

FABRICATION AND CHARACTERIZATION OF BILAYERED TISSUE
SCAFFOLDS INCORPORATING BIOACTIVE AGENTS FOR SKIN TISSUE
ENGINEERING APPLICATIONS

A THESIS SUBMITTED TO
THE GRADUATE SCHOOL OF NATURAL AND APPLIED SCIENCES
OF
MIDDLE EAST TECHNICAL UNIVERSITY

BY

ÖMER AKTÜRK

IN PARTIAL FULFILLMENT OF THE REQUIREMENTS
FOR
THE DEGREE OF DOCTOR OF PHILOSOPHY
IN
ENGINEERING SCIENCES

JANUARY 2015

Approval of the thesis:

**FABRICATION AND CHARACTERIZATION OF BILAYERED TISSUE
SCAFFOLDS INCORPORATING BIOACTIVE AGENTS FOR SKIN TISSUE
ENGINEERING APPLICATIONS**

submitted by **ÖMER AKTÜRK** in partial fulfillment of the requirements for the degree of **Doctor of Philosophy in Engineering Sciences Department, Middle East Technical University** by,

Prof. Dr. Gülbin Dural Ünver
Dean, Graduate School of **Natural and Applied Sciences**

Prof. Dr. Murat Dicleli
Head of Department, **Engineering Sciences**

Assoc. Prof. Dr. Dilek Keskin
Supervisor, **Engineering Sciences Dept., METU**

Dr. Temel Bilici
Co-supervisor, **Paro-TANI Pazarlama ve İletisim Hiz. A.S.**

Examining Committee Members:

Prof. Dr. Ufuk Gündüz
Biology Dept., METU

Assoc. Prof. Dr. Dilek Keskin
Engineering Sciences Dept., METU

Prof. Dr. Emir Baki Denkbaş
Chemistry Dept., Hacettepe University

Assoc. Prof. Dr. Can Özen
Biotechnology Dept., METU

Assoc. Prof. Dr. Senih Gürses
Engineering Sciences Dept., METU

Date: 26.01.2015

I hereby declare that all information in this document has been obtained and presented in accordance with academic rules and ethical conduct. I also declare that, as required by these rules and conduct, I have fully cited and referenced all material and results that are not original to this work.

Name, Last Name : ÖMER AKTÜRK

Signature :

ABSTRACT

FABRICATION AND CHARACTERIZATION OF BILAYERED TISSUE SCAFFOLDS INCORPORATING BIOACTIVE AGENTS FOR SKIN TISSUE ENGINEERING APPLICATIONS

Aktürk, Ömer

Ph. D. , Department of Engineering Sciences

Supervisor : Assoc. Prof. Dr. Dilek Keskin

Co- Supervisor : Dr. Temel Bilici

January 2015, 231 pages

In this study, it was aimed to fabricate tissue scaffolds from different biological polymers (collagen, silk fibroin and sericin) for skin tissue engineering applications. For this purpose, bilayered scaffolds composed of epidermal (collagen/sericin films) and dermal (collagen sponges, collagen matrices or silk fibroin matrices) layers were produced with different biomaterial fabrication methods. Casting and solvent evaporation (film), lyophilization/freeze-drying (sponge) and dry/wet electro-spinning (micro/nanofibrous matrices) methods were used to obtain the scaffolds. Different sizes (10-55nm) of gold nanoparticles (AuNPs) with spherical shapes were synthesized and one size group (37 nm) was incorporated into dermal layers. Collagen based scaffolds were cross-linked with glutaraldehyde and silk fibroin based ones were treated with ethanol to increase the aqueous stability. The suitability of these scaffolds to skin tissue engineering applications was evaluated by means of physicochemical characterization, in vitro biocompatibility, antibacterial assessment,

intra-dermal irritation, skin sensitization, genotoxicity and in vivo rat skin wound healing tests.

The resistance of collagen based scaffolds to hydrolytic and enzymatic degradation was enhanced significantly after cross-linking, on the contrary collagen nanofibrous scaffolds had tendency to degrade quickly. Especially silk fibroin based scaffolds had the lowest degradation levels. Based on water swelling, silk fibroin based scaffolds and collagen sponge groups were similar (10-30 g/g) due to their similar porosities (70-80%) and pore size distributions (10-200 μm). However, water swelling of collagen nanofibrous scaffolds was lower (3 g/g) in comparison due to their low porosity (10%) and small pore sizes (0-8 μm). The water vapor transmission rates of bilayered scaffolds were statistically similar (about 1300-1400 $\text{g}/\text{m}^2/\text{day}$) and they were confirmed to have good oxygen permeability, which was attributed to collagen/sericin film. Tensile strength of collagen based scaffolds enhanced significantly after cross-linking. AuNPs incorporation into collagen based scaffolds did not have a significant effect on tensile strength values. Yet, AuNPs incorporation significantly increased tensile strength of silk fibroin based scaffolds. Also, tensile strength decreased dramatically when the testing was done in wet conditions. On the other hand, elongation at break of all the wet scaffolds were improved significantly reaching to even above 100% values. Elastic modulus of all the scaffolds increased significantly after cross-linking indicating increased hardness, on the contrary elastic modulus decreased significantly in wet conditions as they became more extensible and softer in aqueous environment.

The cytotoxic effect of AuNPs on keratinocyte and fibroblasts were size and dose dependent. None of the scaffolds (epidermal and dermal layers) had a cytotoxic effect (cell viability > 85%) on L929 fibroblasts. Cell seeding tests showed that, fibroblasts and keratinocytes attached and gained their natural morphology (spread or polygonal) in 1 day and proliferated on the scaffolds during 3 days incubation period according to SEM analysis. Antibacterial assessment tests based on the agar disc diffusion method provided strong evidence that AuNPs fabricated in this study had an antibacterial potential against *S. Aureus*. Also, the OD measurement and SEM

analysis showed that *S. Epidermidis* could not attach onto scaffolds containing AuNPs compared to control without AuNPs.

In vivo tests results showed that all the groups had significantly better wound contraction than untreated controls on post-operative 14th day. Early stage re-epithelization started to form in collagen based and silk fibroin based scaffold groups, with low inflammation, and high fibrosis and granulation tissue formation compared to MatridermTM. Also, the groups containing honey or AuNPs started to recover their mechanical properties much quicker than MatridermTM according to biomechanical tests. All these results suggested that all the groups, especially the groups containing honey or AuNPS have equal or slightly better in vivo healing effect than MatridermTM.

According to animal toxicology evaluation and genotoxicity tests on BLCS-AuX, there were no adverse skin reactions (irritation or sensitization) or genotoxicity. As a conclusion, it could be suggested that all of these bilayered skin substitutes, especially the groups containing bioactive agents (honey or AuNPs) could be very valuable skin substitute materials for use in the management of skin wounds.

Keywords: Bilayered skin substitutes, skin tissue engineering, electro-spinning, lyophilization, collagen, sericin, gold nanoparticles

ÖZ

DERİ DOKU MÜHENDİSLİĞİ UYGULAMALARI İÇİN BİYOETKİN AJAN YÜKLÜ İKİ KATMANLI DOKU İSKELELERİ ÜRETİLMESİ VE KARAKTERİZASYONU

Aktürk, Ömer

Doktora, Mühendislik Bilimleri Bölümü

Tez Yöneticisi : Doç. Dr. Dilek Keskin

Ortak Tez Yöneticisi : Dr. Temel Bilici

Ocak 2015, 231 sayfa

Bu çalışmada, deri doku mühendisliği uygulamaları için farklı biyolojik polimerlerden (kollajen, serisin, ipek fibroin) doku iskeleleri üretmek amaçlanmıştır. Bu sebeple epidermal (kollajen/serisin film) ve dermal (kollajen köpük, kollajen matris ya da ipek fibroin matris) eşleniklerden oluşan iki katmanlı deri eşlenikleri farklı biyomalzeme üretim fabrikasyon yolları ile üretilmiştir. İskeleleri üretmek için, solvent dökme ve uçurma (film), liyofilizasyon/dondurup-kurutma (köpük) ve kuru/ıslak elektro-eğirme (mikro/nano fibröz matris) metotları kullanılmıştır. Farklı boyutlarda ve küre şeklinde altın nanoparçacıklar (AuNPs) üretilerek bir boyut grubu (37 nm) dermal katmanlara eklenmiştir. İskelelerin epidermal ve dermal katmanlarının sudaki sağlamlıklarını arttırmak için kollajen temelli iskeleler glutaraldehit (GTA) ile çapraz bağlanmış, ipek fibroin temelli iskeleler ise etanolde kimyasal işlem görmüştür. Bu iskelelerin deri doku mühendisliğine uygunlukları fizikokimyasal karakterizasyon, in vitro biyoyumluluk, antibakteriyellik, deri içi

iritasyon, deri sensitizasyon, genotoksisite, ve in vivo sıçan deri yarası iyileşme testleri ile değerlendirilmiştir.

Çapraz bağlama sonunda kollajen temelli iskelelerin hidrolitik ve enzimatik bozunmaya karşı dirençleri anlamlı bir şekilde artmıştır, bunun aksine kollajen nanofibröz iskeleler daha çabuk bozunmaya meyillidir. Özellikle ipek fibroin temelli iskeleler en düşük bozunmaya sahiptir. Su tutma özelliğine göre, fibroin temelli iskeleler ile kollajen köpükler benzerdir (10-20 gr/gr), çünkü benzer gözenekliliğe (%70-80) ve gözenek boyut dağılımına (10-200 µm) sahiptirler. Bunlara kıyasla kollajen nanofibröz matrikslerin su tutmaları düşük gözeneklilik (%10) ve küçük gözenek boyutları (0-8 µm) yüzünden daha düşüktür (3 gr/gr). İki katmanlı iskelelerin su buharı geçirgenlikleri istatistiksel açıdan benzerdir (1300-1400 gr/m²/gün), ve iyi oksijen geçirgenlikleri olduğu teyit edilmiştir. Bunun sadece kollajen/serisin filme bağlı olduğu düşünülmüştür. Kollajen temelli iskelelerin gerilim kuvveti çapraz bağlama sonucunda anlamlı bir şekilde gelişmiştir. Kollajen temelli iskelelere AuNPs eklenmesinin, gerilim kuvveti üstünde istatistiksel açıdan anlamlı bir etkisi olmamıştır. Ancak, ipek fibroin temelli iskeleye AuNPs eklenmesi gerilim kuvvetini anlamlı bir şekilde arttırmıştır. Ayrıca, gerilim kuvveti, nemli örneklerde dramatik olarak düşmüştür. Diğer yandan, iskelelerin kopma anındaki uzaması, örnekler nemlendirilince %100 değerlerini bile aşarak anlamlı bir şekilde artmıştır. Örneklerin, elastik modülüsü çapraz bağlama sonucunda, sertliğin arttığına işaret olarak, anlamlı bir şekilde artmıştır. Bunun tersine nemli örneklerin elastik modülüsü anlamlı bir şekilde düşmüştür, çünkü örnekler nemli iken daha yumuşak ve daha uzayabilir olmuştur.

Üretilen AuNPs'ların keratinosit ve fibroblastlar üstündeki sitotoksitesinin, boyut ve doza bağlı olduğu görülmüştür. Hiçbir iskele (epidermal veya dermal katmanlar) fibroblastlar üstünde sitotoksik etki göstermemiştir (hücre canlılığı > 85). Hücre yapışma testlerinde, fibroblast ve keratinositlerin 1 günlük süre içinde iskeleler üstüne yapıştığı ve doğal morfolojilerini (uzamış ve poligonal) kazandıkları ve 3 gün sonunda da sayılarının arttığı SEM analizi ile gösterilmiştir. Agar disk difüzyon metoduna dayanan antibakteriyellik değerlendirme testleri bu çalışmada üretilen

AuNPs'lerin *S. Aureous* üstünde antibakteriyel potansiyeli olduğuna yönelik kuvvetli bir delil sağlamıştır. Ayrıca OD ölçümü ve SEM analizi göstermiştir ki *S. Epidermidis*, AuNPs içeren iskelelere AuNPs içermeyen iskelelere kıyasla yok denecek kadar az yapışabilmiştir.

In vivo test sonuçlarına göre; postoperatif 14. gün sonunda bütün gruplar işlem görmemiş kontrol grubundan anlamlı bir şekilde daha iyi yara kapanması göstermiştir. Erken dönem epitelizasyon, kollajen temelli ve ipek fibroin temelli iskele gruplarında, düşük inflamasyon, yüksek fibrosis ve granülasyon dokusu ile Matriderm™'e kıyasla daha iyi oluşmaya başlamıştır. Ayrıca, biyomekanik test sonuçlarına göre, bal ve AuNPs içeren gruplar Matriderm™'den daha hızlı bir şekilde orijinal mekanik özelliklerine kavuşmaya başlamıştır. Bütün bu sonuçlara göre, bütün gruplar, özellikle bal veya AuNPs içeren iskeleler Matriderm™ ile aynı hatta daha iyi in vivo yara iyileşme etkisi göstermiştir.

BLCS-AuX üstünde yapılan hayvan toksikoloji değerlendirilmesi ve genotoksisite testlerine göre; BLCS-AuX için hiç bir ters deri reaksiyonu (iritasyon ya da sensitizasyon) veya genotoksisite sonucu olmamıştır. Sonuç olarak, bütün bu iki katmanlı deri eşleniklerinin, özellikle de biyoaktif ajan (bal veya AuNPs) içeren grupların deri yaralanmalarında kullanılmak için çok değerli deri eşleniği malzemesi olabileceği söylenebilir.

Anahtar Kelimeler: İki katmanlı deri eşleniği, deri doku mühendisliği, elektro-eğirme, liyofilizasyon, kollajen, serisin, altın nanoparçacıklar

Dedicated to my fiancée, Selcan Ekin, who has always supported me more than anyone else during the hard and exhausting course of my doctoral study

ACKNOWLEDGMENTS

I wish to express my deepest gratitude to my advisor Assoc. Prof. Dr. Dilek Keskin and my co-advisor Dr. Temel Bilici for their scientific support and guidance throughout this long research. They have always given their hands whenever I need. I could even establish my own technological start-up company, Remoderm Medical Ltd. Co., with their tremendous helps. Apart from being my scientific advisor, Assoc. Prof. Dr. Dilek Keskin has also become my company advisor and supervised my company project on the fabrication, characterization and commercialization of skin substitutes meticulously and encouraged me during these hard processes. Dr. Temel Bilici was actually my mentor assigned to my company on the framework of TÜBİTAK1512 project. He was a real friend and an asset to my company and tried to lead me and my company to the success road.

One of the other valuable persons, contributed greatly to the success of my TÜBİTAK 1512 project was Prof. Dr. Emir Baki Denkbaşı, deserves my compliments for his huge help.

I would also like to give my special thanks to jury members of this Ph. D. study (Assoc. Prof. Dr. Can Özen and Assoc. Prof. Dr. Senih Gürses) for their priceless suggestions that they have given so far during the thesis meetings.

Many thanks to Prof. Dr. Ufuk Gündüz for participating my Ph. D defense jury.

I would like to give great thanks to my lab friends, whom have recently earned or are still pursuing their academic degrees, for their valuable friendship and huge helps in laboratory works. Dr. Ayşegül Kavas, Dr. Özge Erdemli, Dr. Bengi Yılmaz and Ph. D. candidates Aydın Tahmesebifar and Reza Moonesirad, helped me a lot in the laboratory whenever I need. The insightful advices and friendly supports of them all merit an emphasis. Among them, I would especially like to express my gratitude to Reza Moonesirad for his help in the fabrication of lyophilized scaffolds, a long lasting process continuing even in late nights. Without their help, I would not have

been able to finish my thesis and projects experiments successfully. Not only them, but also M.S. degree candidates and earners; Sibel Ataol, Merve Güldiken, Zeynep Barçın, Nil Göl, Hazal Aydoğdu, Deniz Atila, Ali Deniz, Engin Pazarçeviren, Alişan Kayabölen helped me a lot in the lab. We shared the excessive work load of laboratory and tried to make never lasting laboratory hours more enjoyable. I wish to give all of them many thanks for their intimate friendships and continuous helps. In order to be able to list all the help of my friends I have to add another chapter to my thesis; therefore, to cut it short, many thanks to them for everything.

I would like to thank TÜBİTAK for 1002- Short Term R& D Funding Program (No: 111M810) and 1512- Entrepreneurship and Multistep R& D Funding Program (No: 184210) financial supports.

I would also like to thank the biocompatibility group of Hacettepe University, Faculty of Pharmacy, Department of Pharmacology for conducting toxicology tests.

I would like to give my thanks to Assoc. Prof. Dr. Kemal Kısmet, Prof. Dr. ÇınarYastı and their team (Assoc. Prof. Dr. Muzaffer Çaydere, Assoc. Prof. Dr. Sema Hücümenoğlu, Dr. Serdar Kuru, Dr. Mehmet Esat Duymuş, Dr. Feridun Kaya) for designing and performing in vivo rat full-thickness wound healing experiments, and helping us to analyze the results.

I am very grateful to Assoc. Prof. Dr. Sreeparna Banerjee from Biology Department and Dr. Nusret Taheri from METU Medical Center for allowing me to use their lab facilities for the antibacterial assessment tests.

The last but not the least, I would like to give my special thanks to my parents who have also contributed to the success of this thesis study, maybe more than anybody else. I have always them besides me giving their financial and especially emotional foster and encouraging me whenever I live harsh moments and fall into disappointment in my studies.

TABLE OF CONTENTS

ABSTRACT.....	v
ÖZ.....	viii
ACKNOWLEDGMENTS.....	xii
TABLE OF CONTENTS.....	xiv
LIST OF TABLES.....	xxi
LIST OF FIGURES.....	xxiii
LIST OF ABBREVIATION.....	xxxii
CHAPTERS	
1. INTRODUCTION.....	1
1.1. Skin.....	1
1.1.1. Anatomy of Healthy Skin.....	1
1.1.2. Functions of Skin.....	3
1.1.2.1. Functions of Epidermis.....	3
1.1.2.2. Functions of Dermis.....	3
1.1.3. Biomechanical Properties of Skin.....	4
1.1.4. Skin Wounds.....	6
1.1.5. Repair Mechanism of Skin Wound.....	7
1.2. Skin Substitutes.....	8
1.2.1. The Need for Tissue-engineered Skin Substitutes.....	8
1.2.2. Ideal Properties of Skin Substitutes.....	10
1.2.3. Classification of Skin Substitutes.....	11
1.2.3.1. Epidermal Skin Substitutes.....	12
1.2.3.2. Dermal Skin Substitutes.....	12
1.2.3.3. Dermo-epidermal (Composite) Skin Substitutes.....	13
1.2.3.4. Potential Skin Substitututes.....	20
1.3. General Properties of Materials used in the Study.....	21
1.3.1. Gold.....	22
1.3.1.1. Synthesis of Gold nanoparticles.....	22

1.3.1.2.	Medical Applications of Gold.....	23
1.3.1.2.1.	The Major Therapeutic/Clinical Uses of Gold Nanoparticles.....	23
1.3.1.2.2.	Application of Gold Nanoparticles in Tissue Engineering.....	23
1.3.1.3.	Toxicity of Gold Nanoparticles.....	25
1.3.1.4.	Antibacterial Activity of Gold Nanoparticles.....	27
1.3.1.4.1.	Surface Coating with Gold Nanoparticles.....	27
1.3.1.4.2.	Surface Coating of Antibiotics with AuNPs.....	27
1.3.1.4.3.	Photodynamic Antimicrobial Chemotherapy of Gold Nanoparticles.....	28
1.3.2.	Honey.....	29
1.3.2.1.	Types of Honey.....	29
1.3.2.2.	The Composition of Honey.....	30
1.3.2.3.	Medical Applications of Honey.....	30
1.3.2.3.1.	Wound Healing Effect.....	30
1.3.2.3.2.	Antimicrobial Property of Honey.....	31
1.3.2.3.3.	Anti-oxidant Property of Honey.....	32
1.3.3.	Collagen.....	32
1.3.3.1.	Sources and Refinement.....	32
1.3.3.2.	Molecular Structure.....	33
1.3.3.3.	Types and Distributions.....	34
1.3.3.4.	Mechanical Properties and Stability of Collagen.....	35
1.3.3.5.	Biological Responses to Collagen.....	36
1.3.3.6.	Biomedical Applications of Collagen.....	37
1.3.4.	Silk Fibroin.....	37
1.3.4.1.	Sources and Refinement of Silk Fibroin.....	37
1.3.4.2.	Molecular Structure of Fibroin.....	38
1.3.4.3.	Biological Responses to Fibroin.....	39
1.3.4.4.	Biomedical Applications of Fibroin.....	39
1.3.5.	Silk Sericin.....	40

1.3.5.1.	Sources and Refinement of Silk Sericin.....	40
1.3.5.2.	Molecular Structure.....	40
1.3.5.3.	Biological Responses to Sericin.....	41
1.3.5.4.	Biomedical Applications of Silk Sericin.....	41
1.4.	Aim of the Study.....	42
2.	MATERIALS AND METHODS.....	45
2.1.	Materials.....	45
2.1.1.	Materials and Chemicals for Scaffold Preparation.....	45
2.1.2.	Materials and Chemicals for Gold Nanoparticles Synthesis.....	45
2.1.3.	Materials and Chemicals for Physicochemical Characterization experiments.....	46
2.1.4.	Materials and Chemicals for Cell Culture Studies.....	46
2.1.5.	Materials and Chemicals for In Vivo Studies.....	47
2.2.	Methods.....	47
2.2.1.	Synthesis of Gold Nanoparticles.....	47
2.2.2.	Fabrication of Epidermal Layer of Scaffolds.....	49
2.2.3.	Fabrication of Dermal Layer of Scaffolds.....	49
2.2.3.1.	Collagen Sponges.....	49
2.2.3.1.1.	Preparation of Collagen Sponge Solutions.....	49
2.2.3.1.2.	Lyophilization of Collagen Solutions.....	50
2.2.3.1.3.	Chemical Treatment of Collagen Sponges.....	50
2.2.3.2.	Collagen Nanofibrous Matrices.....	51
2.2.3.2.1.	Preparation of Collagen Spinning Solutions.....	51
2.2.3.2.2.	Electro-spinning of Collagen Solutions.....	51
2.2.3.2.3.	Chemical Treatment of Collagen Nanofibrous Matrices.....	54
2.2.3.3.	Fibroin Micro/Nano Fibrous Matrices.....	54
2.2.3.3.1.	Extraction of Silk Fibroin from Cocoons.....	54
2.2.3.3.2.	Preparation of Fibroin Spinning Solutions.....	55
2.2.3.3.3.	Electro-spinning of Fibroin Solutions.....	56
2.2.3.3.4.	Chemical Treatment of Silk Fibroin Fibrous	

Matrices.....	58
2.2.4. Fabrication of Bilayered Skin Substitutes.....	58
2.2.5. Characterization Tests.....	62
2.2.5.1. Physicochemical Characterization.....	62
2.2.5.1.1. Attenuated Total Reflectance Fourier Transform Infrared Spectrophotometer Analysis.....	62
2.2.5.1.2. Scanning Electron Microscopy.....	63
2.2.5.1.3. Transmission Electron Microscopy.....	63
2.2.5.1.4. Porosity Calculation.....	63
2.2.5.1.5. Pore Size Distribution Analysis.....	64
2.2.5.1.6. Hydrolytic Degradation.....	65
2.2.5.1.7. Enzymatic Degradation.....	65
2.2.5.1.8. Equilibrium Degree of Swelling.....	66
2.2.5.1.9. Water Vapour Transmission Rate.....	67
2.2.5.1.10. Oxygen Permeability Test.....	68
2.2.5.1.11. Mechanical Testing.....	69
2.2.5.2. In Vitro Characterization Tests.....	70
2.2.5.2.1. Cell Culture Conditions.....	70
2.2.5.2.1.1. Fibroblast Cell Line Culture.....	70
2.2.5.2.1.2. Keratinocyte Cell Line Culture.....	70
2.2.5.2.2. Cytotoxicity Tests of Synthesized Gold Nanoparticles.....	71
2.2.5.2.3. Cytotoxicity Tests of Scaffold Extracts.....	71
2.2.5.2.4. Cell Attachment and Proliferation on Scaffolds	73
2.2.5.3. Antibacterial Assessment.....	74
2.2.5.3.1. Antibacterial Tests of Gold Nanoparticles.....	74
2.2.5.3.2. Antibacterial Tests of Scaffolds.....	74
2.2.5.4. In Vivo Characterization Tests.....	75
2.2.5.4.1. Rat Full-Thickness Wound Healing Tests.....	75
2.2.5.4.1.1. Animals and Husbandry.....	75
2.2.5.4.1.2. Full Thickness Wound Model.....	76

2.2.5.4.1.3.	The Optimization of Wound Healing	
	Experimental Procedure.....	76
2.2.5.4.1.4.	Treatments with Scaffolds.....	76
2.2.5.4.1.5.	Histopathological Analysis.....	77
2.2.5.4.1.6.	The Examination of Wound	
	Contraction Rate.....	77
2.2.5.4.1.7.	Biomechanical Tests.....	78
2.2.5.5.	Toxicological Evaluation.....	79
2.2.5.5.1.	Skin Irritation Tests (Animal Intradermal	
	Reactivity Test).....	80
2.2.5.5.2.	Skin Sensitization Tests (Closed-patch Test).....	82
2.2.5.5.3.	Genotoxicity tests (Bacterial Reverse Mutation	
	Test).....	84
2.2.6.	Statistical Analysis.....	86
3.	RESULTS AND DISCUSSION.....	87
3.1.	Synthesis and Characterization of Gold Nanoparticles.....	87
3.1.1.	Characterization of Gold Nanoparticles for Preliminary	
	Synthesis Tests.....	87
3.1.2.	Characterization of Optimized Gold Nanoparticles.....	90
3.2.	Preparation and Morphological Characterization of Collagen	
	Sponges.....	94
3.2.1.	Optimization of Lyophilization Process for Collagen.....	94
3.2.2.	Chemical Treatment of Collagen Sponges.....	94
3.2.3.	Incorporation of Gold Nanoparticles into Collagen Sponges....	95
3.2.4.	Morphology of Collagen Sponges.....	97
3.3.	Preparation and Morphological Characterization of Collagen	
	Nanofibrous Matrices.....	99
3.3.1.	Optimization of the Electrospinning Process for Collagen.....	99
3.3.2.	Incorporation of Gold Nanoparticles into Collagen	
	Nanofibrous Matrices.....	102
3.3.3.	Morphology of Collagen Nanofibrous Matrices.....	105

3.3.4. Chemical Treatment of Collagen Nanofibrous Matrices.....	108
3.4. Preparation and Morphological Characterization of Silk Fibroin Matrices.....	110
3.4.1. Optimization of the Electrospinning Process for Silk Fibroin...	110
3.4.2. Morphology of Silk Fibroin Matrices.....	110
3.4.3. Incorporation of Gold Nanoparticles into SF Matrices.....	114
3.4.4. Chemical Treatment of Silk Fibroin Matrices.....	115
3.5. Characterization of Scaffolds.....	118
3.5.1. Physicochemical Characterization Tests.....	118
3.5.1.1. The Fourier Transform Infrared Spectroscopy Analysis.....	118
3.5.1.1.1. FTIR Analysis of Collagen Sponges.....	118
3.5.1.1.2. FTIR Analysis of Collagen Nanofibrous Matrices.....	119
3.5.1.1.3. FTIR Analysis of Silk Fibroin Matrices.....	121
3.5.1.2. Pore Size Distribution and Porosity of Scaffolds.....	122
3.5.1.3. Hydrolytic Degradation.....	126
3.5.1.4. Enzymatic Degradation.....	127
3.5.1.5. Equilibrium Degree of Swelling.....	131
3.5.1.6. Water Vapor Transmission Rates.....	133
3.5.1.7. Oxygen Permeation.....	134
3.5.1.8. Mechanical Tests.....	135
3.5.1.8.1. Tensile Strength.....	139
3.5.1.8.2. Elongation at Break.....	141
3.5.1.8.3. Tensile Modulus.....	142
3.5.2. In Vitro Characterization Tests.....	145
3.5.2.1. Preliminary Cell Cytotoxicity Tests of Gold Nanoparticles.....	145
3.5.2.2. Cytotoxicity Tests of Optimized Gold Nanoparticles....	150
3.5.2.3. Cytotoxicity Tests of Scaffold Extracts.....	154
3.5.2.4. Cell Adhesion and Proliferation Studies.....	156

3.5.3. Antibacterial Assessment.....	166
3.5.3.1. Antibacterial Tests of Gold Nanoparticles.....	166
3.5.3.2. Antibacterial Tests of Scaffolds.....	168
3.5.4. In Vivo Characterization Studies.....	172
3.5.4.1. In Vivo Rat Full-Thickness Skin Wound Healing Tests.....	172
3.5.4.1.1. The Optimization of Wound Healing Experimental Procedure.....	172
3.5.4.1.2. Wound Contraction.....	174
3.5.4.1.3. Biomechanical Tests.....	178
3.5.4.1.4. Histopathological Analysis.....	183
3.5.4.1.4.1. Epithelization Results.....	183
3.5.4.1.4.2. Repair of the Wound Bed.....	184
3.5.5. Toxicological Evaluation.....	187
3.5.5.1. Intradermal Reactivity.....	187
3.5.5.2. Sensitization.....	188
3.5.5.3. Genotoxicity.....	191
4. CONCLUSION.....	195
REFERENCES.....	197
APPENDICES	
A. ETHICAL APPROVAL FOR ANIMAL TESTS.....	227
VITA.....	229

LIST OF TABLES

TABLES

Table 1.1.	The classification of skin substitutes	11
Table 1.2.	Commercial epidermal skin substitutes	15
Table 1.3.	Commercial dermal skin substitutes	16
Table 1.4.	Commercial dermo-epidermal skin substitutes.....	19
Table 1.5.	The potential collagen based skin substitutes	20
Table 1.6.	The potential skin substitute made of other promising synthetic or biological polymers	21
Table 1.7.	The antibacterial activity of AuNPs in combination with antibiotics.....	28
Table 1.8.	Photodynamic antimicrobial chemotherapy of AuNPs.....	29
Table 1.9.	Collagen types and tissue distribution.....	35
Table 2.1.	Optimization of collagen/PEO spinning solutions added with salt.....	53
Table 2.2.	The groups prepared to study the effect of AuNPs concentration on the electrospinning.....	53
Table 2.3.	Optimization of silk fibroin/PEO spinning blend solutions.....	56
Table 2.4.	Composition of optimized bilayered scaffolds.....	61
Table 2.5.	Qualitative morphological grading of cytotoxicity of extracts.....	73
Table 2.6.	Grading system for intracutaneous (intra-dermal) reactions.....	82
Table 2.7.	Magnusson and Kligman scale.....	83
Table 2.8.	Positive control chemicals for genotoxicity.....	85
Table 3.1.	The properties of nanofibers in the preliminary experimental groups.....	101
Table 3.2.	The properties of nanofibers incorporated with AuNPs.....	103
Table 3.3.	Results obtained in the experimental optimization studies of silk fibroin electrospinning.....	111
Table 3.4.	The properties of fibrous matrices upon chemical treatment.....	116

Table 3.5. Mechanical properties of epidermal and dermal layers of bilayered scaffolds.....	144
Table 3.6. Irritation scores (intracutaneous) in rabbits.....	190
Table 3.7. Mutagenicity of test sample extracts in <i>S.Typhimurium</i> and <i>E. coli</i> test strains.....	193

LIST OF FIGURES

FIGURES

Figure 1.1.	Anatomy of Skin.....	2
Figure 1.2.	A typical stress-strain curve for wet skin.....	5
Figure 1.3.	Collagen Structure : (A) procollagen molecule, (B) collagen molecule, (C) banded structure of collagen fibrils.....	34
Figure 1.4	The main design characteristics of bilayered scaffolds developed in this research.....	44
Figure 2.1.	The schematic figure showing the steps of gold nanoparticles synthesis.....	48
Figure 2.2.	The collagen sponges prepared: (A) CS-Au and, (B) CS.....	50
Figure 2.3.	The electro-spinning system.....	52
Figure 2.4.	The photographs of nanofibrous matrices.....	52
Figure 2.5.	The photographs of nanofibrous matrices after the cross-linking treatment.....	54
Figure 2.6.	A) The photo and B) experimental set-up of wet electrospinning system.....	57
Figure 2.7.	The photo of A) fiber accumulation inside the glass petri plate during electrospinning and B) final freeze-dried electrospun silk fibroin matrix.....	57
Figure 2.8	The photo of optimized experimental groups: A) CS, B) CS-X, C) CS-Au, D) CS-AuX, E) SFM-E, F) SFM-AuE, G) CM-Au, H) CM-AuX, I) C/S, J) C/S-X.....	59
Figure 2.9.	Experimental setup for measuring the hydrolytic and enzymatic degradation.....	66
Figure 2.10.	Experimental setup for measuring water swelling of scaffolds.	67
Figure 2.11.	Experimental set up for testing water vapour transmission rate through bilayered scaffolds.....	68

Figure 2.12.	Experimental set up for testing mechanical properties of scaffolds.....	69
Figure 2.13.	Experimental set up for performing biomechanical tests on rat skin biopsies.....	79
Figure 2.14.	Arrangement of injection sites (1: cranial end, 2: 0.2 ml injections of polar extract, 3: 0.2 ml injections of non-polar extract, 4: 0.2 ml injections of polar solvent control, 5: 0.2 ml injections of non-polar solvent control, 6: caudal end).....	81
Figure 3.1.	The calorimetric verification of gold nanoparticle synthesis.....	87
Figure 3.2.	TEM micrographs and size distribution histograms of synthesized different AuNPs groups: (A1-A2) Au1, (B1-B2) Au2, (C1-C2) Au3 and (D1-D2) Au4.....	89
Figure 3.3.	The spectral scan results of different AuNPs groups between 500 and 700 nm wavelength and their estimated diameters: (A) Au5, (B) Au6, (C) Au7, (D) Au8, (E) Au9, (F) Au10.....	92
Figure 3.4.	CTEM micrographs and size distribution histograms of different AuNPs groups: (A1-A2) Au6, (B1-B2) Au7, (C1-C2) Au8, (D1-D2) Au9 and (E1-E2) Au10.....	93
Figure 3.5.	SEM micrographs of scaffolds incorporated with AuNPs by soaking them into AuNPs solution: (A1-A2) CS-Au, (B1-B2) CS-AuX, or by adding AuNPs into collagen solutions: (C1-C2) CS-Au and D1-D2) CS-AuX. Arrows indicate AuNPs.....	96
Figure 3.6.	SEM micrographs of collagen sponge groups:(A1-A2) CS,(B1-B2) CS-X, (C1-C2) CS-Au and (D1-D2) CS-AuX. Left and right columns indicate the top and side view, respectively.....	98

Figure 3.7.	TEM micrographs of nanofibrous matrix groups: (A1-A2) P2.5Col1Au0, (B1-B2) P2.5Col1Au1, (C1-C2) P2.5Col1Au7 and (D1-D2) P2.5Col1Au14 groups. Red arrows indicate AuNPs. Figures on the right hand side indicate the magnified images.....	104
Figure 3.8	SEM micrographs showing the fiber morphology and fiber diameter distribution of different matrices: (A1-A3) Col1P2Au0 and (B1-B3) Col1P2Au1 group.....	106
Figure 3.9.	SEM micrographs showing the fiber morphology and fiber diameter distribution of different matrices: (A1-A3) Col1P2.5Au0, (B1-B3) Col1P2.5Au1, (C1-C3) Col1P2.5Au7, (D1-D3) Col1P2.5Au14.....	107
Figure 3.10.	SEM micrographs showing the change in nanofiber morphology and pore size of collagen nanofibrous matrices after cross-linking with GTA vapour (3 %) for different time periods: (A1-A2) Col1P2.5Au1 and B1-B2) Col1P2.5Au14.....	109
Figure 3.11.	SEM micrographs and fiber diameter histograms of (A1-A2) degummed pure silk fibroin isolated from silkworm cocoon and SFP2 group with different operation parameters: (B1-B3) flow rate= 2 ml/h, voltage=12 kV, distance=13 cm and (C1-C2) flow rate= 1 ml/h, voltage=17 kV, distance=13 cm. Middle figures are the magnified regions of red rectangles.....	112
Figure 3.12.	SEM micrographs and fiber diameter histograms of SFP2 group collected with the operational parameters: (A1-A3) flow rate= 1 ml/h, voltage=12 kV, distance=20 cm,(B1-B3) flow rate= 0.8 ml/h, voltage=19 kV, distance=23 cm and SFP3 group with the operational parameters of (C1-C3) flow rate= 0.8 ml/h, voltage=19 kV, distance=23 cm. Middle figures are the magnified regions of red rectangles.....	113

Figure 3.13.	SEM micrographs and fiber diameter histograms of SFP3 Au group obtained with the optimized operational parameters (flow rate= 0.8 ml/h, voltage=19 kV, distance=23 cm).....	114
Figure 3.14.	SEM micrographs of silk fibroin matrices treated with different chemical treatment methods:(A1-A2) SFM-E, (B1-B2) SF-M and (C1-C2) SF-G. Figures on the right are the magnified regions of red rectangles.....	117
Figure 3.15.	FTIR-ATR spectra of test groups: (A) CS, (B) CS-Au, (C) CS-X and (D) CS-AuX.....	119
Figure 3.16.	FTIR-ATR spectra of test groups: (A) PEO, (B) collagen type I (C) CM-Au and (D) CM-AuX.....	120
Figure 3.17.	FTIR-ATR spectra of silk fibroin scaffolds: (A) SF film, (B) SF cocoon (C) SFM-E, (D) SFM-M, (E) SFM-G and (F) SFM-AuE.....	122
Figure 3.18.	Porosity and pore size distribution analysis of scaffolds A) CS, B) CS-X, C) CS-Au, D) CS-AuX, E) CM-Au, F) CM-AuX, G) SFM-E and H) SFM-AuE.....	125
Figure 3.19.	Hydrolytic degradation results: (A) collagen sponges (CS, CS-X, CS-Au and CS-AuX) a commercial skin substitute (Matriderm™) and collagen nanofibrous matrices (CM-Au and CM-AuX), (B) silk fibroin matrices (SFM-E and SFM-AuE) and (C) collagen/sericin membranes (C/S and C/S-X).....	129
Figure 3.20.	Enzymatic degradation results:(A) collagen sponges (CS, CS-X, CS-Au and CS-AuX) a commercial skin substitute (Matriderm™) and collagen nanofibrous matrices (CM-Au14 and CM-Au14X), (B) silk fibroin matrices (SFM-E and SFM-AuE) and (C) collagen/sericin membranes (C/S and C/S-X).....	130

Figure 3.21.	EDS of scaffolds. *: Significant difference between the same compositional groups after cross-linking for $p < 0.05$. #: Significant difference between the same compositional groups after AuNPs incorporation for $p < 0.05$. α : Significant difference from Matriderm TM for $p < 0.05$. Values are expressed as mean \pm SD (n=4).....	133
Figure 3.22.	Water vapor transmission rates (WVTR) of bilayered scaffolds. Values are expressed as mean \pm SD (n=4).....	134
Figure 3.23.	Oxygen permeability of bilayered scaffolds. Values are mean \pm SD (n=3).*: Indicates significant difference from the closed control for $p < 0.05$	135
Figure 3.24.	Representative stress-strain curves of scaffolds fabricated in this study: (A) collagen sponges (CS, CS-X, CS-X wet, CS-Au, CS-AuX and CS-AuX wet), Matriderm TM (Matriderm and Matriderm wet) and (B) collagen nanofibrous matrices (CM-Au and CM-AuX).....	137
Figure 3.25.	Representative stress-strain curves of scaffolds fabricated in this study: (A) silk fibroin matrices (SFM-E, SFM-E wet, SFM-AuE and SFM-AuE wet) and (B) collagen/sericin membranes (C/S, C/S-X and C/S-X wet).....	138
Figure 3.26.	Successful tensile break occurred in the middle of the gauge length.....	139
Figure 3.27.	Cytotoxicity tests of different AuNPs on keratinocytes with MTT assay: (A) Au1, (B) Au2 and (C) Au3. *: Significant difference from the control in the same time period #: Significant difference between the groups in the same time period (n=4 \pm SD, $p < 0.05$).....	147

Figure 3.28.	Cytotoxicity tests of different AuNPs groups on 3T3 fibroblasts with MTT assay: (A) Au1, (B) Au2 and (C) Au3.*: Significant difference from the control in the same time period #: Significant difference between the groups in the same time period (n=4 ±SD, p<0.05).....	148
Figure 3.29.	Cytotoxicity tests of different AuNPs groups on keratinocytes: (A) Au7 and (B) Au8.*: Indicating a significant difference from the control in the same time period (n=6 ± SD, p<0.05).....	152
Figure 3.30.	Cytotoxicity tests of different AuNPs groups on 3T3 fibroblasts: (A) Au7 and (B) Au8.*: Indicating a significant difference from the control in the same time period (n=6 ±SD, p<0.05).....	153
Figure 3.31.	The results of extract cytotoxicity tests: (A) epidermal and dermal layers and (B) bilayered scaffolds.....	155
Figure 3.32.	SEM micrographs showing the adhesion and proliferation of L929 fibroblasts on collagen sponge groups in different incubation periods: (A-B) CS and (C-D) CS-Au. Cells were shown with red arrows.....	157
Figure 3.33.	SEM micrographs showing the adhesion of L929 fibroblasts on A-B) CS-X and C-D) CS-AuX collagen sponge groups in different incubation periods. Cells were shown with red arrows.....	158
Figure 3.34.	SEM micrographs showing the adhesion of L929 fibroblasts on A-B) SFM-E and C-D) SFM-AuE silk fibroin groups in different incubation periods. Cells were shown with red arrows.....	159
Figure 3.35.	SEM micrographs showing the adhesion of L929 fibroblasts on A-B) CM-AuX and C-D) and Matriderm™ in different incubation periods. Cells were shown with red arrows.....	160

Figure 3.36.	SEM micrographs showing the adhesion of keratinocytes on A-B) CS and C-D) CS-Au collagen sponge groups in different incubation periods. Cells were shown with red arrows.....	161
Figure 3.37.	SEM micrographs showing the adhesion of keratinocytes on A-B) CS-X and C-D) CS-AuX collagen sponge groups in different incubation periods. Cells were shown with red arrows.....	162
Figure 3.38.	SEM micrographs showing the adhesion of keratinocytes on A-B) SFM-E and C-D) SFM-AuE silk fibroin matrix groups in different incubation periods. Cells were shown with red arrows.....	163
Figure 3.39.	SEM micrographs showing the adhesion of keratinocytes on A-B) CM-AuX and C-D) Matriderm TM groups in different incubation periods. Cells were shown with red arrows.....	164
Figure 3.40.	Agar diffusion tests results showing the transparent zones created around the discs loaded with different doses of AuNPs (Au8 group) alone (top row) and with different doses (5, 10, 20 ppm) of AuNPs (Au8 group) + antibiotic (cefuroxime, 4 µg/ml) at the same time (bottom row).....	168
Figure 3.41.	Antibacterial tests of scaffolds based on OD measurements. *: Indicating a significant difference between the groups. #: Significant difference from the control group (LB) (n=3 ±SD, p<0.05).....	170
Figure 3.42.	SEM micrographs showing the adhered bacteria colonies on A) CS, B) CS-X, C) CS-Au, D) CS-AuX, E) SFM-E and F) SFM-AuE. Arrows and circles in red indicate the bacteria colonies.....	171

Figure 3.43.	The appearance of the wounds on postoperative 14 th day of preliminary experiments with the selected scaffolds: (A) BLCS, (B) BLCS-AuX, and (C) BLSF-X.....	173
Figure 3.44.	The experimental steps to create full-thickness wound model in rats: (A) drawing the wound in the size of 1x2 cm with a mould, (B) incising the wound with a skin scraper and removing the film-like thin muscle tissue under the cut-out skin (panniculus carnosus) (C) applying the test groups onto the wound area and humidifying it with PBS and (D) closing the surface of scaffolds with Ioban TM surgical drape.....	174
Figure 3.45.	Wound contraction rates of different test groups on post-operative 4 th , 7 th , 10 th and 14 th days. #: Significant difference from the untreated control group (n=10 ± SD, p<0.05).....	176
Figure 3.46.	The images showing the wound contraction extent of different test groups and control on post-operative 14 th day: (A) empty control, (B) CS-X, (C) CS-AuX, (D) CS-BX, (E) SFM-E, (F) SFM-AuE, (G) SFM-BE, (H) Matriderm TM	177
Figure 3.47.	Stress-strain curves of skin biopsies taken on post-operative 14 th day.....	179
Figure 3.48.	(A) Tensile strength and (B) the corresponding recovery index of skin biopsies taken on post-operative 14 th day. *: Indicating a significant difference from the unwounded skin. (n≥6 ± SD).....	181
Figure 3.49.	A) Elongation at break (%) and B) elastic modulus of skin biopsies taken on post-operative 14 th day. *: Indicating a significant difference from the unwounded. #: Indicating a significant difference between the test groups for (p<0.05, n≥6 ± SD).....	182

Figure 3.50.	Histopathological scores of test groups (skin biopsies taken on post-operative 14 th day). *: Indicating a significant difference from untreated control. #: Indicating a significant difference between test groups (n=10 ± SD, p<0.05).....	185
Figure 3.51.	Representative images of H&E staining: (A) untreated control, (B) CS-X, (C) CS-AuX, (D) CS-BX (E) SFM-E, (F) SFM-AuE, (G) SFM-BE and (H) Matriderm TM test groups on post-operative 14 th day. Red, yellow and green arrows indicate re-epithelialization (keratinocytes: K, scab: S), granulation/fibrosis (fibroblasts: F, collagen: C, vascularization: V), and inflammatory cells (macrophages: M, lymphocytes: L).....	186

LIST OF ABBREVIATIONS

ANOVA	: Analysis of Variance
ASTM	: American Society for Testing and Materials
AuNPs	: Gold Nanoparticles
DMEM	: Dulbecco's Modified Eagle's Medium
DMSO	: Dimethyl Sulfoxide
DO	: Dissolved Oxygen
EAB	: Elongation at Break
EDC	: N-(3-Dimethylaminopropyl)-N'-ethylcarbodiimide hydrochloride
EDS	: Equilibrium Degree of Swelling
EDTA	: Ethylene Diamine Tetra Acetic acid
EtOH	: Ethanol
E	: Modulus of Elasticity
ED	: Enzymatic Degradation
FBS	: Fetal Bovine Serum
FTIR	: Fourier Transform Infrared Spectrophotometer
GTA	: Glutaraldehyde
HD	: Hydrolytic Degradation
MetOH	: Methanol
MTT	: Thiazolyl Blue Tetrazolium Bromide
NHS	: N-Hydroxysuccinimide
OD	: Optical Density
PBS	: Phosphate Buffered Saline
P	: Porosity
SD	: Standard Deviation
SEM	: Scanning Electron Microscope
TCPS	: Tissue Culture Polystyrene Dishes
TEM	: Transmission Electron Microscopy
UTS	: Ultimate Tensile Stress or Tensile Strength

UV : Ultraviolet

WVTR : Water Vapor Transmission Rate

CHAPTER 1

INTRODUCTION

This study primarily aims to develop a new biomaterial to be used as a skin substitute. Therefore, the general properties of skin, skin wounds, healing processes and the associated treatment methods were described in the introduction part first. Then, skin substitutes investigated in experimental studies and those currently being used in clinical cases were mentioned. Detailed information on the components of skin substitutes, i.e. type I collagen, silk fibroin and sericin polymers and the bioactive agents (honey and gold nanoparticles) used in this study was given in the subsequent section. In the last part, the objectives of the study and reasons of selecting the used materials have been given with a biomimetic approach. At that section, the purposes of performed experimental methods were also discussed in relation to the required properties of a biomaterial for skin wound healing.

1.1. Skin

1.1.1. Anatomy of Healthy Skin

Skin is considered as the largest organ of the body acting as the primary defense system against microorganisms. Anatomically, skin could be divided into three main layers as epidermis, dermis and underlying subcutaneous fat layer (hypodermis) (Augustine et al., 2014).

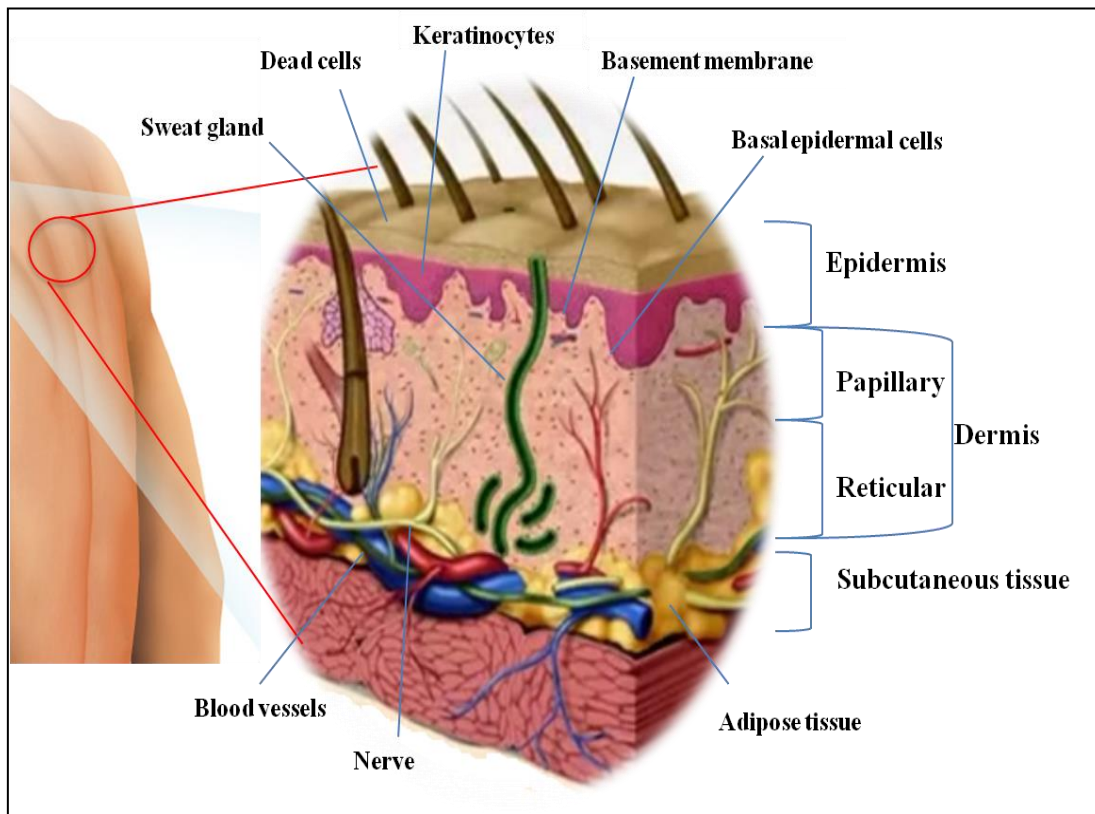


Figure 1.1. Anatomy of skin.

These main layers and functional components of skin are depicted with Figure 1.1. The mission of protection of skin from mechanical damage (wounding) belongs to these layers. The outer and the thinnest layer of skin is called epidermis. In the innermost layer of epidermis, single layer basal epidermal cells proliferate and differentiate into keratinocytes and push already formed cells into upper levels. They finally form flattened, death cells composed of skin proteins called keratins. It does not contain any blood vessels but the nutrients, vitamin and oxygen come from the deeper layers of epidermis with diffusion. At the bottom of epidermis exists a very thin membrane called basement membrane. The boundary between dermis and epidermis contains undulations called rete pegs, which increase the contact area between the layers of skin and aid in preventing the epidermis from being torn. The deeper portion of skin, dermis, contains blood vessels, nerves, and skin appendages such as hair roots, sweat and sebaceous glands. The final layer, hypodermis, is made-

up of fat-filled cells (adipose cells) underlying the dermis. It contains larger blood vessels and nerves so that it contributes to thermoregulation and mechanical properties of skin as well (Metcalf et al., 2007).

1.1.2. Functions of Skin

1.1.2.1. Functions of Epidermis

Briefly, the functions of epidermis could be enumerated as prevention of excess water vapor loss, protection from toxins, heat, UV light and microbial entry (Falanga and Faria, 2007). Keratinocytes are the major cellular component of epidermis. They have a stratified structure for which each layer of cells is attached to each other by desmosomes (Geesin and Berg, 1991). Whereas the outer layer of epidermis is composed of viable (keratinocytes) and death epidermal cells (keratin), inner layer of epidermis is epidermal cells which are inclined to proliferate and migrate to surface and become keratinocytes. Keratin layers create a tough protein surface covering preventing bacteria or toxin entry. At the basal membrane, basal epidermal cells (stem cells) are anchored to basement membrane by adhesion molecules. These epidermal cells also surround the the skin appendages such as hair, sebaceous and sweat glands. Langerhans' cells are (frontline defense of the immune system) and melanocytes (responsible for pigmentation) are also present in the skin.

1.1.2.2. Functions of Dermis

The dermis protects the skin mechanically providing strength, flexibility and elasticity of skin. It is also the factory for all the components required for repair and remodeling of epidermis and dermis. It also acts as a scaffold for cell migration, and control the passage of nutrient and oxygen delivery. In addition to these important functions dermis also regulates the heat of skin by control of skin blood flow and

sweating. It also contains the nerves enabling the sensation (touch, pain, heat and cold) (Falanga and Faria, 2007) Dermis is composed largely of extracellular matrix components including collagen, elastin, fibrillin, hyaluronic acid and proteoglycans. While collagen fibers are responsible for fostering the shape of the skin and preventing the premature mechanical failure, elastin fibers are responsible for elasticity of skin (Geesin and Berg, 1991). The most prevalent cell type in skin is fibroblast. It does not only synthesize and deposit collagen fibers but also recognize, and remove the proteins that are damaged or being recycled (Silver, 1994). The dermis consists of two parts as papillary dermis and reticular dermis. While the upper dermis is named as papillary dermis, the most biologically active part of the dermis, the deeper layer is reticular dermis responsible for durability and anchoring of skin appendages. The predominant protein type in dermis extracellular matrix is collagen type I, followed by fibronectin (the primary adhesive protein playing a major role in healing) elastin and other adhesive proteins. There are also ground substances (glycosaminoglycans) such as carbohydrate protein complexes, hyaluronic acid and chondroitin sulphate. Fibroblasts, macrophages, platelets and stem cells also dwell inside the dermis (Silver, 1994).

1.1.3. Biomechanical Properties of Skin

Collagen and elastin fibers composition in the skin largely determine its mechanical properties. Mechanical strength of skin is due to the mixture of collagen fibers (type I and III) cross-linked as continuous networks inside dermis. This mixture prevents also premature mechanical failure. Strainability of skin is related to elastin with its outstanding elastic property. If skin surface is observed closely it looks creased and an internal tension makes the skin taut. This tension increases to a high extent on the joints (Silver, 1994; Meyers et al., 2008).

Proteoglycans present near the collagen fibrils also affect the mechanical properties of skin, on the other hand the contribution of epidermis to these properties are very

little except in areas of the body where it is thick, such as the palms of the hands and soles of the feet (Silver, 1994; Meyers et al., 2008).

Tensile tests of skin results in a typical increasing slope with increasing strain stress-strain curve (Figure 1.2). Initially the stress does not increase a lot indicating a low modulus region. In this region, undulations in the skin are removed first and collagen fibers are aligned along the tensile load directions. A linear stress-strain relationship prevails throughout the linear region after which the the full load is exerted on collagen fibers. Eventually, skin fails, but skin is known to operate in the first and second regions physiologically (Silver, 1994; Meyers et al., 2008).

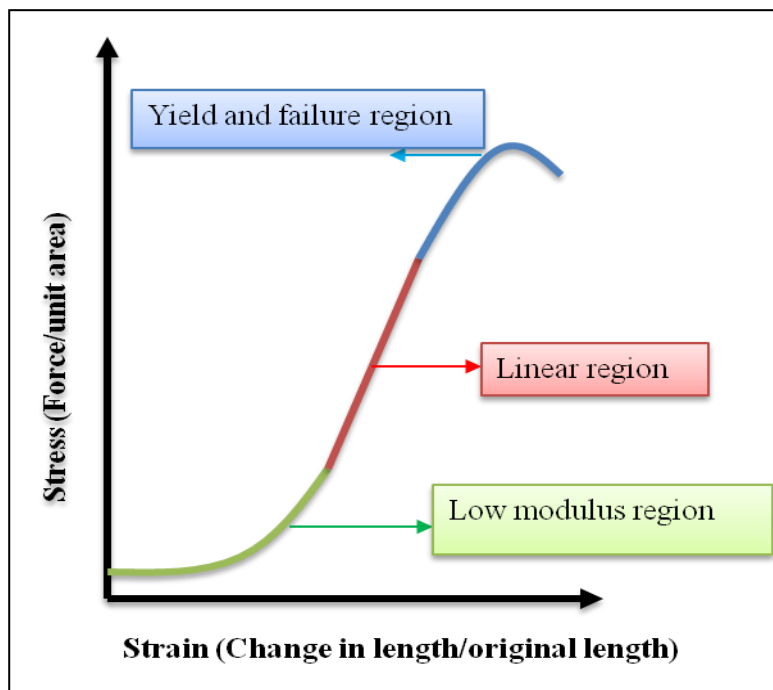


Figure 1.2. A typical stress-strain curve for wet skin (adapted from Silver, 1994).

1.1.4. Skin Wounds

The causes of skin tissue loss could be enumerated such as genetic disorders, acute trauma, and chronic wounds due to diseases or surgical incisions. Thermal trauma is one of the most encountered causes of major skin loss. Large areas of skin are destroyed making it unlikely to regenerate the skin. Severe wounding cases originating from rapid, extensive, deep burns and scalds sometimes cannot be treated with common techniques successfully, and can result in death. Wounds can be classified as epidermal, superficial, partial-thickness, deep partial-thickness and fullthickness according to the thickness of the injury. Different treatment methods are used with respect to the severity of injury (Papini 2004).

For epidermal injuries, only the epidermis is affected. Examples for this type of injury are sunburns, light scalds or grazing, for which erythema and minor pain are the implications. Since that only the epidermis part of skin is wounded, no specific surgical treatment is necessary and no scar tissue is formed as skin regenerates rapidly and extracellular matrix (ECM) deposition does not occur to contribute towards this scar tissue formation (Schevchenko et al., 2010).

Thermal trauma generally cause to superficial partial-thickness wounds which affect the whole epidermis and superficial parts of the dermis. The main indications in these cases are epidermal blistering and severe pain. Epithelialization degree of wound repair starts from the edges of wound, where abundant number of basal membrane epidermal cells is present. These cells differentiate into keratinocytes and start proliferating and covering the defect site. The sources of these migratory epithelial or stem cells are the undisrupted wound edges, hair follicles or sweat gland remnants available in deeper portion of dermis (Papini, 2004; Miller et al., 1998 Blanpain et al., 2004; Tumber et al., 2004; Tumber, 2006).

Larger dermal damage is seen in the case of deep partial-thickness injuries. As compared with superficial partial-thickness wounds scarring is more substantial due

to the high fibroplasias. The number of remaining skin appendages is so less that the duration of healing increases (Schevchenko et al., 2010).

The most severe cases of injuries are full-thickness type. Epithelial-regenerative elements are destroyed completely. The wound healing process commences with contraction followed by epithelialisation from only the edge of the wound. Cosmetic and functional defects are faced frequently. For full-thickness skin wounds which are more than 1 cm in diameter re-epithelialization does not occur on its own without skin grafting, resulting in extensive scarring, limitations in joint mobility and severe cosmetic deformities (Papini, 2004).

1.1.5. Repair Mechanism of Skin Wound

Repair of skin is initiated by bacteriological or viral infection (inflammatory response), chemical burns (degradation of extracellular matrix), electrical burns (tissue necrosis), mechanical trauma (vascular leakage and tissue swelling) and other traumatic stimuli. Before the epidermal repair, dermal repair involving inflammation, immunity, blood clotting, platelet aggregation, fibrinolysis and activation of complement and kinin systems takes place. Blood clotting and platelet aggregation prevents excess bleeding, and plugs leaks in vessel walls, complement is involved in lysis of foreign cells and vasodilation of vessels, fibrinolysis removes blood clots, immunity destroys foreign bacteria, inflammation cleans up dead tissue, kinin is involved in vasodilation (Silver, 1994). Briefly, tissue repair consists of inflammation, proliferation, granulation and remodeling phases.

Blood clotting and platelet aggregation systems are activated as a consequence of damage on the blood vessels of skin and an insoluble fibrin network is formed finally. At first a complex of hyaluronic acid bounded to fibrin is synthesized, and then fibronectin is cross-linked to fibrin in the wound. These complexes are thought to play a role in the granulation and remodeling phases of wound healing and in the attraction, migration and adhesion of inflammatory cells such as polymorphonuclear

leukocytes, respectively. These inflammatory cells secrete factors that have an effect on the migration and proliferation of cells that synthesize extracellular matrix and the recruitment of additional inflammatory cells to the wound. In the first phase of wound healing, inflammation, the dead tissue is removed by these cells also (Silver, 1994; Li et al., 2007; Kondo, 2007).

After the inflammatory phase of wound healing, migratory cells (fibroblasts) starts proliferating, followed by the formation of new blood vessels and the components of extracellular matrix. Fibroblasts attracted by fragments of collagen as well as fibronectin in the blood clot synthesize types I, III and V collagens and proteoglycans. The main elements of granulation tissue are thin randomly organized collagen fibrils (Silver, 1994; Li et al., 2007; Kondo, 2007).

Granulating phase of dermal wound healing is followed by the remodeling of granulation tissue. Thin random collagen fibrils are replaced with oriented large diameter collagen fibrils. There are two possible paths for the removal of collagen fibrils. Collagen fibrils could either be phagocytosized by inflammatory cells, or could be degraded with collagenases synthesized by fibroblasts (Silver, 1994; Li et al., 2007; Kondo, 2007).

As a subsequence of dermal repair, epidermal cells start migrating probably by factors such as fibronectin, epidermal growth factor and interleukin-1 (Silver, 1994; Li et al., 2007; Kondo, 2007).

1.2. Skin Substitutes

1.2.1. The Need for Tissue-engineered Skin Substitutes

Wound treatment can be problematic in several different clinical situations. In one extreme example, massive burn injuries can require replacement of skin covering nearly the entire body surface area. The preferred treatment for coverage of excised

burn wounds is autografting with split-thickness skin (either meshed or unmeshed), yet the availability of donor sites for autograft is limited in patients with very large burns. Therefore, available donor sites are harvested repeatedly in these patients to cover the wound, but this repeated procedure causes to pain and scarring at the donor site and increase the duration of hospital stays (Supp and Boyce, 2005).

Chronic wounds (pressure ulcers and leg ulcers) represent a different kind of challenge for wound healing. A large surface area is not involved in such wounds, but they have more incidence in the general population and so medical and economic impacts are very high. Treatment methods for the chronic wounds include the use of topical agents and occlusive dressings, and grafting of split- or full-thickness skin (Supp and Boyce, 2005).

Congenital skin conditions and diseases (e.g. giant congenital nevi and epidermolysis bullosa) affect a relatively small fraction of the population, but represent significant challenges for wound coverage. Wounds occurring as a result of congenital skin problems are not easy to avoid and tend to heal slowly or progress to chronic wounds. Autografting is not a viable treatment option in these kinds of diseases, because these wounds originate from genetic mutations in proteins of the patient's own skin. Treatment methods are protection from damage and topical therapy, including sterile dressings, antibiotics, and analgesics (Supp and Boyce, 2005; Uitto and Pulkkinen, 2001; Falabella et al., 1999).

As an alternative, safe and effective medical treatment method to above situations, skin substitutes have been developed. Because of the great importance and demand for skin-replacement products, there is a long history of material development, and many research groups worldwide have focused on creating biomaterials for skin substitution. Skin substitute biomaterials are commonly termed as bioengineered skin equivalents, tissue-engineered skin, tissue-engineered skin constructs, biological skin substitutes, bioengineered skin substitutes, skin substitute bioconstructs, living skin replacements and, more recently, as bioengineered alternative tissue (Kim et al. 2006).

1.2.2. Ideal Properties of Skin Substitutes

The ideal skin substitute should have the following characteristics (Sheridan and Tompkins 1999; Ramos-E-Silva and Castro, 2002; Ehrenreich and Ruszczak. 2006):

- ✓ Long shelf life, minimal storage requirements.
- ✓ Appropriate wound drainage (wound dependent).
- ✓ Biocompatibility (tissue compatible, absence of local or systemic toxicity and antigenicity, minimal inflammatory or foreign body response).
- ✓ Facilitation of angiogenesis.
- ✓ Ability to be handled and applied using standard surgical techniques.
- ✓ Minimal pain induction.
- ✓ Impermeability to exogenous microorganisms (barrier layer required).
- ✓ Appropriate mechanical properties (durable, flexible, resistant to linear or shear stresses, good tensile strength to resist fragmentation, elastic to permit motion of underlying tissue).
- ✓ Conformity to surface irregularities, rapid and sustained adherence to wound surface.
- ✓ Controlled water vapor transmission rate (the pooling of exudates and wound desiccation should be avoided to maintain a humid wound environment).
- ✓ Inhibition of bacteria growth.
- ✓ Minimum patient discomfort and nursing care of wound.
- ✓ Low cost.
- ✓ Easy availability.
- ✓ Reduced healing time.
- ✓ Controlled degradation.

1.2.3. Classification of Skin Substitutes

Many different classifications have been made so far for the currently available skin-substitute products (Shevchenko et al., 2010). The classifications were based on different criteria (Table 1.1).

Table 1.1. The classification of skin substitutes

Some of the currently marketed and clinically used skin substitutes were given in Tables 1.2-1.4. These example skin substitutes were organized according to anatomical structure classification.

1.2.3.1. Epidermal Skin Substitutes

There are abundant types of epidermal skin substitutes available in the market (Table 1.2). One of the oldest products (EpicelTM, commercially available in 1988) is based on culturing autologous keratinocytes on a feeder layer of lethally irradiated 3T3 mouse fibroblasts. This technique was not only used in extensive burn wounds (over 95% body surface area) and proved to be life saving, but also found to be beneficial for acute and chronic wounds. The cultured epidermal autograft is used permanently owing to the elimination of rejection problem. Due to the time required for their preparation and the need for biopsy, allogeneic keratinocyte (neonatal foreskin) sheets are preferred to accelerate the preparation. In spite of being a temporary wound covering, it promotes permanent re-epithelialization by host keratinocytes. Since extremely delicate sheets yield poor cosmetic results and blistering of the epidermis, a product (VivoDerm) was produced by seeding hyaluronic acid membrane having laser-drilled microperforations with autologous keratinocytes (Ramos-E-Silva and Castro, 2002; Jones et al., 2002).

1.2.3.2. Dermal Skin Substitutes

In one of the dermal substitutes (TransCyteTM), neonatal (allogeneic) fibroblasts cultured on nylon fibers were used after embedding into a silicone layer for 4 to 6 weeks. These cells form a dense cellular matrix containing high levels of secreted human matrix proteins with several growth factors. The fibroblasts become nonviable after freezing. It is used as a temporary covering for excised deep partial- and full-thickness burns before autografting. Another skin substitute was designed to constitute the epidermal and dermal layers of normal skin composing of skin extracellular materials, collagen and chondroitin-6-sulfate as the dermal substitute and a disposable silicone sheet as the artificial epidermis without any cells (IntegraTM). The porous matrix structure can be controlled by freeze drying process and the vascularized structure formed is suitable for cell ingrowth. It is applied

before grafting of deep partial- or full-thickness burns and silicone epidermis layer is removed when donor sites are available for autografting. Porcine collagen chemically cross-linked with an aldehyde is used as a temporary skin substitute (E-Z-Derm™). It acts as an acellular dermal matrix. Biobrane™ consists of an outer silicone membrane with a nylon fabric partially imbedded into the layer. Porcine collagen is incorporated into the silicone and nylon components of the film by chemical cross-linking. It is used as temporary adherent wound covering for partial-thickness excised burns and donor sites. De-epidermized acellular graft obtained from porcine source (Xenoderm™) or human cadaver (Alloderm™) is also commercially available. Another skin substitute application of porcine source (Oasis™) consists of small intestinal submucosa. The matrix contains collagen type I, II, V and growth factors. Detailed information about these dermal skin substitutes was given in Table 1.3 (Balasubramani et al., 2001; Ramos-E-Silva and Castro, 2002; Boyce S.T., 2001; Shakespeare, 2005).

1.2.3.3. Dermo-epidermal (Composite) Skin Substitutes

The success rate of epidermal grafting depends on the attachment of the keratinocytes to the wound bed, more specifically to basement membrane. However, in full thickness burns where epidermal and dermal layers are annihilated, complete replacement of dermis is necessary to create an attachment site for the subsequent autologous/allogeneic keratinocyte grafting. Also, replacement of the dermis layer is very crucial to prevent excessive formation of granulation tissue which gives rise to scar. Therefore, several skin substitutes consisting of dermal and epidermal layers were produced. Human neonatal fibroblasts (allogeneic) attach, multiply and begin secreting collagens and growth factors when cultured on a bioabsorbable net with circulating nutrients. A solid tissue consisting of collagen proteins and cells is formed (Dermagraft™). The net degrades after 3-4 weeks and the fibroblast collagen matrix is used alone or with possible epidermal cultures. It is used for the treatment of full-thickness chronic diabetic foot ulcers. Apligraf™ consists of both dermal and

epidermal layers. The dermal equivalent matrix made up of type I bovine collagen with human dermal fibroblast (allogeneic), and the overlying epidermal layer cultured with human keratinocytes resembles human skin histologically and produces a great number of cytokines and growth factors. It is used for the treatment of chronic foot ulcers and venous leg ulcers and burn wounds. A composite skin equivalent (OrCel™) consisting of a cross-linked bovine collagen sponge and a nonporous collagen gel is seeded with fibroblasts (allogeneic) on the porous side and with keratinocytes (allogeneic) on the other side. Culturing continues for 10 to 15 days. It is used for the treatment of split-thickness donor sites in patients with burn and surgical wounds. Detailed information about these dermal skin substitutes was given in Table 1.4 (Supp and Boyce, 2005; Ramos-E-Silva and Castro, 2002; Balasubramani et al., 2001; Kearney, 2001; Boyce, 2001).

Table 1.2. Commercial epidermal skin substitutes (adapted from Schevchenko et al., 2010).

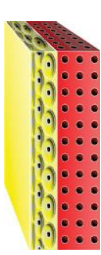
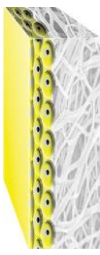
Brand Name	Schematic Representation	Incorporated Human Cells	Scaffold Material	Duration of the Cover
Epicel		Cultured keratinocytes (autogeneic confluent cell sheet)	-	Permanent
EpiDex		Cultured keratinocytes from outer root sheath of scalp hair follicles (autogeneic confluent cell sheet)	-	Permanent
EPIBASE		Cultured keratinocytes (autogeneic confluent cell sheet)	-	Permanent
MySkin		Cultured keratinocytes (autogeneic subconfluent cell sheet)	Silicone	Permanent
Laserskin or Vivoderm		Cultured keratinocytes (autogeneic confluent cell sheet)	Hyaluronic acid	Permanent
Bioseed-S		Cultured keratinocytes (autogeneic subconfluent cell suspension)	Fibrin sealant	Permanent

Table 1.3. Commercial dermal skin substitutes (adapted from Schevchenko et al., 2010).

Brand Name	Schematic Representation	Incorporated Human Cells	Scaffold Material	Duration of the Cover
AlloDerm		-	Human acellular lyophilized dermis	Permanent
Karoderm		-	Human acellular dermis	Permanent
SureDerm		-	Human acellular lyophilized dermis	Permanent
GraftJacket		-	Human acellular pre-meshed dermis	Permanent
Matriderm		-	Bovine non-cross-linked lyophilized dermis, coated with α -elastin hydrolysate	Permanent

Table 1.3. Continued.

Brand Name	Schematic Representation	Incorporated Human Cells	Scaffold Material	Duration of the Cover
OASIS Wound Matrix		-	Porcine acellular lyophilized small intestine submucosa	Permanent
EZ Derm		-	Porcine aldehyde cross-linked reconstituted dermal collagen	Temporary
Integra Dermal Regeneration Template		-	Polysiloxane, bovine cross-linked tendon collagen, glycosaminoglycan	Semi-permanent
Terudermis		-	Silicone, bovine lyophilized crosslinked collagen sponge made of heat-denatured	Semi-permanent
Pelnac Standard/Pelnac Fortified		-	Silicone/silicone fortified with silicone gauze TREX, atelocollagen derived from pig tendon	Semi-permanent
Biobrane/Biobrane-L		-	Silicon film, nylon fabric, porcine collagen	Temporary

Table 1.3. Continued.

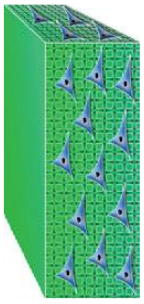
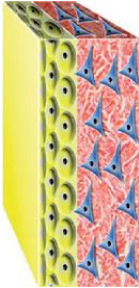
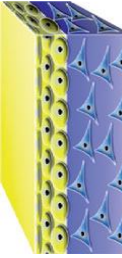
Brand Name	Schematic Representation	Incorporated Human Cells	Scaffold Material	Duration of the Cover
Dermagraft		Cultured neonatal fibroblasts (allogeneic)	polyglycolic acid, polylactic acid, extracellular matrix derived from fibroblasts	Temporary
Hyalomatrix PA		-	hyaluronic acid, silicone	Semi-permanent
Hyalograft 3D		Cultured fibroblasts (autogeneic)	hyaluronic acid membrane	Permanent

Table 1.4. Commercial dermo-epidermal skin substitutes (adapted from Schevchenko et al., 2010).

Brand Name	Schematic Representation	Incorporated Human Cells	Scaffold Material	Duration of the Cover
Allograft (cadaveric) from not for profit skin banks		Native (allogeneic)	Native human skin with dermal and epidermal cells	Temporary
Karoskin Karocell Tissue Engineering AB, Karolinska University Hospital, Stockholm, Sweden		Native (allogeneic)	Native human cadaver skin with dermal and epidermal cells	Temporary
Apligraf Organogenesis Inc., Canton, Massachusetts, CA, USA		Cultured keratinocytes and fibroblasts (allogeneic)	Bovine collagen	Temporary
OrCel Ortec International, Inc., New York, NY, USA		Cultured keratinocytes and fibroblasts (allogeneic)	Bovine collagen sponge	Temporary
PolyActive HC Implants BV, Leiden, The Netherlands		Cultured keratinocytes and fibroblasts (autogeneic)	Polyethylene oxide/polybutylene terephthalate	Temporary

1.2.3.4. Potential Skin Substitutes

Besides the above commercial skin substitutes, the majority of which are based on collagen, a wide variety of different material formulations are currently being investigated as potential skin substitutes as well (Tables 1.5 and 1.6). Most of these investigations are still in the process of physicochemical, in vitro and in vivo characterization. However, some have already passed to stage II–III clinical trials and might probably be on the market for patients and health practitioners soon.

Table 1.5. The potential collagen based skin substitutes.

Skin Substitute Type	References
Collagen/chitosan/polyvinyl alcohol	Lin et al., 2013
Human hair keratin-collagen sponge	Chen et al., 2006
Polycaprolactone (PCL) collagen nanofibrous membrane	Venugopal et al., 2006
Tegaderm/nanofibre construct	Chong et al., 2007
Porcine collagen paste	Shevchenko et al., 2008
Bovine collagen cross-linked with microbial transglutaminase	Garcia et al., 2008
Collagen/glycosaminoglycan/chitosan dermal matrix seeded with fibroblasts	Kellouche et al., 2007
Keratinocytes and fibroblasts grown on Collatamp	Johnen et al., 2008

Table 1.6. The potential skin substitute made of other promising synthetic or biological polymers.

Skin Substitute Type	References
Hyaluronan coupled with fibronectin functional domains	Ghosh et al., 2006
Polycaprolactone (scaffolds incorporated with ZnO nanoparticles)	Augustine et al., 2014
Cellulose acetate/gelatin membranes	Vatankhah et al., 2014
Gelatin and polycaprolactone	Duan et al., 2013
Polyvinyl alcohol/chitosan/fibroin blended sponge	Yeo et al., 2000
Bacterial cellulose	Helenius et al., 2006
ICX-SKN skin graft replacement	Boyd et al., 2007
Composite nano titanium oxide/chitosan artificial skin	Peng et al., 2008
Deacetylated chitin or plant cellulose transfer membranes	Johnen et al., 2008

1.3. General Properties of Materials Used in the Study

There are many natural and synthetic materials used in skin tissue engineering applications. Most common examples of natural polymers are collagen, chitosan, fibrin, elastin, gelatin, and hyaluronic acid while the examples of synthetic materials are polyurethane, polyglycolic acid, polylactic acid, poly (l-lactide), and polycaprolactone. The natural materials are superior to the synthetic ones in that they are biodegradable, biocompatible and have proven to be successful in wound healing. However, synthetic polymers could be preferred due to problems occurring with natural polymers such as low mechanical strength, shrinkage/contraction, difficulty in handling, and risks of immunological rejection (Zhong et al., 2010).

1.3.1. Gold

1.3.1.1. Synthesis of Gold nanoparticles

Gold nanoparticles (AuNPs) can be prepared via various synthesis routes including chemical, sonochemical, or photochemical path ways (Daniel and Astruc, 2004). The most common chemical route is redox reaction of the gold nanoparticles in aqueous solution from a dissolved gold precursor. For instance; gold salt could be used to synthesize AuNPs together with a reducing agent such as sodium citrate, ascorbic acid, sodium borohydride, or block copolymers. These reducing agents (e.g., sodium citrate) could also act as capping/stabilizing agent that prevents agglomeration or further growth of the particles. In some of the cases a further stabilizing agent might be required.

AuNPs have been prepared in different organic or aqueous solvents (Volkert et al., 2011; Oh et al., 2010; Martin et al., 2010; Brust et al., 1994; Templeton et al., 1998; Waters et al., 2003). Among these synthesis methods, the citrate reduction method could be said to be the best candidate since it is an inexpensive reducing agent and non-toxic water solvent (Turkevich et al., 1953; Frens, 1973; Ji et al., 2007; Biggs et al., 1993). These AuNPs are biocompatible and easily handled in applications (Nguyen et al., 2010). Therefore, citrate reduction method is commonly used in many gold nanoparticle based biological and biomedicine systems (Zhao et al. 2006; Li et al., 2010; Kim et al., 2008; Liu et al., 2005).

Turkevich et al. (1953) was the first to report the basic experimental approach and the effect of temperature and reagent concentration upon the nanoparticle size and size distribution in his work. Then, Frens (1973) published the control of size variation of gold nanoparticles by changing the concentration of sodium citrate. A sol formation mechanism and a particle growth model were later published by Chow and Zukoski (1994). In addition to these studies, the decisive role of sodium citrate on the pH value of the reaction mixture and the nanoparticle size was demonstrated in later studies (Ji et al., 2007; Yang et al., 2007; Kumar et al., 2007).

1.3.1.2. Medical Applications of Gold

AuNPs have been used in clinical cases as therapeutic agent for a long time and have attracted increased attention in biological application areas due to their unique properties. Especially the studies of gold nanoparticles on biomedical application areas such as drug and gene delivery systems have been very encouraging because they have nontoxic, bio-inertness and easily producible nature (Pissuvan et al., 2011). The study of Shukla et al. (2005) underlined the potential of gold nanoparticles in application areas of nanoimmunology, nanomedicine, and nanobiotechnology because their results suggested that gold nanoparticles were noncytotoxic, nonimmunogenic, and biocompatible.

1.3.1.2.1. The Major Therapeutic/Clinical Uses of Gold Nanoparticles

The therapeutic use of gold can be traced back to the Chinese medical history in 2500 BC (Mahdihassan, 1985). Gold also has been used as nervine, a substance that could revitalize people suffering from nervous conditions, long before in history in the western world. In the 16th century gold was recommended for the treatment of epilepsy and in the beginning of the 19th century it was used in the treatment of syphilis. No sooner than that Robert Koch discovered the bacteriostatic effect of gold cyanide towards the tubercle bacillus, gold based therapy was applied for the treatment of tuberculosis in 1920s (Shaw, 1999). Rheumatic diseases including psoriasis, juvenile arthritis, planindromic rheumatism and discoid lupus erythematosus are also treated gold compounds (Felson et al., 1990).

1.3.1.2.2 Application of Gold Nanoparticles in Tissue Engineering

AuNPs are used in many biological application areas such as contrast agents (Miladi et al., 2014), radiotherapy agents (Yang et al., 2014), biomarkers (Nunes Pauli et al.,

2014; Haller et al., 2015) and biosensors (Gong et al., 2015). Their unique properties such as enhanced mechanical stability and resistance against enzymatic degradation (Grant et al., 2014; Deeken et al., 2011), easy incorporation of antibodies (Obaid et al., 2015), growth factors (Paviolo et al., 2014), cell adhesion molecules and peptides (Gopalakrishnan et al., 2015) by their immobilization at the gold surface, enhanced biocompatibility (Cui et al., 2014; Hung et al., 2014), possible antioxidant (Balasubramani et al., 2014; Sanna et al., 2014) and antimicrobial behavior (Regiel-Futyra et al., 2015; Ehmann et al., 2015; Li et al., 2014) makes them promising candidates in tissue engineering applications such as vascular (Hung et al., 2014), cardiac (Schevach et al., 2014; Ravichandran et al., 2014) bone (Ko et al., 2015), skin (Labala et al.; 2015; Silveira et al., 2014; Cozad et al., 2011).

It was demonstrated that keratinocyte could adhere fast to the AuNPs /chitosan film scaffold and a low concentration of AuNPs (a concentration of 5 ppm) enhanced the proliferation of keratinocytes (Lu et al., 2010). AuNPs with collagen form an efficient matrix for the growth of hydroxyapatite and the mineralized collagen can be potentially applied in bone tissue repair and regeneration (Aryal et al., 2006). In addition, gold nanoparticles have already been used in conjugation with electrospun fibers in a series of studies related to tissue engineering applications. For example; McKeon-Fisher and Freeman (2011) fabricated electrospun poly (L-lactide) and AuNPs composite scaffolds for skeletal muscle tissue engineering and suggested that lower amounts of AuNPs may be utilized to create a biodegradable, biocompatible and conductive scaffold for skeletal muscle repair. In another example; collagen/hyaluronic acid polymer blend conjugated with AuNPs were electrospun into a scaffold material for the treatment of osteoporosis disease (Fisher et al., 2012). Nanocomposite scaffold, integrating coiled electrospun fibers with gold nanoparticles were also reported for cardiac tissue engineering (Fleisher et al., 2014). The polymethylglutarimide nanofibers functionalized by the grafted AuNPs, which were labeled with cell-adhesive peptides, enhanced HeLa cell attachment and potentiated cardiomyocyte differentiation of human pluripotent stem cells (Jung et al., 2012).

1.3.1.3. Toxicity of Gold Nanoparticles

There is the problem of nanotoxicity for nanosized materials. Copper and zinc based nanomaterials appeared to be very toxic. On the other hand, titania, alumina, ceria, silver, nickel and zirconia-based nanomaterials showed low to moderate toxicity, and no toxicity was observed for tungsten carbide (Lanone et al., 2009). It was shown that cytotoxicity of AuNPs was dependent on the shape, size, dose and the type and charge of surface capping/reducing agents as well as cell type.

For instance; it was demonstrated that smaller AuNPs (1.4 nm) were cytotoxic for connective tissue fibroblasts, epithelial cells, and macrophages and melanoma cells whereas bigger AuNPs in the 15 nm size range were nontoxic even at high concentrations (Pan et al., 2007). The higher surface area to volume ratio of AuNPs might lead to more intense interactions with cellular components and the penetration of smaller sized AuNPs into intracellular locations like nucleus could be easier, thus cause to cytotoxicity (Pan et al., 2007). It was stressed in a study that keratinocyte proliferation was inhibited at doses of AuNPs (34 nm) higher than 10 ppm, on the other hand lower doses (5 ppm) was shown to enhance the cellular activity for 5 days of incubation (Lu et al., 2010). With increasing concentration of AuNPs, cell area decreased along with cell number and density of actin fibers indicating some cytotoxic effects. The observed cellular changes were both dose and time dependent (Pernodet et al., 2006).

Also, gold nanorods have been shown to be more cytotoxic than AuNPs; however, the reason for this was attributed to the coatings, such as cetyl-trimethylammonium bromide (Wang et al., 2008).

It was suggested that the cationic AuNPs were more cytotoxic than the same-size anionic ones due to the affinity of cationic particles to the negatively charged cell membrane (Goodman et al., 2004). It was also found that citrate-capped AuNPs were not cytotoxic to baby hamster kidney cells and human hepatocellular liver carcinoma cells, but cytotoxic to human carcinoma cells at certain concentrations (Patra et al.,

2007). Monkey kidney cells were transfected with polyethylenimine (PEI)-modified AuNPs. The results showed that after exposure to PEI–AuNPs complexes, cell viability was 80% and further decreased to 70% upon exposure to AuNPs with dodecyl–PEI complexes due to higher transfection observed (Thomas and Klibanov, 2003). The effect of size and different surface modifications on uptake and acute toxicity of AuNPs was studied in human leukemia cells. The sizes ranged between 4 and 18 nm with surface modifiers including biotin, CTAB, cysteine, citrate, and glucose. After three days of exposure, the largest nanoparticle with citrate and biotin surface modifiers did not appear to be toxic at concentrations up to 250 mM (Connor et al., 2005)

In another study examining four different peptide/BSA/AuNPs conjugates in three cell lines (HeLa, 3T3/NIH, and HepG2), differing effects of the nanoparticles was reported. This suggests that the nuclear delivery of the peptide/BSA/AuNPs influences cell viability due to particle interactions with cellular DNA (Tkachenko et al., 2004). In a different study, the effect of AuNPs exposure was tested in multiple cell lines again (COS- 1 cells, red blood cells, and Escherichia coli cultures). These cells were incubated with cationic (ammonium-functionalized) and anionic (carboxylate-functionalized) AuNPs at 0.38–3 mM concentrations for 24 hours. The cationic nanoparticles were found to be more cytotoxic than the anionic and similar toxicity levels were measured for these different cell types (Goodman et al., 2004). The effect of AuNPs on the proliferation of RAW264.7 macrophage cells was tested. Macrophage cells showed greater than 90% viability with no increase in pro-inflammatory cytokines (TNF- α and IL-1 β) after 48 hours of up to 100 mM AuNPs (Shukla et al., 2005).

1.3.1.4. Antibacterial Activity of Gold Nanoparticles

1.3.1.4.1. Surface Coating with Gold Nanoparticles

A wide variety of surfaces (implants, fabrics) were coated with AuNPs for treatment of wounds. Glass surfaces were also coated with AuNPs to maintain hygienic environments in hospitals and other places (Das, 2009). The inhibitory activity of AuNPs against a wide range of bacteria (*S.aureus*, *K.*, *pnemoniae*, *P aureginosa*, *E. Coli*, *L. monocytogenes*, *B. cereus*, *S. typhimurium*) was reported in different studies (Zawrah and El-Moes, 2011; Geethalakshmi and Sarada 2012). Bactericidal property of AuNPs was confirmed in a study by measuring the minimum bactericidal concentration (12-16 ppm) and minimum inhibitory concentration (4 ppm) (Cui et al., 2012).

1.3.1.4.2. Surface Coating of Antibiotics with Gold Nanoparticles

The antibacterial activity of AuNPs was enhanced (Table 1.7) when it is used in combination with antibiotics (Burygin, 2009).

Table 1.7. The antibacterial activity of AuNPs in combination with antibiotics.

Antibacterial agent	Effect	References
Vancomycin coated with AuNPs	Enhanced antimicrobial activity against vancomycin resistant enterococci	Gu et al., 2003
Aminoglycosidic antibiotics coated with AuNPs	Antibacterial effect on a range of Gram-positive and Gram-negative bacteria	Grace and Pandian, 2007; Saha, 2007
Cefaclor reduced gold nanoparticles	Potent antimicrobial activity on both Gram-positive (<i>S. aureus</i>) and Gram-negative bacteria (<i>E. coli</i>)	Rai et al., 2010

1.3.1.4.3. Photodynamic Antimicrobial Chemotherapy of Gold Nanoparticles

Au-based nanomaterials (nanospheres, nanocages, and Au nanorods) can destroy cancer cells and bacteria via photothermal heating at near infrared irradiation. Au-based nanoparticles can be combined with photosensitizers for photodynamic antimicrobial chemotherapy. The examples are listed in Table 1.8.

Table 1.8. Photodynamic antimicrobial chemotherapy of AuNPs.

Antibacterial agent	Effect	References
Au nanorods conjugated with photosensitizers (such as toluidine blue O)	Kill methicillin-resistant <i>Staphylococcus aureus</i> by photodynamic antimicrobial chemotherapy and NIR photothermal radiation	Kuo, 2009; Pissuwan et al., 2009; Gil-Tomas, 2007; Perni, 2009
Light absorbing gold nanoparticles conjugated with specific antibodies	Photothermally kill <i>S. aureus</i> by using laser	Zharov, 2006
Functionalized gold nanoparticles as photothermal agents	Hyperthermally kill pathogens	Norman, 2008; Simon-Deckers, 2008; Huang, 2007

1.3.2. Honey

1.3.2.1. Types of Honey

The floral source of honey changes its composition and physicochemical properties (Chen et al., 2000). The unique name of honey comes from the geographical location where the honey is produced, or the floral source of the honey or the trees on which the hives are found (Lusby et al., 2002). Manuka honey, pasture honey, jelly bush honey and African jungle honey are among the most well-researched honey types.

1.3.2.2. The Composition of Honey

The main constituents of honey are sugars (mostly monosaccharides and oligosaccharides) and water. The most abundant sugar in honey is fructose (White and Doner, 1980; Bogdanov et al., 2008; Ajibola et al., 2007). There are lots of vitamins; especially vitamin B complex, vitamin C and ascorbic acid, pantothenic acid, niacin and riboflavin and minerals; calcium, copper, iron, magnesium, manganese, phosphorus, potassium and zinc in honey (Ajibola et al., 2012). Honey contains at least 181 constituents (Bogdanov et al., 2008; Gheldof et al., 2002). The other constituents are amino acids, antibiotic-rich inhibine, proteins and phenol antioxidants (Wang and Li, 2011). Bioactive substances in honey are phenolic constituents, flavonoids, organic acids, carotenoid-derived compounds, nitric oxide metabolites, amino acids and proteins (Arriaga et al., 2011; Beretta et al., 2010). Also, some varieties of honey contain kynurenic acid (a tryptophan metabolite with neurological activity) which may contribute to its antimicrobial properties (Beretta et al., 2007). Enzymes prevailing inside honey are glucose oxidase, diastase, invertase, phosphatase, catalase and peroxidase (Crane, 1975).

1.3.2.3. Medical Applications of Honey

1.3.2.3.1. Wound Healing Effect

The medical properties of honey such as its antimicrobial property and wound-healing activities have been known since ancient times. Its use as a drug and an ointment was first mentioned in a Sumerian tablet writing dating back to 2100-2000 BC. Aristotle (384-322 BC) mentioned pale honey as being “good for wounds” (Mandal and Mandal, 2011). Honey does not only maintain a moist wound condition and provide a protective barrier to prevent infection due to its high viscosity, but it also has antibacterial activity and immune-modulatory property. These effects contribute to the healing property of honey (Bilsel et al., 2002).

Honey has been applied for accelerating wound healing since ancient times. The positive effect of honey in wound healing process has been shown repeatedly (Molan, 1998; Molan, 1999). Treating ulcers, bed sores and other skin infections resulting from burns and wounds with honey has gained acceptance (Molan, 1999; Blassa et al., 2006). The effectiveness of honey as dressing of wounds, burns, skin ulcers and inflammations were reported; the growth of new tissue is accelerated with the anti-bacterial properties of honey, thereby assisting the wound healing (Medhi et al., 2008). The medihoney and manuka honey have been shown to have *in vivo* activity and are suitable for the treatment of ulcers, infected wounds and burns (Prakash et al., 2008; Aljadi and Kamaruddin, 2004).

1.3.2.3.2. Antimicrobial Property of Honey

Honey has antimicrobial effects, which are attributed to the osmotic effect of the sugars, the low pH (3.2-4.5), and particularly to its peroxidase activity (H_2O_2). The antimicrobial effects are also due to the presence of non peroxidase substances such as phenolic acids, flavonoids, and lysozymes (Tan et al., 2009; Al-Jabri et al., 2005; Ghazali, 2009; Nasir et al., 2010)

Natural, unheated honey have been reported by many researchers to have a broad-spectrum antibacterial activity when tested against pathogenic bacteria, oral bacteria, as well as food spoilage bacteria (Kwakman et al., 2010). The *Leptospermum scoparium* honey, one of the best known with standardized levels of anti-bacterial activity, has been reported to have an inhibitory effect on around 60 species of bacteria, including aerobes and anaerobes, gram-positives and gram-negatives (Mundo et al., 2004).

1.3.2.3.3. Anti-oxidant Property of Honey

Chronic or degenerative diseases are more susceptible to oxidative stress. Honey has antioxidant activities that can suppress oxidative stress (Mohamed et al., 2010). The antioxidants in honey are flavonoids, phenolic acids, amino acids, proteins, and some enzymes (Kishore et al., 2011; Khalil et al., 2011).

1.3.3. Collagen

1.3.3.1. Sources and Refinement

There are various sources of collagen on earth. Bovine skin and tendons, porcine skin and rat tail are the common sources of collagen for tissue engineering applications. Collagen extracted from marine sponges (Exposito et al., 2002; Exposito et al., 1999), fish (Sugiura et al. 2009), and jellyfish (Song et al., 2006) are widely used in the industry, but it is not the preferred option for research and clinical usage. Collagen properties changes from one animal to another, and that is why all these collagen types merit investigation (Lin and Liu, 2006). Apart from these collagens recombinant human collagen, which is potentially less immunogenic than animal sources and identical in composition to collagen is produced by Fibrogen® has been proposed as the future of collagen scaffolds (Yang et al., 2004). Decellularized ECM (mostly composed of collagen) serves as as a scaffolding material for tissue regeneration in biomedical applications. Acellular ECM is typically produced from human or porcine dermis or from swine intestine or bladder submucosa (Badylac, 2004).

1.3.3.2. Molecular Structure

The primary structure of collagens can be represented by the motif of Glycine-Proline-Hydroxyproline-Glycine-X-Y where X and Y can be any amino acids. This sequence forms an alpha chain and every collagen molecule contains a triple α -helix, which is the molecular basis of tropocollagen, precursor of collagen. According to the type of tissues the individual α -chains differ. For instance, type I collagen consists of three coiled subunits composed of two α -1 (I) chains and one α -2 (I) chain. Each α chain winds around each other to form a right-handed triple helix. The three chains are held together strongly by H bonds between glycine residues and between the hydroxyl (-OH) groups of hydroxyprolines. In addition, there are cross-linkages via lysine among α helixes. Hence, the amino acid composition of a collagen species also affects cross-linking and thereby mechanical properties. Lysine and hydroxylysine are necessary for natural intra- and inter-molecular cross-linking of collagen (Angele et al., 2004). Therefore, the more lysine and hydroxylysine are present in a collagen molecule, the more it will be resistant to enzymatic and thermal degradation.

Hydroxyproline is present in minute amounts in other proteins so, it is considered as unique to collagen. For this reason assays of hydroxyproline are frequently used to determine the collagen content in a given tissue. Propeptide regions, which are thought to play a role in the initial assembly of the triple helix, are present at the ends of procollagen molecules (Figure 1.3.A). After secretion from cells, the propeptides are enzymatically cleaved from the procollagen molecules to form collagen molecules with diameter of 1.5 nm, and length about 300 nm (Figure 1.3.B). Collagen molecules undergo a self assembly process to form collagen fibrils (10-300 nm in diameter). This assembly results in staggered array of collagen molecules, in which overlapping rows of collagen molecules are staggered with respect to one another by a distance of 64 to 67 nm forming a banded structure (Figure 1.3.C) (Dee et al, 2002; Park and Bronzino, 2003; Meyers et al., 2008).

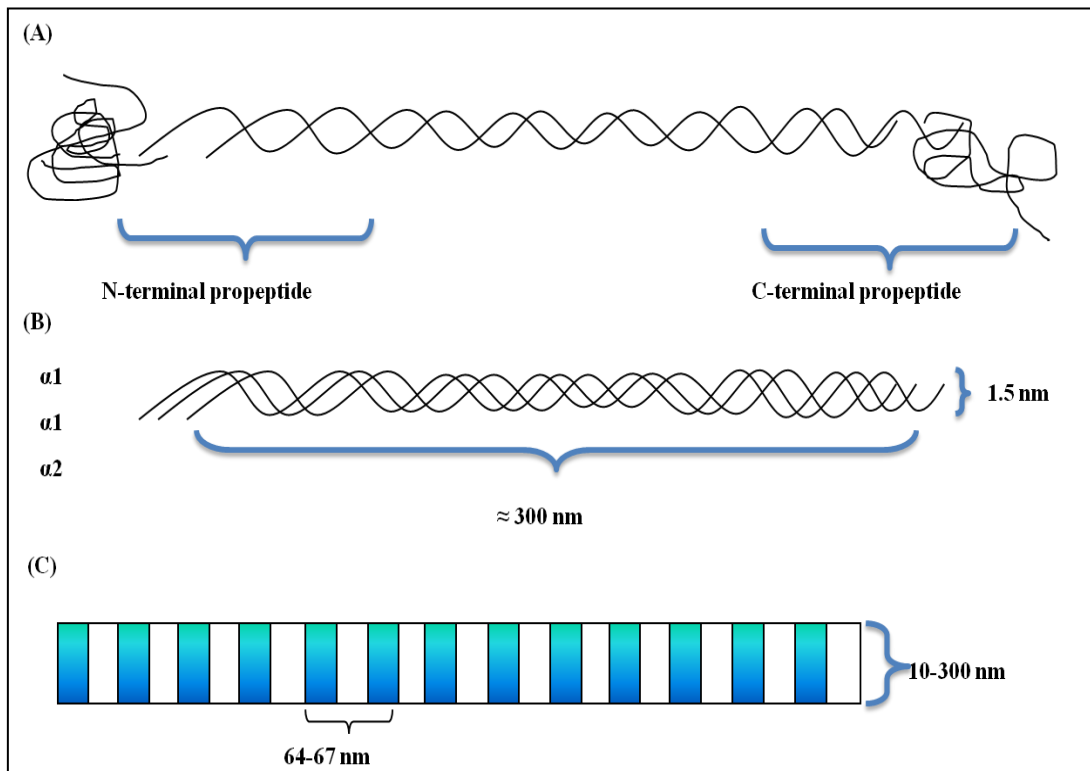


Figure 1.3. Collagen Structure: (A) Procollagen molecule, (B) collagen molecule. (C) banded structure of collagen fibrils (Adapted from Dee et al., 2002)

1.3.3.3. Types and Distributions

There are approximately twenty-five different α chain conformation, each produced by their unique gene. So, 29 types of collagen have been identified. The most common are briefly described in Table 1.9. Only a few types of collagen (mainly type I collagen) are used to produce collagen based biomaterials in the field of tissue-engineering. Type I collagen is distributed in most tissues and comprises the largest proportion of the total collagen within the human body (Fung, 1993). Type I collagen is found mainly in bone, tendons, ligaments, and skin (Guelcher and Hollinger, 2006).

Table 1.9. Collagen types and tissue distribution (adapted from Albert et al., 2002).

	Type	Molecular formula	Tissue distribution
Fibril-Forming (fibrillar)	I	$[\alpha 1(\text{I})]_2\alpha 2(\text{I})$	bone, skin, tendons, ligaments, cornea (represent 90% of total collagen of the human body)
	II	$[\alpha 1(\text{II})]_3$	cartilage, intervertebrate disc, notochord, vitreous humor in the eye
	III	$[\alpha 1(\text{III})]_3$	skin, blood vessels
Fibril associated	IX	$\alpha 1(\text{IX})\alpha 2(\text{IX})\alpha 3(\text{IX})$	Cartilage
	XII	$[\alpha 1(\text{XII})]_3$	tendons, ligaments
Network forming	IV	$[\alpha 1(\text{IV})]_2\alpha 2(\text{IV})$	basal lamina
	VII	$[\alpha 1(\text{VII})]_3$	beneath stratified squamous epithelia

1.3.3.4. Mechanical Properties and Stability of Collagen

Different characteristics of the collagen in the aspect of chemical and mechanical properties could be obtained since there are over 29 types of collagen. Yet, some of the fundamental mechanical properties (and structure-property relationships) of collagen needs to be fully explored. Collagen being the basic structural component in our body plays the same role as steel does in structures (Guelcher and Hollinger, 2006).

In general, temperature and pH are known to affect stability of collagen, although its material behavior is relatively unaffected over the range of temperature from 0 to 37 °C. However, triple-helix structure of collagen could easily be denatured upon exposing to temperatures above 37 °C or to a low pH solvent causes (Guelcher and Hollinger, 2006).

The tensile modulus (obtained from the linear portion of the stress-strain curve) for collagen fibers has a reported range between 350 and 1000 MPa (Fung, 1993;

Gentlemen et al., 2003). The tensile strengths for collagen fibers were shown to range from 50 to 100 MPa (Fung, 1993). When compared to large diameter fibers, smaller diameter collagen fibers tend to display larger values of modulus and peak stress. It has been suggested that larger-diameter fibers are more likely to possess defects and thus break more easily. Besides that smaller fibers have a larger surface-to-volume ratio and allow greater number of cross-links per fiber unit length, which would make the fiber stiffer (Gentleman et al., 2003). The tangent modulus is a material property and therefore should be independent of the size of the specimen. However, different lengths of collagen fibers, either fabricated in the same way or dissected from the same tissue, have been shown to have significantly different moduli (Guelcher and Hollinger, 2006; Gentlemen et al., 2003).

1.3.3.5. Biological Responses to Collagen

One property of biomaterials based on natural materials like collagen is that the materials are normally known by the living system. As one consequence of this, collagenases and metalloproteinases that are produced by cells easily degrade collagen based biomaterials in tissues. The products of this degradation will be amino acids that the body copes with in the course of its normal metabolic processes (Guelcher and Hollinger, 2006).

The interaction of collagen with the surrounding environment is regulated with its quaternary structure. For example, platelet aggregation has been shown to be a property of the quaternary structure (Yannas, 1996). Collagen acts as chemo-attractant to leukocytes and fibrogenic cells (Gentlemen et al., 2003) and binds to growth factors and cytokines (Gelse et al., 2003).

The triple helix structure of collagen is present in many species. Especially, type I collagen is abundant in most organisms, and therefore a better tolerance across species and a lower immune response than other collagen types are expected (Yannas, 1996). Patients awaiting an implant were tested to determine whether they

have a pre-existing allergy to collagen and it was reported that only up to 4 % of a population a pre-existing allergy to bovine collagen exists (Cukier et al., 1993; Soo et al., 1993; Cretel et al., 2001). The adverse reactions to implanted collagen in patients without pre-existing allergies were also found to be rare (< 3%) (Guelcher and Hollinger, 2006; Lynn et al., 2004).

1.3.3.6. Biomedical Applications of Collagen

Collagen could easily be processed into various forms including films, fibers, gels and sponges for skin (Chan et al., 2015) urethral (Wei et al., 2015) ocular (Zhou et al., 2014) bone (Quinlan et al., 2015) and cartilage (Zhao et al., 2014) tissue engineering applications.

Collagen-based wound dressings have been applied long before for skin wounds (Yannas et al., 1982; Doillon and Silver, 1986). Since that time new skin tissue scaffolds have been investigated with melanocytes (Regnier et al., 1997), a capillary-like network (Tremblay et al., 2005), dendritic cells (Bechetoille et al., 2007), sensory innervation (Blais et al., 2009) and adipose tissue (Trottier et al, 2008).

1.3.4. Silk Fibroin

1.3.4.1. Sources and Refinement of Silk Fibroin

The most economically important silk-producing animal is mulberry silkworms (*Bombyx mori*) since they could be kept in captivity. When the caterpillars came out from the eggs of the adult moth they start eating fresh mulberry leaves for a month. When they are mature enough for metamorphosis into a moth, they start constructing a protective cocoon of silk. Upon completion of the cocoon, it is subjected to hot water/steam and the caterpillars inside the cocoon are killed, and the silk is

harvested. The crude silk fiber is degummed (cleared of from the glue-like protein, sericin) and processed before being used (Hardy et al., 2008).

1.3.4.2. Molecular Structure of Fibroin

The diameter of fibers of domesticated *B. mori* silkworm are about 10–25 μm and composed of two proteins as a light (≈ 26 kDa) and heavy (≈ 390 kDa) chain linked by a single disulfide bond (Zhou et al., 2000). Sericin (20–310 kDa), known to be a hydrophilic protein coat the fibroin fibers (Kaplan et al., 1998; Zhou et al., 2000; Yamaguchi et al., 1989; Inoue et al., 2000). The disulfide linkages between the heavy light chain holds the fibroin together (Tanaka et al., 1999). Sericin forms about 25 to 30 % of the silk cocoon mass and its removal process is carried out during the degumming process (Vepari and Kaplan, 2007). Silk fibroin from *B. mori* is mainly composed of glycine (43%), alanine (30%) and serine (12%) (Kaplan et al., 1998).

There are a number of silk polymorphs. These are glandular state prior to crystallization (silk I), the spun silk state which consists of the β -sheet secondary structure (silk II), and an air/ water assembled interfacial silk (silk III, with a helical structure) (Kaplan et al., 1998; Jin and Kaplan, 2003; Motta et al., 2002). The silk I structure (the water-soluble state) is easily converted to a silk II structure when it is exposed to heat or physical spinning. The silk I structure is also converted to a β -sheet structure when exposed to methanol or potassium chloride (Huemmerich et al., 2006). The asymmetrical structures of β -sheets are due to occupation of hydrogen side chains from glycine and the methyl side chains from the alanines. The formation of the intersheet stacking in the crystals is resulted from the interaction of the methyl groups and hydrogen groups of opposing sheets. A thermodynamically stable structure is formed by virtue of the strong hydrogen bonds and Van der Waals forces (Kaplan et al., 1998). Between amino acids perpendicular to the axis of the chains and the fiber, inter- and intra-chain hydrogen bondings are created (Kaplan et al., 1998). Water is not included in the silk II structure is not soluble in several solvents such as mild acid and alkaline solutions, and many chaotropes.

1.3.4.3. Biological Responses to Fibroin

Hypersensitivity results of sutures made from virgin silk and sutures from de-gummed silk were found to be different (Altman et al., 2003). According to the comparison of the inflammatory response between of de-gummed silk fibroin and polystyrene and poly (2-hydroxyethyl methacrylate) less in vitro adhesion of immuno-competent cells was demonstrated (Santin et al., 1999). Inflammatory responses of silk films implanted in vivo were compared with collagen and PLA films, and lower responses were reported for the former (Meinel et al., 2005). A weak foreign body response and no fibrosis were induced in silk fibroin non-woven mats implanted subcutaneously in rats. During the six months of in vivo study, there was little lymphocytes invasion, and slight inflammatory pathway upregulation at the implantation site (Dal Pra et al., 2005).

1.3.4.3. Biomedical Applications of Fibroin

Silk fibroin was fabricated in the forms of fibers (Dal Pra et al., 2005; Unger et al., 2004; Jin et al., 2004; Min et al., 2004; Li et al., 2006; Kim et al., 2005) hydrogels (Motta et al., 2004; Fini et al., 2005), foams (Meinel et al., 2004; Kim et al., 2005; Wang et al., 2006; Aoki et al., 2003) and films (Wang et al., 2005; Jin et al., 2004; Hu et al., 2006) for different tissue engineering applications such as skin, bone and cartilage tissue engineering. Also, silk fibroin scaffolds were reported to promote cell attachment and proliferation of a variety of cells such as keratinocytes, fibroblasts (Unger et al., 2004), human fibroblasts (Petrini et al., 2003; Chiarini et al., 2003) endothelial cells (Unger et al., 2004), human mesenchymal stem cells (Jin et al., 2004), osteoblast-like cells (Motta et al., 2004) and chondrocytes (Wang et al., 2006). In vivo studies with silk fibroin also gave promising results. For example; enhancement in bone healing were observed (Kim et al., 2005; Fini et al., 2005) skin (Yeo et al., 2000; Sugihara et al., 2009).

1.3.5. Silk Sericin

1.3.5.1. Sources and Refinement of Silk Sericin

Silk derived from silkworm *Bombyx mori* is mainly composed of sericin and fibroin proteins. Sericin constituting 25–30 % of silk envelops the fibroin fibers with successive sticky layers that help in the formation of a cocoon. It is estimated that 1 million tons of cocoons (fresh weight) is produced worldwide and sericin is discarded as a waste product. Although at present, sericin is mostly discarded in silk processing wastewater, the recovery and recycling of this protein could provide a significant economic and social benefit because depletion of 50,000 tons of sericin from 400,000 tons of dry cocoon is a great loss.

Sericin is a water soluble protein. When dissolved in a polar solvent, hydrolyzed in acid or alkaline solutions, or degraded by a protease, different molecular size distributions (≤ 20 kDa or ≥ 20 kDa) of the resulting sericin molecules occur depending on factors such as temperature, pH, and the processing time.

The small sericin peptides are soluble in cold water and can be recovered at early stages of raw silk production while the larger sericin peptides are soluble in hot water and can be obtained at the latter stages of silk processing or from silk degumming processes (Zhang, 2002).

1.3.5.2. Molecular Structure

Sericin having a wide molecular weight range of about 10 to over 300 kDa is a macromolecular protein. It is made of 18 amino acids most of which have strongly polar side groups such as hydroxyl, carboxyl, and amino groups. In addition, the amino acids, serine and aspartic acid constitute approximately 33.4% and 16.7% of sericin, respectively. Serine is thought to make sericin an excellent moisturizing agent (Zhang, 2002; Kundu et al., 2008).

1.3.5.3. Biological Responses to Sericin

The silk was known to cause allergic reactions (Hollander, 1994; Zaoming et al., 1996; When et al., 1990; Kurosaki et al., 1999). The glue-like protein sericin has been implicated as the causative agent for immune responses to silk, but only when it is found in conjunction with fibroin. Sericin by itself did not elicit an immune response (Panilaitis et al., 2003). Meinel et al. (2005) showed that the inflammatory tissue reaction and foreign body response to silk films was similar or less than collagen films.

1.3.5.4. Biomedical Applications of Silk Sericin

Various biomedical application areas of sericin were reviewed by Zhang et al. (2002) and Kundu et al. (2008). Generally, it was used in the form of solutions/creams hydrogels, foams and films.

Tsubouchi (1999) developed a fibroin-mixed-sericin wound dressing that could accelerate healing and could be peeled off without disturbing the newly formed skin. Minoura et al. (1995) and Tsukada et al. (1999) investigated the attachment and growth of animal cells on films made of sericin and fibroin. Films of pure component proteins (i.e., fibroin or sericin) permitted cell attachment and growth comparable to that on collagen, a widely used substrate for mammalian cell culture. In another study made by Murase (1994), films made of sericin and fibroin were found to have excellent oxygen permeability and showed high similarity to human cornea in its functional properties. Hence, it was thought as promising to form artificial corneas. The effect of sericin on the attachment of primary cultured human fibroblasts was studied by Tsubouchi et al. (2005). It was found that the attachment of these cells was enhanced with sericin.

The studies conducted by Aramwit and Sangcakul (2007) about the wound healing effect of sericin cream in rats suggested that sericin had wound healing effects

without causing allergic reactions. The antioxidant action of sericin was shown by Kato et al. (1998). Antioxidant potential and photoprotective effect of silk protein sericin against hydrogen peroxide-induced oxidative stress in skin fibroblasts and skin keratinocytes was studied by Dash et al. (2008a and 2008b). A novel mucoadhesive polymer has been prepared by template polymerization of acrylic acid in the presence of silk sericin (Ahn et al., 2001). It was also shown by Tamada (1997) that biomaterials with anticoagulant properties could be prepared by sulfonation treatment of sericin and fibroin proteins. The anticoagulant activity of sulfated sericin was estimated to be at 1/10 to 1/20 of heparin (Tamada et al. 2004). The findings of Zhaorigetu et al. (2003) suggest that sericin has suppressing activity against both chemical and UV radiation induced skin tumorigenesis by reducing oxidative stress.

1.4. Aim of the Study

The substantial aim of this Ph. D study is to develop new biomaterials as potential skin substitutes and to provide alternative and efficient treatment methods to clinical cases (Figure 1.4). To reach this aim, the following tests and analysis were performed:

- ✓ Green synthesis of the scaffolds with little or non cytotoxic solvents (d-water or aqueous acetic acid) and chemical agents (ethanol and glycine blocked GTA).
- ✓ Development of bilayered skin substitutes composed of epidermal (collagen/sericin membranes: C/S) and dermal (collagen sponges: CS, collagen matrices: CM or silk fibroin matrices:SF) layers with different fabrication methods. Casting and solvent evaporation (film), lyophilization/freeze-drying (sponge) and dry/wet electro-spinning (fibrous matrices) methods were used to obtain the scaffolds. Epidermal and dermal layers were glued to each other with natural honey to form the bilayered structure. Bilayered skin substitutes were labelled as BLCS, BLCS-Au, BLCS-AuX, BLCM-Au, BLCM-AuX, BLSF, BLSF-Au. Sericin/collagen film (epidermal layer) may act as a membrane that

allows the controlled oxygen/carbon dioxide exchange, controls the water vapor permeation rate and avoids the bacteria penetration, while dermal part may act as a suitable substrate for cell adhesion, proliferation and migration. Therefore; bilayered design of the scaffold may enhance the properties of the scaffold as a skin substitute by mimicking the roles of natural skin's layers.

- ✓ Fabrication of 3D scaffolds (0.5 mm-2 mm) with suitable micro/nano architectures (randomly oriented nanofibrous collagen or fibrous silk fibroin sponges and porous collagen sponges) which are also water-stable.. To achieve this stability, collagen based scaffolds were x-linked with GTA (C/S-X, CS-X and CM-X) and silk fibroin based scaffolds were treated with ethanol to increase the stability in water.
- ✓ Characterization of the scaffolds with physical (water swelling, water vapour transmission rate, oxygen permeability, fiber/pore size and distribution analysis and interconnectivity with SEM and TEM, porosity calculation and mechanical properties with tensile strength, elongation at break and tensile modulus) and chemical (hydrolytic and enzymatic degradation, FTIR analysis) laboratory tests to select the best groups as skin substitute.
- ✓ Synthesis of gold nanoparticles with different sizes and concentrations to incorporate into scaffolds.
- ✓ Characterization of the nanogold for shape and size distribution with TEM
- ✓ Determination of the nontoxic sizes of gold nanoparticle and doses with in vitro cytotoxicity studies (MTT analysis)
- ✓ Development of the scaffolds with the nontoxic gold nanoparticles to observe the AuNP incorporation and distribution inside the nanofibers with TEM. Gold nanoparticles (AuNPs) were incorporated into dermal substitutes (CS-Au, CS-AuX, CM-Au, CM-AuX, SFM-AuE) to obtain an antibacterial biomaterial surface and to investigate the effect of AuNPs on cell adhesion, spreading and proliferation.
- ✓ Assessment of the in vitro biocompatibility of scaffolds incorporated with gold nanoparticles (cell viability assay according to ISO 10993-5).

- ✓ Confirmation of the antibacterial effect of gold nanoparticles (agar disc diffusion method) in the selected size and dose with *S. Aureus* and to confirm the bacterial growth inhibition effect of gold nanoparticles (OD measurement and SEM imaging) on scaffolds incorporated with gold nanoparticles with *S. Epidermidis*.
- ✓ Seeding the cells (fibroblasts and keratinocytes) into scaffolds and observe the cell/biomaterial interactions (cell adhesion, spreading and proliferation).
- ✓ Investigation of the wound healing effect of final optimized scaffolds loaded with different bioactive agents (AuNPs or honey) on full-thickness wound of rats by comparing the results of the scaffolds developed in this study with a commercial skin substitute (Matriderm™).
- ✓ Toxicological evaluation of one of the best scaffold groups by skin irritation (ISO 10993-10), sensitization (ISO 10993-10) and genotoxicity (ISO 10993-3, OECD471) tests.

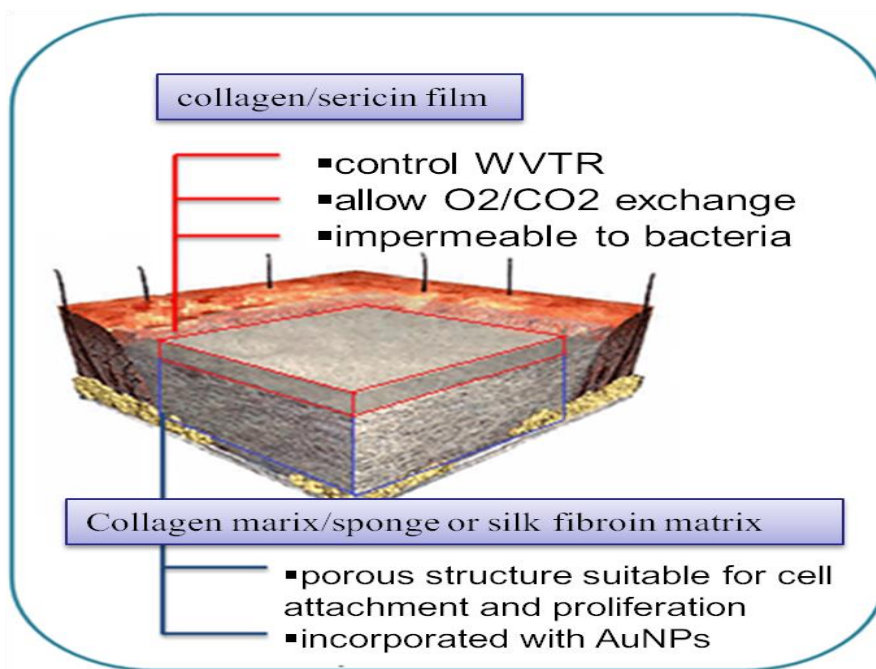


Figure 1.4. The main design characteristics of bilayered scaffolds developed in this research.

CHAPTER 2

MATERIALS AND METHODS

2.1. Materials

2.1.1. Materials and Chemicals for Scaffold Preparation

Commercial sericin was purchased from Nembri Industrie Tessili s.r.l. (CAS no: 60650-88-6; 60650-89-7, MW: ca.138 kDa) and collagen (Gelfix® lyophilized type I collagen pad) was obtained from Isse International Eurosearch (Italy). Silk cocoon of *Bombyx mori* origin was bought from Kirman İplik Ltd. Sti. (Bursa, Turkey). Collagen from bovine achilles tendon (powder), acetic acid (ReagentPlus®, ≥99%), glutaraldehyde solution (GTA, Grade I, 25% in H₂O) hexamethyldisilazane (HMDS, reagent grade, ≥99%), poly(ethylene oxide) (PEO, average M_v ~4,000,000), lithium bromide (ReagentPlus®, ≥99%), sodium carbonate (anhydrous, powder, 99.999%), dialysis tubing cellulose membrane (avg. flat width 25 mm) ethanol (CHROMASOLV®, for HPLC, ≥99.8%), methanol (CHROMASOLV®, for HPLC, ≥99.9%), *N*-(3-Dimethylaminopropyl)-*N'*-ethylcarbodiimide hydrochloride (EDC, commercial grade, powder) and *N*-Hydroxysuccinimide (NHS, 98%) were purchased from Sigma-Aldrich (Germany). Glycine (electrophoresis purity reagent) was obtained from Bio-Rad Laboratories (USA).

2.1.2. Materials and Chemicals for Gold Nanoparticles Synthesis

Hydrogen tetrachloroaurate (III) (HAuCl₄·3H₂O) was obtained from Applichem (Germany), trisodium citrate dihydrate (Na₃C₆H₅O₇·2H₂) was obtained from Sigma-

Aldrich (Germany), Millex[®] syringe filter units (disposable, Durapore[®] 0.1 μm, PVDF) was obtained from Merck Millipore (Germany).

2.1.3. Materials and Chemicals for Physicochemical Characterization Experiments

Magnesium chloride hexahydrate (99.995% trace metals basis, MgCl₂·6H₂O), LB broth (Miller, liquid microbial growth medium), collagenase from *Clostridium histolyticum* (Type I-A, lyophilized powder) were purchased from Sigma-Aldrich (Germany), formvar carbon film coated (200 mesh) copper grids for TEM was bought from Electron Microscopy Sciences (USA).

2.1.4. Materials and Chemicals for Cell Culture Studies

DMEM (1x) (D-Glucose (4.5g/l), NaHCO₃ (3.7 g/l), stable glutamine, Na-Pyruvate), penicillin/streptomycin (100x), D MEM (1x) (D-Glucose (4.5g/l), NaHCO₃ (3.7 g/l) Na-Pyruvate, w/o phenol red), fetal bovine serum (FBS) and trypsin-EDTA solution (0.25%/0.02% w/v in PBS w/o Ca⁺², Mg⁺²) were obtained from Merck Millipore (Germany). Ethylene diamine tetraacetic acid disodium salt dihydrate (EDTA, 99%), thiazolyl blue tetra-zolium bromide (MTT bromide, approx. 98 % TLC), trypan blue solution (0.4%) were purchased from Sigma-Aldrich (Germany). Prestoblue was obtained from Life Technologies, Thermo Fisher Scientific Inc., USA). Dimethyl sulfoxide (DMSO, cell culture grade, min. 99.5%) was obtained from AppliChem (Germany). Ethanol (absolute extra pure) was purchased from Merck (Germany).

2.1.5. Materials and Chemicals for In Vivo Studies

Ketamine hydrochloride (Ketalar, Parke-Davis- Eczacıbaşı, Istanbul, Turkey) povidone-iodine and surgical drapes (Ioban™ incise drape, 3M Health Care, USA) were bought from pharmacies (Turkey). Eighty healthy adult male Wistar albino rats weighing 200–250 gr and also the standard rat chow and wood shaving were obtained from Kobay D.H.L A.Ş. (Turkey).

2.2. Methods

2.2.1. Synthesis of Gold Nanoparticles

Gold ions (Au^{+3}) were reduced to neutral gold atoms by means of citrate ions acting as both reducing and capping agent. Gold nanoparticles of different sizes were synthesized using the citrate reduction method also known as Turkevich method (Kimling et al., 2006). The formation of gold nanoparticles was confirmed with the red color. Briefly, the experimental steps were as follows:

- 1) The hydrogen tetrachloroaurate ($\text{HAuCl}_4 \cdot 3\text{H}_2\text{O}$, 10 mM) stock solution was prepared
- 2) By diluting the stock with distilled water, 1 mM solution was obtained (Solution I).
- 3) From the solution I, 20 ml was taken and poured it into a Erlenmeyer flask and it was left to boil while stirring at high speeds (800 rpm). At boiling point, previously prepared 1 % trisodium citrate dihydrate ($\text{Na}_3\text{C}_6\text{H}_5\text{O}_7 \cdot 2\text{H}_2\text{O}$) solution (Solution II) was added at different volumes (1-4 ml) slowly to avoid the aggregate formation.
- 4) Different sizes (diameters) of gold nanoparticles were prepared by altering the volumetric ratio of gold salt ($\text{HAuCl}_4 \cdot 3\text{H}_2\text{O}$) to reducing agent ($\text{Na}_3\text{C}_6\text{H}_5\text{O}_7 \cdot 2\text{H}_2\text{O}$) (Frens, 1973; Chithrani et al., 2009). The change in color of the solution from pale

blue (nucleation) to deep red (ruby red) is an indication that gold (III) has been reduced and gold nanoparticles have been formed.

Some modifications on the protocol were made to get larger (30-50 nm) and more uniform distribution of size and shape. For modification; i) 0.1 % trisodium citrate dihydrate ($\text{Na}_3\text{C}_6\text{H}_5\text{O}_7 \cdot 2\text{H}_2\text{O}$) solution (Solution II) was added in different 5-10 ml volumes to solution I. ii) Solution II was passed through 0.2 μm filter and it was heated mildly with a heater before adding to Solution I. Accordingly, the problems related with the temperature difference (temperature gradient) between Solution I and Solution II was tried to be evaded. When the color of the solution starts to turn from pale blue (nucleation) to deep red (ruby red) the stirring at boiling point was continued for 15 minutes more. Immediately after this step, flask containing the solution was soaked into an ice bath to stop the reaction in an intention to form particles with a more uniform size distribution. Finally, the gold nanoparticle suspensions was topped to 30 ml and passed through 0.1 μm filter (Figure 2.1).

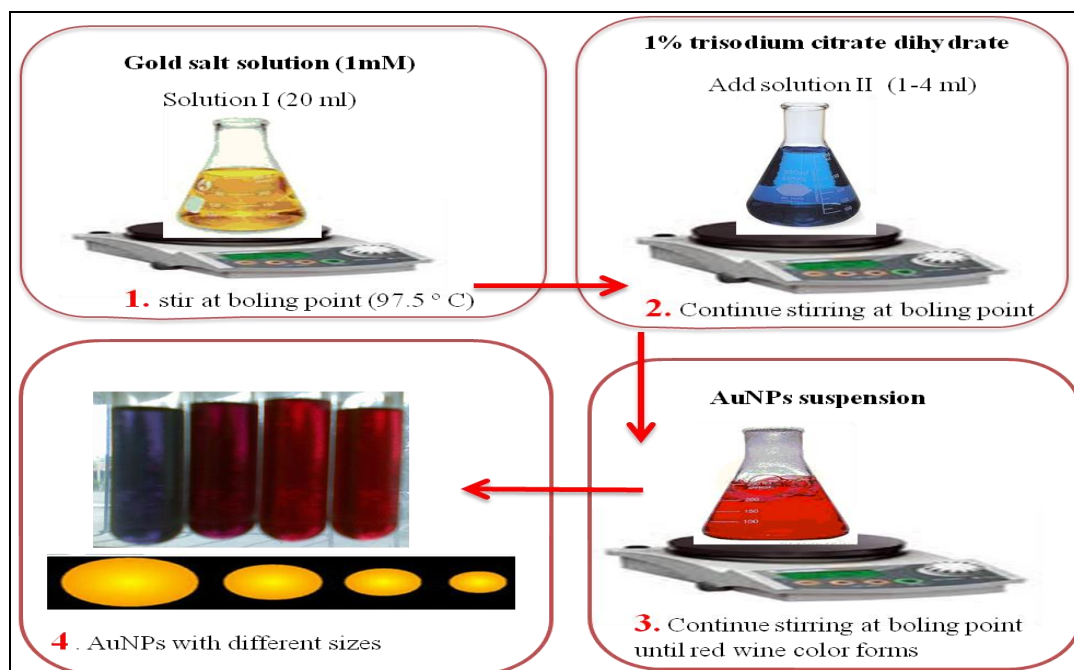


Figure 2.1. The schematic figure showing the steps of gold nanoparticles synthesis.

2.2.2. Fabrication of Epidermal Layers of Scaffolds

Collagen/sericin films (epidermal layer) were fabricated as it was described before with some slight modifications (Akturk et al., 2011). Briefly, sericin and collagen suspensions having 1% concentrations were prepared in 0.5 M acetic acid and blended in collagen/sericin ratios of 2:1 w/w. The mixture (120 ml) was then cast onto glass petri plates (12 cm) and left to air drying in room temperature. The dried film was first subjected to dehydrothermal cross-linking in vacuum oven at 120 °C for 2 hours before chemical cross-linking with GTA (3%) for two hours. Then, cross-linked films were rinsed with distilled water thoroughly and held in 0.2 M glycine solution for 30 minutes to deactivate the toxic aldehyde residues.

2.2.3. Fabrication of Dermal Layer of Scaffolds

2.2.3.1. Collagen Sponges

2.2.3.1.1. Preparation of Collagen Sponge Solutions

Different collagen solutions (0.1-2 %) were prepared by dissolving collagen type I in 0.5 M acetic acid solution. To maintain the structural properties (characteristic triple helix) of the protein, collagen solutions were stirred at ice cold conditions (4 °C). The prepared groups were homogenized with a blender and air bubbles were removed by sonication before the lyophilization. Collagen sponges incorporated with AuNPs (CS-Au) were obtained by adding the AuNPs into collagen solutions before freeze/drying process with lyophilisation. 10 ml of collagen solution (1 %) was added with 1 ml AuNPs (157 ppm) to get final concentration of AuNPs in the blends as 14.27 ppm.

2.2.3.1.2. Lyophilization of Collagen Solutions

After preparing the sponge solutions, they were casted onto moulds (glass petri plates or tissue culture 6 well plates). Sponges (Figure 2.2) were prepared by lyophilizing the frozen collagen solutions (-80 °C) for 8 hours in a freeze-dryer (FreeZone Plus 12, Labconco, USA).

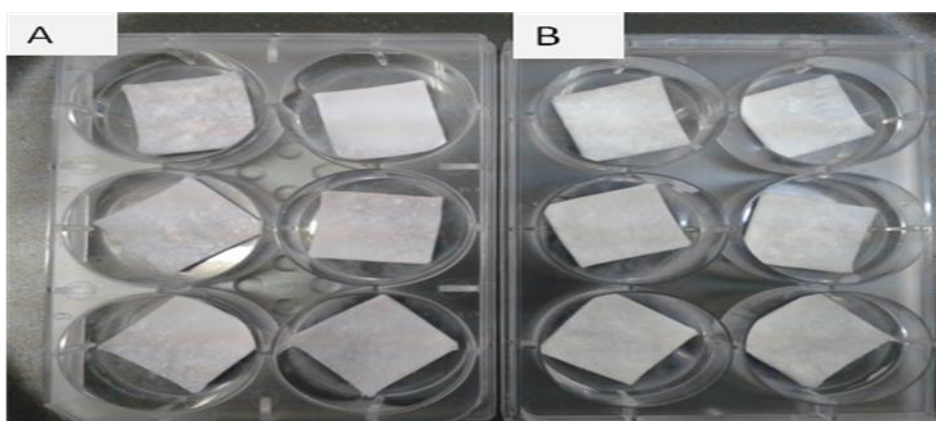


Figure 2.2. The collagen sponges prepared: (A) CS-Au and, (B) CS.

2.2.3.1.3. Chemical Treatment of Collagen Sponges

The collagen sponges were known to lose their 3D structure in aqueous environment, so they were cross-linked with glutaraldehyde (GTA) solution (% 3) for 2 hours. Sponges were soaked in distilled water briefly to swell the pores before cross-linking. Unreacted aldehyde groups were blocked in glycine solution (0.2 M) for 30 minutes after cross-linking. For complete dehydration, the scaffolds were freeze-dried. Finally, the scaffolds were stored in a desiccator at room temperature.

2.2.3.2. Collagen Nanofibrous Matrices

2.2.3.2.1. Preparation of Collagen Spinning Solutions

Collagen type I solutions (1 %, 2 %) were prepared by dissolving them in acetic acid solution (0.5 M). In order to be able to perform the electrospinning successfully, a transparent, thoroughly dissolved polymer solution was necessary. Therefore, the collagen solutions prepared were heated up to boiling point and awaited at the boiling point for 5-15 minutes. Afterwards, the transparent solution was filtered through 100 µm pore sized filter. The concentration of the final solution was checked by drying a sample solution in an oven and measuring the dry weight.

2.2.3.2.2. Electro-spinning of Collagen Solutions

For electrospinning collagen, PEO was utilized as the second polymer. In order to increase the conductivity and to get uniform nanofibers, NaCl was added into solutions (Table 2.1). The effect of AuNPs on the electrospinning process was investigated by preparing different test groups which were given in Table 2.2. The flow rate of the collagen solutions dripping out from the of syringes (blunt needle, 18 G) was adjusted as 0.8-1 ml/h with syringe pump (New Era, USA). The electrospun fibers were collected on a stationary aluminium collector located in a 20-26 cm distance away from the syringe needle. By adjusting the voltage (15-20 kV) of the high voltage power supply (Gamma, USA) connected to the needle tip, the continuity of the solution jet flow and the nanofiber accumulation on the screen (liquid droplets or white fibrous mats) was observed (Figure 2.3). The nanofibrous matrices (Figure 2.4) were peeled off from the collectors with a tweezer and stored in desiccators until characterisation.

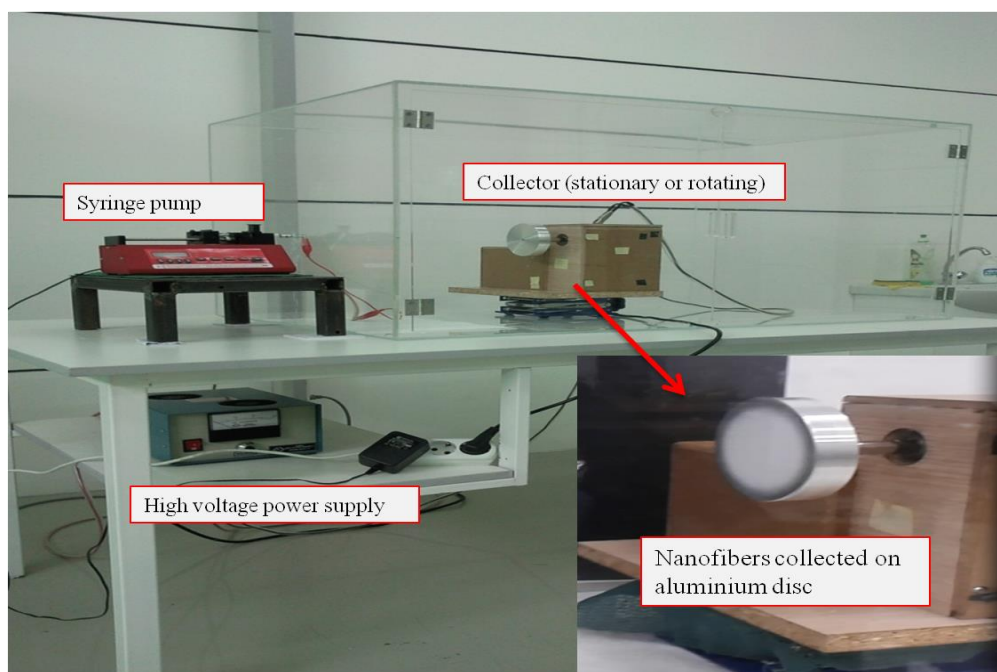


Figure 2.3. The electro-spinning system.



Figure 2.4. The photographs of nanofibrous matrices

Table 2.1. Optimization of collagen/PEO spinning solutions added with salt.

Groups	Collagen concentration in final solution (% w/v)	PEO concentration in final solution (% w/v)	Polymer ratio C:PEO (w/w)	Total polymer concentration (% w/v)	Salt amount in final solution (mM)
Col1S	1	-	1:0	1	40
Col2S	2	-	2:0	2	40
Col1P1S	1	1	1:1	2	40
Col1P1.5S	1	1.5	1:1.5	2.5	40
Col1P2.5S	1	2.5	1:2.5	3.5	40
Col2P1.5S	2	1	2:1	3	40
Col2P1.5S	2	1.5	2:1.5	3.5	40
Col2P2.5S	2	2.5	2:2.5	4.5	40

Table 2.2. The groups prepared to study the effect of AuNPs concentration on the electrospinning.

Groups	Collagen concentration in final solution (% w/v)	PEO concentration in final solution (% w/v)	Blend ratio, PEO:C (wt/wt)	Total blend concentration (% w/v)	The volume of AuNPs added (157 ppm, μl)
Col1Au0	1	-	1:0	1	0.14
Col2Au0	2	-	2:0	2	0.14
Col1 P2Au0	0.91	1.8	1:2	2.73	0.14
Col1 P2Au1	0.91	1.8	1:2	2.73	1.42
Col1 P2.5Au0	0.91	2.27	1:2.5	3.18	0.14
Col1 P2.5Au1	0.91	2.27	1:2.5	3.18	1.42
Col1 P2.5Au7	0.91	2.27	1:2.5	3.18	7.13
Col1 P2.5Au14	0.91	2.27	1:2.5	3.18	14.27

2.2.3.2.3. Chemical Treatment of Collagen Nanofibrous Matrices

Since the electrospun matrices were observed to lose their structural integrity to a large extent in aqueous environment, they were cross-linked with GTA vapor (% 3) for 2 hours. To prevent the contraction of the scaffolds during cross-linking treatment, they were glued to circular glass caps from the edges (Figure 2.5). In this manner, their size and shape were maintained. Unreacted aldehyde groups during cross-linking were blocked in glycine solution (0.2 M) for 30 minutes. Graded ethanol series (% 20-100) were used for dehydration or rehydration of scaffolds. The scaffolds were stored in desiccator until they were used in tests.



Figure 2.5. The photographs of nanofibrous matrices after the cross-linking treatment.

2.2.3.3. Fibroin Micro/Nano Fibrous Matrices

2.2.3.3.1. Extraction of Silk Fibroin from Cocoons

Dry silk cocoons (without silk worm) were severed into small pieces and boiled for 30 min in an aqueous solution of 0.02M Na₂CO₃ (5g cocoon in 2L) and then rinsed thoroughly with distilled water 3 times (20 min each) for 1 hour to extract the glue-like sericin proteins. Approximately 3.5 g of sericin free silk (fibroin) remained out of 5 g cocoon after this process. The silk fibroin (3.5 g) was then dissolved in 9.3M

LiBr solution (14 ml) at 60 °C, yielding a highly concentrated gel-like solution. This solution was dialyzed against distilled water using a dialysis membrane for 3 days, changing the distilled water two times every day. Finally, the pure fibroin solution in d-water was filtered through 100 µm filter and put in a refrigerator at 4 °C. The final concentration of silk fibroin in aqueous solution was about 5-10 wt %, which was determined by weighing the remaining solid after drying a particular volume of this solution in an oven (60 °C) for 2-3 hours. Concentrated silk fibroin solution (10-20 wt %) was also obtained by heating the solution at 55-60 °C while continuously stirring at 250 rpm.

2.2.3.3.2. Preparation of Fibroin Spinning Solutions

During preliminary studies, pure silk fibroin solutions were prepared at different concentrations (1-20%, in d-water). Groups of silk fibroin/PEO solutions used to generate stable, continuous spinning were summarized in Table 2.3. For instance; SFP3 solution was prepared by adding 1 ml of PEO solution (2 % in d-water) to 5 ml SF solution (8.6 % in d-water). Homogeneous solutions were obtained by mildly stirring for at least 2 hours at room temperature. The solutions could be waited at 4 °C as long as 2 weeks without any observable changes (premature β -sheet formation) in the blends.

Table 2.3. Optimization of silk fibroin/PEO spinning blend solutions.

Groups	Silk Fibroin concentration in final solution (% w/v)	PEO concentration in final solution (% w/v)	Polymer ratio, SF:PEO (w/w)	Total polymer concentration (% w/v)
SF1	1	-	1:0	1
SF2	2	-	2:0	2
SF3	3	-	3:0	3
SF4	4	-	4:0	4
SF5	5	-	5:0	5
SF10	10	-	10:0	10
SF20	20	-	20:0	20
SFP1	4.6	0.4	11:1	5
SFP2	8.3	0.3	25:1	8.7
SFP3	7.2	0.3	21.5:1	7.5

2.2.3.3.3. Electro-spinning of Fibroin Solutions

The flow rate of the silk fibroin solutions dripping out from the syringes (blunt needle, 18 G) was adjusted as 0.8-2 ml/h with syringe pump (New Era, USA). As the main difference from collagen electrospinning, here, the fibers were collected in ethanol bath (96 %) placed on metal collector rotating at 30-60 rpm speed and located perpendicular in a 12-26 cm distance away from the syringe needle (Figure 2.6, wet electrospinning). By adjusting the voltage (10-20 kV) of the high voltage power supply (Gamma, USA) connected to the needle tip, the continuity of the solution jet flow and the fiber accumulation inside the ethanol bath (Figure 2.7 A) was achieved. The electrospun fibers in ethanol were then transferred into glass beakers and stored at 4 °C overnight.

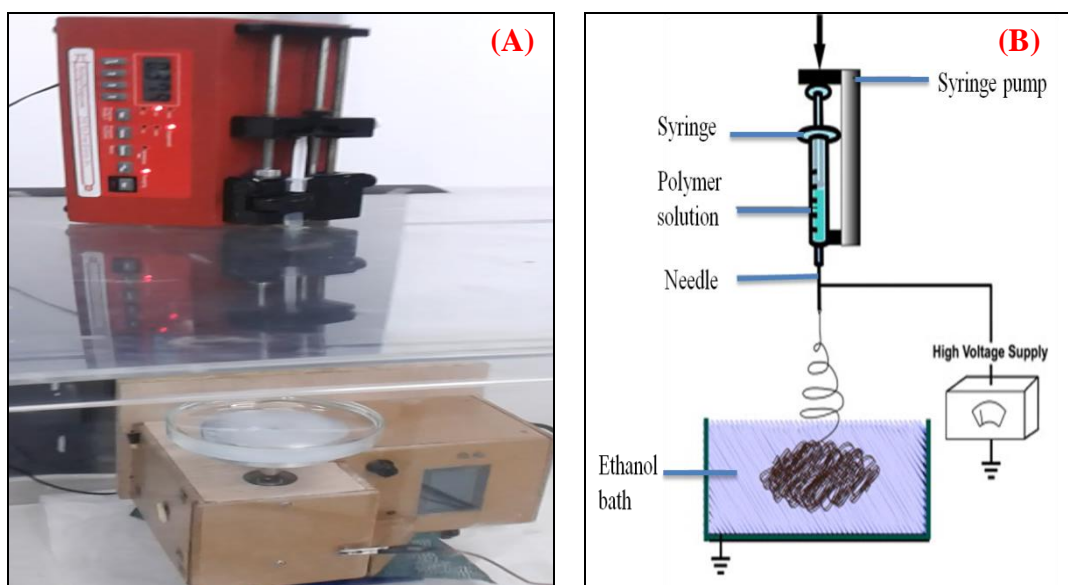


Figure 2.6. A) The photo and B) the experimental set-up of wet electrospinning system.

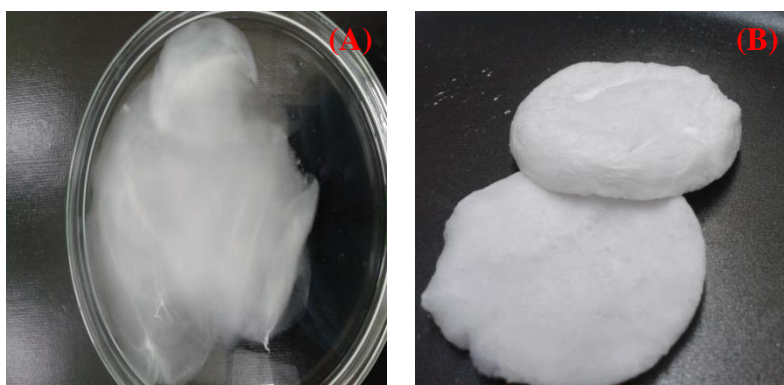


Figure 2.7. The photo of A) fiber accumulation inside the glass petri plate during electrospinning and B) final freeze-dried electrospun silk fibroin matrix.

Silk fibroin fibrous suspensions were subjected to sonication for 5-10 minutes in order to avoid fiber fusion. Afterwards, the ethanol in silk fibroin fibrous suspensions was removed followed by rinsing thoroughly with d-water. Finally, suspensions were kept in an oven at 37 °C for 1 hour. D-water was removed from suspensions

prior to freezing. The wet fibrous mat spontaneously got the shape of mould (glass petri dish or 6 well plates) when it was frozen at - 20. The frozen fibrous mat was freeze-dried for 2 days and a silk fibroin dermal substitute with spongy form (about 1-2 mm) and silky soft surface was obtained (Figure 2.7 B).

2.2.3.3.4. Chemical Treatment of Silk Fibroin Fibrous Matrices

Different chemical treatment methods such as ethanol (96%), methanol (100%), EDC/NHS (10 mM each in absolute ethanol) and GTA (3% in d-water) were tried to enhance the stability of the silk fibroin matrix (SFP3 group) in aqueous environment. In order to form β -sheets, silk fibroin fiber suspension was hold in ethanol overnight at 4 °C (SFM-E), then additionally put into methanol for 5 min (SFM-M), or EDC/NHS solution (SFM-E/N), or 3% GTA (SFM-G). All the treated groups were rinsed with d-water afterwards and freeze-dried as mentioned previously. The solubility, brittleness, FTIR spectra and SEM micrographs of all 4 chemically treated groups of electrospun fibrous matrices were assessed later.

2.2.4. Fabrication of Bilayered Skin Substitutes

Eventually, lyophilized or nanofibrous scaffolds (dermal layer) and 2:1 collagen/sericin films (epidermal layer) were glued to each other with natural honey to form the final optimized bilayered structures (Figure 2.8). The bilayered scaffolds were kept in a desiccator until they were used in tests. Compositions of prepared bilayered scaffolds were given Table 2.4.

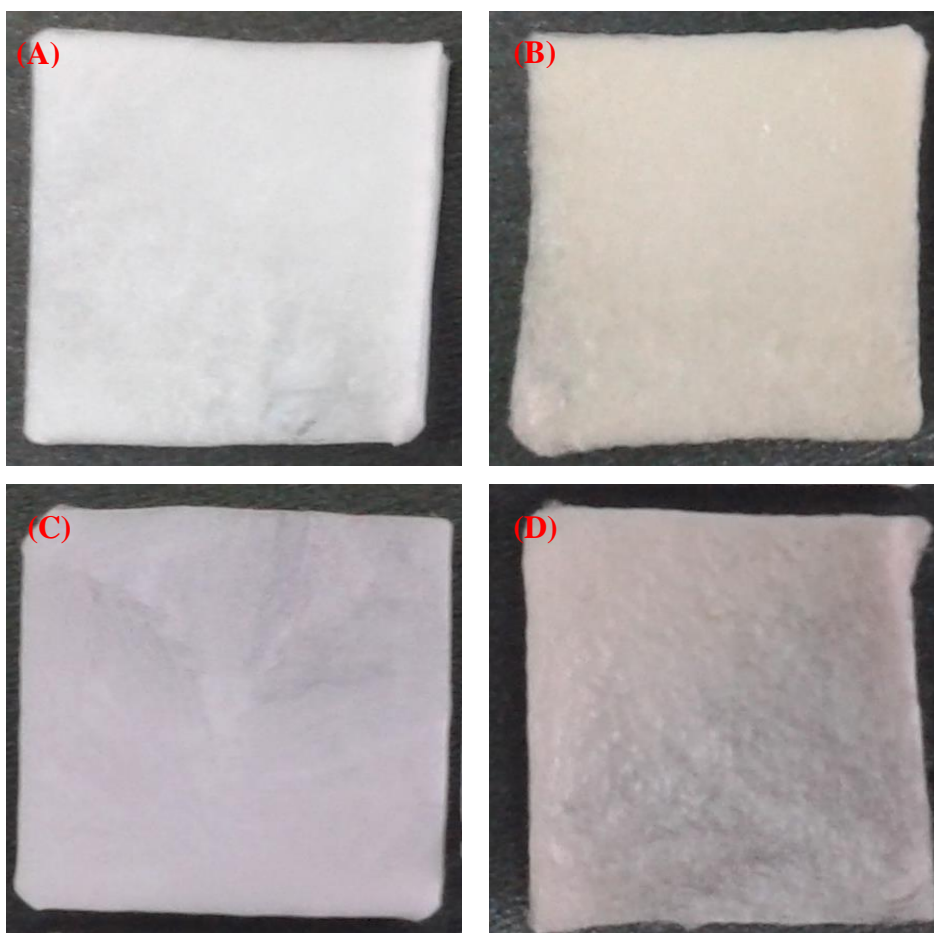


Figure 2.8. The photo of optimized experimental groups: (A) CS, (B) CS-X, (C) CS-Au, (D) CS-AuX.

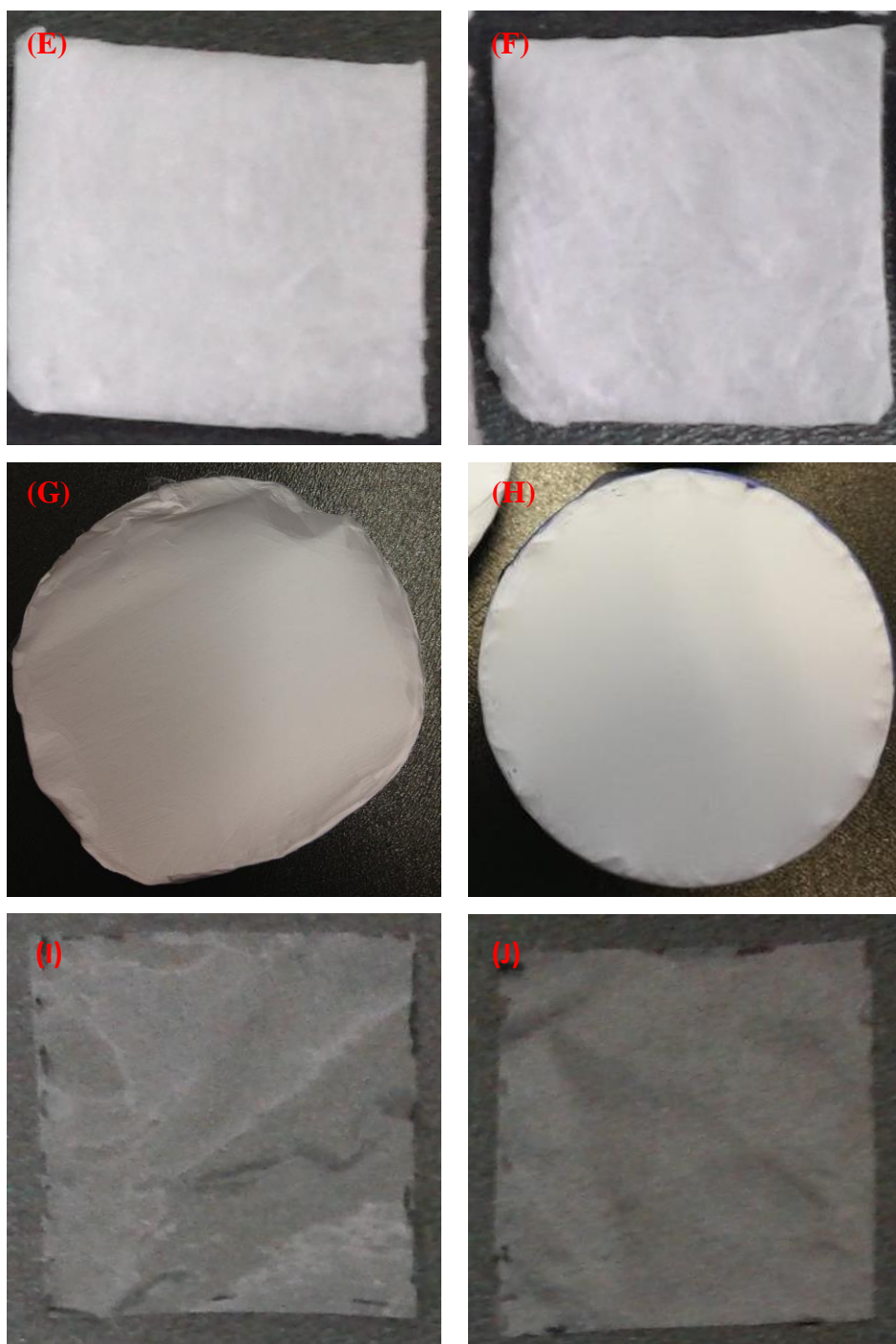


Figure 2.8. Continued: (E) SFM-E, (F) SFM-AuE, (G) CM-Au, (H) CM-AuX, (I) C/S, (J) C/S-X.

Table 2.4. Composition of optimized bilayered scaffolds.

Groups	Epidermal layer	Dermal layer
BLCS	Collagen/sericin membrane (2:1 w/w) obtained by casting and solvent evaporation (C/S)	Lyophilized collagen sponge obtained from 0.91% collagen solution (CS)
BLCS-X	GTA cross-linked collagen/sericin membrane (2:1 w/w) obtained by casting and solvent evaporation (C/S-X)	GTA solution cross-linked lyophilized collagen sponge obtained from 0.91% collagen solution (CS-X)
BLCS-Au	Collagen/sericin membrane (2:1 w/w) obtained by casting and solvent evaporation (C/S)	Lyophilized collagen sponge obtained from 0.91% collagen solution incorporated with AuNPs (14.27 ppm) (CS-Au)
BLCS-AuX	GTA cross-linked collagen/sericin membrane (2:1 w/w) obtained by casting and solvent evaporation (C/S-X)	GTA solution cross-linked (3%, 2 h) lyophilized collagen sponge incorporated with AuNPs (14.27 ppm). (CS-AuX)
BLCM-Au14	Collagen/sericin membrane (2:1 w/w) obtained by casting and solvent evaporation (C/S)	Electrospun collagen nanofibrous matrix obtained from collagen/PEO blends (1:2.5, w/w) incorporated with AuNPs (14.27 ppm) (CM-AuX)
BLCM-Au14X	GTA cross-linked collagen/sericin membrane (2:1, w/w) obtained by casting and solvent evaporation (C/S-X)	GTA vapour cross-linked (3%, 2h) electrospun collagen nanofibrous matrix obtained from collagen/PEO blends (1:2.5, w/w) incorporated with AuNPs (14.27 ppm) (CM-AuX).
BLSFM	GTA cross-linked collagen/sericin membrane (2:1, w/w) obtained by casting and solvent evaporation (C/S-X)	Wet electrospun and lyophilized silk fibroin matrix obtained from SF/PEO (21.5:1, w/w) blends (SFM-E)
BLSFM-Au	GTA cross-linked collagen/sericin (2:1, w/w) membrane obtained by casting and solvent evaporation (C/S-X).	Wet electrospun and lyophilized silk fibroin matrix obtained from SF/PEO (21.5:1, w/w) blends (SFM-AuE).

2.2.5. Characterization Tests

At first the physicochemical (attenuated total reflectance Fourier transform infrared spectral scans, Scanning Electron Microscopy, Transmission Electron Microscopy, hydrolytic and enzymatic degradation, water swelling, water vapor transmission rate, oxygen penetration, mechanical tests, fiber and pore size distribution, porosity, particle size and distribution and attenuated total reflectance Fourier transform (ATR-FTIR) characterization tests were performed on the scaffolds. After this, the selected groups were subjected to in vitro biocompatibility analysis (cell cytotoxicity, cell adhesion, spreading, and proliferation) and in vivo rat wound healing tests to determine their success in wound healing of full-thickness skin wound model. Finally, in vivo toxicological evaluation tests (skin sensitization, irritation and genotoxicity tests) were carried out on one of the most successful bilayered scaffold groups chosen according to evaluation of the results of all the previous tests.

2.2.5.1. Physicochemical Characterization

2.2.5.1.1. Attenuated Total Reflectance Fourier Transform Infrared Spectrophotometer Analysis

Infrared spectra were measured with an attenuated total reflectance Fourier transform (ATR-FTIR) (IFS/66S, Hyperion 1000) spectrophotometer in Central Laboratory at METU. Each spectrum was acquired in transmittance mode on a ZnSe ATR crystal cell by accumulation of 256 scans with a resolution of 4 cm^{-1} and a spectral range of $4000\text{-}400\text{ cm}^{-1}$.

2.2.5.1.2. Scanning Electron Microscopy

The morphology of the scaffolds was examined using SEM. To prepare the samples for SEM analysis, they were completely dehydrated by lyophilization. Finally, samples were sputter coated with gold and the surface properties were analyzed with Scanning Electron Microscope (JSM-6400 Electron Microscope, JEOL Ltd., Japan) at the Department of Metallurgical and Materials Engineering in METU.

2.2.5.1.3. Transmission Electron Microscopy

High contrast transmission electron microscope (CTEM) (FEI Tecnai G² Spirit BioTwin) analysis was made in Central Laboratory at METU to understand whether the AuNPs had the desired size. Before the analysis, gold nanoparticles were subjected to sonication and vortexing processes to prevent agglomeration and aggregation, so more uniform distribution of the nanoparticles along the water was enabled. Nanogold size distribution analysis was done to at least 300 particles imaged with CTEM with the help of image J programme. Also, the nanogold distribution inside the nanofibers was examined with CTEM. CTEM samples were prepared such that the nanogold loaded nanofibers were collected on carbon coated copper grids.

2.2.5.1.4. Porosity Calculation

The porosity of the sponge form scaffolds (BLCS, BLCS-X, BLCS-Au, BLCS-AuX, BLSF, BLSF-Au) were measured by liquid displacement method. Hexane was used as the displacement liquid since it is nonsolvent for both collagen and silk fibroin and is able to easily permeate through the scaffold and do not cause swelling or shrinkage, unlike ethanol (Bhardwaj et al., 2014). A picnometer was used for porosity calculation. First, the empty (W_0), and the full weight (W_1) of picnometer

with n-Hexane was measured. Dry sample (W_s) was immersed in picnometer topped with hexane and air bubbles were removed by vacuuming for 10 minutes. Afterwards the weight of picnometer with wet sample (W_2) was measured. Finally, the wet sample (W_3) was taken out. The following equations were used for the porosity calculations:

$$W_{W1} = W_1 - W_0 \quad (1)$$

$$W_{W2} = W_2 - W_0 - W_s \quad (2)$$

$$V_S = \frac{W_{W1} - W_{W2}}{D_{Hexane}} \quad (3)$$

$$V_P = \frac{W_3 - W_s}{D_{Hexane}} \quad (4)$$

$$P = \frac{V_P}{V_P + V_S} \times 100 \quad (5)$$

V_S , V_P and P are skeletal volume, pore volume and porosity of sample, respectively and D_{Hexane} (0.6548 gr/ml) is the density of n-hexane.

The porosity of the nanofibrous scaffolds (BLCM-Au, BLCM-AuX) was measured with mercury porosimeter (Quantachrome Corporation, Poremaster 60) in high pressure analysis mode (0- 55,000 psi) in Central Laboratory at METU.

2.2.5.1.5. Pore Size Distribution Analysis

For measuring the pore size distribution of selected groups of scaffolds (CS, CS-X, CS-Au, CS-AuX, SF, SF-Au, CM-Au, and CM-AuX), mercury porosimeter (Quantachrome Corporation, Poremaster 60) was used. Low pressure analysis (0-50

psi) was conducted for CS, CS-X, CS-Au, CS-AuX, SF and SF-Au, on the other hand high pressure analysis (0- 55,000 psi) was conducted on CM-Au, CM-AuX.

2.2.5.1.6. Hydrolytic Degradation

The degradation of scaffolds in aqueous environment was analyzed. The samples were cut in 1x1 cm² pieces and put into PBS (pH: 7.2, 0.01 M). They were incubated at 37°C until the structural integrity is disrupted. Gravimetical analysis was carried out by removing the scaffolds at different time intervals and measuring their weights after complete drying. The freeze-dried samples (1x1 cm) were weighed initially (W_d) then put in sample bottles containing PBS. These samples waited in water bath at 37°C and at different time intervals the samples were taken out from the bottles, rinsed with d-water and freeze-dried. The gravimetical analysis was carried out by measuring the dry weights (W_t) again. After weighing them, the samples were put into dissolution liquid and the incubation continued (Figure 2.9). Degradation at different time periods (D_t) was calculated using the following equation:

$$D_t = \frac{W_d - W_t}{W_d} \times 100 \quad (6)$$

2.2.5.1.7. Enzymatic Degradation

In vitro degradation of the scaffolds was performed by incubating in PBS solution (0.01 M, 5 ml) containing type I collagenase solution (1 mg/ml, 60 μ l). The mass loss of collagen from the scaffolds was measured with a gravimetical analysis as described before for hydrolytic degradation (Figure 2.9).

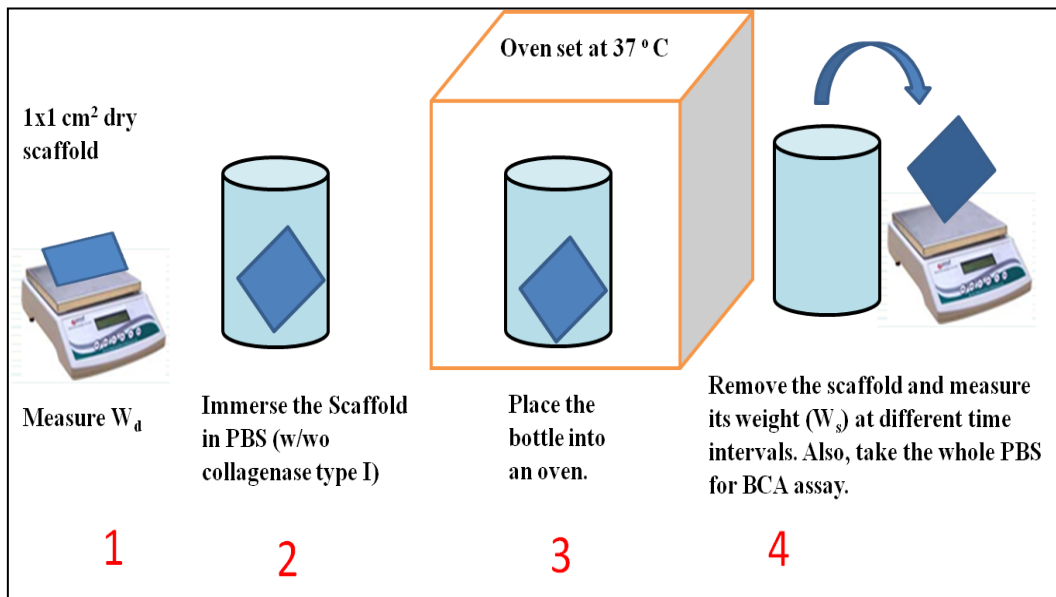


Figure 2.9. Experimental setup for measuring the hydrolytic and enzymatic degradation

2.2.5.1.8. Equilibrium Degree of Swelling

A general gravimetric method was used to measure the water absorption of scaffolds. Scaffolds were cut into 1x1 cm² pieces and their dry weights (W_d) were measured. Each scaffold was immersed in de-ionized water in plastic bottles and incubated at 37 °C in an oven. The weight of each bottle was measured initially. All bottles were capped tightly to prevent any evaporative water loss. At different time intervals water inside the bottles were removed and excess surface water on swollen scaffolds was gently blotted with filter paper. The weights of these scaffolds were measured together with empty bottles and weights of swollen scaffolds (W_s) were obtained by taring. Equilibrium degree of swelling (EDS) was calculated using the following equation:

$$\text{EDS} = \frac{W_s - W_d}{W_d} \quad (7)$$

Accordingly, the water uptake values were normalized with dry scaffold weights. The schematic representation of water uptake studies is shown in Figure 2.10. The tests were carried out at least in quadruplets ($n \geq 4$)

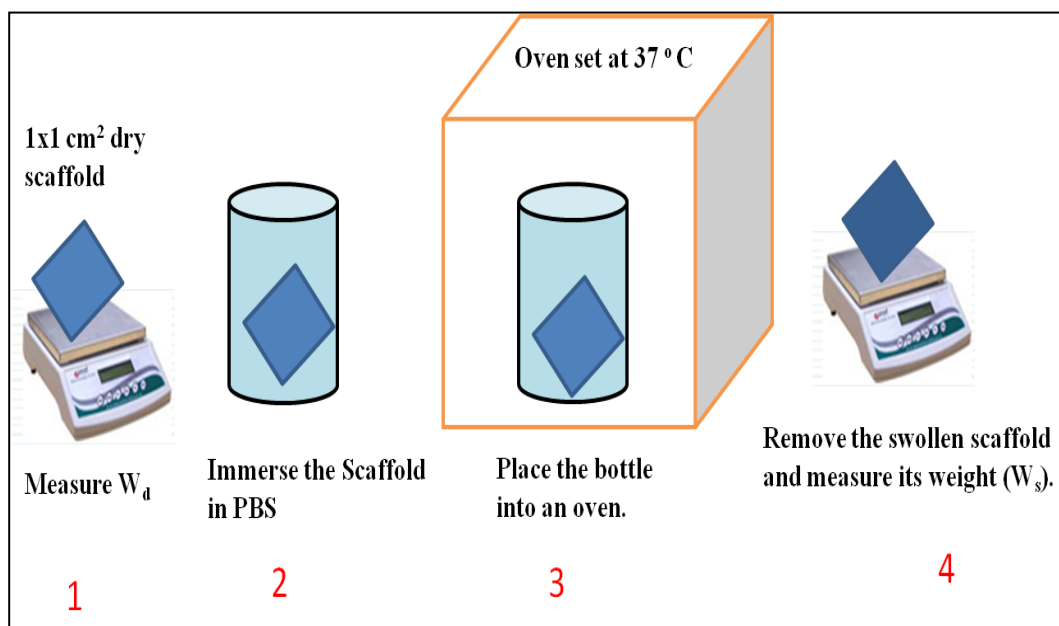


Figure 2.10. Experimental setup for measuring water swelling of scaffolds

2.2.5.1.9. Water Vapour Transmission Rate

Water vapour transmission rates (WVTR) were determined according to the ASTM method E96-90, Procedure D. An evaporimeter was constructed in a closed chamber to prevent variations owing to ambient conditions. Briefly, the system consists of a plastic box with an air tight cover and isothermal ambience at 35 °C, a digital hygrometer with a continuous percent relative humidity (RH) and temperature display, and a reservoir of a saturated magnesium chloride solution to maintain the relative humidity at $40 \pm 2\%$ after equilibration. A cylindrical, plastic permeability cup filled with 20 g of de-ionized water and sealed with the test scaffold at the top was placed inside the system. Evaporation of water through the test scaffold was monitored by measuring weight change in plastic cup as an indication of daily loss of

water. Then, the water vapour transmission rate (WVTR) was found by dividing the daily loss of water with the evaporation area of the permeability cup (Figure 2.11). The water vapor evaporation studies were carried out at least in quadruplets ($n \geq 4$).

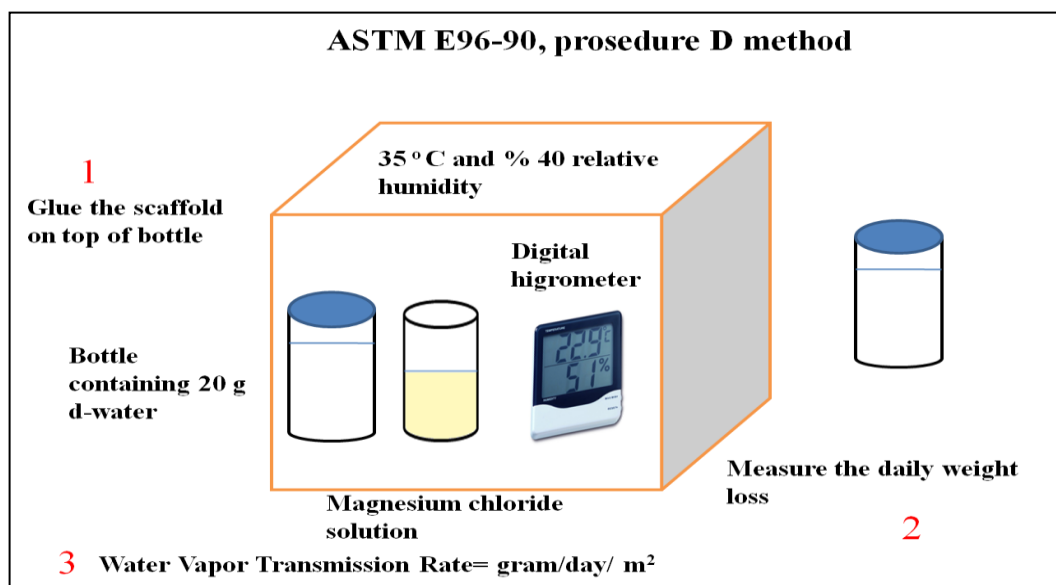


Figure 2.11. Experimental set up for testing water vapour transmission rate through bilayered scaffolds.

2.2.5.1.10. Oxygen Permeability Test

Oxygen permeation of bilayered scaffolds was verified with a home-made system. The system consists of a two headed bottle, a dissolved oxygen meter, and digital stirrer. One of the heads of the bottle was covered with scaffolds (open and closed head bottles were used as controls) and from its other head the probe of oxygen meter was passed through and its surrounding was covered tightly to prevent air entrance. The probe stayed continuously inside the water. The water inside the bottle agitated with rapid stirring (800 rpm). At the end of one day the dissolved oxygen inside d-water was measured ($n \geq 3$) at room temperature (25.5 °C).

2.2.5.1.11. Mechanical Testing

The mechanical properties of scaffolds were evaluated by applying tension test with Lloyd LS500 Material Testing Machine (Lloyd, England) using Nexygen computer software. Rectangular samples (5 x 30 mm) were cut from scaffolds. To prevent slippage from the grips they were covered with sand paper at the grip side. The gauge length and width were 10 and 5 mm, respectively. The thickness of the test samples were calculated by means of Vernier calliper. The crosshead speed of the system was adjusted to 10 mm/min to get a constant strain rate of 100 %/min. The tests were also performed by wetting the tests samples with PBS (0.01 M, pH: 7.4) for 5 minutes (Figure 2.12) The results of both dry and wet samples were obtained as load versus deflection curves which were then converted into stress-strain data by the computer program. Modulus of elasticity (E), ultimate tensile strength (UTS) and percent elongation at break (EB) was calculated ($n \geq 6$) from the stress-strain curves of samples.

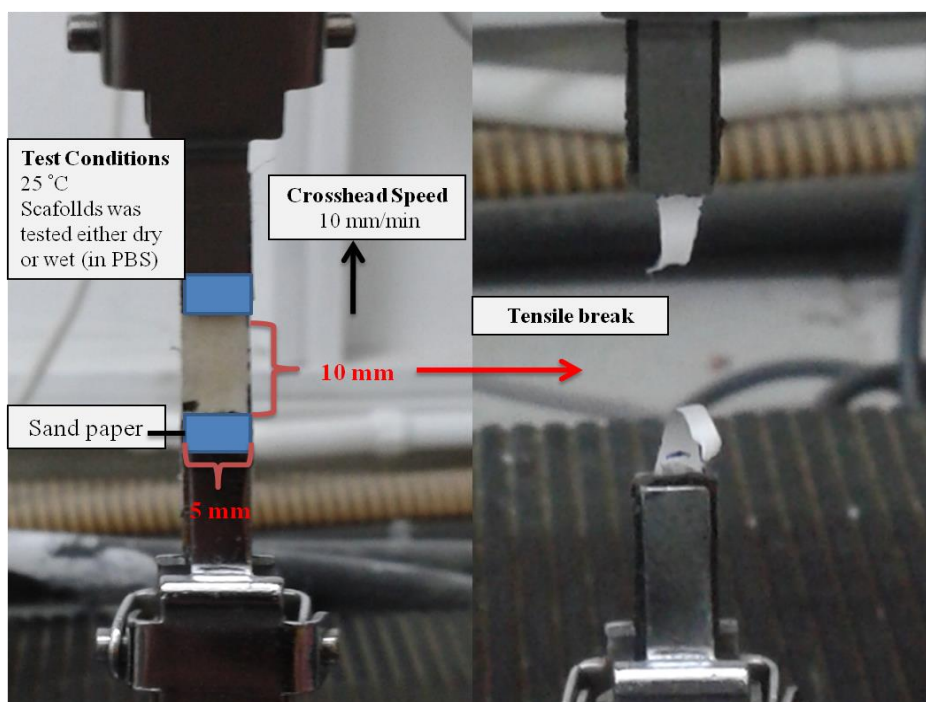


Figure 2.12. Experimental set up for testing mechanical properties of scaffolds.

2.2.5.2. In Vitro Characterization Tests

Biocompatibility of scaffolds was studied with three different cell lines; 3T3 fibroblasts (An1 Swiss albino mouse fibroblast, obtained from Foot-and-Mouth Disease Institute of Ministry of Agriculture and Rural Affairs of Turkey), L-929 fibroblasts (Mouse, ATCC), and keratinocytes (HaCat human keratinocyte, obtained from DSMZ, Braunschweig). Light microscopy and SEM pictures were taken to examine the cell-biomaterial interactions (i.e. cell morphology; adherence onto scaffolds, distribution-spread, roundness etc.). Cytotoxicity tests were also conducted with AuNPs alone and with scaffold extracts.

2.2.5.2.1. Cell Culture Conditions

2.2.5.2.1.1. Fibroblast Cell Line Culture

The 3T3 or L-929 fibroblast cell lines were cultured in Dulbecco's modified Eagle's medium (DMEM high glucose-glutamine) supplemented with fetal bovine serum (FBS, 10%, v/v) and penicillin/streptomycin (10 U/ml) at 37°C under humidified atmosphere of 5% CO₂- 95 % air in incubator (5215, SHEL LAB, USA). The medium was refreshed 2 times a week. When the cells reached at least 80-90 % confluency, they were trypsinized with trypsin-EDTA (0.1% in PBS) and passaged in 1:3 ratios.

2.2.5.2.1.2. Keratinocyte Cell Line Culture

The HaCat keratinocyte cell line was cultured in Dulbecco's modified Eagle's medium (DMEM high glucose-glutamine) supplemented with fetal bovine serum (FBS, 10%, v/v) and penicillin/streptomycin (10 U/ml) at 37°C under humidified atmosphere of 5% CO₂- 95 % air in incubator (5215, SHEL LAB, USA). The

medium was refreshed 2 times a week. When the cells reached at least 80-90 % confluency (approximately 7 days), they were first rinsed with EDTA (0.05 % in PBS) and incubated in EDTA (0.05 %) for 10-20 minutes at 37°C and then trypsinized with trypsin-EDTA (0.1 % in PBS) for 5-10 minutes and passaged in 1:5-1:10 ratios.

2.2.5.2.2. Cytotoxicity Tests of Synthesized Gold Nanoparticles

Keratinocytes and 3T3 fibroblasts were seeded onto 12-well plates at seeding density of 100 cells/ μ l (30,000 cells/well). After 1 day incubation period, AuNPs were added to cell seeded 12-well plates at different concentrations (10, 20 ppm). The desired nanoparticle concentration was achieved by diluting the stock AuNP suspension (157 ppm) with complete cell culturing medium. The cytotoxic effect of AuNP was evaluated with methylthiazolyldiphenyl-tetrazolium bromide (MTT) cell viability assay for 1, 4 and 7 day incubations. Medium containing AuNPs was refreshed every other day for longer incubations. Briefly, MTT stock solution (5mg/ml) was prepared by dissolving in PBS buffer. The test MTT solution was prepared by diluting this stock in 1/10 ratio with DMEM (without phenol red). At the end of each time period, the medium was removed and washed with PBS. Subsequently, 500 μ l MTT test solution was added to each well. The test wells were incubated at 37°C in a dark environment for 4 hours. Afterwards, MTT test solution was removed and 500 μ l DMSO was added and wells were shaken at 200 rpm for 15 minutes. Spectrophotometric measurements were done at 550 nm wavelength with microplate reader.

2.2.5.2.3. Cytotoxicity Tests of Scaffold Extracts

Cytotoxicity tests were carried out according to the protocols of ISO 10993-5 standards with either qualitative or quantitative means. Qualitative morphological

grading system was given in Table 2.5. Epidermal layers (C/S, C/S-X), dermal layers (CS, CS-Au, CS-X, CS-AuX, CM-Au, CM-AuX, SF, SF-Au) of scaffolds and bilayered scaffolds glued to each other by honey (BLCS, BLCS-Au, BLCS-X, BLCS-AuX, BLCM-AuX, BLSF and BLSF-Au) were sterilized in 70% ethanol supplemented with antibiotics (penicillin/streptomycin, 10 U/ml) overnight. After sterilization, the samples were rinsed with sterile d-water completely and held in complete cell culture medium (DMEM with 10% FBS) temporarily. Finally, they were incubated in extract medium (complete medium) at 37°C for 24 hours while shaking at 200 rpm. Extraction was done in accordance with ISO 10993-12 standards. Complete medium without any scaffolds were used as control. After seeding L-929 cells on 96 well plates (10,000 cells/well) for 1 day, the cells were checked for subconfluency. Then, medium was removed and refreshed with extract medium of samples. Cell viability was evaluated with methylthiazolyldiphenyl-tetrazolium bromide (MTT) cell viability assay after 1 day. Briefly, MTT stock solution (5mg/ml) was prepared by dissolving in PBS buffer. The test MTT test solution was prepared by diluting the MTT stock solution in 1/10 ratio with DMEM (without phenol red). At the end of 24 hours, the medium was removed and washed with PBS. Subsequently, 100 µl MTT test solution was added to each well. The test wells were incubated at 37°C in a dark environment for 4 hours. Afterwards, MTT test solution was removed and 100 µl DMSO was added and wells were shaken at 200 rpm for 15 minutes. Spectrophotometric measurements were done at 570 nm primary wavelength and 650 nm reference wavelength. The % cell viability was calculated by normalizing the extract sample OD results to that of control.

Table 2.5. Qualitative morphological grading of cytotoxicity of extracts

Grade	Reactivity	Conditions of all cultures
0	None	Discrete intracytoplasmatic granules, no cell lysis, no reduction of cell growth
1	Slight	Not more than 20% of the cells are round, loosely attached and without intracytoplasmatic granules, or show changes in morphology; occasional lysed cells are present; only slight growth inhibition observable
2	Mild	Not more than 50% of the cells are round, devoid of intracytoplasmatic granules, no extensive cell lysis; not more than 50 % growth inhibition observable.
3	Moderate	Not more than 70% of the cell layers contain rounded cells or are lysed; cell layers not completely destroyed, but more than 50% growth inhibition observable
4	Severe	Nearly complete or complete destruction of the cell layers.

2.2.5.2.4. Cell Attachment and Proliferation on Scaffolds

The sterilized scaffolds were cut in circular shapes (D: 10 mm) and put on sterile 24 well suspension plates. Before the cell seeding, the samples were kept in DMEM briefly. Afterwards, fibroblasts or keratinocytes were seeded onto scaffolds at a seeding density of 100 cells/ μ l (100,000 cells/well) and held in a CO₂ incubator for 1 and 3 days. The cell culture medium inside the wells refreshed every other day. Eventually, the medium was removed and the scaffolds seeded with cells were fixed in 3% GTA (in PB) solution for 1 h at room temperature. They were completely dehydrated in a lyophilizator. Then, they were coated with gold and analyzed with Scanning Electron Microscope (JSM-6400 Electron Microscope, JEOL Ltd., Japan) at the Department of Metallurgical and Materials Engineering in METU.

2.2.5.3. Antibacterial Assessment

2.2.5.3.1. Antibacterial Tests of Gold Nanoparticles

Bactericidal capacity of the AuNPs was assessed by applying agar disc diffusion method on petri plates seeded with *Staphylococcus aureus* (*S.aureus*) bacteria. The sterile discs (6 mm) used in antibiogram tests were dipped into gold nanoparticle suspensions having different concentrations (0, 5, 10, 20 ppm). Also, in order to search for the combined antibacterial effect of gold nanoparticles and an antibiotic (cefuroxime) known for its bactericidal effect against *S.aureus*, discs were loaded with both gold nanoparticles (5, 10, 20 ppm) and cefuroxime (4 µg/ml). Discs loaded with gold nanoparticles (Au8 group) and antibiotics were put onto agar in petri plates. Plates were seeded with *S.aureus* previously after culturing on blood agar plates at 37 °C. After incubating at 37 °C for 24 hours, the transparent inhibitory zone around each disc was measured with a ruler (Park et al., 2004, modified method). Empty discs were used as control.

2.2.5.3.2. Antibacterial Tests of Scaffolds

Agar petri plates were prepared by dissolving 2.5% Luria Broth (LB) and 1.5% agar in d-water and then the mixture was sterilized by autoclaving. The solution was poured onto plates to cool down. Frozen cultures of bacterial strain (*S. epidermidis*) grown on petri plates were inoculated into suspension flasks (2.5% LB) first and were incubated at 37°C under gentle rocking in a thermostatically controlled incubator overnight. Then, OD of the suspending bacteria was measured at 562 nm wavelength. An OD value of 0.52 was found to be corresponding to 9×10^8 bacteria/ml bacteria concentration. The OD measurement below this value was increased by concentrating the bacteria suspension with centrifugation. The bacteria seeding density was adjusted (1.6×10^6 bacteria/cm²). The test samples (1 x1 cm) were sterilized with ethanol solution (70 %) overnight in 24-well tissue culture

plates. The bacteria were seeded at the predetermined density onto the sterilized test samples containing 1.5 ml LB broth. Controls consisted of bacterial controls (cultures alone) and sample controls (samples without bacteria). All these test plates were incubated at 37°C for 48h. Subsequently, first 100 µl of the supernatant of the test wells (bacteria inoculated sample wells, culture alone wells and wells without bacteria) were removed and transferred into 96 well plates. To assess the adhered bacteria on the samples, the test samples were transferred to flasks containing fresh LB and vortexed for 1 minute to suspend the bacteria inside the solution and transferred into 96 well plates as well. Finally, OD values were obtained at 562 nm wavelength. The bacteria seeded scaffolds were initially fixed with GTA solution (3% in PB) for 1 hour before SEM examination. Then, they were coated with gold and analyzed with Scanning Electron Microscope (JSM-6400 Electron Microscope, JEOL Ltd., Japan) at the Department of Metallurgical and Materials Engineering in METU.

2.2.5.4. In Vivo Characterization Tests

2.2.5.4.1. Rat Full-Thickness Wound Healing Tests

2.2.5.4.1.1. Animals and Husbandry

Healthy adult male Wistar albino rats (80) weighing 200–250 g were used in experiments. The rats were housed in stainless steel cages in an animal room maintained at 22 °C with a 12 hour alternating dark–light cycle. All were fed with the same rat chow diet and water and fasted for 12 hours before the operations. The procedures in this experimental study were performed in accordance with the National Guidelines for the Use and Care of Laboratory Animals and approved by the Animal Ethics Committee of Ankara Research and Training Hospital.

2.2.5.4.1.2. Full Thickness Wound Model

Eight groups were randomly constituted of 10 rats each. The rats were anaesthetised with intramuscular injections of 50 mg/kg ketamine hydrochloride. The operation sites were shaved and disinfected with povidone-iodine. A 2 × 1 cm rectangular-shaped incision was made on the back of the rats centred on the midline, then a standard full-thickness skin defect, including panniculus carnosus, was created on this site.

2.2.5.4.1.3. The Optimization of Wound Healing Experimental Procedure

For optimization of the wound healing experiments, 4 different bilayered scaffold groups (BLCS, BLCS-X, BLCS-AuX and BLSF) were selected. The tests were conducted on different rats. Full-thickness wound model was created as defined above. In the study groups, the wounds were cleaned with PBS, and 1 sample from some groups, BLCS, BLCS-X, BLCS-AuX and BLSF, were applied. All wounds were followed for 14 days and no complications developed during this period. On the 14th day, all the wounds were photographed with a digital camera. The wound contraction of all the study groups was compared with the control group (no intervention was made on the dermal wounds) referring to previous study of Doç. Dr. Kemal Kismet.

2.2.5.4.1.4. Treatments with Scaffolds

All scaffolds were cut off into the same size with skin wound area and subsequently each wound was softly covered with; CS-X, CS-AuX, CS-BX, SFM, SFM-Au, SFM-B or MatridermTM ($n = 10$). In the control group (untreated control), defects moisturised with saline were covered with only surgical drapes (IobanTM incise drape, 3M Health Care, USA). In the study groups, CS-X, CS-AuX, CS-bX, SFM,

SFM-AuE, SFM-bE and Matriderm were applied onto previously moisturised defect sites and covered with Ioban™ surgical drapes again. All wounds were followed for 14 days and no complications developed during this period. All rats were euthanized with high-dose ketamine hydrochloride on postoperative 14th day.

2.2.5.4.1.5. Histopathological Analysis

The wound area was excised together with the scar tissue. All specimens were fixed in 10% phosphate-buffered formaldehyde solution for 24 hours at room temperature. Histopathological assays were performed in a blind manner by a pathologist. Specimens were washed in tap water and dehydrated through graded alcohol series. After passing through the routine histological series, tissues were embedded in paraffin blocks. Sections of 5 µm were cut, deparaffinised and rehydrated. Sections were counterstained with haematoxylin and eosin (H&E). The histopathological scores were given with respect to re-epithelization, inflammation, fibrosis and granulation tissue formation degrees. The intensities of polymorphonuclear leucocytes and mononuclear leucocytes and the extent of fibroblast proliferation and vascular proliferation were evaluated by inflammatory scoring to determine the general characteristics of scar tissue in the sections stained with H&E. The number of polymorphonuclear leucocyte and mononuclear leucocyte (inflammation) and the degrees of vascular proliferation (fibrosis) and fibroblast proliferation (granulation tissue) were measured on a numerical scale from 0 to 3 to determine inflammatory scores. Also, the degree of re-epithelization was scored on a numerical scale from 0 to 2.

2.2.5.4.1.6. The Examination of Wound Contraction Rate

Open wounds were drawn on graph acetate paper with a marker pen at day 0 and at 4th, 7th, 10th and 14th days. The surface area of the wounds was measured with a

planimetric programme on computer after scanning the acetate sheets. The percentage of contraction was calculated by the following formula:

$$\text{Percentage of contraction (at } n^{\text{th}} \text{ day)} = 100 - \frac{A_t}{A_0} \quad (8)$$

Where A_t and A_0 denotes total wound area at n^{th} day and total wound area at day 0, respectively.

2.2.5.4.1.7. Biomechanical Tests

Biomechanical testing was performed at 14th days of wounding. The mechanical properties of the harvested biopsy specimens were evaluated by applying tension test with Lloyd LS500 Material Testing Machine (Lloyd, England) using Nexygen computer software. Rectangular samples (5 x 50 mm) were cut from wound sites. After harvesting skin samples, they immediately underwent biomechanical testing. Cranial–caudal orientation was preserved and the healed wound, if present, was centrally located within the testing unit. The gauge length and width were 20 and 5 mm, respectively. The thickness of the test samples were calculated by means of vernier calliper and found to be about 1-2 mm. The crosshead speed of the system was adjusted to 10 mm/min to get a constant strain rate of 50 %/min. Before tests, all specimens were preloaded at 5 N to flatten the skin samples. To prevent slippage of the membranes from the grips they were covered with sand paper (60 grids) at the attachment site (Figure 2.13). The results of tests were obtained as load versus deflection curves which were then converted into stress-strain data by the computer program. Modulus of elasticity (E), ultimate tensile strength (UTS) and percent elongation at break (EB) was calculated ($n \geq 6$) from the stress-strain curves of samples. The recovery index was also calculated as the tensile strength of a treated specimen divided by the tensile strength of an unwounded specimen from the same rat.

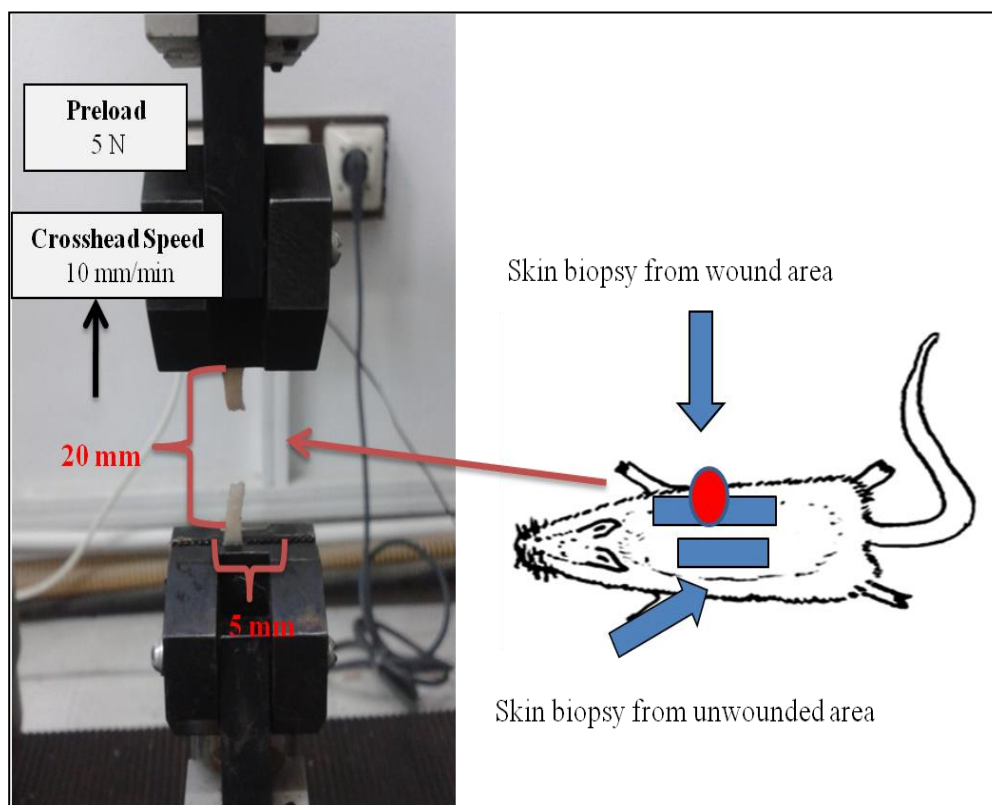


Figure 2.13. Experimental set up for performing biomechanical tests on rat skin biopsies

2.2.5.5. Toxicological Evaluation

The animal toxicology evaluation of one of the bilayered scaffold group (BLCS-AuX) containing all the possible toxic components and reagents (i.e., GTA and AuNPs) was made with intradermal irritation tests (ISO 10993-10: Animal intradermal reactivity test), skin sensitization (ISO 10993-10: Closed-patch test) and genotoxicity tests (ISO 10993-3, OECD 471: Bacterial reverse mutation test). All these tests were conducted by biocompatibility group in Hacettepe University, Faculty of Pharmacy Department of Pharmacology. Animal tests were approved by the Laboratory Animals Ethics Committee of Hacettepe University.

2.2.5.5.1. Skin Irritation Tests (Animal Intradermal Reactivity Test)

For medical devices intended to be used as an implant, the use of an intracutaneous (intradermal) reactivity test is indicated. An assessment is made of the potential of the material under test to produce irritation following intradermal injection of extracts of the material.

The test sample extract was prepared in accordance with ISO 10993-12. As there are multiple test sites on each animal, several test samples were applied together with the appropriate negative controls or blank. Healthy young adult albino rabbits of either sex from a single strain, weighing 2-3 kg, were used. The animals were acclimatized and cared for as specified in ISO 10993-2. Three animals were used to evaluate the test material.

Within a 4 h to 18 h period before testing, the fur on the backs of the animals was closely clipped, allowing a sufficient distance on both sides of the spine for injection of the extracts. 0.2 ml of the extract obtained with polar (physiological saline, 0.9 % m/v NaCl) or non-polar solvent (sesame oil) at five sites on one side of each rabbit was injected intracutaneously. The arrangements of the injection sites were presented in Figure 2.14. So, 0.2 ml of the polar or non-polar solvent control on five sites of the contralateral side of each rabbit was injected.

The appearance of each injection site was graded by an experienced person immediately after injection and at 24, 48 and 72 hours after injection. Tissue reaction for erythema and oedema were graded according to the system given in Table 2.6 for each injection site and at each time interval observed, and the results were recorded.

After the 72 hours grading, all erythema grades plus oedema grades 24, 48 and 72 hours were totalled separately for each test sample or blank for each individual animal. To calculate the score of a test sample or blank on each individual animal, each of the totals was divided by 15 (3 scoring time points \times 5 test or blank sample injection sites). To determine the overall mean score for each test sample and each corresponding blank, the scores for the three animals were added and divided by

three. The final test sample score was obtained by subtracting the score of the blank from the test sample score. The requirements of the test were met if the final test sample score was 1 or less.

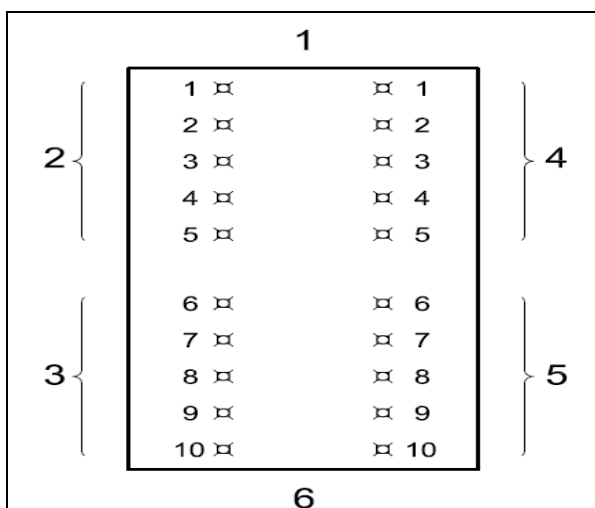


Figure 2.14. Arrangement of injection sites (1: cranial end, 2: 0.2 ml injections of polar extract, 3: 0.2 ml injections of non-polar extract, 4: 0.2 ml injections of polar solvent control, 5: 0.2 ml injections of non-polar solvent control, 6: caudal end).

Table 2.6. Grading system for intracutaneous (intradermal) reactions

Reaction	Numerical grading
Erythema and eschar formation	
No erythema	0
Very slight erythema (barely perceptible)	1
Well-defined erythema	2
Moderate erythema	3
Severe erythema (beet-redness) to eschar formation preventing grading of erythema	4
Oedema formation	
No oedema	0
Very slight oedema (barely perceptible)	1
Well-defined oedema (edges of area well-defined by definite raising)	2
Moderate oedema (raised approximately 1 mm)	3
Severe oedema (raised more than 1 mm and extending beyond exposure area)	4
Maximal possible score for irritation	8
Other adverse changes at the injection sites shall be recorded and reported.	

2.2.5.5.2. Skin Sensitization Tests (Closed-patch Test)

An assessment is made of the potential of the material under test to produce skin sensitization in guinea pigs. The test sample was prepared according to ISO 10993-12. Healthy young adult albino guinea pigs of either sex from a single outbred strain,

weighing 300 g to 500 g at the start of the test, were used. The animals were acclimatized and cared for as specified in ISO 10993-2. Ten animals were treated with the test sample, and five animals acted as a solvent control group.

The fur on all treatment sites prior to all steps in the test procedure was closely clipped or shaved. For all topical applications, a patch of the appropriate dimensions (25 mm x 25 mm) was saturated with the extract (0.5 ml) and applied to the clipped area under an occlusive dressing for 6 hours. The test sample was administered by topical application to the clipped left upper back region of each animal using appropriate patches soaked. The restrainer of any occlusive dressings and patches were removed after 6 hours. This procedure was repeated on three days a week for three weeks. The control animals were treated similarly, using the blank liquid alone. At 14 days after the last induction application, all test and control animals were challenged with the test sample. The test sample was administered by a single topical application to a clipped untested area of each animal using appropriate patches soaked in the test sample. The restrainer and occlusive dressings and patches were removed after 6 hours. At 24 hours and 48 hours after removal of the challenge patch, the test sites were graded using the scale given in Table 2.7.

Table 2.7. Magnusson and Kligman scale

Patch test reaction	Grading scale
No visible change	0
Discrete or patchy erythema	1
Moderate and confluent erythema	2
Intense erythema and/or swelling	3

The Magnusson and Kligman grading scale given in Table 2.7 were applied. Grades of 1 or greater in the test group generally indicate sensitization, provided that grades of less than 1 are seen on control animals. If grades of 1 or greater are noted on control animals, then the reactions of test animals which exceed the most severe control reaction are presumed to be due to sensitization.

2.2.5.5.3. Genotoxicity Tests (Bacterial Reverse Mutation Test)

Fresh cultures of bacteria were grown up to the late exponential or early stationary phase of growth (approximately 10^9 cells per ml). At least five strains of bacteria were used according to OECD 471 standards. The bacteria strains were: 1) *S. typhimurium* TA1535, 2) *S. typhimurium* TA1537, 3) *S. typhimurium* TA98, 4) *S. typhimurium* TA100, 5) *E. coli* WP2 uvrA. An appropriate minimal agar (e.g. containing Vogel-Bonner minimal medium E and glucose) and an overlay agar containing histidine and tryptophan, to allow for a few cell divisions, is used. Metabolic activation system was a cofactor supplemented post-mitochondrial fraction (S9) prepared from the livers of rodents treated with enzyme-inducing agents (Aroclor 1254). The post-mitochondrial fraction was used at concentrations of 30% v/v in the S9-mix. Negative controls solvents were physiological saline and DMSO, on the other hand positive control chemicals were given in Table 2.8.

Table 2.8. Positive control chemicals for genotoxicity.

Control chemicals	Solvent	Strain
2-Aminoatrasen	DMSO	Salmonella strains + S9 E.Coli strains + S9
9-Aminoacridine HCl	Distilled water	TA1535
4-nitroquinoline 1-oxide	DMSO	TA100; EC002; EC188
N4-Aminocytidine	Distilled water	TA100; TA1535
2-Nitrofluorene	DMSO	TA98

Scaffolds were extracted according to ISO 10993-12 standards. Test sample extracts were obtained in both physiological saline (0.9 % m/v NaCl) (test extract 1) and dimethyl sulfoxide (DMSO) (test extract 2) during 72 hours incubation period at 37 °C. Negative controls were physiological saline (negative control 1) and DMSO (negative control 2).

MOLTOX® FTTM test kit was used to assess the mutation effect of test sample such that either *Salmonella typhimurium* or *Escherichia coli* (amino-acid requiring strain histidine or tryptophan, respectively) could produce a strain independent of histidine (his + revertant) and tryptophan (trp + revertant). With MOLTOX® FTTM test kit, the defined bacteria strains (approximately 10^7 bacteria cells) were incubated in medium containing test samples, positive and negative controls and a specified amount of histidine (*Salmonella typhimurium*) or tryptophan (*Escherichia coli*) concentration to doubled population. After the incubation period, bacteria cultures were diluted in chemical medium with pH indicator and without histidine or tryptophan. These bacteria dilutions subjected to different test groups were transferred to 48 wells (50 µl) of 384 well plates. After 48 hours incubation period, bacteria (his+ revertant and trp + revertant) proliferation caused to a change of colour

in wells from purple to yellow due to increase in medium acidity. The blurry and yellow colour inside wells indicated changing bacteria populations. Spectrophotometric measurements were done at 600 nm wavelength to determine the bacteria number. The reversed bacteria number in wells containing tests sample was compared to the reversed bacteria number in wells containing negative controls. The genotoxicity of test sample metabolites was assessed with metabolic activation system blend 30 % S9. When the p value of test samples were less than 0.05 ($p < 0.05$) compared to the negative controls (One-way Analysis of Variance and post-hoc Bonferroni tests), this implied biological significance, that is mutagenic activity was induced in the treated population significantly.

2.2.6. Statistical Analysis

In comparing the groups for a single parameter One-way Analysis of Variance (ANOVA) test was done with Tukey's, or Bonferroni Multiple Comparison Test for the post-hoc pairwise comparisons using SPSS-22 Software Programme (SPSS Inc., USA). Differences were considered significant for $p < 0.05$.

CHAPTER 3

RESULTS AND DISCUSSION

3.1. Synthesis and Characterization of Gold Nanoparticles

3.1.1. Characterization of Gold Nanoparticles for Preliminary Synthesis Tests

AuNPs in the size range of 12 to 55 nm were synthesized with citrate reduction and capping method in the first set of experiments. For synthesis, gold salt solution temperature (boiling point), stirring rate (800 rpm), the molarity of gold salt (1 mM), the start volume (20 ml) and the concentration of the trisodium citrate were all kept constant (1%). The only variable was the volume of the citrate added (1-5 ml). Therefore, AuNPs synthesized with this method were labelled as Au1 (1 ml citrate), Au2 (2 ml citrate), Au3 (3 ml citrate), and Au4 (4 ml citrate). Formation of AuNPs was observed with calorimetric differences initially (Figure 3.1).

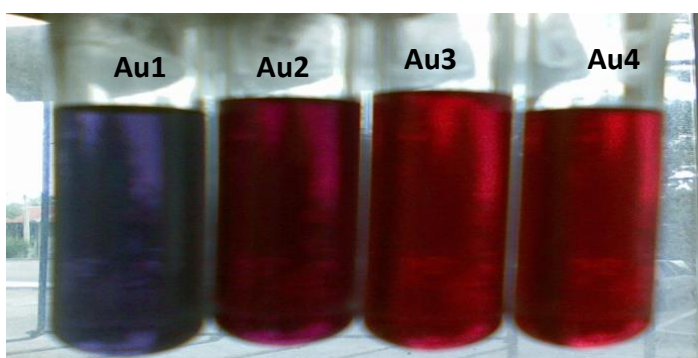


Figure 3.1. The calorimetric verification of gold nanoparticle synthesis.

The synthesized AuNPs had stock concentration of 157 ppm in distilled water at the end of the experiment and were diluted to the desired concentrations for further characterization tests. The stability of the AuNPs in d-water was high, but after a certain period of time they tended to agglomerate and settle down to the bottom of the tube. To overcome this problem, AuNPs were prepared freshly before the experiments and/or subjected to vortexing and sonication processes at specific time intervals when they were stocked for longer periods of time. Especially the bigger nanoparticles were more prone to agglomerate, thereby to settling. These nanoparticles were also more difficult to separate from each other. The size of AuNPs tended to decrease when the volume of citrate increased until a certain degree (citrate volume= 3ml). Au1 group nanoparticles had the largest average diameter (55.34 ± 8.53 nm) with statistically significant difference from the other groups. Also, Au2 group had bigger AuNPs than the other groups; Au3 and Au4. However, there were no significant size differences between groups Au3 and Au4 (13.09 ± 1.72 nm and 11.57 ± 1.22 nm, respectively) (Figure 3.2). Size distribution of Au1 and Au2 groups were not uniform, but a more uniform distribution was obtained for Au3 and Au4 groups. Also, in Au1 group, different shaped particles (pyramid, cylindrical rods, triangles and rectangular) were formed as distinct from spherical ones. Upon increasing the citrate volume, the number of spherical particles increased. Considering all these experimental results, sufficient control over the particle size, size distribution and shape of AuNPs was thought to be too difficult for obtaining larger particles.

To increase the control on particle size distribution and shape for larger particle sizes (>20 nm), variations in experimental conditions (temperature control, stirring rate) and/or related with preparation of reaction solutions (adjusting the molarity of low concentrations and obtaining homogenous solutions) were evaluated. The temperature of the gold salt was tried to be kept constant during the reduction reaction of AuNPs synthesis. The volume of the boiling gold salt solution was maintained by closing the top of the flask. For this purpose, reflux systems were used generally, but it was stated that reflux systems would likely to produce heat gradient in the solution (Kimling et al., 2006).

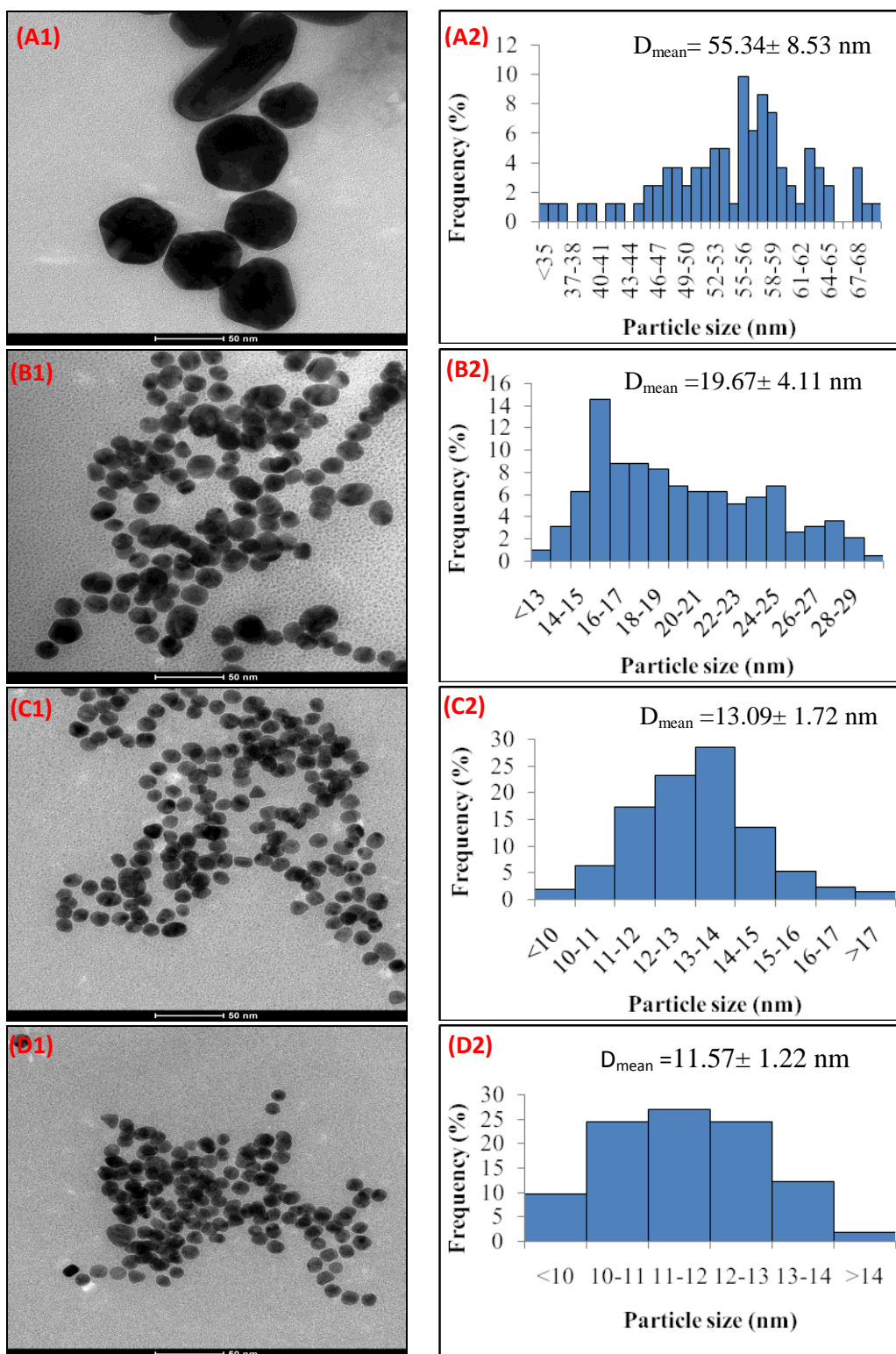


Figure 3.2. TEM micrographs and size distribution histograms of synthesized different AuNPs groups: (A1-A2) Au1, (B1-B2) Au2, (C1-C2) Au3 and (D1-D2) Au4.

Apart from these, reaction temperature for the AuNPs synthesis (here the reaction occurs at boiling point, around 100 ° C) could be lowered to 70-85 ° C. At lower temperatures, the reaction rate slows down and the control over particle size distribution was enhanced (Li et al., 2011). The alkalinity of the gold salt solution could also be increased with bases for better control (Li et al., 2011). In the literature, replacing the reducing agent (citrate) with ascorbic acid or initiating the reduction reaction with UV radiation at room temperature 25 °C instead of heating process was suggested for obtaining a more uniform particle size distribution and more spherical particles for AuNPs (Kimling et al., 2006).

3.1.2. Characterization of Optimized Gold Nanoparticles

Considering the above tips for optimizations, AuNPs having a larger size range (between 20 and 50 nm) were synthesized in the second set of experiments. At the step of AuNPs synthesis, again gold salt solution temperature (boiling point), stirring rate (800 rpm), the molarity of gold salt (1 mM), the start volume of it (20 ml) were all kept constant, but the concentration of the trisodium citrate solution (0.1%) and volume of the citrate added (5-10 ml) were varied. By virtue of this, the synthesized AuNPs were labelled as Au5 (5 ml citrate), Au6 (6 ml citrate), Au7 (7 ml citrate), Au8 (8 ml citrate), Au9 (9 ml citrate), Au10 (10 ml citrate). Eventually, spectrophotometric measurements were made to determine the approximate size of AuNPs before the exact assessment with TEM analysis. The average particle size was estimated from the peak absorbance wavelength using the experimental results as described by Kimling et al. (2006). The relationship between particle diameter and peak wavelength was derived graphically with a least-squares cubic polynomial best-fit line. Sizes were estimated according to the following equation derived from the data of Kimling et al. (2006).

$$\lambda_m = 5 \times 10^{-5} d^3 - 0.0058 d^2 + 0.6335 d + 510.83 \quad (1)$$

In equation 1, d is the average AuNPs diameter and λ_m is the peak absorbance wavelength. For this experiment, Equation 1 can be used iteratively to estimate the AuNPs diameter which closely approximates the respective peak absorbance wavelength. The spectral scan results of the second set of AuNPs groups (Au5-Au10) and their approximated diameters derived by using equation 1 were given in Figure 3.3.

According to TEM results, meaningful differences were not encountered with the amount of sodium citrate added, except for Au10 group (Figure 3.4). Nevertheless, when the citrate was increased the size distribution and uniformity of shape of the AuNPs were enhanced. Different AuNPs shapes (rectangular, triangular or rod-like) other than spherical particles were observed more pronouncedly with lower volumes of citrate (Au6, Au7). After this volume, the number of spherical particles in the AuNPs solutions was dominant (Au8, Au9 and Au10). The shape and size distribution of Au8 and Au9 groups were very similar. Au10 group had AuNPs smaller than 20 nm, which was supposed to have a potential to cause nanotoxicity according to preliminary cytotoxicity tests. Considering all of these results, Au7 and Au8 groups were selected to be used for further in vitro cell viability experiments and Au8 was decided to be the most appropriate group to be used in electrospinning solutions after preliminary cytotoxicity tests.

Similar spherical and monodispersed AuNPs with the size range of 10-30 nm were obtained in different studies using Turkevich method (Zhou et al., 2012; Schlinkert et al., 2015; Agarwal et al., 2014). Nanoparticles were shown to have tendency to aggregate and they subsequently precipitate (Zhou et al., 2012; Agarwal et al., 2014). In this study, this common problem was tried to be solved by applying sonication and vortexing the stock AuNPs before the tests. When the original red color, a clear indication of AuNPs, shifted to blue, this was accepted as sign of aggregation of AuNPs. AuNPs synthesized in this study absorb at 500-600 nm as a result of the excitation of surface plasmons, which shift to longer wavelengths when aggregates form.

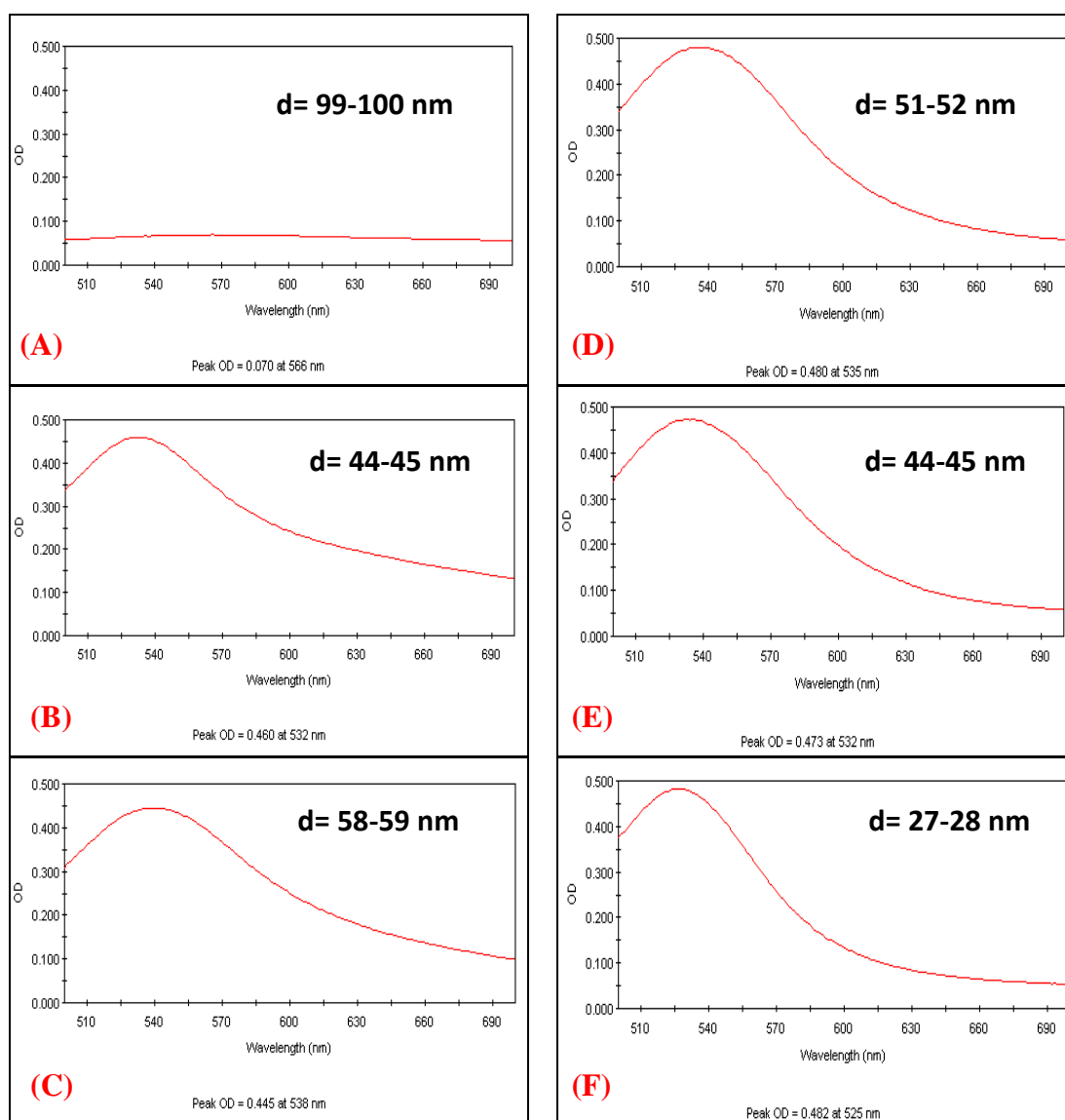


Figure 3.3. The spectral scan results of different AuNPs groups between 500 and 700 nm wavelength and their estimated diameters: (A) Au5, (B) Au6, (C) Au7, (D) Au8, (E) Au9, (F) Au10.

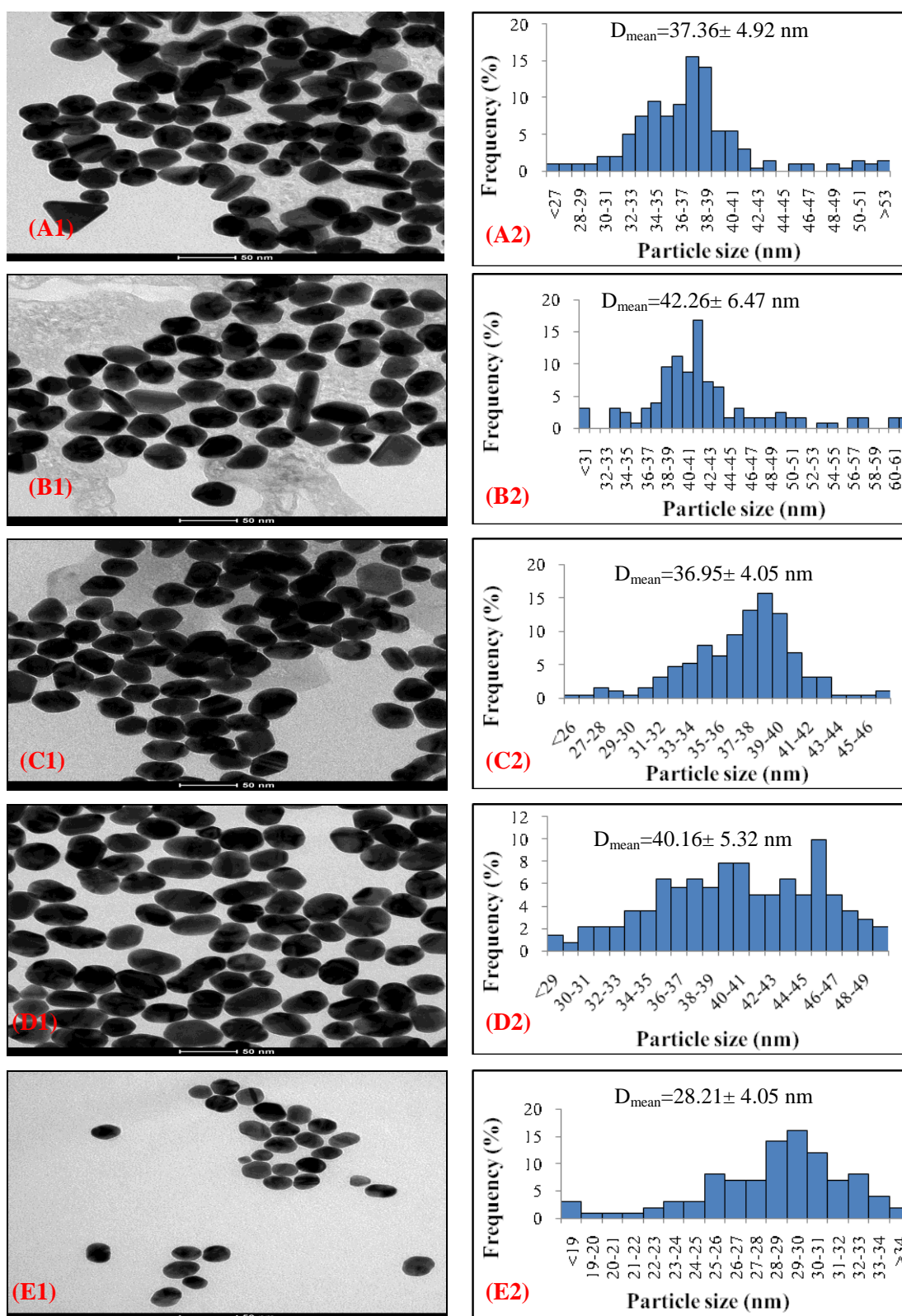


Figure 3.4. CTEM micrographs and size distribution histograms of different AuNPs groups: (A1-A2) Au6, (B1-B2) Au7, (C1-C2) Au8, (D1-D2) Au9 and (E1-E2) Au10.

3.2. Preparation and Morphological Characterization of Collagen Sponges

3.2.1. Optimization of Lyophilization Process for Collagen

According to our optimization studies related to the lyophilisation of collagen, mainly two parameters, that is collagen solution concentration and freezing temperature affected the final product properties. Different collagen concentrations were tried (0.4, 1 and 2%) and it was concluded that 1 % was the best concentration. Sponges produced using 0.4% collagen concentration was too porous, and soft. Upon contact with aqueous environments, the 3D structure of sponges deteriorated immediately. On the contrary, 2% concentration was too high yielding very solid and nearly non-porous structures. As a result, the medium solution concentration of collagen (1%) was selected to be the optimum one.

3.2.2. Chemical Treatment of Collagen Sponges

GTA cross-linking has been selected for cross-linking of collagen based scaffolds due to the reasons that it is a bi-functional cross-linking reagent that can bridge amino groups between two adjacent polypeptide chains and has become the predominant choice in skin tissue engineering because of its water solubility, high cross-linking efficiency and low cost (Jorge Herrero et al., 1999). While cross-linking the collagen sponges the free amino groups of collagen and lysine or hydroxylysine amino acid residues of the polypeptide chains react with the aldehyde groups of GTA. After GTA treatment for 2 hours, the white color of collagen sponges shifted to yellowish. This colour change is due to the establishment of $\text{CH}\equiv\text{N}$ linkages between the free amine groups of collagen and GTA (Zhang et al., 2006). The sponges did not shrink dimensionally, because all the scaffolds were rehydrated in d-water for 15 min firstly before GTA cross-linking. The prospective toxicity problems related to GTA in further in vitro or in vivo studies was avoided by

using a low concentration (3%) and by blocking the un-reacted aldehyde residues with glycine solution.

3.2.3. Incorporation of Gold Nanoparticles into Collagen Sponges

Two different methods were tried to load AuNPs into scaffolds. In the first method, scaffolds were incorporated with AuNPs by soaking them into a solution containing 14.27 ppm AuNPs. In the second method, AuNPs were added into collagen solutions to impregnate them inside the scaffold before the lyophilisation process. AuNP distribution within the collagen sponges was uniform in the first method (Figure 3.5 A-B). Especially, AuNPs could be seen more clearly on the cross-linked collagen sponge (Figure 3.5B). On the contrary, it was very hard to distinguish AuNPs that were impregnated inside the collagen sponges (Figure 3.5C-D). AuNPs situated on the surface layer of sponges could be traced hardly. Therefore, it was supposed that AuNPs dwelled in the deeper portion of sponges or even embedded within the polymer matrix of the sponges.

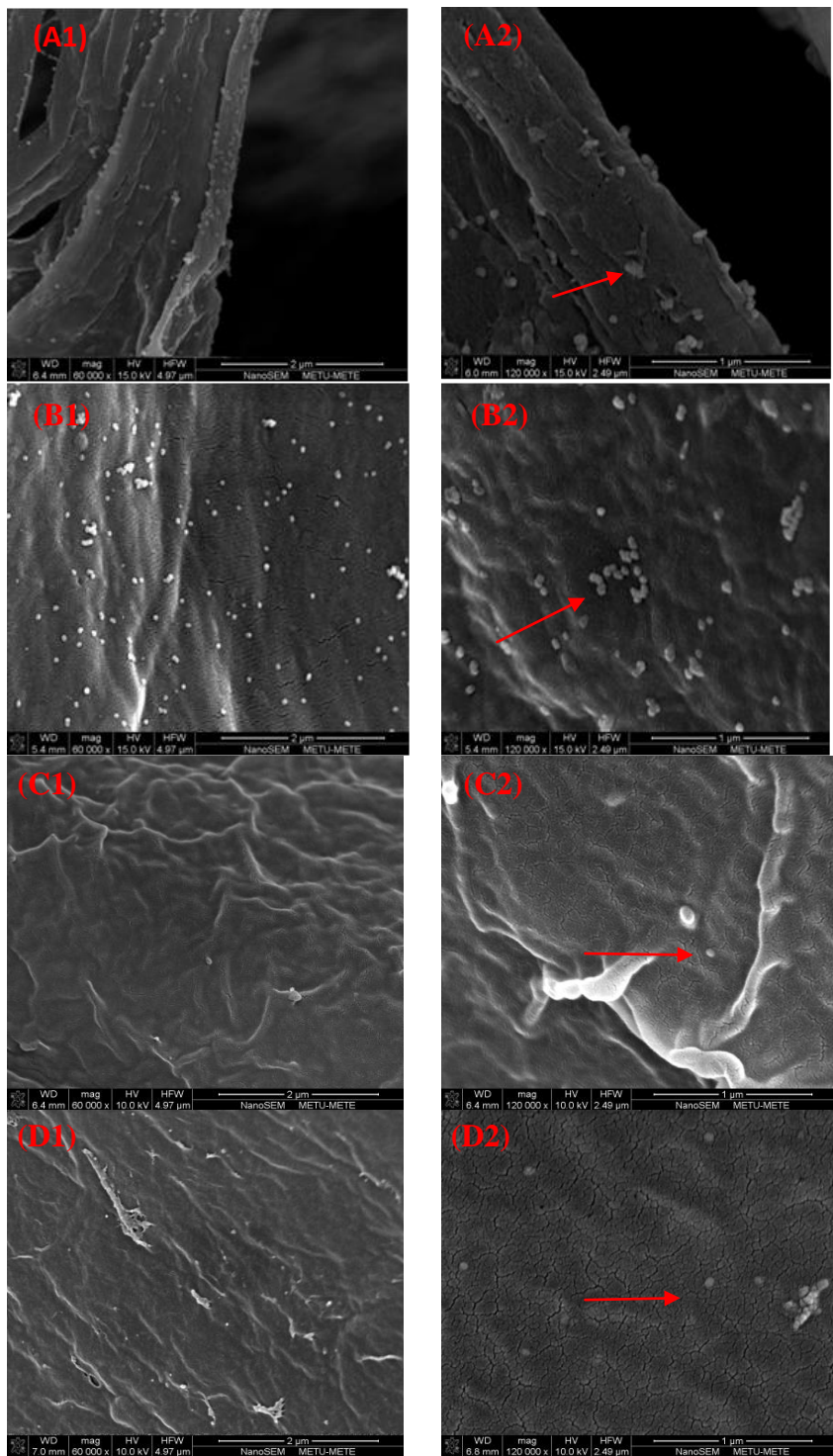


Figure 3.5. SEM micrographs of scaffolds incorporated with AuNPs by soaking them into AuNPs solution: (A1-A2) CS-Au, (B1-B2) CS-AuX, or by adding AuNPs into collagen solutions: (C1-C2) CS-Au and (D1-D2) CS-AuX. Arrows indicate AuNPs.

3.2.4. Morphology of Collagen Sponges

It is known that the microstructure such as pore size and its distribution, porosity as well as pore shape has prominent influence on cell intrusion, proliferation and function in tissue engineering. The top and side view morphologies of the collagen sponge scaffolds before (CS and CS-Au) and after (CS-X, and CS-AuX) GTA cross-linking were shown in Figure 3.6. The pore sizes of the uncross-linked scaffolds were quite large (10-200 μm), interconnected with cylindrical channels and tubular structures suggesting their suitability to cell migration (Figure 3.6 A and C). The interconnected 3D porous structures of the scaffolds were retained after GTA treatment; however, some significant changes occurred with respect to pore size and morphology (Figure 3.6 B and D). It was observed that the size of the pores was decreased and some cylindrical channels and tubular structures had shrunk slightly after cross-linking and subsequent drying processes. The pores almost merged to each other in some regions of sponges, but there were still tubular passage connections between the pores. It was supposed that the morphology difference was caused by both GTA and re-lyophilization process after the GTA cross-linking treatment. The additional refreeze-drying might have induced the collagen fibers to be combined again to form sheets, leading to the fusion of some smaller pores to generate larger ones. On the other hand, the GTA treatment had an opposite effect to the pore fusion; i.e., reducing the pore size. These two competing processes having antagonistic effects caused to the final structure of the collagen sponges.

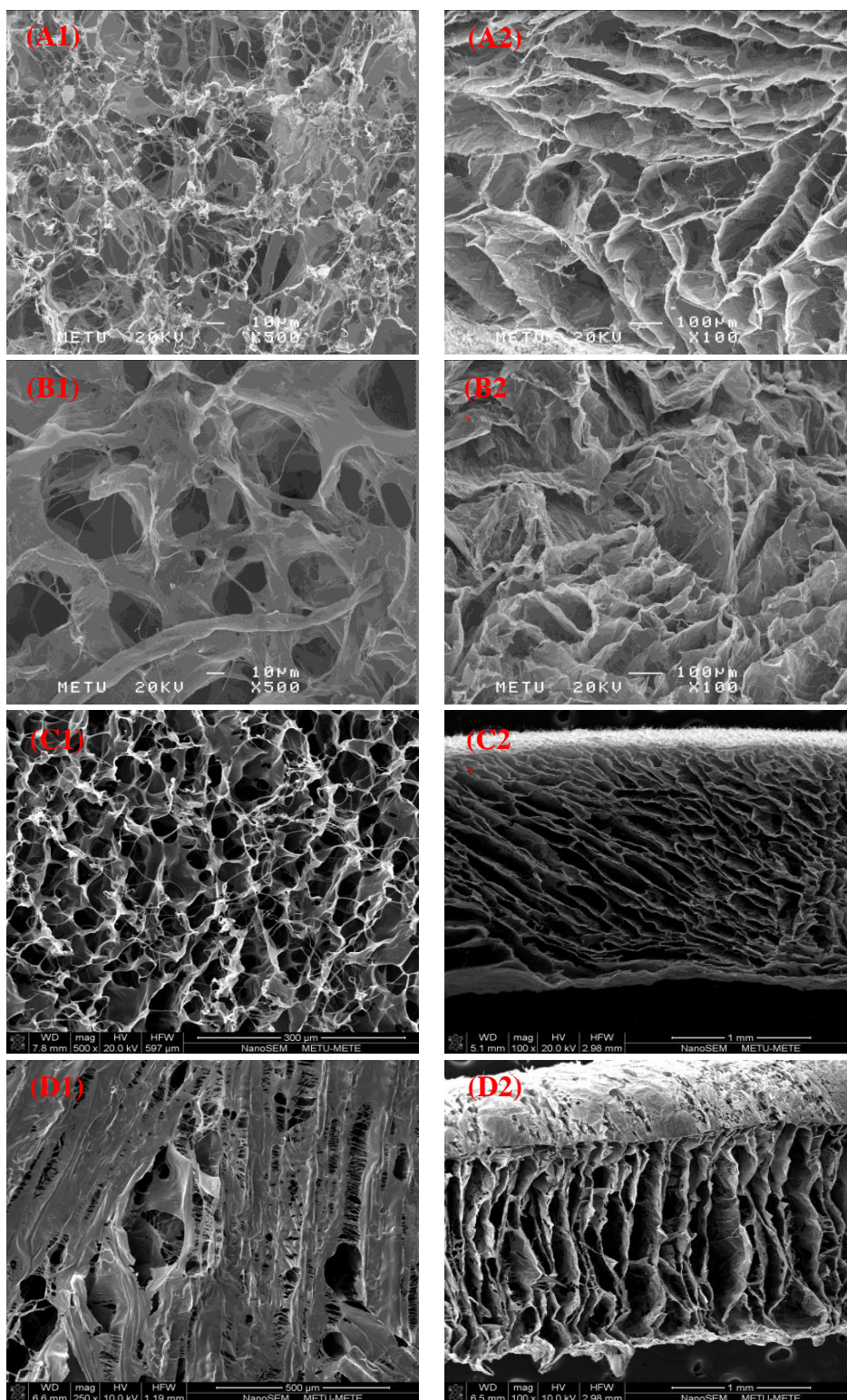


Figure 3.6. SEM micrographs of collagen sponge groups: (A1-A2) CS, (B1-B2) CS-X, (C1-C2) CS-Au and (D1-D2) CS-AuX. Left and right columns indicate the top and side view, respectively.

3.3. Preparation and Morphological Characterization of Collagen Nanofibrous Matrices

3.3.1. Optimization of the Electrospinning Process for Collagen

According to our preliminary studies, electrospun matrices could not be obtained from only collagen solutions dissolved in 0.5 M acetic acid solvent. Collagen dissolved in dilute acetic acid could not form nanofibers during electrospinning due to their low charges and low viscosities. Similarly, Huang et al. (2001) could not achieve to prepare continuous collagen fibers from collagen solutions, so they used poly (ethylene oxide) (PEO) to aid in the electrospinning process as well. The same strategy was used by other researchers to improve the electrospinnability of collagen/elastin (Buttafoco et al., 2006), collagen/chitosan (Chen et al., 2008), chitosan (Bhattacharai et al., 2005), and silk fibroin (Jin et al., 2004) solutions. Hence, following the same strategy, PEO was used in this study to increase the spinnability of solutions. The best electrospinning processing parameters, that is the optimum collagen and PEO concentration, total polymer concentration, voltage, flow rate, and needle to collector gap distance were tried to be determined. After numerous trials, P1.5 (1.5% PEO) and P2.5 (2.5% PEO) groups were decided to be appropriate for electrospinning collagen solution, but P3.5 group (3.5% PEO) was too viscous to be electrospun. Addition of PEO to collagen solutions resulted in the formation of nanofiber accumulation on the collector, but still these nanofibrous matrices could not be obtained intact during removal from the collector. It was stated in literature that the nanofibers fused to each other in cases that collagen was not dissolved well (Zeugolis et al., 2008). For this reason, a short heat treatment was applied to collagen solutions and they were filtered through 100 μm to improve the homogeneity of the solution before mixing them with PEO solutions. Successful electrospun matrices were obtained from only PEO solutions (1.5% and 2.5%) and from mixtures of PEO and collagen. However, the nanofibrous mats obtained from the blends had abundance of liquid droplets.

It was recommended that a certain amount of salt would increase the conductivity when added to the collagen/PEO blend solutions to solve the morphological problems related to the nanofibers and to get a more uniform nanofiber distribution (Chen et al., 2011). Therefore, 40 mM salt was also added to the blend mixtures (Table 3.1). However, successful nanofibrous structures could not be formed with only collagen solutions (Col1S, Col2S) containing 40 mM salt. Therefore, it was concluded that it was nearly unlikely to obtain successful nanofibers from collagen only solutions, even with salt supplement. Collagen/PEO blend groups supplemented with salt (Col1P1S, Col1P1.5S, Col1P2.5S, Col2P1S, Col2P1.5S, and Col2P1.5S) provided fibrous structures, but at the same time showed morphological defects such as small droplets. In none of the salt supplemented groups, a matrix with the desired properties (that could be peeled off from the collector without any deformation) could be obtained. Electrospun matrices obtained from the blends of collagen and PEO had deformations (such as beads, liquid droplets etc).

Table 3.1.The properties of nanofibers in the preliminary experimental groups

Groups *	The properties of the structure accumulated on the collector	Properties of the solution
Col1S	No fibrous structure	Low viscosity, transparent solution.
Col2S	No fibrous structure	Viscosity is higher than C1t, solution is transparent.
Col1P1S	Fibrous structure, but many liquid droplets.	Viscosity is suitable for electrospinning, solution is transparent.
Col1P1.5 S	Fibrous structure, but many liquid droplets (Less than Col1SP1).	Viscosity is higher than Col1P1S, solution is transparent.
Col1P2.5S	Fibrous structure, but many liquid droplets (Less than Col1P1.5S)	Viscosity is higher than Col1P1.5 S, solution is transparent.
Col2P1S	No continuous fiber jet flow, many liquid droplets	Viscosity is very high, solution is transparent.
Col2P1.5S	No continuous fiber jet flow, many liquid droplets	Viscosity is very high, solution is transparent.
Col2P2.5S	No continuous fiber jet flow, many liquid droplets	Viscosity is very high, solution is transparent.

* Types of the polymers in the groups and their ratios in the blends were given in Table 2.1.

3.3.2. Incorporation of Gold Nanoparticles into Collagen Nanofibrous Matrices

In order to be able to alleviate the problems encountered so far, AuNPs were added to Collagen/PEO blends. As a result, more successful nanofibrous structures were obtained (Table 3.2). The spinnability of collagen only solutions supplemented with AuNPs was also checked before electrospinning experiments of blend solutions supplemented with AuNPs. As expectedly, no fibers were obtained for these groups. In the col/PEO blend groups to which different amounts (0.14, 1.42, 7.13, 14.27 ppm) of AuNPs were added, it was accomplished to get nanofibrous matrices. As it was decided in the previous electrospinning optimization studies, the most successful matrices were again obtained in the groups having 2.5% PEO. Increasing the collagen concentration from 1% to 2% resulted in an unexpected increase in the viscosity. Consequently, this prevented the continuous and uniform fiber jet outflow from the syringe tip during electrospinning process. Hence, 1% collagen concentration was selected to be the most appropriate concentration for electrospinning with AuNPs. Also, the increase in the amount of AuNPs added to collagen solutions enhanced the morphology and size distribution of nanofibers (Table 3.2). As a result of the previous studies, AuNPs from the Au8 group were incorporated into collagen/PEO solutions. The collagen nanofibrous matrix (P2.5Col1Au14) selected as the best group in our study had collagen nanofiber diameter similar to human ECM (Duan et al., 2013). Collagen nanofiber diameters produced in other studies related to skin tissue engineering were in the range of about 100-500 nm (Zhou et al., 2015.; Hsu et al., 2010; Rho et al., 2006; Chen et al., 2008), similar to the nanofiber size range of our study.

The appearance of AuNPs inside the nanofibers was viewed with TEM (Figures 3.7). Identification of the AuNPs inside the nanofibers was very difficult for lower concentrations of AuNPs (Figure 3.7). However, detecting the AuNPs in the nanofibers became much easier in the groups in which greater amounts of AuNPs (7.13 and 14.27 ppm) were supplemented.

Table 3.2. The properties of nanofibers incorporated with AuNPs

Groups *	The properties of the structure accumulated on the collector	Properties of the solution
Col1Au0	Only liquid droplets	Viscosity is very low, solution is transparent.
Col2Au0	Only liquid droplets	Viscosity is very low (higher than Col1Au10), solution is transparent
Col1P2Au0	Fibrous structure, no liquid droplets.	Viscosity is suitable for electro-spinning, solution is transparent
Col1P2Au1	Fibrous structure, no liquid droplets.	Viscosity is suitable for electro-spinning, solution is transparent
Col1P2.5Au0	Fibrous structure, no liquid droplets.	Viscosity is suitable for electro-spinning, solution is transparent
Col1P2.5Au1	Fibrous structure, no liquid droplets.	Viscosity is suitable for electro-spinning, solution is transparent
Col1P2.5Au7	Fibrous intact structure	Viscosity is suitable for electro-spinning, solution is transparent
Col1P2.5Au14	Fibrous intact structure	Viscosity is suitable for electro-spinning, solution is transparent

* Types of the polymers in the groups and their ratios in the blends were given in Table 2.2.

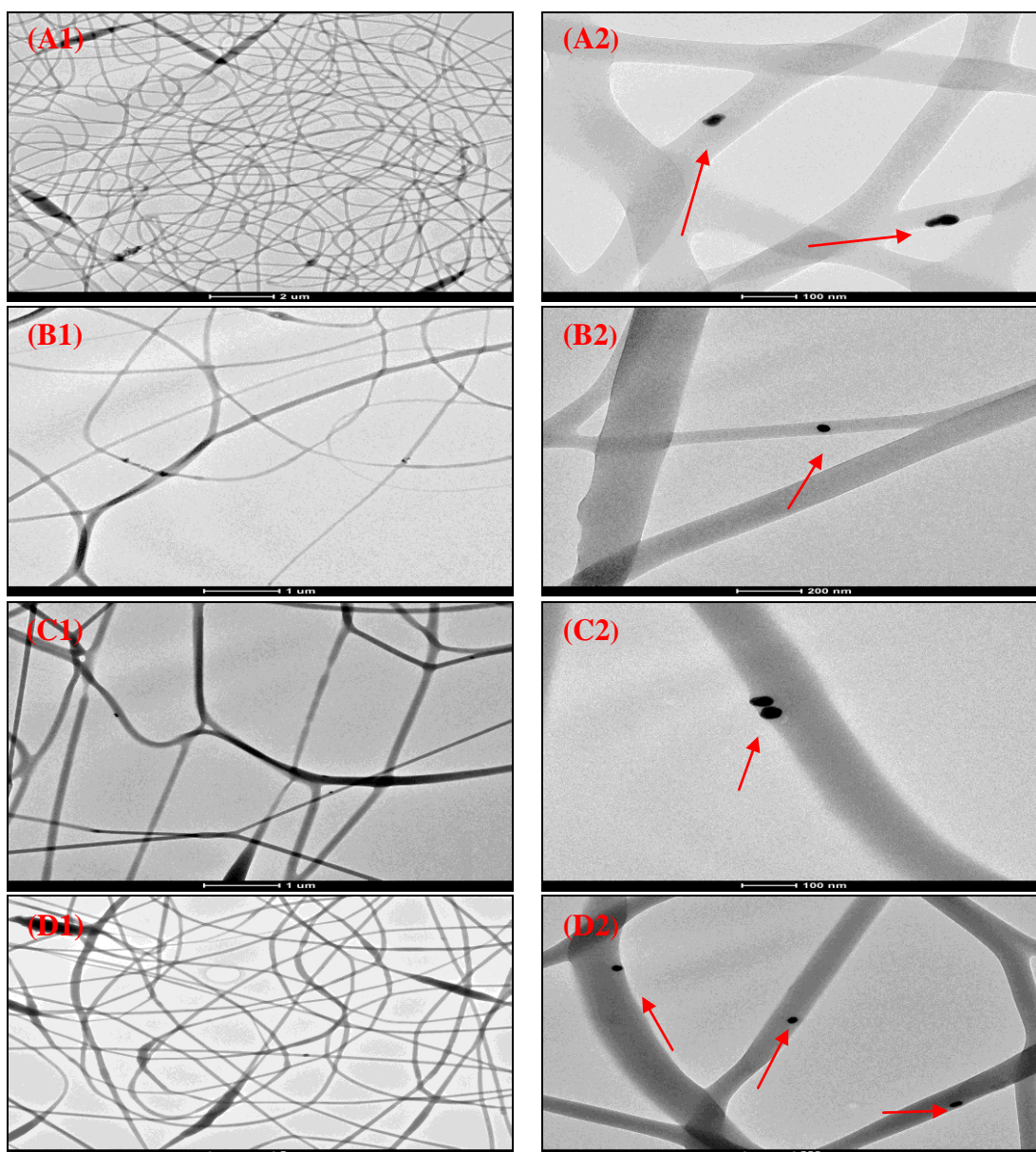


Figure 3.7. TEM micrographs of nanofibrous matrix groups: (A1-A2) P2.5Col1Au0, (B1-B2) P2.5Col1Au1, (C1-C2) P2.5Col1Au7 and (D1-D2) P2.5Col1Au14 groups. Red arrows indicate AuNPs. Figures on the right hand side indicate the magnified images.

3.3.3. Morphology of Collagen Nanofibrous Matrices

Although nanofibrous matrices were obtained successfully in groups to which AuNPs were added, micron sized film-like structures (droplet shape) were recognized in the matrices. In the case of collagen/PEO blends (1:2) with the low AuNPs concentrations (0.14 and 1.42 ppm) these morphological defects were more distinct (Figure 3.8). In order to diminish the micro droplets, the first step was to increase the PEO concentration from 2% to 2.5%. Together with this, as the amount of AuNPs was increased from 0.14 ppm to 1.42 ppm, there was a pronounced decrease in the number of droplets and enhancement in the uniformity of nanofibers (Figure 3.9 A-B). Eventually, the concentration of PEO was selected as 2.5% PEO and AuNPs amount was increased still further (7.13 and 14.27 ppm). So, almost all the micro droplets disappeared and the nanofiber structure were improved (Figures 3.9 C-D). Therefore, a skin tissue scaffold with a homogenous structure and negligible structural deformations were successfully fabricated from the group containing 14.27 ppm AuNPs.

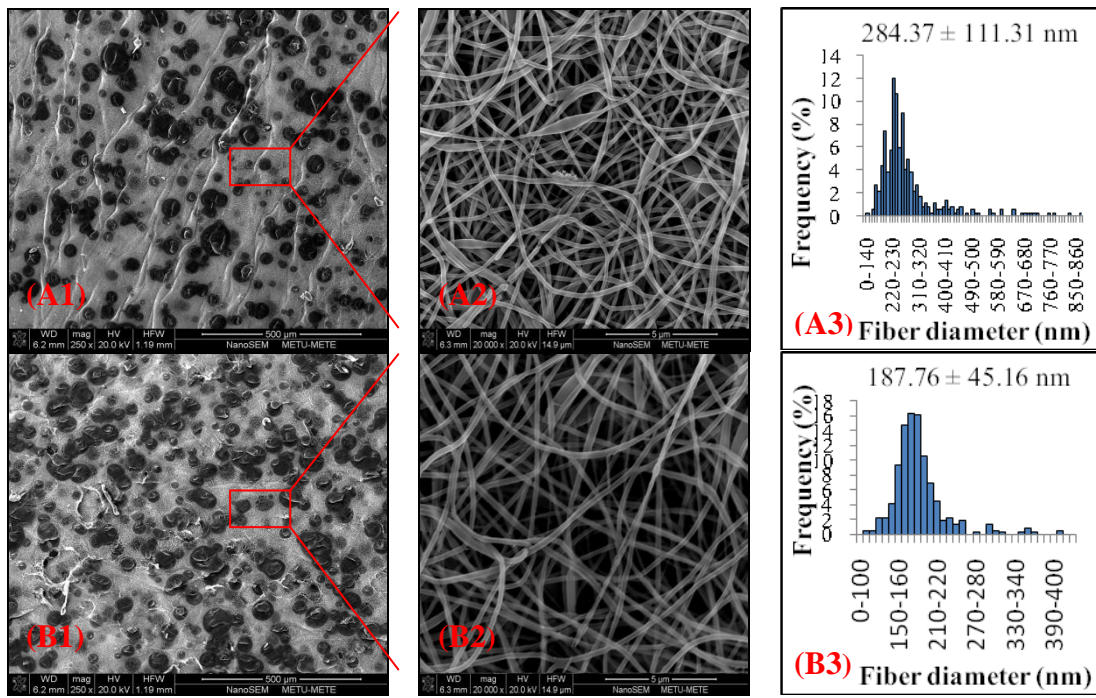


Figure 3.8. SEM micrographs showing the fiber morphology and fiber diameter distribution of different matrices: (A1-A3) Col1P2Au0 and (B1-B3) Col1P2Au1 group.

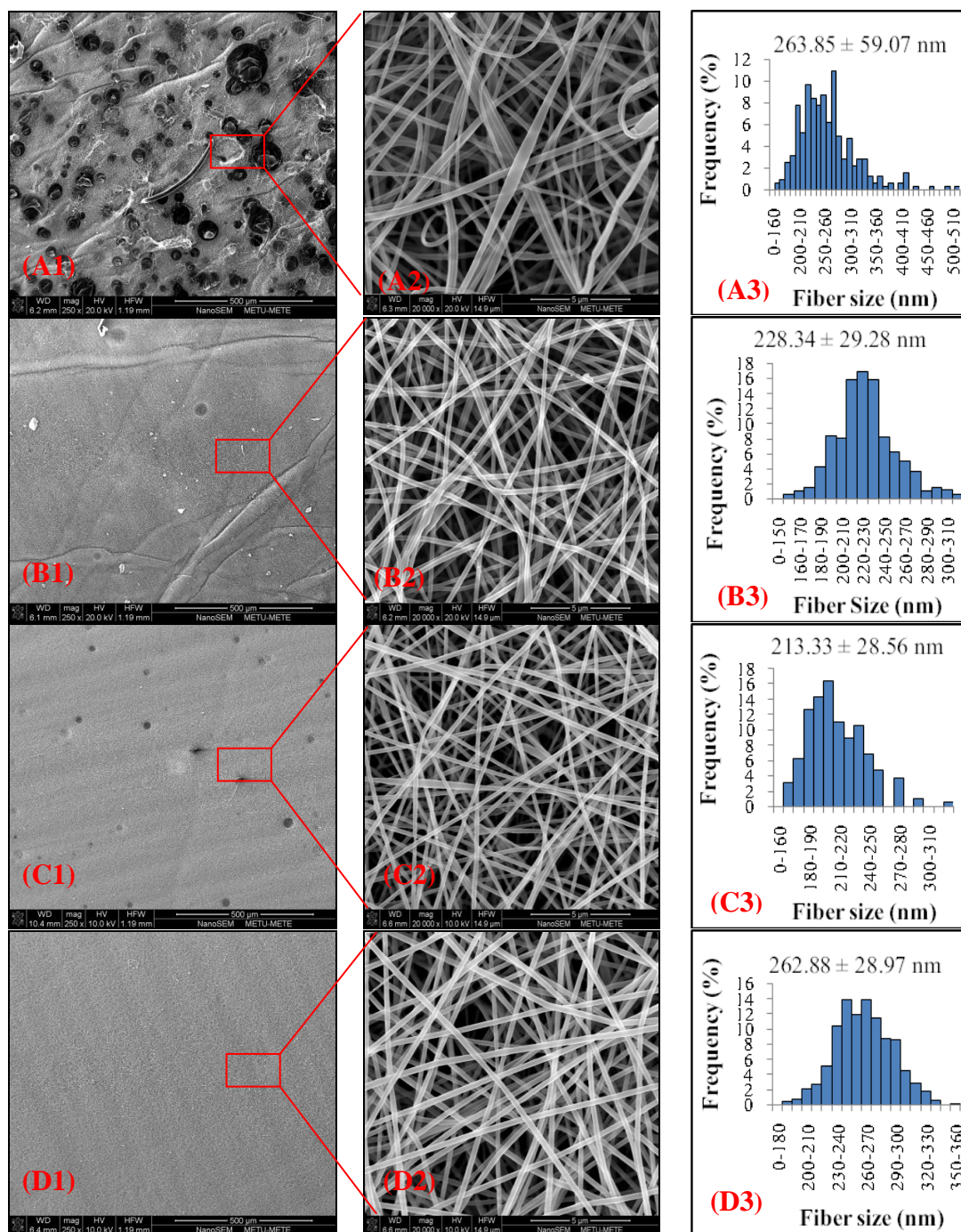


Figure 3.9. SEM micrographs showing the fiber morphology and fiber diameter distribution of different matrices: (A1-A3) Col1P2.5Au0, (B1-B3) Col1P2.5Au1, (C1-C3) Col1P2.5Au7, (D1-D3) Col1P2.5Au14.

3.3.4. Chemical Treatment of Collagen Nanofibrous Matrices

As stated previously in the optimization studies of collagen electrospinning process, randomly oriented collagen/PEO/AuNPs nanofiber matrices could be obtained in desired morphology by electrospinning. However, the nanofibers containing collagen were too vulnerable to disintegration in aqueous environment. Even when placed in a high humidity environment, electrospun fibers fused at the fiber junctions. Owing to the sensitivity to water or high humidity, the conventional cross-linking approach of immersing samples into aqueous GTA solution was not feasible for cross-linking these collagen/PEO/AuNPs matrices. Hence, by placing the nanofibers into a closed chamber containing GTA solution in another bottle, the GTA vapour was able to crosslink collagen/PEO/AuNPs matrix. After GTA vapor cross-linking, the fiber matrix became visibly yellowish as in the case of collagen sponges and they shrunk slightly.

Nanofibrous structure of the scaffolds was protected to a great extent (Figure 3.10) after cross-linking treatment with GTA vapour (3 %) at different time periods (2 and 4 hours). With respect to the cross-linking treatment done with groups containing different amounts of AuNPs (1.42 and 14.27 ppm) the pores of the scaffolds were closed too much when cross-linking duration was 4 hours. Hence, the cross-linking duration of 2 hours was decided to be more convenient. The pore sizes of the groups cross-linked for shorter time (2 hours) was in the range of 500 nm- 3 μ m. This size is appropriate for cell migration into the scaffold. Furthermore, the group including more AuNPs among the cross-linked groups preserved its nanofibrous structure more.

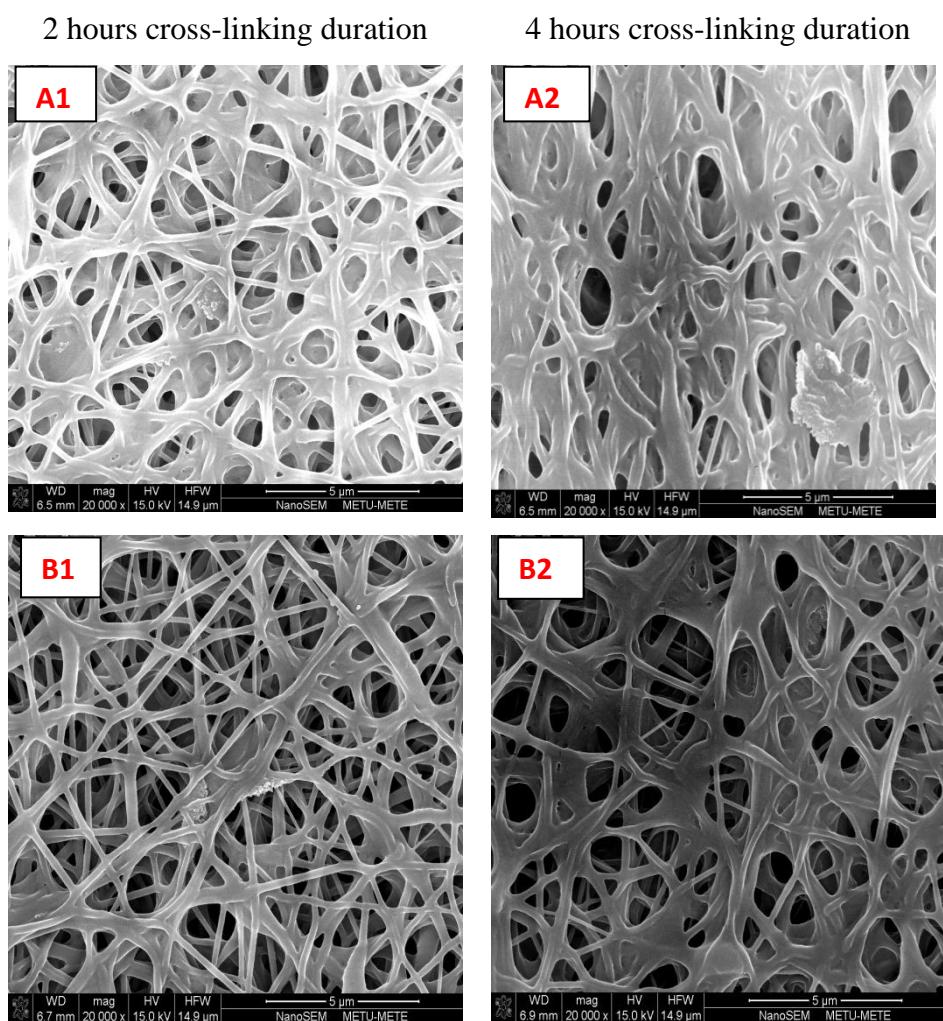


Figure 3.10. SEM micrographs showing the change in nanofiber morphology and pore size of collagen nanofibrous matrices after cross-linking with GTA vapour (3 %) for different time periods: (A1-A2) Col1P2.5Au1 and B1-B2) Col1P2.5Au14.

3.4. Preparation and Morphological Characterization of Silk Fibroin Matrices

3.4.1. Optimization of the Electrospinning Process for Silk Fibroin

According to the electrospinning experiments, fibrous structures could not be formed with only silk fibroin solutions (Table 3.3). Therefore, obtaining nanofibers from silk fibroin solutions (1-20% dissolved in d-water) was thought to be difficult. In order to electrospin the silk fibroin successfully, an additional polymer seemed to be necessary. Therefore, as it was used before for the spinning of collagen, PEO which could dissolve well in d-water was used. PEO solution in d-water was prepared separately since addition of solid PEO into silk fibroin solution resulted in the premature β -sheet formation and complete gelation at room temperature.

Small amounts of PEO (0.3-0.4%) was enough to form continuous fiber jets and to form homogenous fibers. Small amounts of PEO could be leached out from the structures more easily while rinsing. In SFP1 group, the fibers obtained were not intact while handling. High concentrations of silk fibroin (10-20%) would probably form very large diameter fibers ($> 50 \mu\text{m}$). Hence 6-8% silk fibroin concentrations (SFP2 and SFP3) were found to be optimum to form smaller diameter fibers not more than a few microns

3.4.2. Morphology of Silk Fibroin Matrices

The operating parameters (flow rate, voltage, and distance) of SFP2 and SFP3 groups were evaluated and optimized for fiber morphology (Figures 3.11-3.12). Upon adjusting the operating parameters of the wet electrospinning system, changing the fiber size (0.7-20 μm) was accomplished. The most successful (homogenous fiber size distribution, fiber size innanometer range, and smooth fibers) matrices were obtained in the SFP3 group having 0.3% PEO and 7.2% silk fibroin concentration as confirmed with SEM analysis (Figure 3.12 C). Silk fibroin fibers were connected to

each other and created numerous pores whose size reached up to several tens of microns.

Table 3.3. Results obtained in the experimental optimization studies of silk fibroin electrospinning

Groups *	The properties of the structure formed	Properties of the solution
SF1	No fibrous structure	Low viscosity. Solution is transparent.
SF2	No fibrous structure	Low viscosity but viscosity is higher than SF1
SF3	No fibrous structure	Low viscosity but viscosity is higher than SF2
SF4	No fibrous structure	Low viscosity but viscosity is higher than SF3
SF5	No fibrous structure	Low viscosity but viscosity is higher than SF4
SF10	No fibrous structure	Viscosity is too high. Not spinnable
SF20	No fibrous structure	Viscosity is very high. Solution is not dripping out from syringe tip.
SFP1	Stable continuous fiber jet flow, fiber accumulation in the bath	Viscosity is medium, solution is transparent.
SFP2	Stable continuous fiber jet flow, fiber accumulation in the bath	Viscosity is medium, solution is transparent.
SFP3	Stable continuous fiber jet flow, fiber accumulation in the bath	Viscosity is medium, solution is transparent.
SFP3-Au	Stable continuous fiber jet flow, fiber accumulation in the bath	Viscosity is medium, solution is transparent.

* Types of the polymers in the groups and their ratios in the blends were given in Table 2.3.

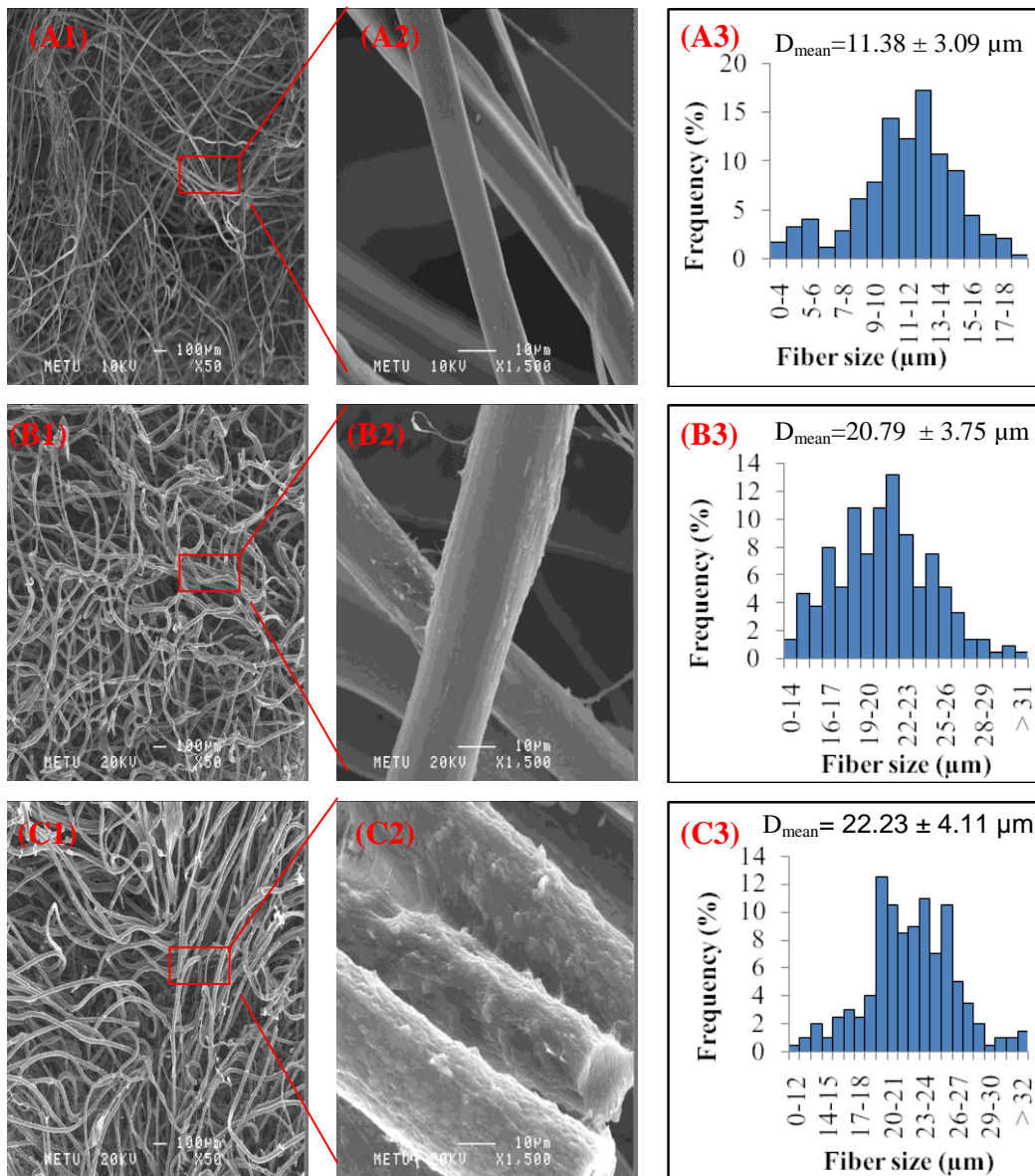


Figure 3.11. SEM micrographs and fiber diameter histograms of (A1-A2) degummed pure silk fibroin isolated from silkworm cocoon and SFP2 group with different operation parameters: (B1-B3) flow rate= 2 ml/h, voltage=12 kV, distance=13 cm and (C1-C2) flow rate= 1 ml/h, voltage=17 kV, distance=13 cm. Middle figures are the magnified regions of red rectangles.

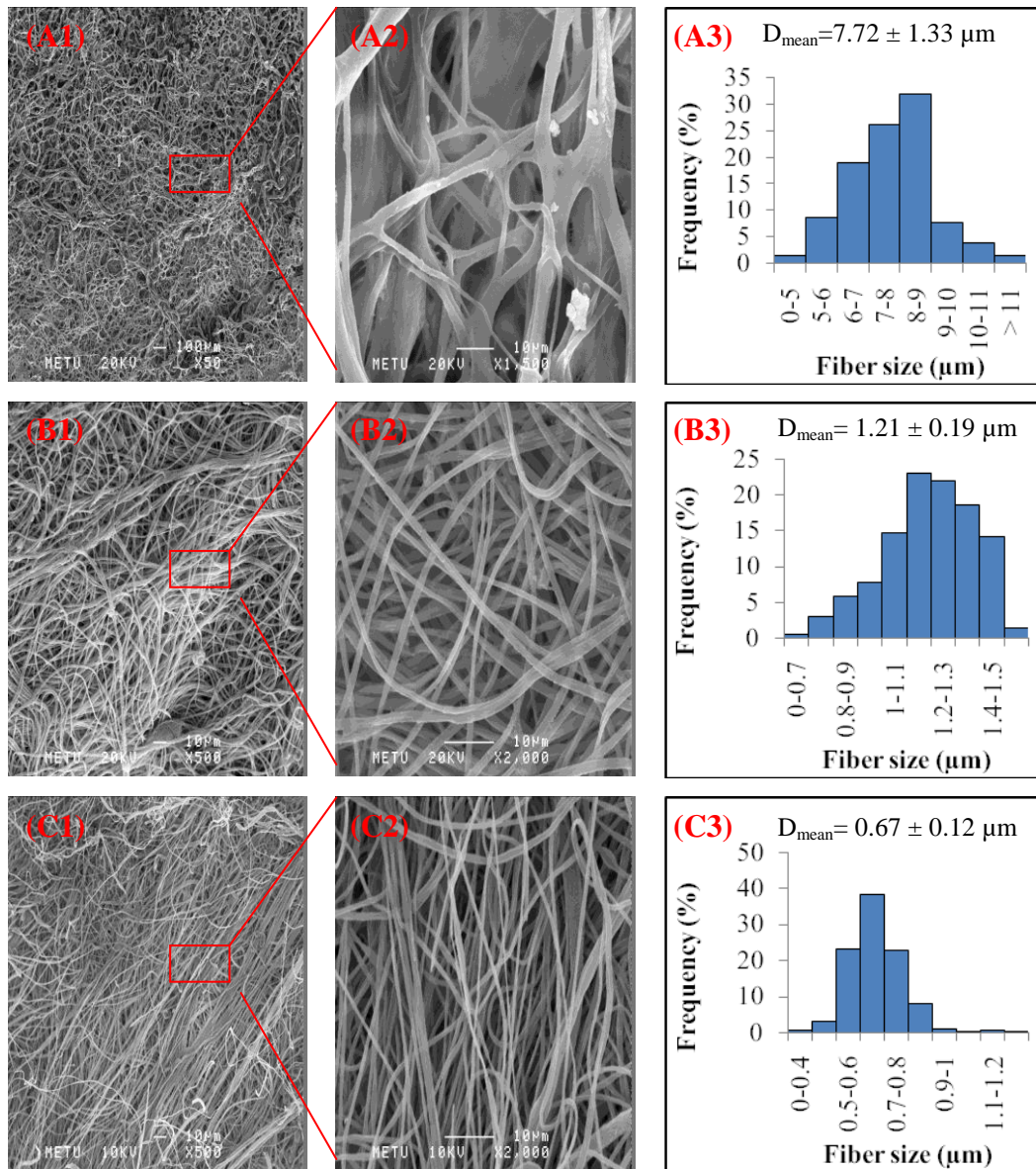


Figure 3.12. SEM micrographs and fiber diameter histograms of SFP2 group collected with the operational parameters: (A1-A3) flow rate=1 ml/h, voltage=12 kV, distance=20 cm, (B1-B3) flow rate=0.8 ml/h, voltage=19 kV, distance=23 cm and SFP3 group with the operational parameters of (C1-C3) flow rate=0.8 ml/h, voltage=19 kV, distance=23 cm. Middle figures are the magnified regions of red rectangles.

3.4.3. Incorporation of Gold Nanoparticles into SF Matrices

AuNPs were added into silk fibroin solution (SFP3-Au group) before the electrospinning process. AuNPs concentration in the silk fibroin solution was the same with those used in the preparation of other scaffold groups (14.27 ppm). In comparison to the silk fibroin group containing no AuNPs (SFP3 group), SFP3Au group had slightly smaller diameter nanofibers, but the size distribution range was a little bit wider with smaller and larger nanofibers (Figure 3.13). AuNPs were thought to be distributed inside the nanofibers, but this was not detectable with TEM analysis as done before for collagen nanofibers. Since the silk fibroin fibers were electrospun into ethanol bath, the fibers were not able to be collected on copper grids.

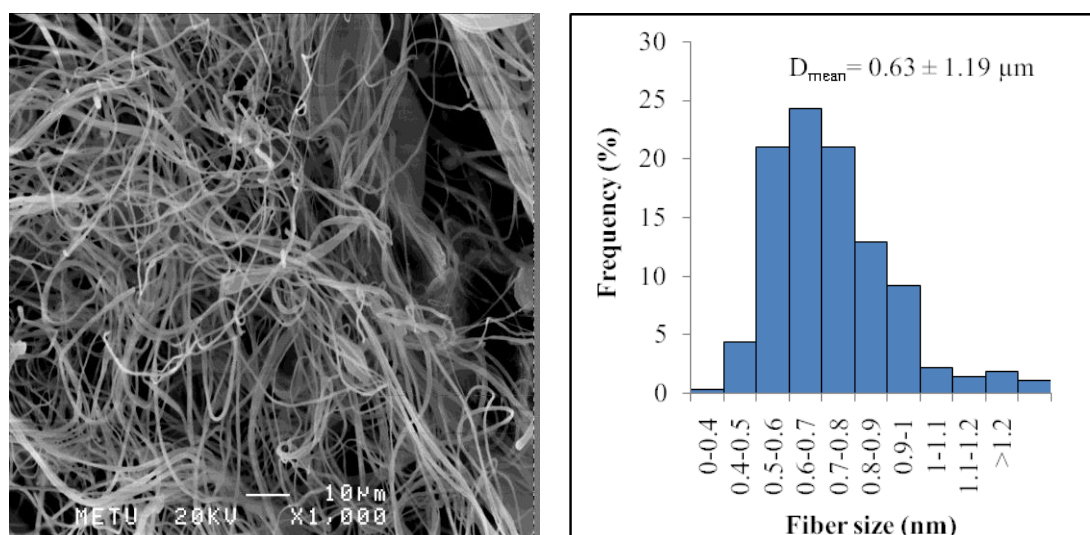


Figure 3.13. SEM micrographs and fiber diameter histograms of SFP3Au group obtained with the optimized operational parameters (flow rate=0.8 ml/h, voltage=19 kV, distance=23 cm).

3.4.4. Chemical Treatment of Silk Fibroin Matrices

It was recognized in the preliminary studies that to make water resistant silk fibroin could be problematic. As a result, different chemical treatments were applied. Chemical treatment of silk fibroin matrix with different chemicals showed that the fibers became more brittle after any of the treatments (EtOH, MetOH, EDC/NHS and GTA) and they were prone to breakage. They also disintegrated rapidly in d-water. However, the integrity of the scaffolds was protected to a great extent while using only EtOH in comparison to the others. Among these groups, only SFM-E and SFM-M were extensible without any breakage. The other two groups, SFM-E/N and SFM-G, especially the former one was highly brittle with fracturing tendency in d-water. Silk fibroin is insoluble in water while β -sheet conformation prevails. Apart from these reasons related to the solubility or brittleness issues, organic solvents such as MetOH and GTA can pose toxicity problems when the processed materials are exposed to cells in vitro and in vivo. Although chemical treatment of SF fiber with MetOH (Li et al., 2006; Meinel et al., 2009) and GTA (Ki et al., 2008) was reported in the literature a lot the biocompatibility concerns were also noted. Hence, avoiding the use of such organic solvents can enhance the potential biocompatibility of the electrospun fibers. All of the results related to the structural properties, brittleness and solubility of the chemically treated SF were summarized in Table 3.4. In addition, the physical effects of these chemical treatment methods were studied with SEM analysis (Figure 3.14) and hence no clear change was observed for any of the chemically treated groups (SFM-E, SFM-M, and SFM-G). As a whole, it was decided to use pure ethanol to induce a β -sheet conformation transition. The mechanism of conformation transition of silk fibroin with ethanol treatment was explained in a study (Cao et al., 2009). Essentially, the conformation transition is a process of hydrogen bond rearrangement. When the electrospun matrix is immersed in ethanol, it swells and its free volume increases and there is enough space for the molecule chains to rearrange.

Table 3.4. The properties of fibrous matrices upon chemical treatment.

Groups	The structural properties of the fibrous matrices	Brittleness	Solubility in d-water
SFM-E	Fibrous intact structure. Soft silky surface.	Extensible with no crack formation	Insoluble. No observable dissolution
SFM-M	Fibrous intact structure. Smooth surface	Extensible but cracks form after a certain degree	Insoluble. No observable dissolution
SFM-E/N	Fibrous intact structure. Smooth surface. Irregularities such as cracks.	Highly brittle	Insoluble, but fibers starts breaking into small pieces
SFM-G	Fibrous intact structure. Hard dense structure. Irregularities and yellowish color.	Brittle	Insoluble. Fiber breaking occurs

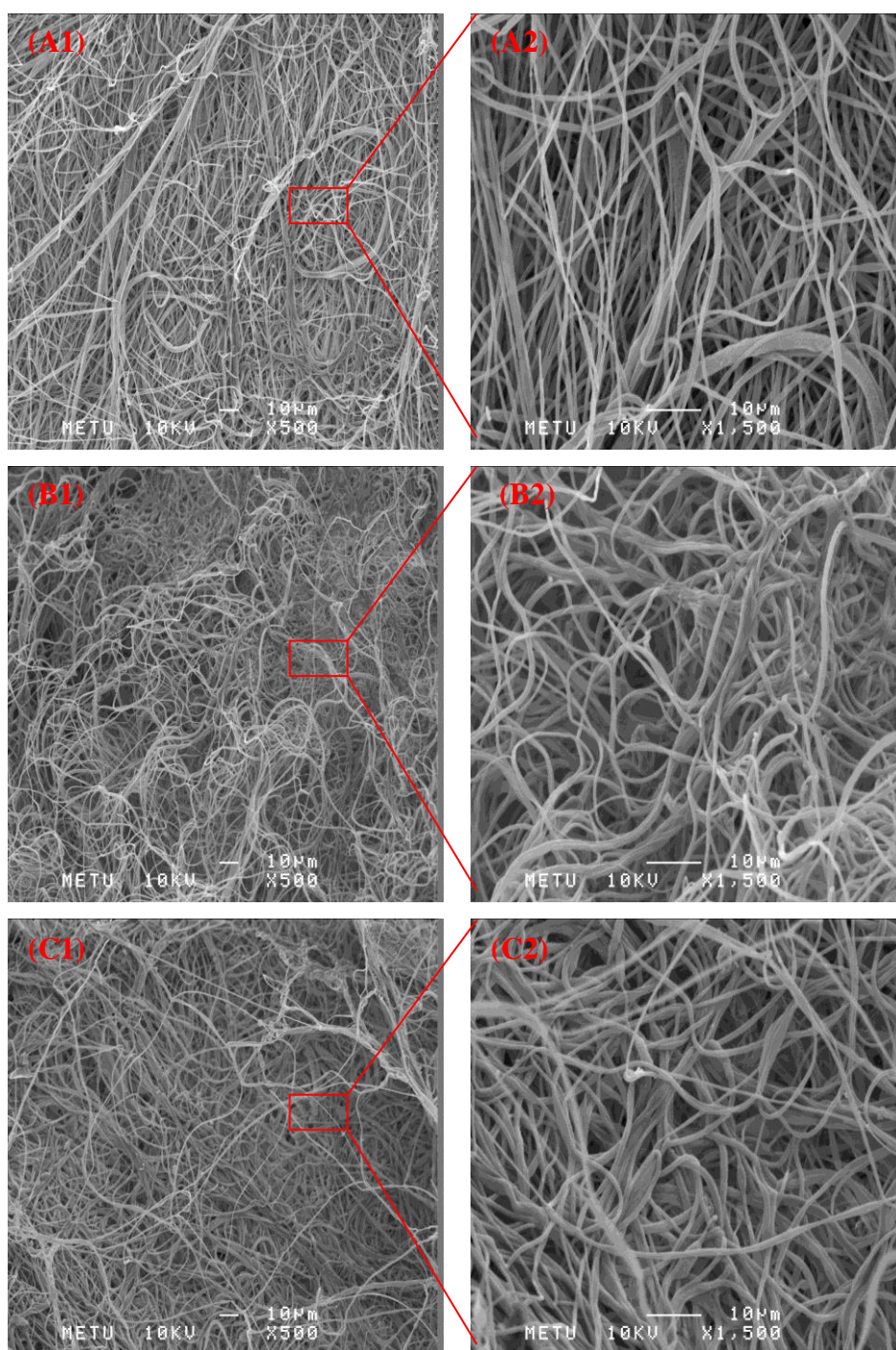


Figure 3.14. SEM micrographs of silk fibroin matrices treated with different chemical treatment methods: (A1-A2) SFM-E, (B1-B2) SFM-M and (C1-C2) SFM-G. Figures on the right are the magnified regions of red rectangles.

3.5. Characterization of Scaffolds

3.5.1. Physicochemical Characterization Tests

3.5.1.1. The Fourier Transform Infrared Spectroscopy Analysis

3.5.1.1.1. FTIR Analysis of Collagen Sponges

All the collagen sponge groups (CS, CS-Au, CS-X and CS-AuX) were characterized by FTIR spectroscopic analysis. The infrared-active modes of the peptide backbone are expressed in the amide bands. The spectrum of collagen depicts characteristic absorption bands at 1600-1700, 1500-1550 and 1200-1300 cm^{-1} , which respectively represent the amide I (C=O stretching), amide II (N-H bending and C-N stretching) and amide III (C-N stretching and N-H deformation) bands of collagen (Sionkowska et al., 2010). The main amide characteristic absorption band of collagen sponge groups was observed at 1630-1628 cm^{-1} (amide I), 1530-1540 cm^{-1} (amide II), 1234-1235 cm^{-1} (amide III) as shown in Figure 3.15.

The absorption bands at 2900-3300 cm^{-1} are the O-H stretching contribution of collagen. The region from 970 to 1200 cm^{-1} is also distinct in collagen, with two small maxima observed at 1030 and 1082 cm^{-1} (CS), 1030 and 1080 cm^{-1} (CS-Au), 1030 and 1082 cm^{-1} (CS-X), 1031 and 1081 (CS-AuX), generally ascribed to C-O vibrations of alcohols, either from hydroxyproline or from the glycosidic side chain of collagen (Chang and Tanaka, 2002). The bands at 1336-1448 cm^{-1} (CS) and 1447-1448 cm^{-1} (CS-Au) 1447-1448 cm^{-1} (CS-X) 1447-1448 cm^{-1} (CS-AuX) correspond to C-H and O-H bending vibrations. The bands between 3300 and 3500 cm^{-1} are reported to occur due to N-H amine group stretching vibrations superimposed on the side of O-H hydroxyl group stretching bands (Kumari et al., 2012). Also, it was shown that the amide absorption bands of the groups did not change significantly after the conjugation with AuNPs and GTA cross-linking, which was an indication of undisturbed α -helix secondary structure of collagen, but both the cross-linking with GTA or AuNPs incorporation decreased the amide I, II and III absorption bands.

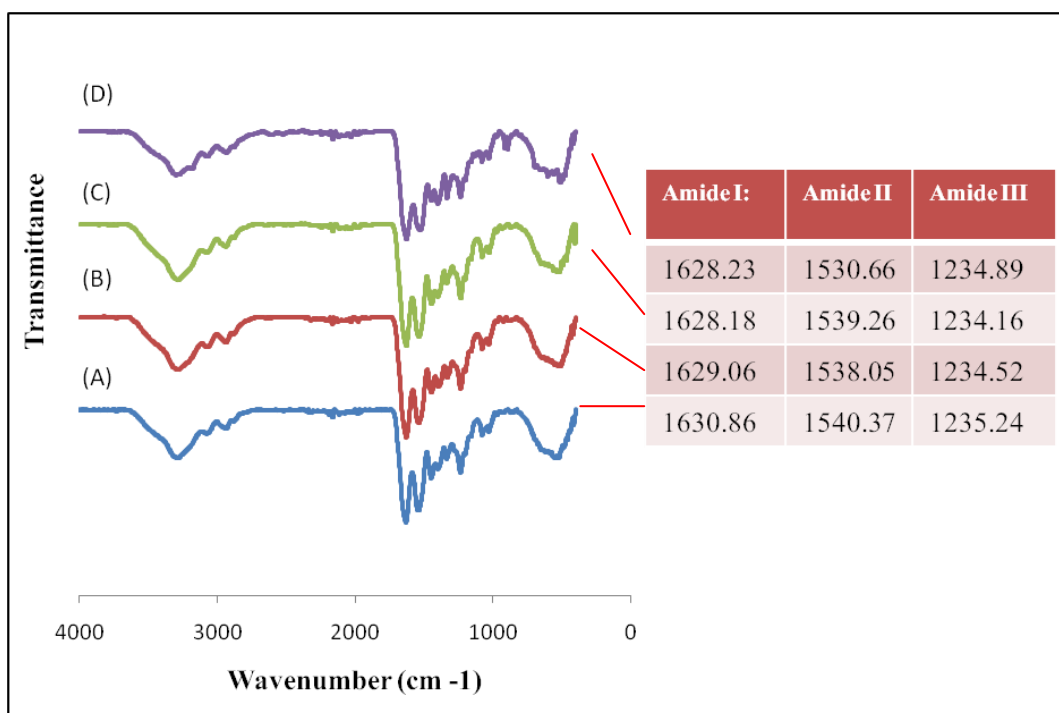


Figure 3.15. FTIR-ATR spectra of test groups:(A) CS, (B) CS-Au, (C) CS-X and (D) CS-AuX.

3.5.1.1.2. FTIR Analysis of Collagen Nanofibrous Matrices

The final optimized collagen nanofibrous groups (CM-Au and CM-AuX) and their matrix constituents (PEO and collagen type I) were also characterized by FTIR spectroscopic analysis. The infrared-active modes of the peptide backbone are expressed in the amide bands. The main amide characteristic absorption bands of collagen type I and collagen matrices were observed at 1630-1651 cm^{-1} (amide I), 1538-1544 cm^{-1} (amide II), and 1235-1240 cm^{-1} (amide III) as shown in Figure 3.16. The region from 970 to 1200 cm^{-1} is also distinct in collagen, with the highest absorption bands observed at 1060 cm^{-1} (collagen type I), 1098 cm^{-1} (CM-Au), and 1097 cm^{-1} (CM-AuX), generally ascribed to C–O vibrations of alcohols, either from hydroxyproline or from the glycosidic side chain of collagen (Chang and Tanaka, 2002). The absorption peaks at 839 cm^{-1} , 944 cm^{-1} and 959 cm^{-1} (=CH₂ bending),

1090 cm^{-1} , 1240 cm^{-1} and 1278 cm^{-1} (O-C stretching) 1359 and 1466 cm^{-1} (O-H bending) and 2859 cm^{-1} (O-H stretching) were clearly observed in for PEO.

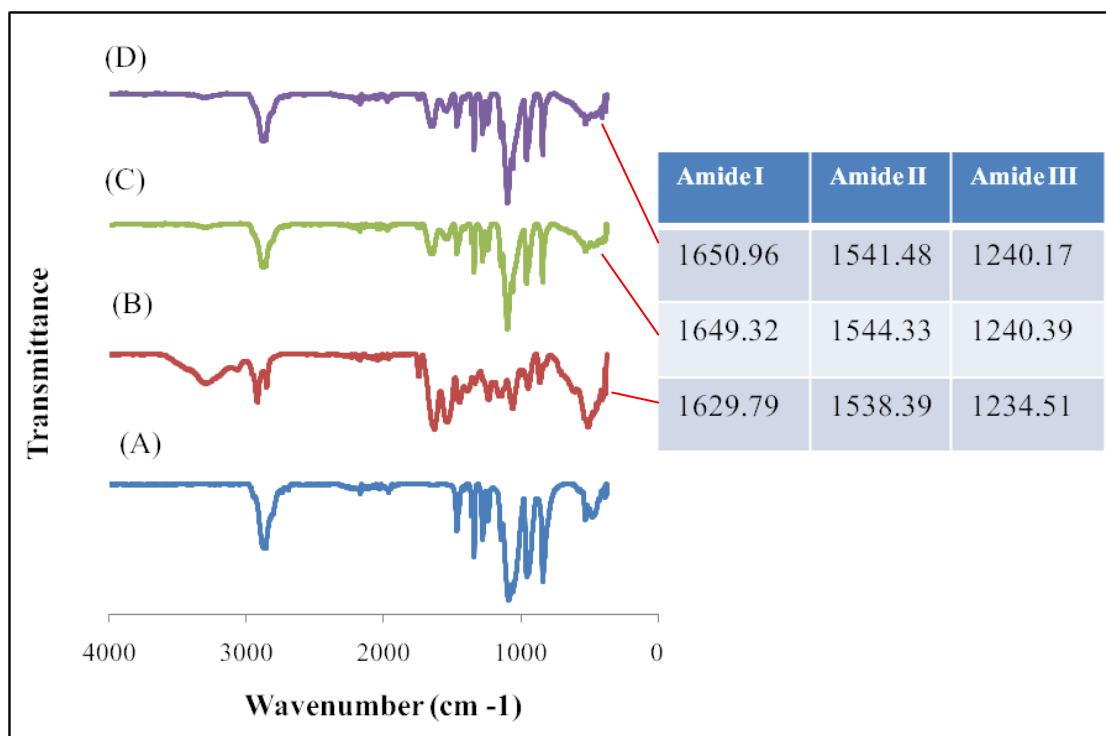


Figure 3.16. FTIR-ATR spectra of test groups: (A) PEO, (B) collagen type I (C) CM-Au and (D) CM-AuX.

For CM-Au and CM-AuX groups, each absorption peak of collagen and PEO and were identified, which confirms that both collagen nanofibrous matrices were composed of these polymers. However, the absorption peak of $-\text{N}=\text{CH}-$ (1622 cm^{-1}), which represents the imide bond formation between aldehyde and amino groups during the crosslinking step, cannot be clearly identified due to interference from $1649\text{-}1651 \text{ cm}^{-1}$ (amide I) peak (Chen et al., 2008). The absorption bands at $2500\text{-}3300 \text{ cm}^{-1}$ are the O-H stretching contribution of collagen. The addition of AuNPs into collagen/PEO matrices caused to disappearance of O-H bands of collagen type I observed at $2500\text{-}3300 \text{ cm}^{-1}$, with only remaining O-H stretching

band at about 2900 cm^{-1} that might be attributed to PEO. It was also found that the peak intensities of collagen nanofibrous matrices (CM-Au and CM-AuX) and collagen type I changed. It is well known that proteins can bind to gold AuNPs either through free amine groups or cysteine residues in the proteins and therefore, AuNPs might have been stabilized by binding to surface proteins (Kumari et al., 2012). These results suggested that collagen/PEO stabilized AuNPs (Fathi-Azarbayjani et al., 2010). Also, it was shown again that the amide absorption bands of the groups did not change significantly, which was an indication of undisturbed α -helix secondary structure of collagen, but both the cross-linking with GTA or AuNPs incorporation increased the amide I, II and III absorption bands.

3.5.1.1.3. FTIR Analysis of Silk Fibroin Matrices

Infrared spectroscopy was applied to study the molecular conformation of silk fibroin scaffolds fabricated in this study. Random coil showed strong absorption bands at 1665 cm^{-1} (amid I), 1540 cm^{-1} (amid II) and 1235 cm^{-1} (amid III), while the β -sheet showed absorption bands at 1628 cm^{-1} (amid I), 1533 cm^{-1} (amid II) and 1265 cm^{-1} (amid III) (Ayutsede et al., 2005). As shown in Figure 3.17 the structure of all chemically treated silk fibroin matrices (SFM-E, SFM-M, SFM-GTA and SFM-Au) and silk fibroin film (SF film) obtained after drying in an oven at $60\text{ }^{\circ}\text{C}$ was characterized by absorption bands at $1620\text{-}1622\text{ cm}^{-1}$ (amid I) and $1503\text{-}1513\text{ cm}^{-1}$ (amid II), attributed to the β -sheet conformation. The characteristic β -sheet absorptions at wavenumbers; 1620 , 1503 and 1221 cm^{-1} (unprocessed silk fibroin cocoon fibers: SF) were present in all of the SF groups (SFM-E, SFM-M, SFM-G, SFM-Au and SF film). However, the intensity of SF film was too low compared to other groups, showing weak β -sheet conformation. As a result, to create β -sheet conformation similar to the natural fibroin, EtOH chemical treatment was determined to be sufficient. Formation of β -sheet conformation was required to fabricate water stable silk fibroin scaffolds. In addition, washing of chemicals used for the treatment of scaffolds at $37\text{ }^{\circ}\text{C}$ for 1 hours resulted in the loss of typical PEO absorption peaks

at 1090 cm^{-1} , 959 cm^{-1} and 839 cm^{-1} , suggesting that the water soluble PEO had been extracted completely.

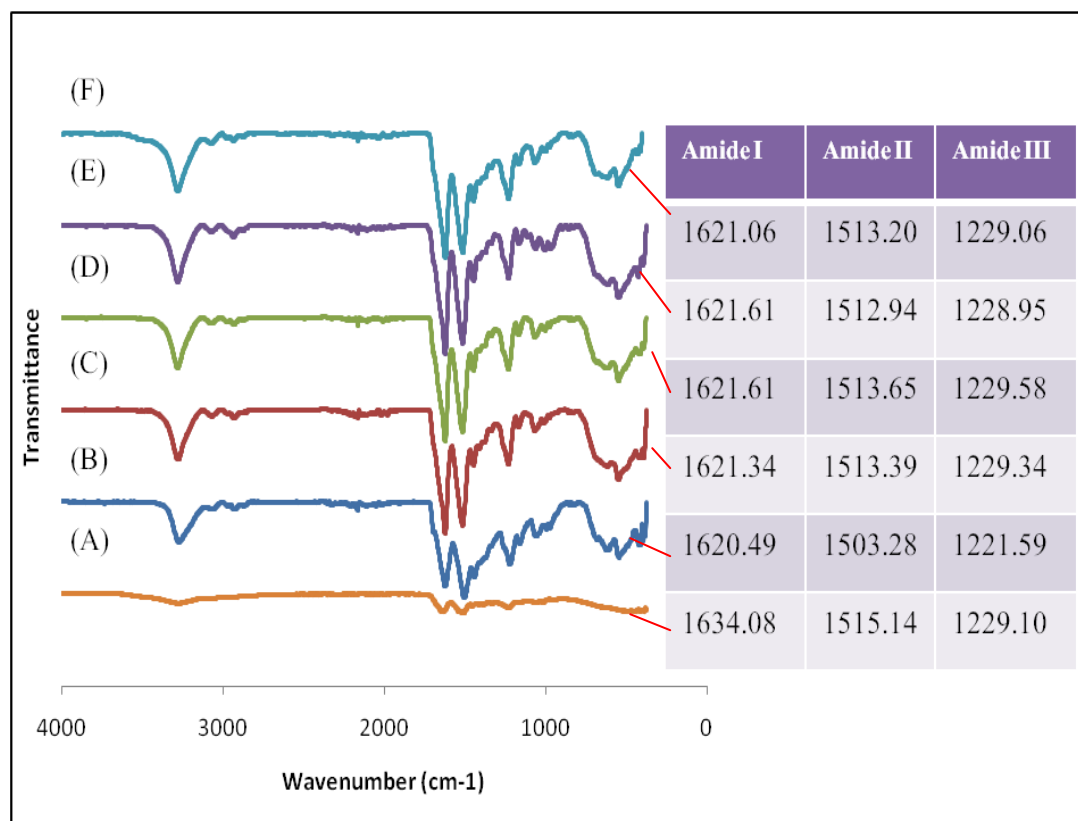


Figure 3.17. FTIR-ATR spectra of silk fibroin scaffolds: (A) SF film, (B) SF cocoon (C) SFM-E, (D) SFM-M, (E) SFM-G and (F) SFM-AuE.

3.5.1.2. Pore Size Distribution and Porosity of Scaffolds

The porosity (P) of collagen sponges (CS: $72.9 \pm 1.02\%$, CS-Au: $78.58 \pm 2.21\%$) was not influenced explicitly by the cross-linking treatment (CS-X: $72.55 \pm 3.29\%$, CS-AuX: $70.88 \pm 3.52\%$). The P values changed in the range of 71-79%. However, P of CS-Au group was significantly higher than the other groups. According to the pore size distribution analysis (Figure 3.18 A-D); the scaffolds had a wide range of pore size distribution (0-200 μm). After cross-linking, pores having sizes up to 20 μm

were mostly closed resulting in abrupt decrease of pores below this size range and pores were concentrated in 20-50 μm size range. Pore size distribution was unimodal for CS-AuX group while it was bimodal for the other collagen sponge groups (CS, CS-Au, and CS-X).

P of the CM-Au had a small decrease after cross-linking (Figure 3.18 E-F). The cross-linking treatment did not have any pronounced effect on P of collagen nanofibrous matrices (CM-Au: 10.93% and CM-AuX: 9.08%), but after cross-linking, small pores (0-7 μm) were closed completely and there were only pores in the size range of 7-10 μm . It was verified before with SEM imaging that the nanofibrous matrices fabricated had a dense structure (small pores and low porosity). However, it was anticipated that the PEO inside the scaffolds would act like a porogen increasing evidently P and pore size of the scaffolds when subjected to aqueous environment.

P of silk fibroin matrices (SFM-E and SFM-AuE) was similar (67-69%) having similar porosities to the collagen sponges. Like the collagen sponge groups, the pore size distribution analysis showed that the scaffolds had a wide range of pore size distribution (0-200 μm), mostly around 0-50 μm (Figure 3.18 G-H).

Porosity measurement of scaffolds was done by the liquid displacement method using hexane as the displacing liquid. Hexane was chosen because it permeates into scaffolds without causing shrinkage or swelling compared to other organic solvents including ethanol (Bhardwaj et al., 2014). A scaffold used for tissue engineering requires a porous structure with a high porosity and interconnected pores which allow cell migration, mass transport, growth, gene expression and new tissue formation in three dimension (Muthukumar et al., 2014). Generally, the porosity values of different studies related to tissue engineering applications focused on obtaining collagen scaffolds having porosity not less than 70% and well above 90% porosity values (Bhardwaj et al., 2014; Muthukumar et al., 2014; Gaspar et al., 2011; Davidenko et al., 2012). The pore structure of the scaffolds in this study was formed as a result of the lyophilization process. Previous studies showed that the morphology of the pores

is dependent upon the freezing temperature of the mixture before lyophilization (Bhardwaj et al., 2014, Davidenko et al., 2012). The freezing temperature of -80 °C used in this study was decided to be suitable as regards the results of porosity and pore size distribution analysis. Pore sizes concentrating between 20 and 200 µm are thought to be optimal for improved initial cell attachment. Therefore, due to their porous nature of large pore sizes, collagen sponge and silk fibroin matrix groups would be more successful in absorbing the wound exudates in comparison to collagen nanofibrous matrices.

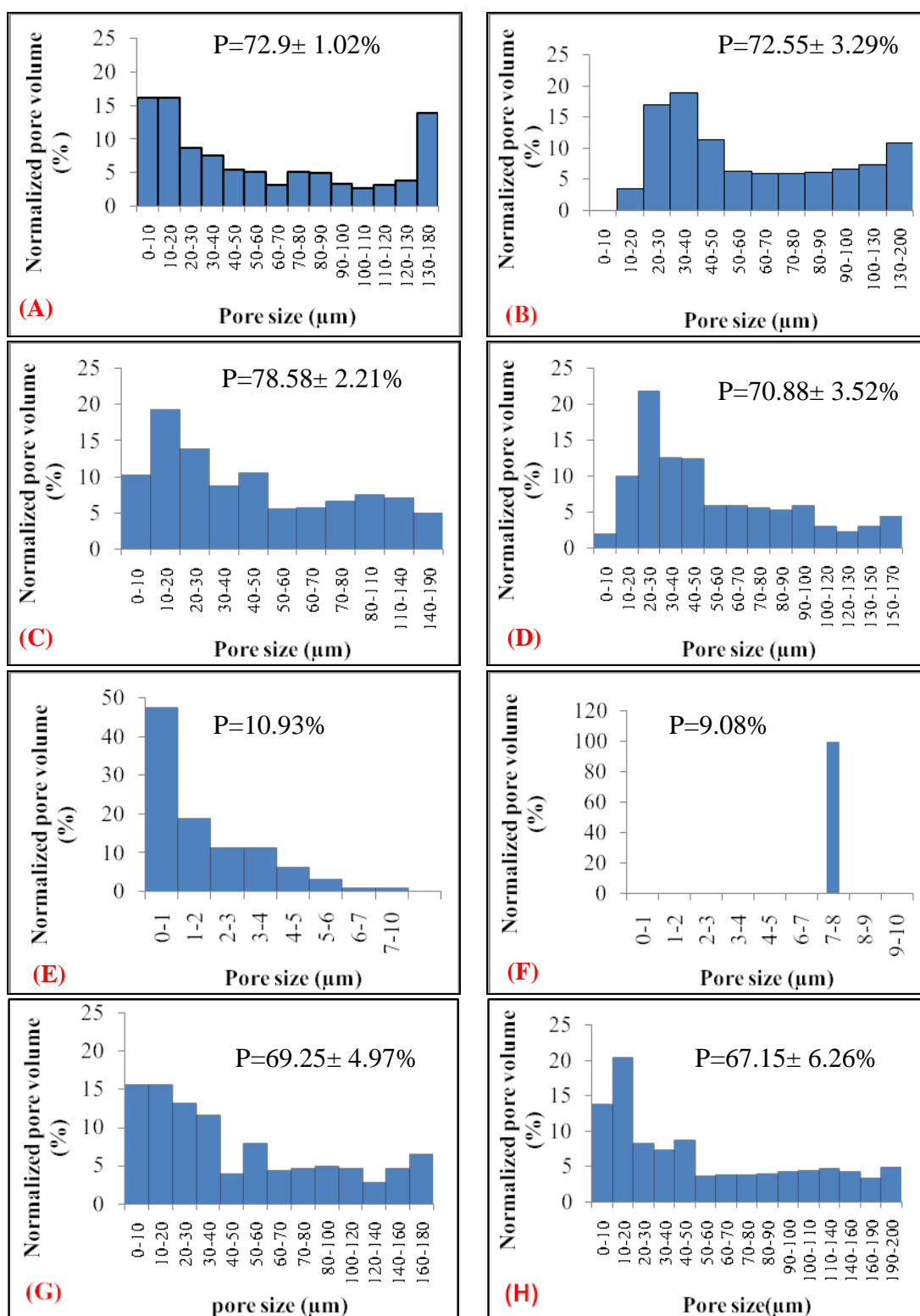


Figure 3.18. Porosity and pore size distribution analysis of scaffolds: (A) CS, (B) CS-X, (C) CS-Au, (D) CS-AuX, (E) CM-Au, (F) CM-AuX, (G) SFM-E and (H) SFM-AuE.

3.5.1.3. Hydrolytic Degradation

The resistance of the scaffolds to hydrolytic degradation (HD) was generally high for cross-linked collagen scaffolds. The cross-linked collagen sponges maintained their 3 dimensional structures in aqueous environment to a large extent (17-18%) as long as 2 weeks while uncross-linked collagen samples contracted at 37 °C in 1 day to a great extent, and degraded almost completely in 1 and 2 weeks for CS (100%) and CS-Au (65%), respectively (Figure 3.19 A). So it could be resulted that degradation of collagen sponges differed with respect to AuNPs incorporation for uncross-linked sponges, but the same effect was not so clear for cross-linked sponges (CS-X and CS-AuX). With the cross-linking treatment and AuNPs incorporation, the purpose of maintaining the structural integrity was fulfilled. The degradation profile of collagen sponges fabricated in this study was compared to a commercial skin substitute (MatridermTM) since it is a collagen/elastin sponge similar to our collagen sponges. Degradation profile of MatridermTM was similar to our uncross-linked collagen sponges. HD of MatridermTM was slow during 4 days (30%) with a steady increase during 14 days. HD of MatridermTM was comparable to CS-Au group after 7 days. Cross-linked collagen sponge groups (CS-X and CS-Au) were both way better than MatridermTM in terms of HD.

CM-Au degraded immediately in PBS at 37 °C, whereas after cross-linking (CM-AuX), it had a very high first day hydrolytic degradation result (85%) which slowed down in the following days and its structural stability was maintained as long as 7 days (Figure 3.19 A). As a whole, the cross-linking treatment increased the resistance of collagen based scaffolds against HD.

The scaffold groups containing the highest resistance capacity against HD was silk fibroin scaffolds either with or without AuNPs (SFM-E and SFM-AuE). HD of SFM-E was barely detectable in 4 days incubation period. Yet, after 1 week HD increased slightly and was constant during 2 weeks (18%). Similarly HD of SF-Au was on 3% level during 2 weeks (Figure 3.19 B).

Film layers of bilayered scaffolds in both uncross-linked (C/S) and cross-linked (C/S-X) state were examined separately as well. C/S showed an initial abrupt degradation in 1 day (85%) and maintained its integrity during 7 days until complete disruption. On the other hand, cross-linking treatment enhanced the degradation profile very much as expectedly such that HD was on 4% level during 14 days (Figure 3.19 C).

3.5.1.4. Enzymatic Degradation

According to the enzymatic degradation (ED) results, uncross-linked collagen sponges (CS and CS-Au), MatridermTM and both uncross-linked and cross-linked collagen nanofibrous matrices (CM-Au and CM-AuX) degraded soon after 2 hours; on the other hand, cross-linked collagen sponges (CS-X and CS-AuX) maintained their structural stability for 72 hours with a steady increase (Figure 3.20 A). A continuous increase in degradation profiles was observed for both CS-X and CS-AuX during this incubation period but the difference between the first day results of these two groups was not significant. However, the degradation of CS-AuX seemed to slow down after this point resulting in a slightly better stability than CS-X. Thus, it could be concluded that AuNPs incorporation might have a decreasing effect on enzymatic degradation of GTA cross-linked collagen sponge. The resistance of silk fibroin scaffolds (SFM-E and SFM-AuE) against ED was clearly higher than any of the other groups; so, they had very low enzymatic degradation (16-27%) during 2 weeks of incubation period (Figure 3.20 B). Again ED of film layers were examined separately and it was confirmed again that after cross-linking the resistance of films against ED was increased and the structural integrity was conserved as long as 3 days while C/S film degraded immediately in 2 hours (Figure 3.20 C).

Different studies showing the enhanced resistance of GTA cross-linked collagen matrices to collagenase degradation were reported before (Lai et al., 2013). Also, there are studies stating that EDC-NHS mediated functionalized AuNPs cross-linked to collagen scaffolds had enhanced resistance against enzymatic degradation (Grant

et al., 2014, Castaneda et al., 2008; Deeken et al., 2011). It is believed that attachment of the AuNPs on the collagenase binding sites and many intermolecular cross-links formed after GTA cross-linking might have caused enzymes to have difficulty in reaching these attack sites in the collagen sponge groups. However, the high hydrolytic and enzymatic degradation results of collagen matrices developed in this study could be due to the ineffectiveness of GTA cross-linking for collagen alone and the denatured structure of collagen after heat treatment. It was stated in a study (Lin et al., 2013) that collagen type I alone could be insufficient for the provision of free $-NH_2$ and the triple-helix structure of collagen might have caused to steric hindrance. All these might have resulted in deterioration of the cross-linking efficiency of GTA. Not only this low cross-linking efficiency could have caused the quick disruption of collagen matrices (CM-AuX) in enzymatic environment, but also the high concentration of the collagenase type I used in this study could be one another reason. It was reported before that biodegradation rate of scaffolds made of silk fibroin differed with respect to the type of enzyme (α -chymotrypsin, collagenase IA, and protease XIV) used (Li et al., 2003). The strength of these enzymes was classified as follows: protease XIV > collagenase IA > α -chymotrypsin. Thus the low degradation profile of silk fibroin matrices could also be related to the type of enzyme used in this study. It is known that results of enzymatic degradation are not only related to intrinsic property of the fabricated material but also to type and concentration of the collagenase used. In natural skin tissue, the concentration of the enzyme will likely to differ with respect to wound level or to the type of the wounded tissue; therefore, faster or slower rates of degradation could be encountered. The fact that the cross-linked samples degraded completely in 3 days in biodegradation tests could be explained with the high concentration of the collagenase. Such a disruptive environment might not exist in wounded skin areas normally.

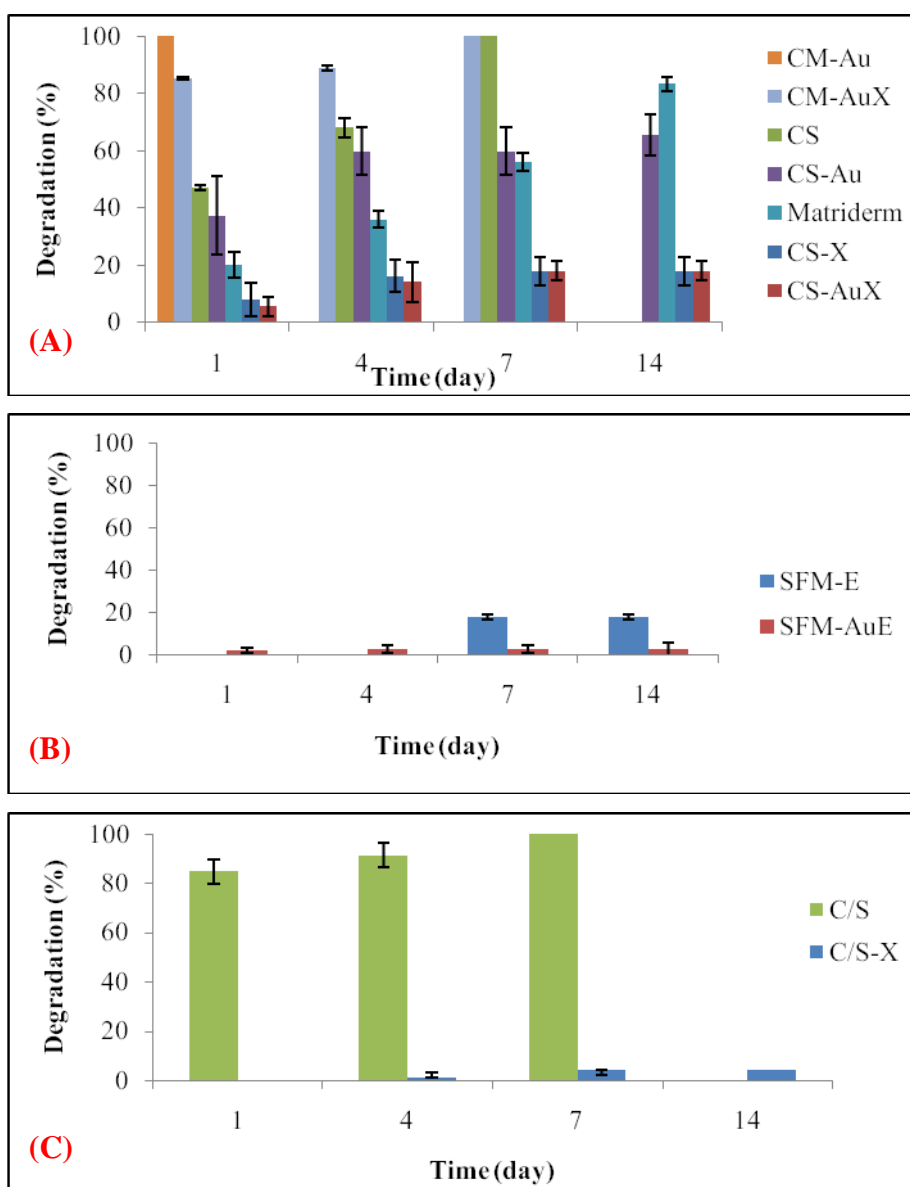


Figure 3.19. Hydrolytic degradation results: (A) collagen sponges (CS, CS-X, CS-Au and CS-AuX) a commercial skin substitute (MatridermTM) and collagen nanofibrous matrices (CM-Au and CM-AuX), (B) silk fibroin matrices (SFM-E and SFM-AuE) and (C) collagen/sericin membranes (C/S and C/S-X).

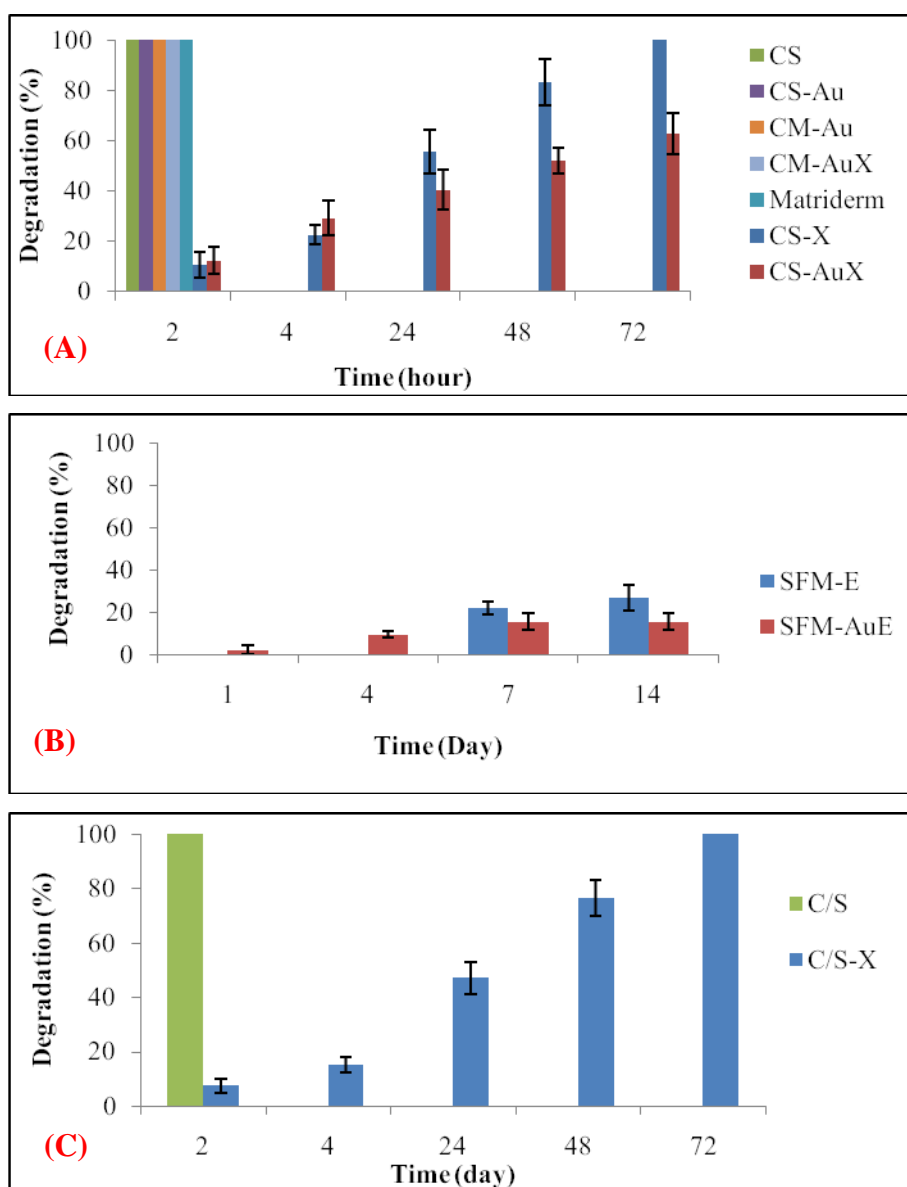


Figure 3.20. Enzymatic degradation results: (A) collagen sponges (CS, CS-X, CS-Au and CS-AuX) a commercial skin substitute (Matriderm™) and collagen nanofibrous matrices (CM-Au14 and CM-Au14X), (B) silk fibroin matrices (SFM-E and SFM-AuE) and (C) collagen/sericin membranes (C/S and C/S-X).

3.5.1.5. Equilibrium Degree of Swelling

The equilibrium degrees of swelling ratios (EDS) of epidermal (C/S and C/S-X) and dermal (CS, CS-X, CS-Au, CS-AuX, CM-AuX, SFM-E and SFM-AuE) layers of all the scaffolds fabricated in this study and a commercial skin substitute (Matriderm™) were shown in Figure 3.21. It was observed that EDS of the scaffolds reached to equilibrated levels at the end of 1st day. The EDS values of dermal layers were calculated as 7-61 g/g. EDS of collagen sponges (CS: 18.89 ± 3.68 g/g) increased after cross-linking (CS-X: 61.17 ± 6.00 g/g) in a statistically meaningful manner. Similarly, EDS of collagen sponges incorporated with AuNPs (CS-Au: 13.48 ± 1.81 g/g) increased significantly after cross-linking (CS-AuX: 38.54 ± 4.50 g/g). The increase in EDS after cross-linking was supposed to be mainly due to high contraction (shrinkage) and rapid degradation of uncross-linked collagen scaffolds in water at 37 °C during 1 day compared to cross-linked samples. The water inside the sponges was more inclined to be imprisoned inside the cross-linked samples; on the contrary, it spilled out from the uncross-linked samples easily. Opposing to the GTA treatment, AuNPs incorporation decreased the EDS values of uncross-linked and cross-linked collagen scaffolds significantly.

EDS of silk fibroin scaffolds without (SFM-E: 19.91 ± 1.98 g/g) and with AuNPs (SFM-AuE: 24.60 ± 2.30 g/g) were statistically different. AuNPs incorporation into silk fibroin scaffolds increased EDS.

EDS of cross-linked collagen nanofibrous matrices (CM-AuX: 7.26 ± 2.62 g/g) were significantly lower than any other dermal layer groups. Their water swelling values were thought to be very low due to the fact that these scaffolds contained small pores and had a dense structure with less porosity (9-10%) than the scaffolds fabricated in the sponge forms. Their EDS were statistically similar to collagen/sericin films (C/S: 4.59 ± 0.58 g/g and C/S-X: 2.79 ± 0.43 g/g), since the films had also a very dense structure.

The ability of a scaffold to preserve water is an important aspect to evaluate its property for skin tissue engineering. The water uptake ability of the scaffolds could be attributed to their hydrophilicity, their morphology (pore size, pore size distribution, and porosity) and the maintenance of their 3D structure. In general, EDS is decreased as the cross-linking degree is increased because of the decrease of the hydrophilic groups (Bhardwaj et al., 2014). Also, EDS decreases when the pore size and porosity decreases too (Park et al., 2002). However, cross-linking with GTA clearly increased EDS of bilayered scaffolds in this study, probably due to the decrease in dimensions of the uncross-linked scaffolds with substantial contraction and/or degradation in aqueous environment. EDS values obtained in different studies related to skin tissue engineering applications varied greatly. Silk fibroin 3D scaffolds as skin dermal substitutes (Bhardwaj et al., 2014) had varying swelling ratios (20-30 g/g). Electrospun collagen blends as skin substitutes had swelling ratios of 0.5-2 (Lin et al., 2013). EDS value of collagen-chitosan nanofibrous scaffolds was 9 g/g (Chen et al., 2008) Chitosan wound dressings cross-linked with GTA (Adekogbe et al., 2005) had EDS value range of 29.9-31 g/g. EDS values of nanofibrous matrices obtained by electrospinning of polylactide-polyglycolide/collagen blends ranged between 1.8-2.2 g/g (Liu et al., 2010). EDS values of the scaffolds in the literature were similar to the values in our study. As a whole, the EDS values of the bilayered skin substitutes prepared in our study were thought to be appropriate for skin tissue engineering applications.

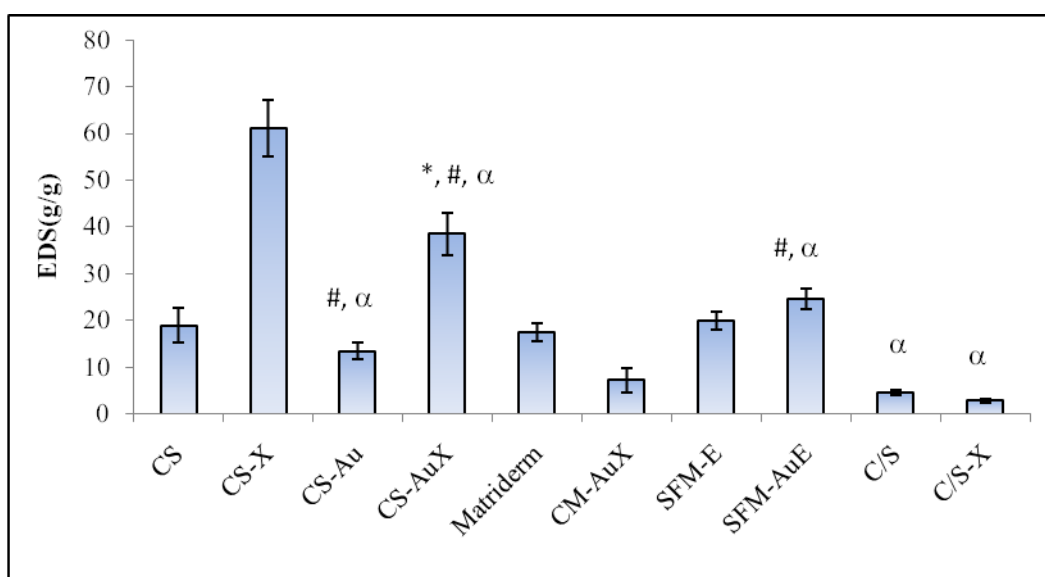


Figure 3.21. EDS of scaffolds. *: Significant difference between the same compositional groups after cross-linking for $p < 0.05$. #: Significant difference between the same compositional groups after AuNPs incorporation for $p < 0.05$. α : Significant difference from MatridermTM for $p < 0.05$. Values are expressed as mean \pm SD (n=4).

3.5.1.6. Water Vapor Transmission Rates

Water vapour transmission rate (WVTR) values (about 1300 g/m²/day) of bilayered scaffolds were found to be statistically similar (Figure 3.22). Therefore, WVTR values were thought to be controlled mainly by sericin/collagen membrane layer.

In fact, a moist environment is desired for quick healing of wound, but at the same time excessive pooling of exudates below the wound bed should be avoided to decrease the risk of infection. On the other hand, wound dehydration would result in death cell debris creating a scar tissue. Therefore, it should be taken into consideration that a skin substitute might be able to control the water vapour loss from the wound at an optimal rate. It was shown that WVTR for normal skin is 204 g/m²/day, and this value changes with respect to the exudates level of wound type. For instance; WVTR for injured skin could be as low as 279 g/m²/day for a first-

degree burn and this could increase up to 5138 g/m²/day for a granulating wound. Owing to the fact the WVTR varies with respect to the type of wound, it might be suggested that the values about 1300 g/m²/day measured for the bilayered skin substitutes are likely to be suitable for low to medium exudating wounds (Yannas and Burke, 1980).

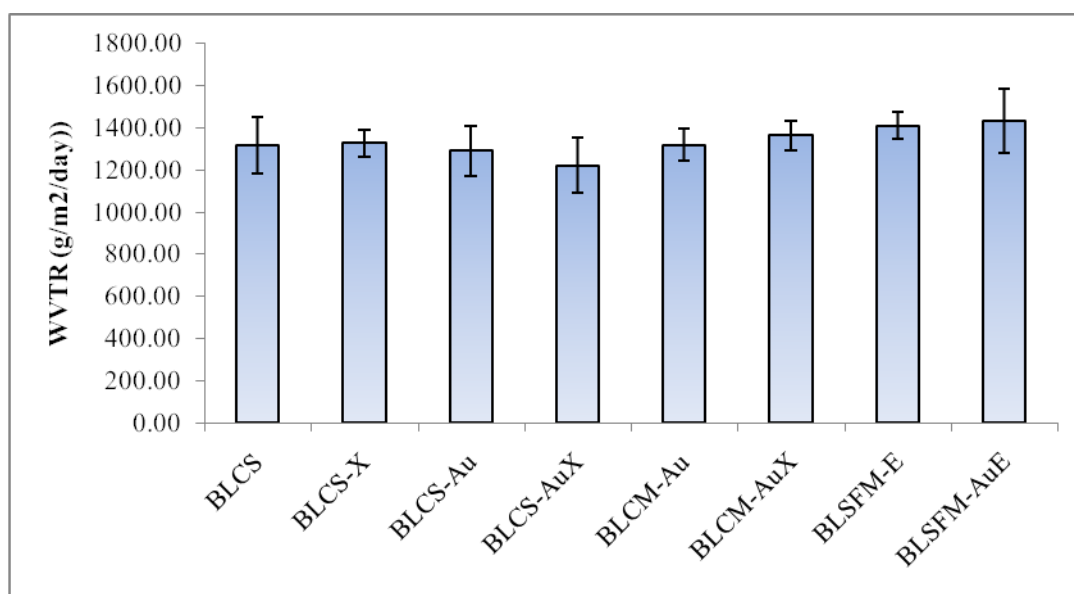


Figure 3.22. Water vapor transmission rate (WVTR) of bilayered scaffolds. Values are expressed as mean \pm SD (n=4).

3.5.1.7. Oxygen Permeation

Oxygen permeability (OP) tests were based on measuring the amounts of dissolved oxygen (DO) in the media isolated from air by the bilayered scaffolds separately. Hence, the measured parameter, DO, was considered to be a direct result of OP character of bilayered scaffolds. OP characteristic of bilayered scaffolds were shown in Figure 3.23. The open control was measured to have a DO value of 7.33 ± 0.02 mg/L, but the closed control had DO as 7.11 ± 0.01 mg/L. DO of all of the bilayered scaffolds and the open control were almost the same (about 7.33 mg/L) having

statistically insignificant difference. On the other hand, the closed group had significantly lower mean DO value than all the bilayered scaffold groups. As a consequence, all of these results suggested that all of the bilayered scaffolds were said to be highly permeable to oxygen.

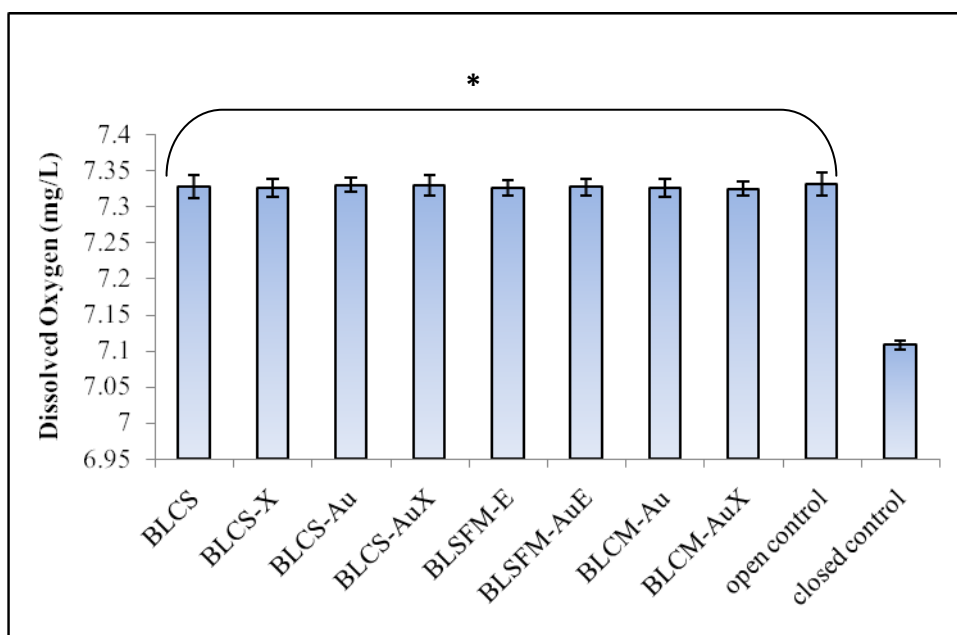


Figure 3.23. Oxygen permeability of bilayered scaffolds. Values are mean \pm SD (n=3).*: Indicates significant difference from the closed control for $p < 0.05$.

3.5.1.8. Mechanical Tests

The representative stress-strain curves of epidermal (C/S and C/S-X) and dermal (CS, CS-X, CS-Au, CS-AuX, CM-Au, CM-AuX, SFM-E and SFM-AuE) layers of all the bilayered scaffolds (in both dry and wet testing) conditions were given in Figure 3.24 and 3.25 to give a rough idea about the general mechanical characteristics of bilayered scaffolds fabricated in this study. The typical collagen sponge stress-strain curve was such that initially the stress did not increase a lot while the strain does creating a toe region as explained in detail in the introduction part. In order to circumvent this toe region, the scaffolds were gripped tautly between

the jaws by exerting a very low pretension. It must be noted that, especially for the delicate scaffolds (here in this study CS, CS-Au, SFM-E and SFM-AuE, C/S and C/S-X), pretension caused premature failures. Therefore, pretension was adjusted meticulously for such scaffolds. When tension was exerted, the crimping collagen fibers elongated to a specific extent after which the cross-links holding them become stressed, and the stress-strain curve became linear as shown in the initial part of the stress-strain curves (Figure 3.24 and 3.25). After cross-linking, this linear region became more distinct. After a specific degree of tensile stress (proportional limit), the linear relationship between stress and strain was lost. Then, the scaffolds behaved nonlinearly until reaching a maximum stress value (ultimate tensile stress or tensile strength) at or after which it broke. In the stress-strain curves of collagen sponges (CS, CS-X, CS-Au, CS-AuX), silk fibroin matrices (SFM-E and SFM-AuE) and collagen/sericin films (C/S and C/S-X) and Matriderm™, generally the plastic region was barely realized or completely lost in dry experimental conditions. Only collagen nanofibrous matrices (CM-Au) had a very short linear elastic region followed by a long nonlinear plastic region. Plastic region of this group also became smaller after cross-linking. When the mechanical tests were performed in wet conditions the plastic region could be seen more pronouncedly.

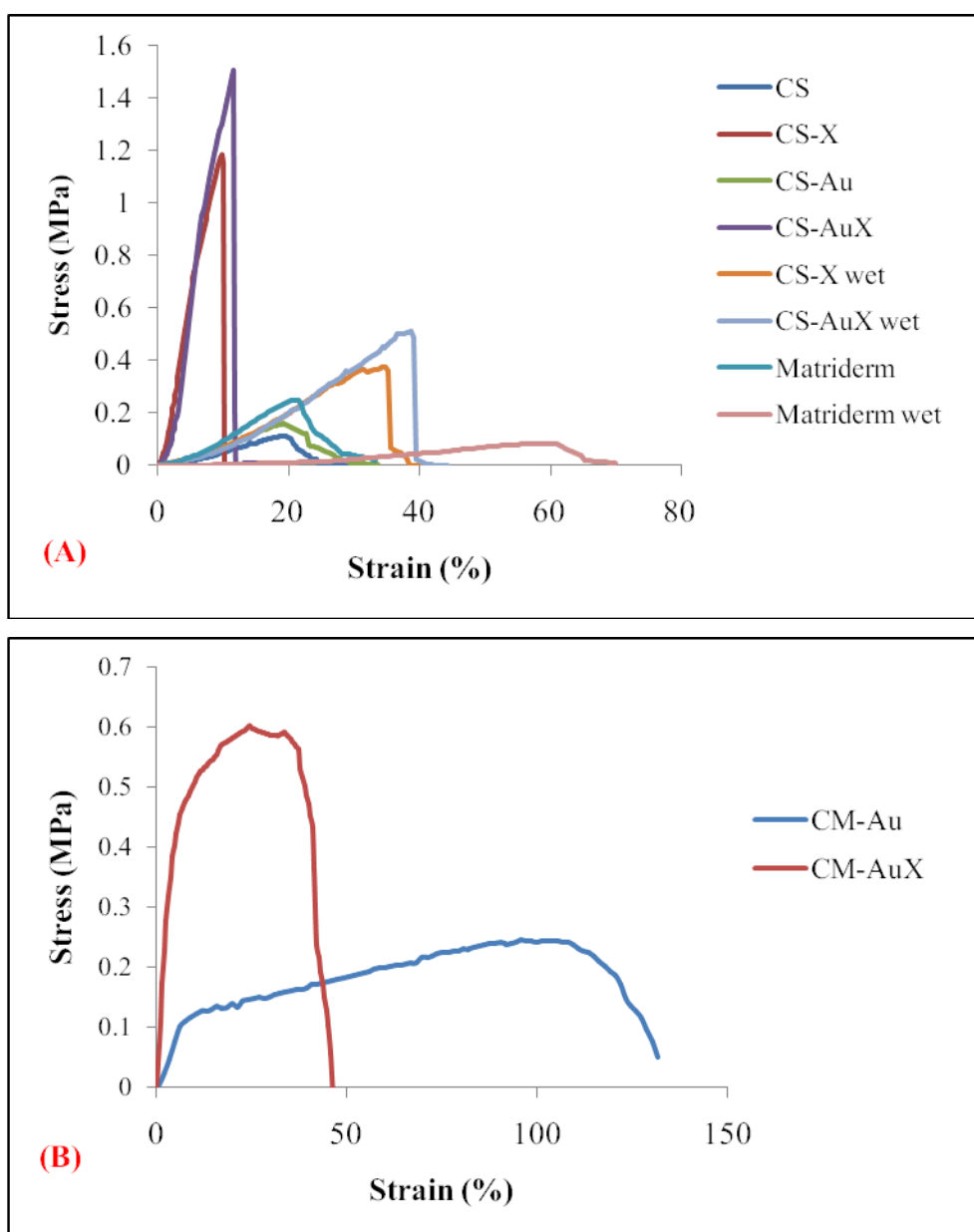


Figure 3.24. Representative stress-strain curves of scaffolds fabricated in this study: (A) collagen sponges (CS, CS-X, CS-X wet, CS-Au, CS-AuX and CS-AuX wet), MatrigelTM (Matrigel and Matrigel wet) and (B) collagen nanofibrous matrices (CM-Au and CM-AuX).

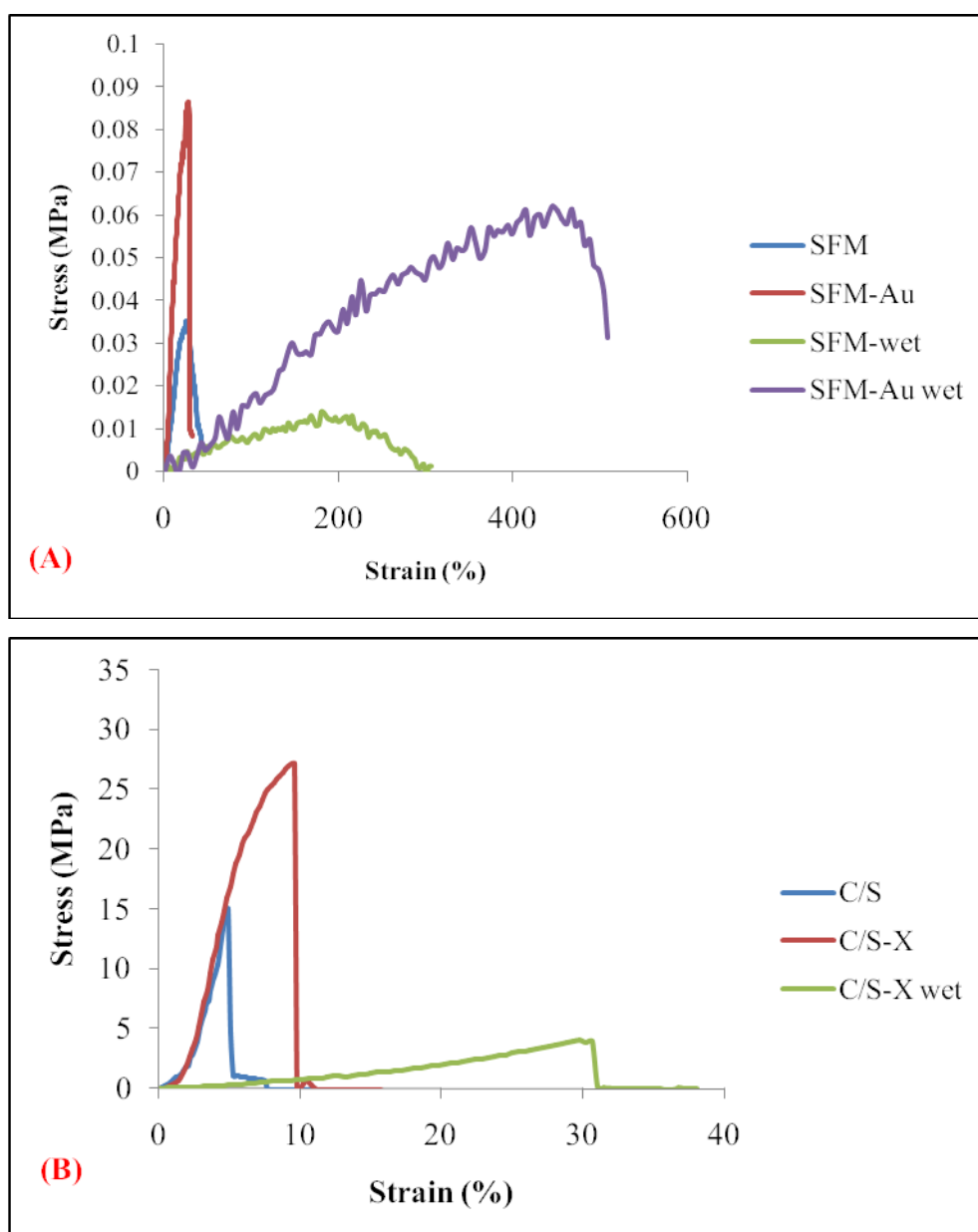


Figure 3.25. Representative stress-strain curves of scaffolds fabricated in this study: (A) silk fibroin matrices (SFM-E, SFM-E wet, SFM-AuE and SFM-AuE wet) and (B) collagen/sericin membranes (C/S, C/S-X and C/S-X wet).

The tensile test was accepted as successful when the failure occurred in the middle of the gauge region of samples (Figure 3.26). Tensile strength is an intrinsic property of materials, and consequently does not depend on the size of the specimen. However, it

is affected by the preparation procedures of the specimen and the temperature of the test environment and material. Hence, mechanical tests were carried out at the same laboratory environment (standard room conditions) for all samples.

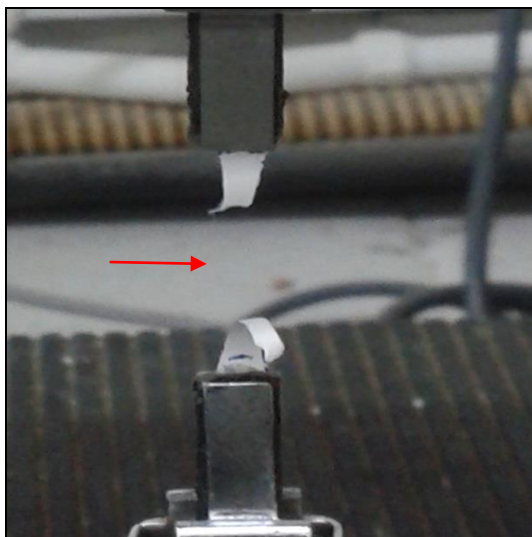


Figure 3.26. Successful tensile break occurred in the middle of the gauge length.

3.5.1.8.1. Tensile Strength

Ultimate tensile stress or tensile strength (UTS) of scaffolds was found to range from very low values for silk fibroin matrices (0.011 MPa) in wet conditions to very high UTS for collagen/sericin films (24 MPa) (Table 3.5). UTS of collagen sponge groups, collagen nanofibrous matrices and collagen/sericin films increased significantly after cross-linking. In contradiction to the increasing effect of cross-linking, performing the tests in wet conditions decreased UTS significantly for all the groups. AuNPs incorporation into collagen sponges and silk fibroin matrices tended to increase UTS, though it was not statistically meaningful for collagen sponge group. The same increase effect of AuNPs on strength of scaffold was encountered in other studies as well such as chitosan-AuNPs nanocomposite (Lin et al., 2008) and poly (L-lactide)-AuNPs composite scaffolds (McKeon-Fischer and Freeman, 2011).

Cross-linked collagen sponge groups had statistically better UTS than Matriderm™, whereas uncross-linked collagen sponges had diminished UTS.

In this study, it was aimed to mimic tensile strength of skin with the scaffolds as much as possible. However, it was not possible to reach the reported tensile strength (2.5-16 MPa) of human skin (Silver, 1994) with the scaffolds developed in this study. The tensile strength values of the collagen sponges (0.1-1.2 Mpa), silk fibroin matrices (0.08-0.01 MPa) and collagen nanofibrous matrices (0.3-0.5 MPa) fabricated in this study were lower than the tensile strength of skin, but these results were similar with the UTS values measured for different studies related to the skin tissue engineering in the literature. In order to improve the mechanical properties of collagen based scaffolds, generally a variety of cross-linking agents were used such as GTA (Muthukumar et al., 2014), genipin (Bi et al., 2011), EDC(Powel and Boyce, 2006). Although these cross-linkers succeeded in to improve the mechanical properties of collagen based scaffolds considerably, they did not reach the reported values specified for skin as well. For example; collagen sponge incorporated with *Macrotyloma uniflorum* had 0.6-3MPa UTS (Muthukumar et al., 2014) and collagen-GAG sponge had 0.03-0.07- MPa UTS (Powel and Boyce, 2006). There are also some variations on the tensile strength of collagen nanofibers fabricated in different studies probably due to the differences in collagen nanofiber diameter, thickness, cross-linking treatment and etc. For instance; UTS of GTA cross-linked collagen nanofibers had 7-11 MPa in dry and wet testing conditions (Rho et al., 2006). Collagen/chitosan nanofibrous wound dressing had 0.5-1 MPa UTS (Chen et al., 2008). Electrospun matrices as wound dressing prepared from *Rana chensinensis* skin collagen/poly(L-lactide) mixtures had UTS values of 0.2-3 MPa (Zhang et al., 2015). UTS of nanofibrous matrices obtained by electrospinning of collagen/polyvinyl alcohol/chitosan blends were about 1-7 MPa UTS (Lin et al., 2013). Electrospun type I collagen/polycaprolactone blends had 0.8-1.9 MPa UTS (Chakrapani et al., 2012).

3.5.1.8.2. Elongation at Break

In the present study, elongation at break (EAB) values of different scaffolds changed in a very wide spectrum ranging from very low values of 3-9% for collagen/sericin films (C/S and C/S-X) in dry conditions to very high EAB reaching to 168-301% for silk fibroin matrices (SFM-E and SFM-AuE) (Table 3.5). It was found that the collagen sponge groups could elongate as much as the MatridermTM with similar elongation characteristics. Cross-linking treatment seemed to decrease EAB of collagen sponges; though it did not have a significant effect on collagen sponges without AuNPs, the decrease became significant in dry conditions. The difference became pronounced in wet conditions. In a similar way, cross-linking treatment decreased EAB of collagen nanofibrous matrices and collagen/sericin membranes significantly in dry conditions. Performing the test in wet conditions increased EAB of all the groups significantly. AuNPs incorporation did not have a significant influence on collagen sponges or silk fibroin matrices.

Ultimate elongation of skin is 78% (Park and Lakes, 1992). The maximum strain of collagen was reported as in the 10-20% range (Meyers et al., 2008). In this study, it was aimed to mimic the mechanical properties of skin with the scaffolds as much as possible. However, it was not possible to reach the reported EAB values of skin values in dry conditions with any of the scaffolds except for CM-Au group exceeding 100% elongation. Yet, this high EAB was sacrificed after cross-linking treatment dropping to 29% levels for CM-AuX. Again the EAB values of different studies in the literature varied a lot, but EAB values in none of these studies exceeded 100% levels. Generally, EAB values were higher for nanofibrous matrices reaching to 54-61% for electrospun type I collagen/ polycaprolactone (Chakrapani et al., 2012), 5-50% for collagen/polyvinyl alcohol/chitosan (Lin et al., 2013) and 5-40% for *Rana chensinensis* skin collagen/poly(L-lactide) (Zhang et al., 2015). On the other hand, EAB of scaffolds in the sponge form such as for collagen sponge incorporated with *Macrotyloma uniflorum* (Muthukumar et al., 2014) and collagen-GAG sponge (Powell and Boyce, 2006) were in the range of 12-16% and 23-62%, respectively. The EAB range of other scaffolds fabricated in this study was soundly lower than

that of skin. However, the EAB of scaffolds increased evidently in wet form. Considering that the wound area is generally moist owing to the exudate discharge from the skin, it is thought that the dressing would get wet and become more extensible. Adekogbe and Ghanem (2005) showed that the elongation of dry chitosan scaffolds increased from 20% to 80% when they got wet. In addition, EAB of cross-linked dry collagen films of Wang et al. (2003) increased from 2.3% to 36.5% when they were wet. Hence, the measured strains of wet scaffolds are expected to increase in *in vivo* conditions as well.

As seen, the mechanical results of the scaffolds developed in this study are compatible with the literature data. In addition, the mechanical properties the scaffolds developed in this study were comparable to or even better than that of commercial skin substitute, MatridermTM. This indicated that these scaffolds would probably provide a similar or even better level of mechanical stability when applied in the wound treatment procedure.

3.5.1.8.3. Tensile Modulus

Since extensibility is a selection criterion for skin substitutes, a low modulus of elasticity (E) with high extensibility was sought. In this study, E had the highest values for the most brittle scaffold, i.e. collagen/sericin films, and on the contrary had the lowest values for the softest silk fibroin scaffolds as measured to range from 621 MPa to 0.0052 MPa (Table 3.5). E of collagen sponge groups, collagen nanofibrous scaffolds and collagen/sericin films increased significantly after cross-linking. In contrast, E of all groups decreased significantly in wet conditions. E value of CS-X wet, CS-AuX wet, CM-Au and MatridermTM were very close. Due to the fact silk fibroin scaffolds were very soft, they had the lowest E values. There was not a clear change in E values when AuNPs were incorporated into scaffolds.

The E range of collagen sponges (0.4-12 MPa), silk fibroin matrices (0.01-0.3 MPa), collagen nanofibrous matrices (2-6 MPa) and collagen/sericin films (14-621 MPa)

developed in this study are in the range or close the lower E limit of human skin. E for skin was found between 6-40 MPa (Silver, 1994). Also, the range of E values in the literature was compatible with the E values of our scaffolds. E increased significantly as a result of AuNPs incorporation as mentioned before. The same increase effect of AuNPs on elastic modulus of scaffold was encountered in other studies as well (Lin et al., 2008; McKeon-Fischer and Freeman, 2011). Collagen/chitosan nanofibrous wound dressing (Chen et al., 2008) had very low E values (0.3-0.7 MPa) similar to values obtained for uncross-linked sponges (CS and CS-Au) and silk fibroin matrices (SFM-E and SFM-AuE). *Rana chensinensis* skin collagen/poly(L-lactide) electrospun matrices (Zhang et al., 2015) and collagen/polyvinyl alcohol/chitosan nanofibrous matrices (Lin et al., 2013) had E values of 32-38 MPa and 5-50 MPa, respectively. These values were also similar with the E values of cross-linked collagen sponges (CS-X and CS-AuX) and collagen nanofibrous matrices (CM-AuX). The same decrease in E values of scaffolds was observed when the tests were performed with wet samples in the literature. For instance; cross-linked dry collagen films of Wang et al. (2003) had E value of 1.16 GPa approximately, but decreased to 5.8 MPa in wet form.

Table 3.5. Mechanical properties of epidermal and dermal layers of bilayered scaffolds.

Groups	Tensile Strength (MPa)	Elongation at Break (%)	Elastic Modulus (MPa)
CS	0.099 ±0.022 ^d	15.43± 2.38 ^d	0.73± 0.16
CS wet	NA	103.43± 16.70 ^{ad}	NA
CS-X	0.97 ±0.13 ^{bd}	10.36± 2.19 ^d	10.10± 1.68 ^b
CS-X wet	0.38 ±0.081 ^a	33.63± 4.58 ^{ad}	1.18± 0.20 ^a
CS-Au	0.097 ±0.038 ^d	27.16± 8.63 ^c	0.44± 0.23
CS-Au wet	NA	101.84± 15.57 ^{ad}	NA
CS-AuX	1.19 ±0.40 ^{bd}	9.86± 1.99 ^d	12.47± 4.19 ^b
CS-AuX wet	0.47 ±0.099 ^a	39.46± 9.10 ^{ad}	1.44± 0.44 ^a
Matriderm TM	0.33 ±0.077	22.41± 2.55	1.67± 0.31
Matriderm TM wet	0.093 ±0.013 ^a	56.59± 7.52 ^a	0.19±0.035 ^a
CM-Au	0.29 ±0.031	106.90± 14.97	1.82± 0.38
CM-AuX	0.53 ±0.079 ^b	28.64± 4.23 ^b	6.38± 1.96 ^b
SFM-E	0.032 ±0.0091	21.58± 10.96	0.26± 0.19
SFM-E wet	0.011 ±0.0029	168.35± 29.16 ^a	0.0052± 0.0013 ^a
SFM-AuE	0.077 ±0.023 ^c	29.53± 4.84	0.27± 0.15
SFM-AuE wet	0.041 ±0.015 ^a	301.40± 81.26 ^{ac}	0.013±0.0047 ^a
C/S	15.00 ±2.68	3.00± 1.30	620.60± 250.41
C/S wet	NA	67.69± 12.11 ^a	NA
C/S-X	24.30 ±2.42 ^b	8.75± 1.80 ^b	328.00± 49.59 ^b
C/S-X wet	3.81 ±0.58 ^a	28.02± 4.99 ^{ab}	13.76± 1.54 ^a

Data are expressed as mean ± SD (n ≥6).

^asignificant difference observed between the same groups when the tests were performed in wet conditions for p<0.05.

^bsignificant difference observed between the same groups when they were cross-linked for p<0.05.

^csignificant difference between the same groups when they contain AuNPs.

^d significant difference from MatridermTM for p<0.05.

NA: Scaffolds are not applicable to the testing.

3.5.2. In Vitro Characterization Tests

3.5.2.1. Preliminary Cell Cytotoxicity Tests of Gold Nanoparticles

In preliminary cytotoxicity tests, the cytotoxic effect of AuNPs having different sizes (Au1: 55 nm, Au2: 20 nm and Au3: 13 nm) and different doses (5, 10, 20 ppm) were evaluated on HaCat keratinocyte and 3T3 fibroblast in terms of OD values and the corresponding % cell viabilities (Figures 3.27 and 3.28). OD results were used to show the proliferation of cells between time points, as the cell viability results were used to show cytotoxicity. Reduction of cell viability by more than 30% is considered as a cytotoxic effect according to ISO 10993-5 standards.

At 1st day, there was no significant difference between the OD values of control group (no AuNPs) and any dose groups (5, 10 and 20 ppm) of Au1 for both cell types (Figures 3.27 A and 3.28 A). While keratinocyte cell viabilities were 92-108%, fibroblast cell viabilities were 84-89% for Au1 dose groups. Although statistically significant OD differences were found between all the doses of Au2 and Au3 and control, these differences were very small due to less number of cells grown at 1st day for both cell types (Figures 3.27 B-C and 3.28 B-C). As keratinocyte cell viabilities were 64-71% and 61-79%, fibroblast cell viabilities were 67-72% and 61-73% for Au2 and Au3 dose groups, respectively. Also, there was no significant difference among the test doses of Au1, Au2 and Au3 at 1st day (Figures 3.27 and 3.28). These results showed that AuNPs having bigger sizes (55 nm) did not have any cytotoxic effect on neither keratinocytes nor 3T3 fibroblasts, but Au2 and Au3 were slightly cytotoxic at the tested doses during 1 day time period.

At 7th day, all the doses (except for 20 ppm dose) of Au1 group had OD values statistically similar to control group for both cell types (Figures 3.27 A and 3.28 A). The OD value differences of the same doses of Au1 between different time periods were again significant for both cell types at 7th day. While keratinocyte cell viabilities were 68-87%, fibroblast cell viabilities were 85-91% for Au1 dose groups. After 7 days of incubation period, the proliferation of keratinocytes slowed down

substantially for any doses of Au2 and Au3 in comparison to control, but OD values between the same doses increased significantly between the time points (Figures 3.27 B-C). However, the proliferation of 3T3 fibroblasts was comparable to control for any doses of Au2 and Au3 except for the 20 ppm dose of Au3 (Figures 3.28 B-C). As keratinocyte cell viabilities were 26-35% and 28-49%, fibroblast cell viabilities were 121-139% and 50-97% for Au2 and Au3 dose groups, respectively. Only bigger nanoparticles (Au1: 55 nm) were found to be nontoxic on keratinocytes with slight cytotoxic effect of its 20 ppm dose only, on the contrary, the other AuNPs were highly toxic on keratinocytes in 7 days. As a consequence, cytotoxic effect of AuNPs on keratinocytes was clearly size dependent. None of the AuNPs (Au1, Au2 and Au3) were toxic on fibroblast, that is, toxicity was not size dependent in 7 days. Only 20 ppm dose of Au3 was moderately toxic on fibroblasts. To clarify these results, AuNPs having larger sizes (sizes between 20-50 nm) and a more uniform size distribution was synthesized and investigated for its cytotoxicity.

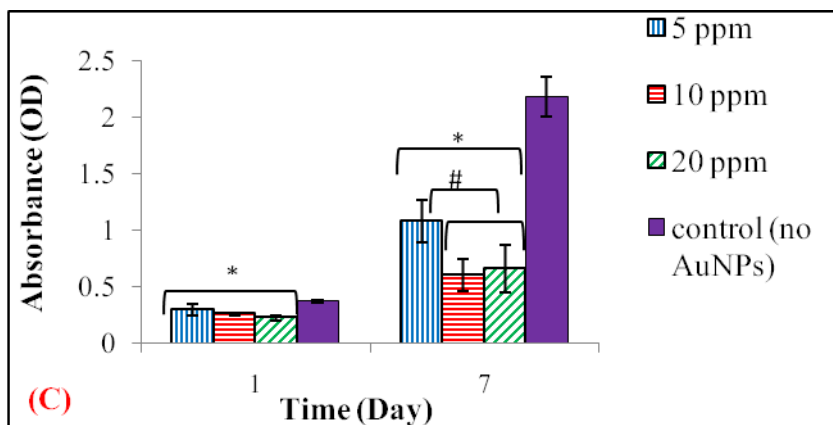
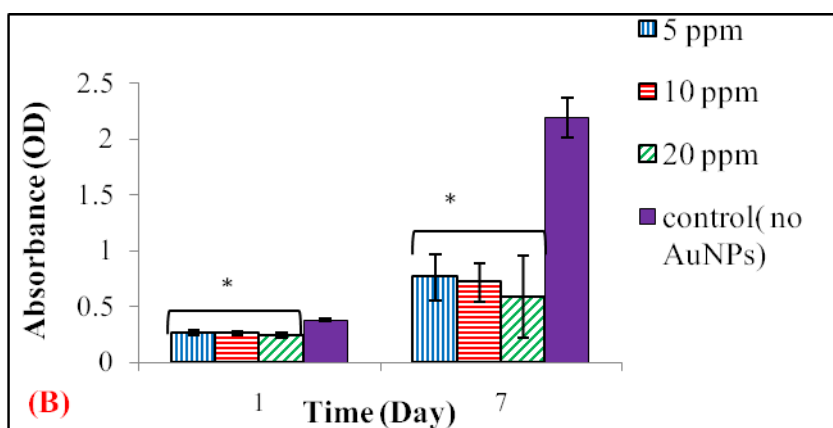
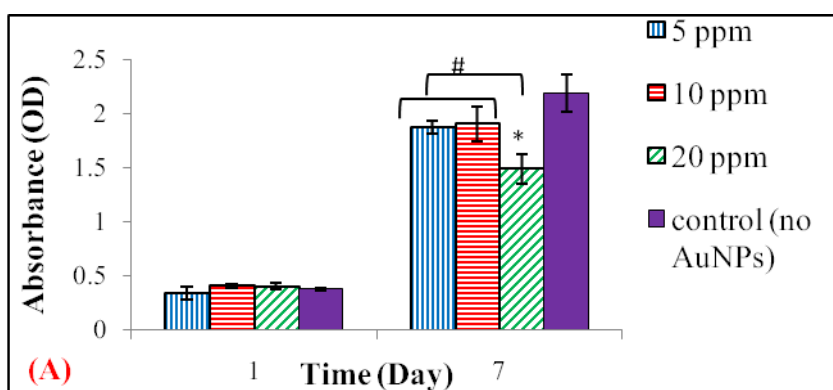


Figure 3.27. Cytotoxicity tests of different AuNPson keratinocytes with MTT assay: (A) Au1, (B) Au2 and(C) Au3. *: Significant difference from the control in the same time period. #: Significant difference between the groups in the same time period. (n=4 ±SD, p<0.05).

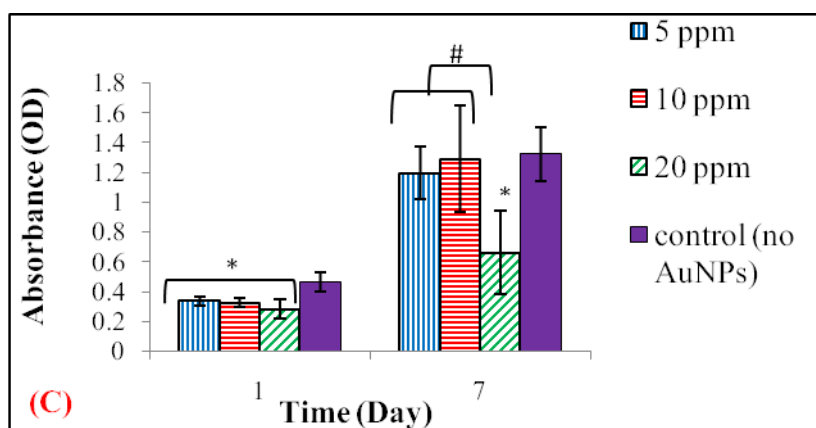
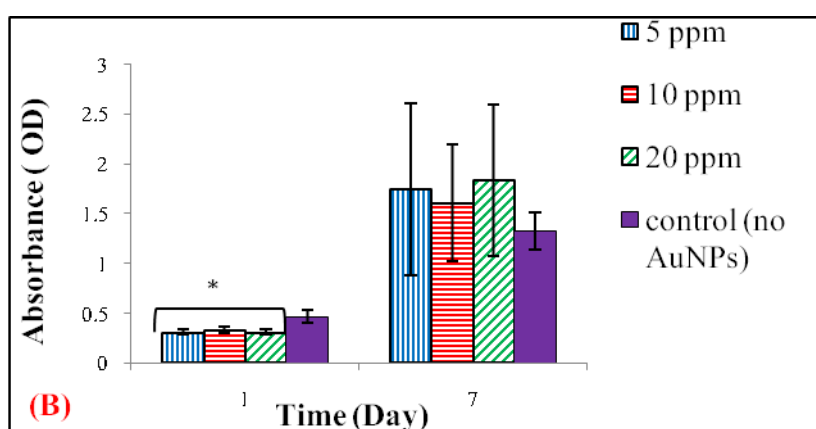
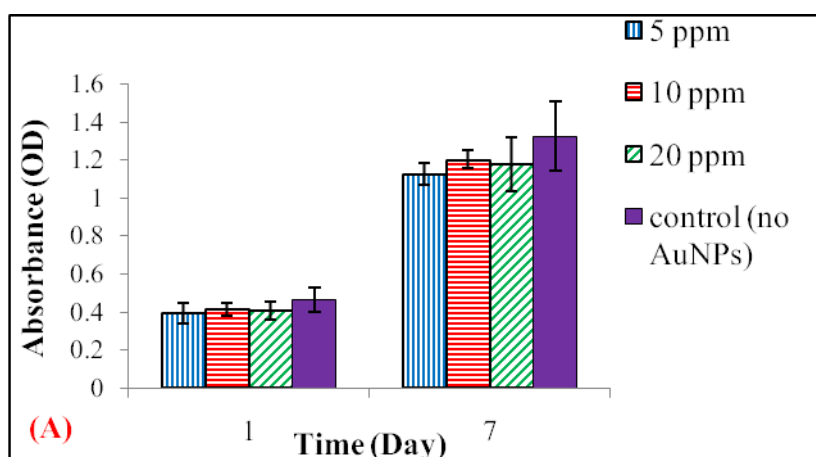


Figure 3.28. Cytotoxicity tests of different AuNPs groups on 3T3 fibroblasts with MTT assay: (A) Au1, (B) Au2 and (C) Au3. *: Significant difference from the control in the same time period #: Significant difference between the groups in the same time period. (n=4 \pm SD, p<0.05).

In our study, in order to be able to synthesize potentially biocompatible AuNPs, key parameters, such as size and shape of the nanoparticles were considered at first, because it was shown that cytotoxicity of AuNPs was dependent on the shape, size, dose and the type and charge of surface capping/reducing agents as well as cell type. For instance; it was demonstrated in a study that smaller AuNPs (1.4 nm) were cytotoxic for connective tissue fibroblasts, epithelial cells, and macrophages and melanoma cells whereas bigger AuNPs in the 15 nm size range were nontoxic even at high concentrations (Pan et al., 2007). The higher surface area to volume ratio of AuNPs might lead to more intense interactions with cellular components and the penetration of smaller sized AuNPs into intracellular locations like nucleus could be easier, thus cause to cytotoxicity (Pan et al., 2007). Also, gold nanorods were shown to be more cytotoxic than AuNPs; however, the reason for this was attributed to cetyl-trimethylammonium bromide surface coating (Wang et al., 2008). It was suggested that the cationic AuNPs were more cytotoxic than the same-size anionic ones due to the affinity of cationic particles to the negatively charged cell membrane (Goodman et al., 2004). It was also found that citrate-capped AuNPs were not cytotoxic to baby hamster kidney cells and human hepatocellular liver carcinoma cells, but cytotoxic to human carcinoma cells at certain concentrations (Patra et al., 2007). It was stressed in a study that keratinocyte proliferation was inhibited at doses of AuNPs (34 nm) higher than 10 ppm, on the other hand lower doses (5 ppm) was shown to enhance the cellular activity for 5 days of incubation (Lu et al., 2010). We also came up with a similar conclusion that toxicity of keratinocytes were dose dependent for bigger nanoparticles (37 and 42 nm), but 20 ppm was the toxic dose limit. Yet, slight differences between different studies related to the AuNPs cytotoxicity are not surprising due to the tendency of AuNPs to aggregation in cell culture media (Wang et al., 2008).

After performing the preliminary cytotoxicity tests for different size and concentration of AuNPs, we also reached to the conclusion that the cytotoxicity of AuNPs synthesized in this study was also size and dose dependent as reported in the literature. Appropriate size of AuNPs for in vitro tests was selected as greater than 20

nm but less than 50 nm. AuNPs having larger size than 50 nm was not preferred since that shape and size uniformity became worse for bigger AuNPs.

3.5.2.2. Cytotoxicity Tests of Optimized Gold Nanoparticles

Second set of cytotoxicity tests were carried out for bigger AuNPs (Au7: 42 nm and Au8: 37 nm) on keratinocytes and 3T3 fibroblasts again. Dose (10, 20 ppm) and time effect (1, 4 and 7 days) of AuNPs cytotoxicity on these cells were investigated as well. According to 1st day results, there was no significant difference between different doses of Au7 and Au8 groups and the control group for keratinocytes (Figure 3.29 A-B), but significant difference between different doses of Au7 and Au8 groups and the control group were observed for 3T3 fibroblasts (Figure 3.30A-B). Keratinocyte cell viabilities were 98-88% for Au7 and 90-92% for Au8 at 1st day. On the other hand, fibroblast cell viabilities were 67-70% for Au7 and 68-72% for Au8 at 1st day. These results verified that, these doses (10-20 ppm) of Au7 and Au8 were non-cytotoxic on keratinocytes, but slightly cytotoxic on fibroblast in 1 day.

After 4 days, there were significant differences between dose groups of Au7 and Au8 and the control for both cell types except for the OD of 10 ppm dose of Au7 for fibroblast (Figure 3.29 A-B and 3.30 A-B). While keratinocyte cell viability results were 65-73% for Au7 and 87-88% for Au8 at 4th day, fibroblast cell viabilities were 85-91% for Au7 and 79-82% for Au8 at 4th day. According to these results, the defined doses of Au8 were non-cytotoxic on keratinocytes or fibroblasts, but slight cytotoxic effect of Au7 was observed on keratinocytes in 4 days. In addition, no statistically meaningful difference occurred among the doses of Au7 and Au8 at 4th day for both cell types.

According to the OD results measured after an incubation period of 7 days, the OD results in all of the AuNPs groups were statistically similar to the control for both cell types, except for the OD values of 20 ppm dose group of both Au7 and Au8 for fibroblasts (Figure 3.29 A-B and 3.30 A-B). Keratinocyte cell viabilities were 91%

for Au7 and 90-97% for Au8 at 7th day. On the other hand, fibroblast cell viabilities were 80-86% for Au7 and 84-95% for Au8 at 7th day. These results verified that, the defined doses of Au7 or Au8 were non-cytotoxic on keratinocytes or fibroblasts in 7 days. Also, between each time periods, the cells proliferated significantly for all of the doses of Au7 and Au8.

As a consequence, the AuNPs in these sizes were supposed to have no clear adverse effect on cell proliferation or cell viability of fibroblasts and keratinocytes for short or long time periods. Taking into consideration all of these results, AuNPs groups did not have any cytotoxic effect on the cells during different incubation periods, but it should be noted that as the dose increased, cell viabilities decreased slightly. Especially, fibroblasts seemed to be more sensitive to dose increase of these AuNPs sizes. It was concluded that bigger AuNPs (37 and 42 nm) used in the second set of cytotoxicity tests appeared not to cause any cytotoxic effect on fibroblasts and keratinocytes, especially at low concentrations (5, 10 ppm). Hence, the fabricated scaffolds in this study were incorporated with these AuNPs having the aforementioned properties.

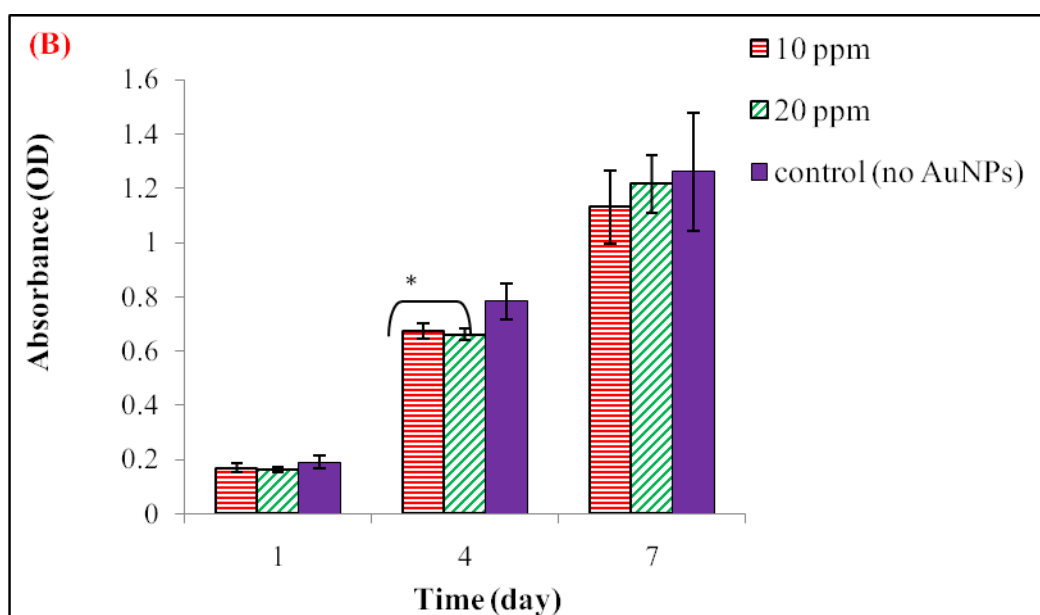
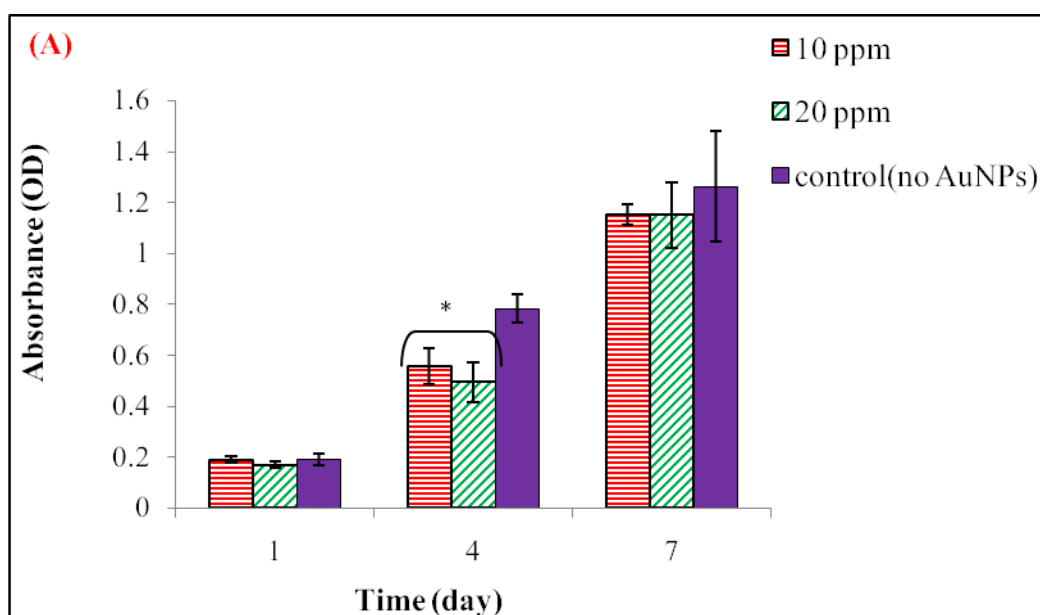


Figure 3.29. Cytotoxicity tests of different AuNPs groups on keratinocytes: (A) Au7 and (B) Au8. *: Indicating a significant difference from the control in the same time period (n=6 ±SD, p<0.05).

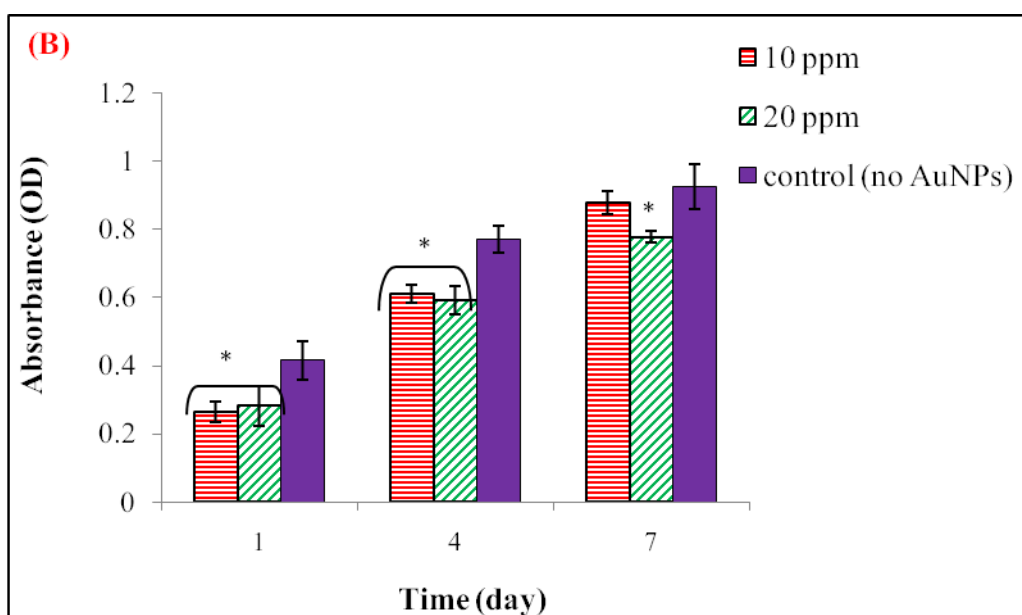
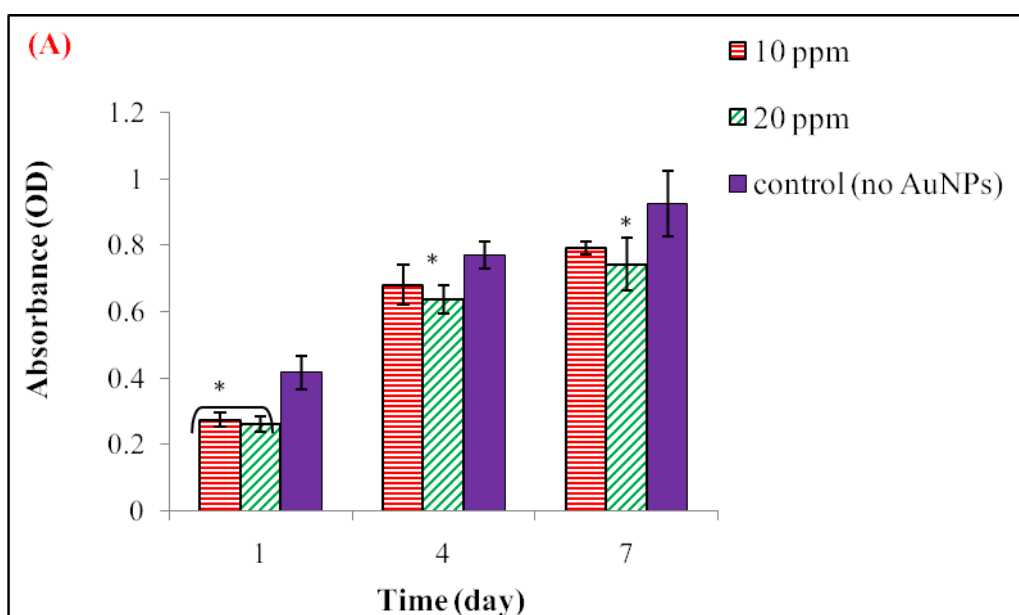


Figure 3.30. Cytotoxicity tests of different AuNPs groups on 3T3 fibroblasts: (A) Au7 and (B) Au8. *: Indicating a significant difference from the control in the same time period ($n=6 \pm SD$, $p<0.05$).

3.5.2.3. Cytotoxicity Tests of Scaffold Extracts

Cytotoxic effects of scaffold extracts were determined by either qualitative or quantitative means. According to qualitative morphological observation of L-929 cells subjected to extracts of epidermal, dermal layers of scaffolds and bilayered scaffolds, 0 grade (none reactivity) was given for each scaffold. The grading system was given in Table 2.5.

Reduction of cell viability by more than 30% is considered as a cytotoxic effect. The cell viability of dermal (CS, CS-X, CS-Au, CS-AuX, SF, SF-Au, CM-AuX) and epidermal layers (C/S and C/S-X) of scaffolds were generally above 90% (Figure 3.31A). Furthermore, the bilayered scaffolds (BLCS, BLCS-X, BLCS-Au, BLCS-AuX, BLSF, BLSF-Au, and BLCM-AuX) were considered non-cytotoxic since the cell viability of all groups was again above 90% (Figure 3.31 B).

Generally, the nontoxicity results of different AuNPs concentrations and leached out AuNPs from scaffolds in our culture conditions could be explained by the lower phagocytic capability of L-929 cells and shorter cultivation period (1 day) used for cell viability assay. L-929 cells are phagocytic (Vukovic et al., 2009), but the inhibitory effect of AuNPs on the metabolic activity of these cells was seen after prolonged cultivation periods (Rudolf et al., 2012). After longer incubation periods, the ingested AuNPs reduced cellular proliferation by inducing a transient oxidative stress (Soenen et al., 2009), or affecting cytoskeleton architecture (Pernodet et al., 2006). It is also possible that proliferation processes may be influenced by disturbing cell-cell contacts by AuNPs attached to the surface of L-929 cells. In addition, AuNPs might have partially been agglomerated in the complete cell culture medium before the tests. Furthermore, a re-aggregation process which occurred in the culture medium, leading to formation of some micron-sized particles, might have decreased phagocytosis.

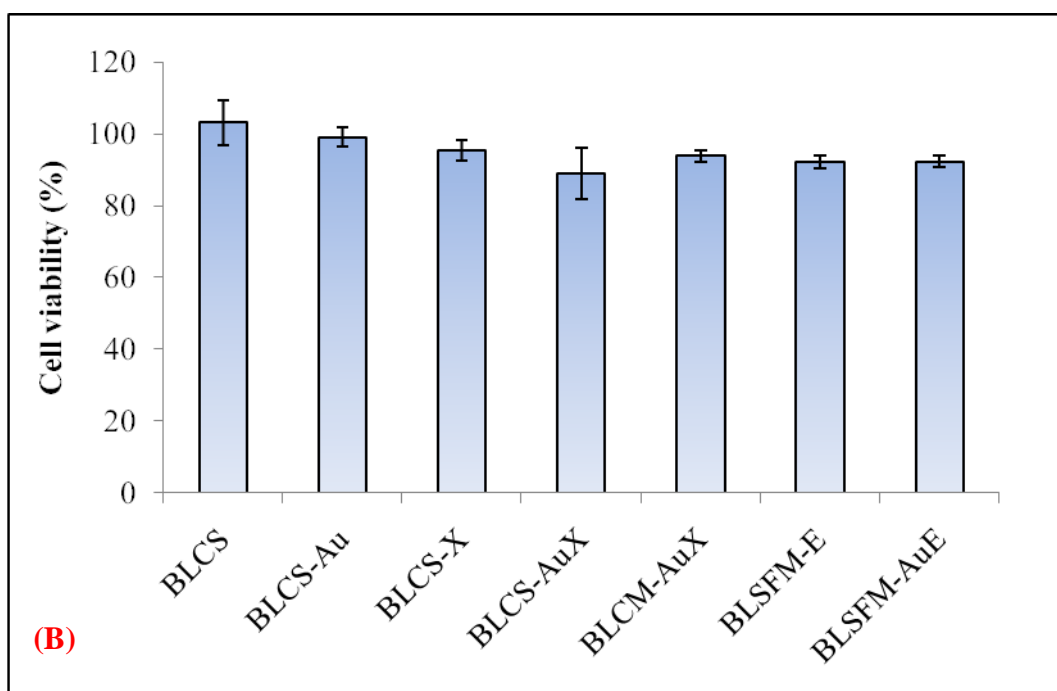
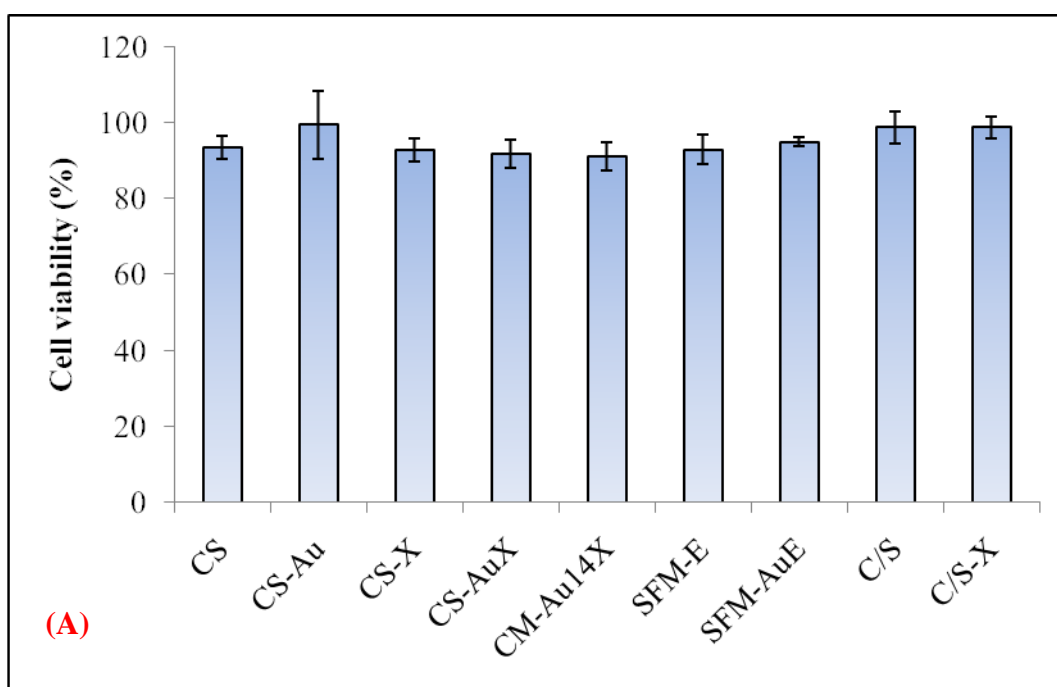


Figure 3.31. The results of extract cytotoxicity tests: (A) epidermal and dermal layers and (B) bilayered scaffolds.

3.5.2.4. Cell Adhesion and Proliferation Studies

Besides cytotoxicity tests, it is imperative to show cell attachment and proliferation on scaffolds that are to be utilized in skin tissue regeneration. Cell infiltration and proliferation are crucial for a scaffold to support and guide new tissue formation.

SEM micrographs revealed that fibroblasts adhered on the walls of the each dermal layer of scaffold group (CS, CS-X, CS-Au, CS-AuX, SF, SF-Au, and CM-AuX) tightly with typical spindle-like shape and out-stretched pseudopods spreading over scaffold surface in 1 day (Figures 3.32-3.35). Proliferation of cells on the scaffolds was also shown during 3 days incubation period with an increase in globular cells observed especially for scaffolds containing AuNPs. Since there were also lots of spindle-like shape in these groups, the increase is likely due to overcrowding of cells. This behavior was also previously verified by culturing the cells to over confluency on cell-culture flasks. Thus, it could be suggested that AuNPs might have an accelerating effect on the proliferation of L-929 cells.

According to SEM analysis HaCat keratinocytes attached to the surface of the each dermal layer of scaffold group (CS, CS-X, CS-Au, CS-AuX, SF, SF-Au, and CM-AuX) with typical polygonal morphology spreading over scaffold surface in 1 day (Figures 3.36-3.39). In line with the results of fibroblasts, keratinocytes also proliferated on the surface of scaffolds during the incubation time (Figures 3.36-3.39). As distinct from fibroblasts, it was observed that keratinocytes formed sheet like structures conforming to the topography of scaffold surfaces after 3 days. So, detecting them with SEM imaging was very difficult. Lu et al. (2010) showed that keratinocytes could adhere fast to the AuNPs/chitosan film scaffold and a low concentration of AuNPs (5 ppm) enhanced the proliferation of keratinocytes

These results proved that the scaffolds fabricated in this study preserve the original good cytocompatibility of collagen or silk fibroin. Potential cytotoxicity of GTA residue or AuNPs was not evidenced; on the contrary, AuNPs incorporation into scaffolds seemed to have an enhancing effect on cell proliferation. This result was

also tried to be confirmed further by analyzing the skin tissue responses to the scaffolds in vivo.

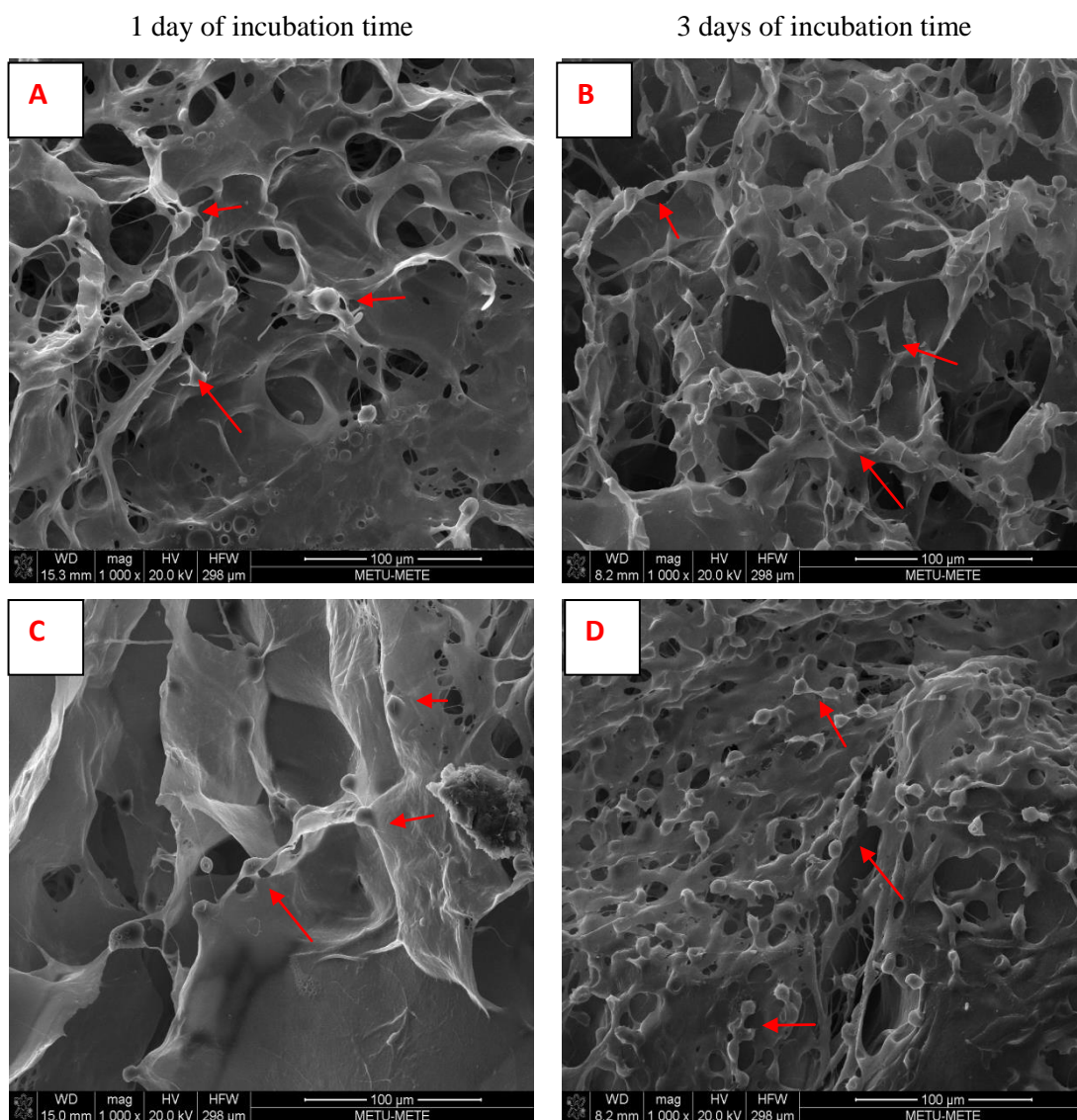


Figure 3.32. SEM micrographs showing the adhesion and proliferation of L929 fibroblasts on collagen sponge groups in different incubation periods: (A-B) CS and (C-D) CS-Au. Cells were shown with red arrows.

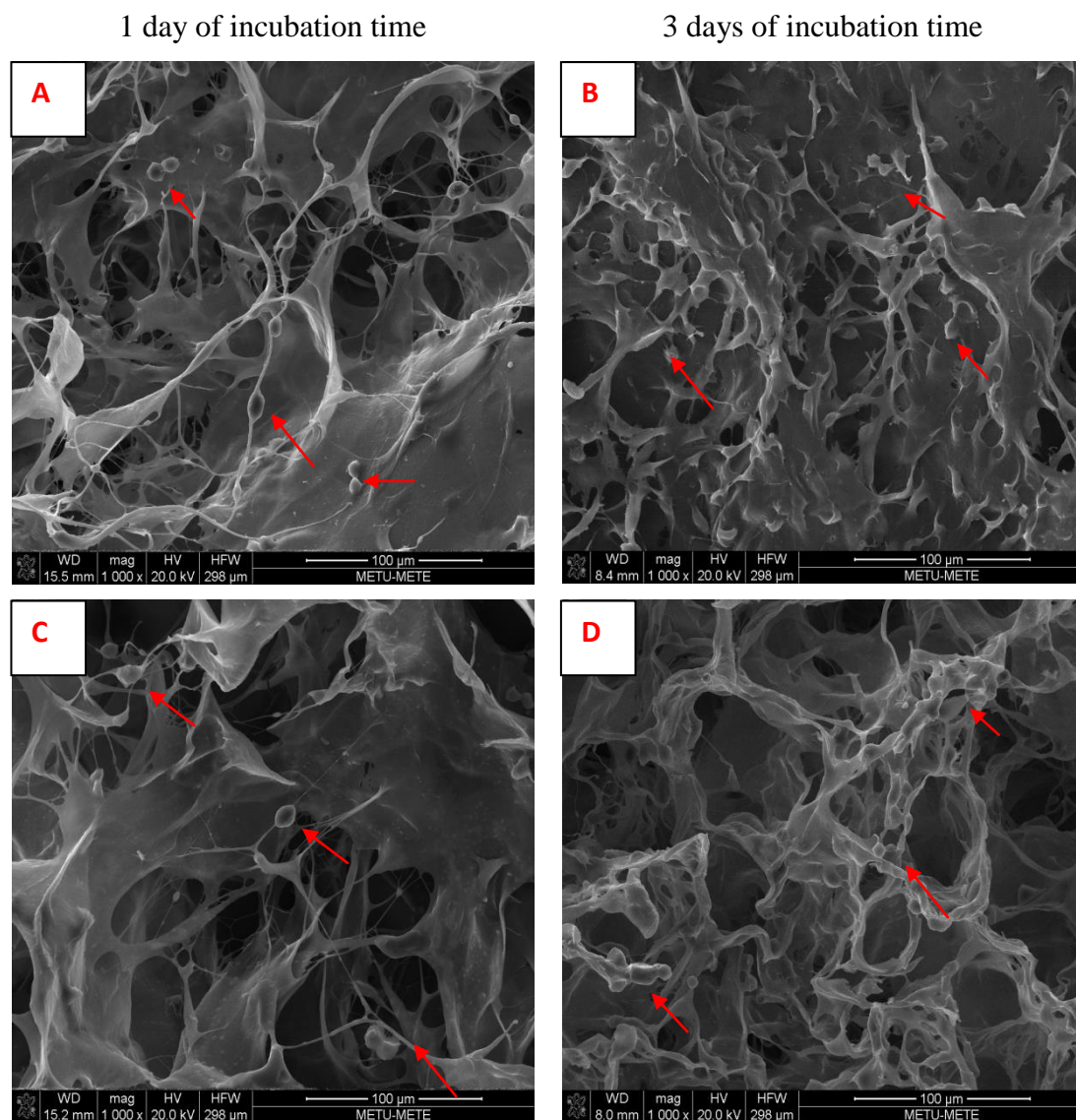


Figure 3.33. SEM micrographs showing the adhesion of L929 fibroblasts on A-B) CS-X and C-D) CS-AuX collagen sponge groups in different incubation periods. Cells were shown with red arrows.

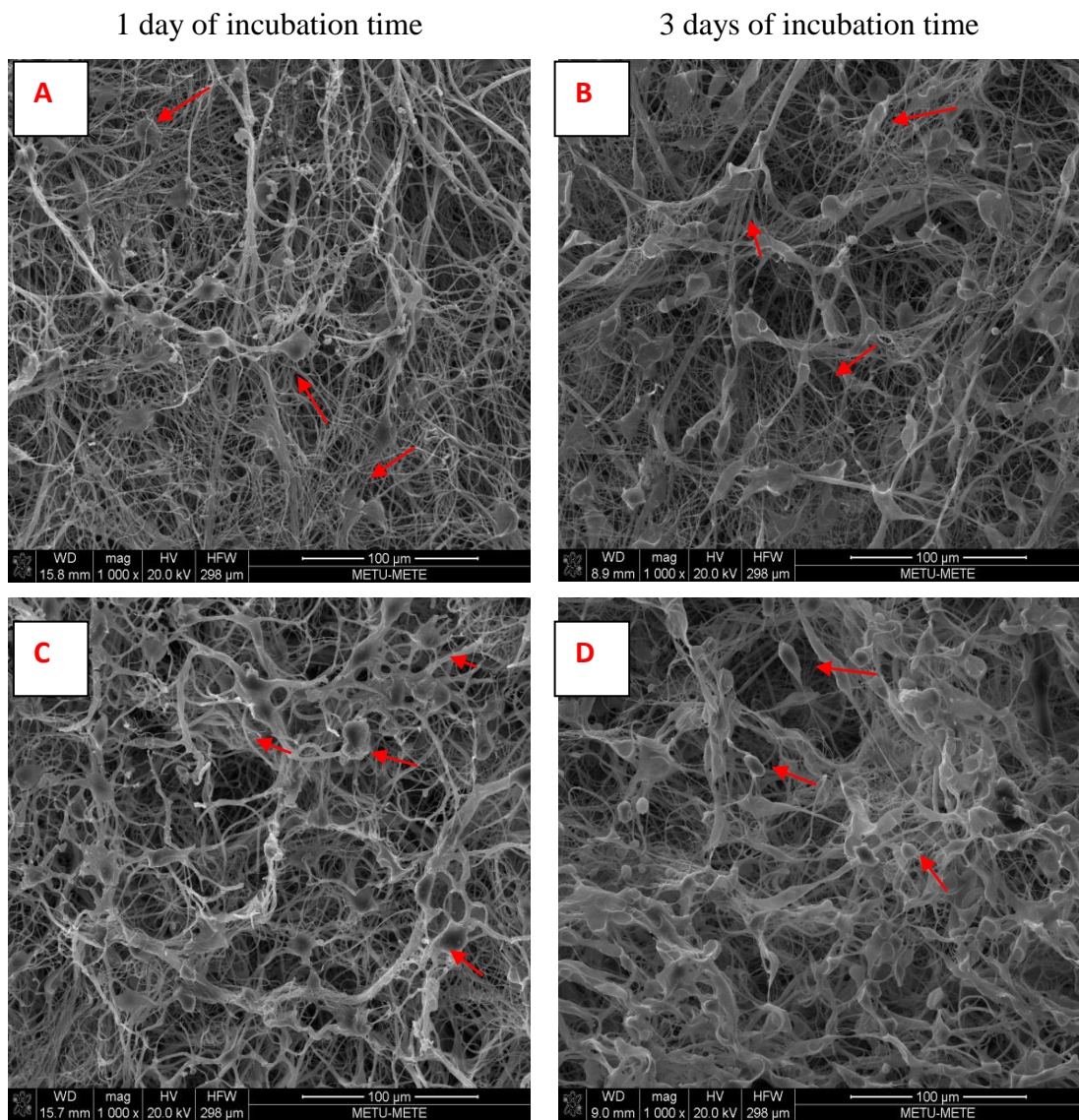


Figure 3.34. SEM micrographs showing the adhesion of L929 fibroblasts on A-B) SFM-E and C-D) SFM-AuE silk fibroin groups in different incubation periods. Cells were shown with red arrows.

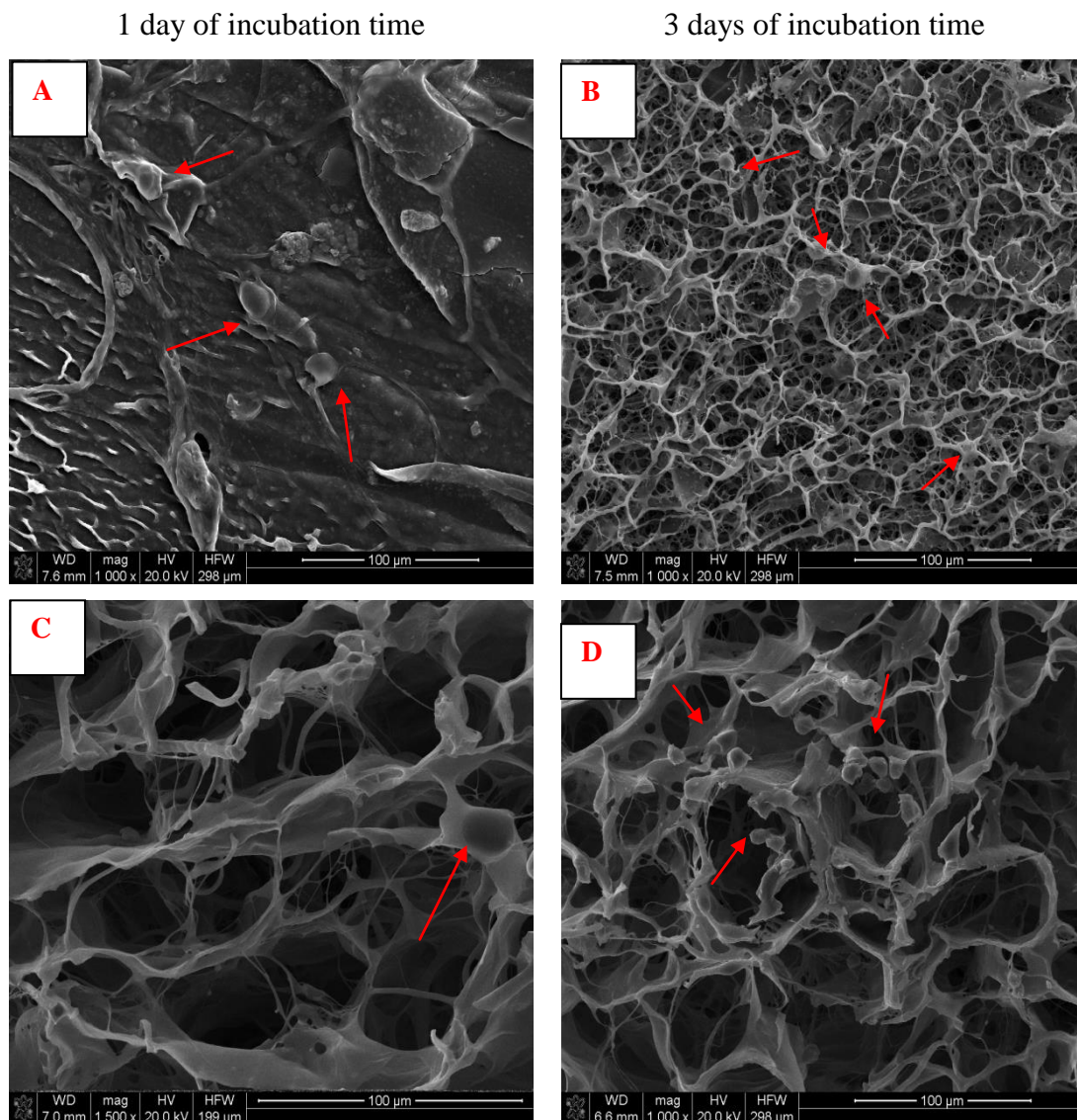


Figure 3.35. SEM micrographs showing the adhesion of L929 fibroblasts on A-B) CM-AuX and C-D) and Matriderm™ in different incubation periods. Cells were shown with red arrows.

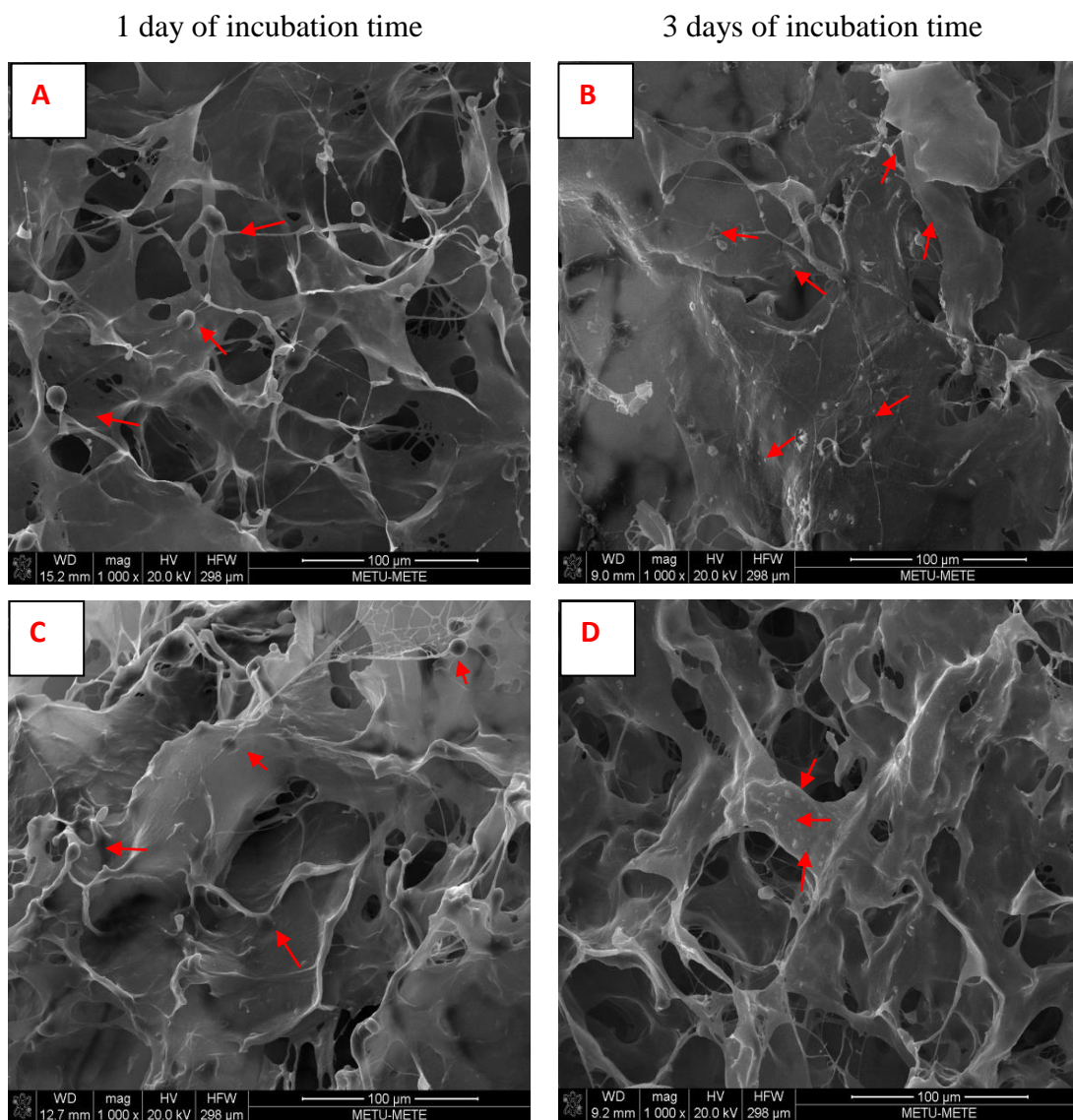


Figure 3.36. SEM micrographs showing the adhesion of keratinocytes on A-B) CS and C-D) CS-Au collagen sponge groups in different incubation periods. Cells were shown with red arrows.

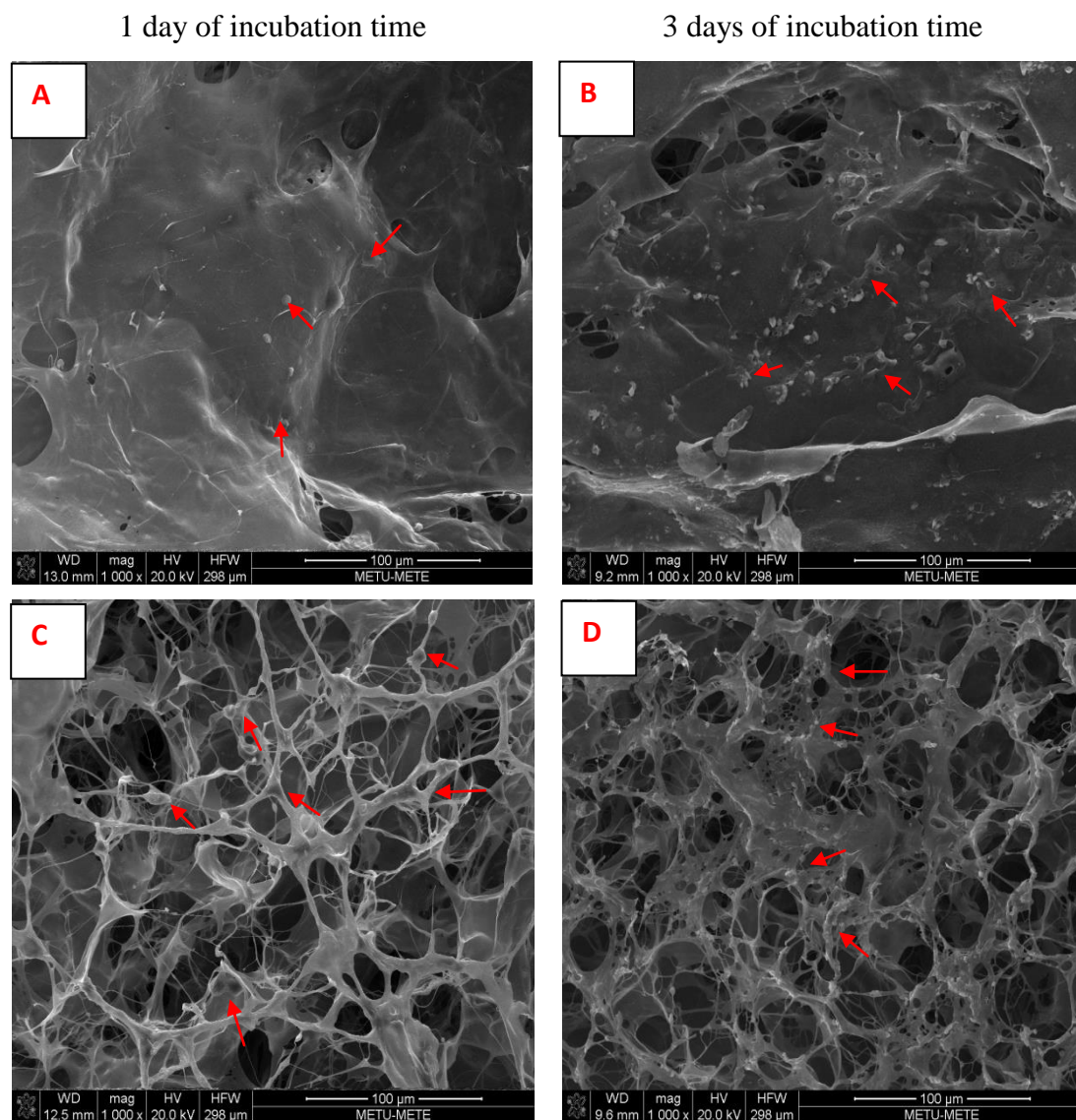


Figure 3.37. SEM micrographs showing the adhesion of keratinocytes on A-B) CS-X and C-D) CS-AuX collagen sponge groups in different incubation periods. Cells were shown with red arrows.

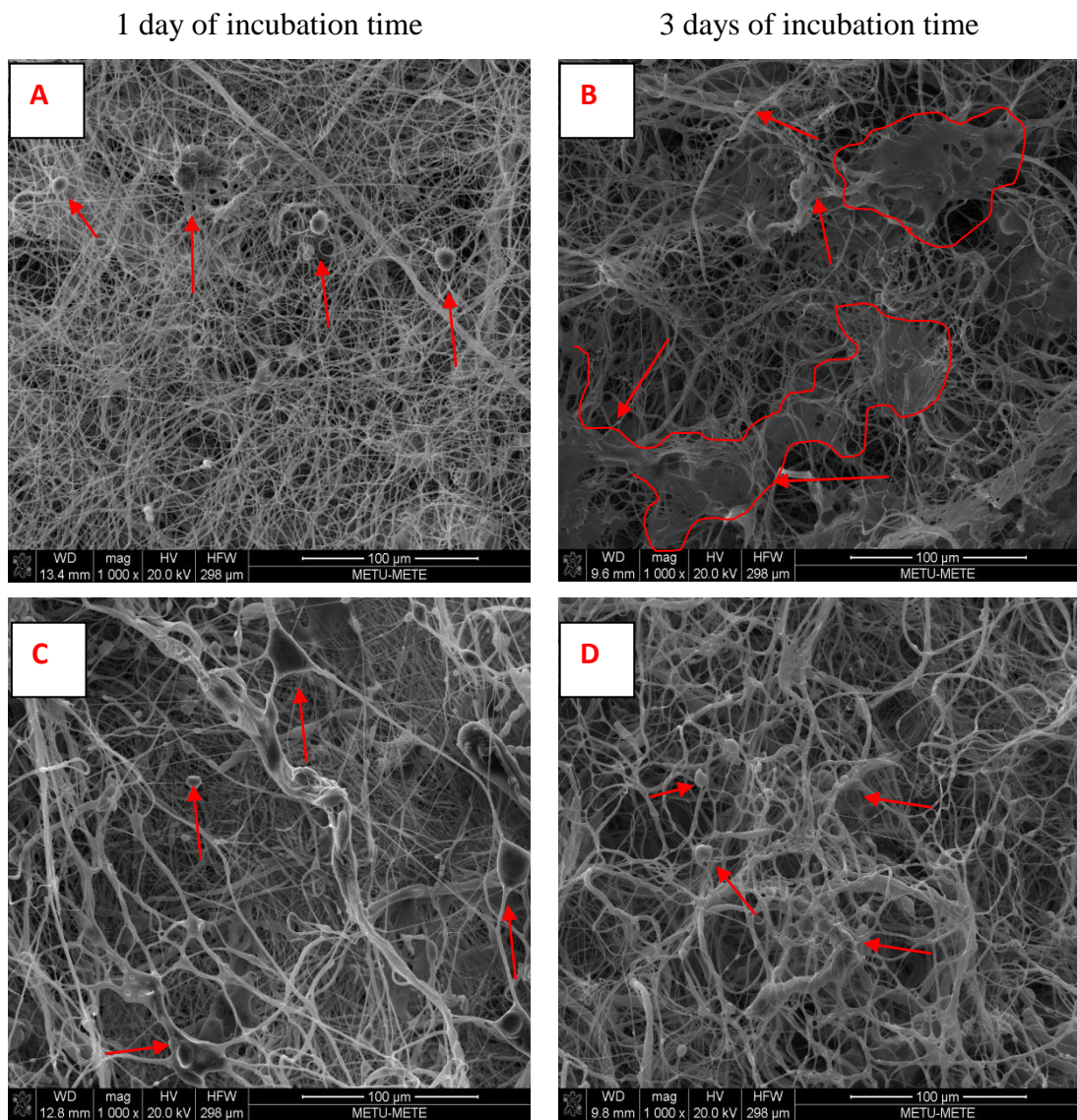


Figure 3.38. SEM micrographs showing the adhesion of keratinocytes on A-B) SFM-E and C-D) SFM-AuE silk fibroin matrix groups in different incubation periods. Cells were shown with red arrows.

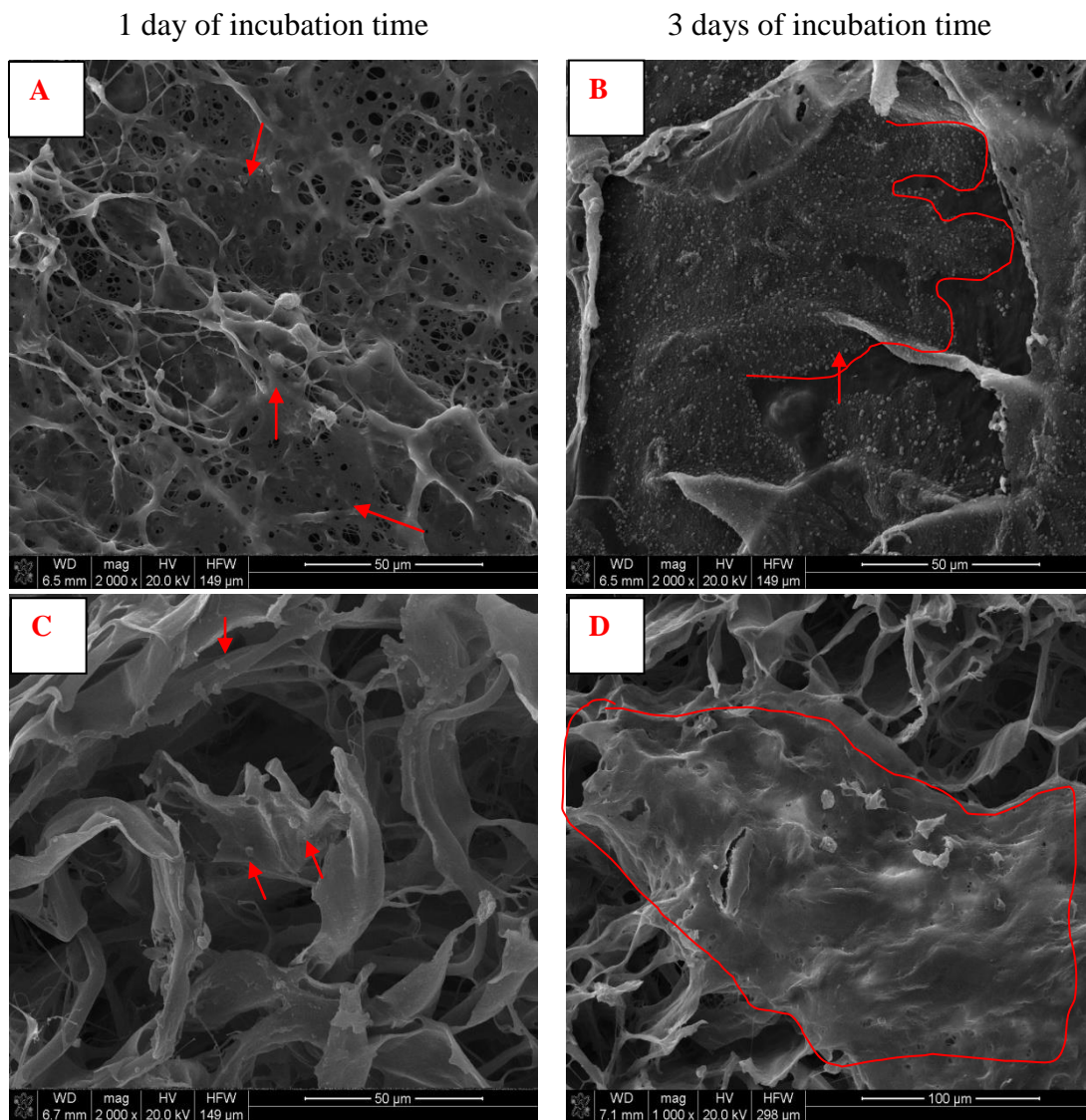


Figure 3.39. SEM micrographs showing the adhesion of keratinocytes on A-B) CM-AuX and C-D) MatridermTM groups in different incubation periods. Cells were shown with red arrows.

A similar strategy of incorporating AuNPs into tissue scaffolds such as decellularized porcine diaphragm (Cozad et al., 2011) collagen gel (Grant et al., 2014), polyethylene terephthalate mesh (Whelove et al., 2011) polypropylene mesh (Grant et al., 2011) was adopted for enhanced cell attachment and/or proliferation. To generalize these studies, specific amount of AuNPs was observed to enhance cell attachment and/or proliferation on tissue scaffolds. For instance; AuNPs (100 nm) incorporated collagen gels were not cytotoxic and the proliferation of cells seemed to be better than collagen gels without AuNPs. However, they also showed that the initial cell attachment was better in the collagen gels without AuNPs (Grant et al., 2014). In line with this study, collagen gels with AuNPs (2.4 nm) were not toxic at the concentrations (5mM) used in synthesis (Castaneda et al. 2008).

Like the collagen nanofibrous matrices developed in our study, AuNPs were also incorporated into nanofibrous structures made up of different materials such as poly L-lactide (McKeon-Fisher and Freeman, 2011), polyvinyl alcohol (Manjumeena et al., 2015) and polymethylglutarimide nanofibers (Jung et al., 2012). Electrospun poly (L-lactide) and AuNPs (5 nm) composite scaffolds were fabricated for skeletal muscle tissue engineering and specific amounts (7%) of AuNPs made the scaffolds biocompatible. In a similar way, 0.1% loading of AuNPs (15 nm) into electrospun PVA nanofibers increased the hydrophilicity and this led to good cell adhesion and proliferation when tested for biocompatibility on Vero cell lines (Manjumeena et al., 2015). It was reported that loading AuNPs (15 nm) into polymethylglutarimide nanofibers enhanced HeLa cell attachment and potentiated cardiomyocyte differentiation of human pluripotent stem cells (Jung et al., 2012).

In addition, silk fibroin nanofibers were reported to have good effect on cell attachment and spreading of normal human keratinocytes and fibroblasts in vitro (Min et al., 2004). Furthermore, silk fibroin extracted from different types of silkworm exhibited similar (*Bombyx mori* domestic silkworm) or better attachment (*Antheraea pernyi* wild silkworm) and proliferation of fibroblast cells as compared with collagen (Minoura et al., 1995).

3.5.3. Antibacterial Assessment

Antibacterial properties of the scaffolds are important for secondary infections after application to the wounded skin. In this research, presence of AuNPs in the scaffolds was considered as a positive enhancement of scaffold properties towards antibacterial role. Hence, two common pathogens of skin wounds, *S. aureus* and *S. Epidermidis*, were used in this study for evaluation of antibacterial properties.

3.5.3.1. Antibacterial Tests of Gold Nanoparticles

Antibacterial effect of AuNPs (with or without antibiotics) on *S.aureus* bacteria was investigated by measuring the transparent area (bacteria growth inhibitory zone) on the agar bacteria culture plate. As demonstrated in Figure 3.40, the antibacterial effect of discs containing only AuNPs increased as directly proportional with its concentration (5 -20 ppm). However, the transparent zone of samples containing the minimum AuNPs concentration (5 ppm) was unclear. The diameter of the zone was as small as the control group (empty discs). Yet, the zone of inhibition increased when the concentration of AuNPs increased still further.

Similar to our study, the inhibitory activity of AuNPs against a wide range of bacteria (*S.aureus*, *K. pneumoniae*, *P. aureginosa*, *E. Coli*, *L. monocytogenes*, *B. cereus*, *S. typhimurium*) was reported in different studies (Zawrah and El-Moes, 2011; Geethalakshmi and Sarada 2012). Bactericidal property of AuNPs was confirmed in a study by measuring the minimum bactericidal concentration (12-16 ppm) and minimum inhibitory concentration (4 ppm) (Cui et al., 2012). Hence, AuNPs in our study might not only have inhibited the growth of bacteria (5-10 ppm) but also killed them (20 ppm) for the selected test concentrations. The antimicrobial ability of citrate capped AuNPs against *S.aureus* in our study might be referred to their small size (about 37 nm) which is 40 times smaller than a bacterium. This makes them easier to adhere with the cell wall of the microorganisms causing its destruction and leads to the death of the cell. AuNPs possess well-developed surface

chemistry, chemical stability and appropriate smaller size, which make them easier to interact with the microorganisms (Nirmala and Pandian, 2007).

The combined effect of cefuroxime and AuNPs was also studied. The antibacterial effect of AuNPs was enhanced with the addition of antibiotic cefuroxime and the transparent zone became clearer (Figure 3.40). It is indicated that the best results were obtained when the concentration of AuNPs was the highest similar to the results when no antibiotic was used. By increasing the number of gold atoms, more amount of drug gets adsorbed on the nanoparticle surfaces when the number of drug molecules increase, they act more effectively against the microorganisms. This means that the AuNPs can act as an effective carrier to the drugs (Nirmala and Pandian, 2007). Drugs capped AuNPs act as a single unit against the microorganism and this leads to the increase in zone of inhibition (Zawrah and El-Moes, 2011). AuNPs act as a good vehicle carrying more amounts of drugs on its surface via electrostatic attraction between the amine groups of drugs and nanoparticles. Increasing the number of gold atoms, surrounded by a number of drug molecules makes an effective approach of the drug molecules as a group rather than acting alone towards the bacterial organisms (Nirmala and Pandian, 2007). Other studies indicated that drugs capped AuNPs are effective against various isolates of bacteria when compared with the pure drugs. The process of targeting by AuNPs can minimize treatment durations and side effects of drugs (Thomas and Klibanov, 2003; Tkachenko et al. 2004; Connor et al. 2005 and Mukherjee et al. 2007).

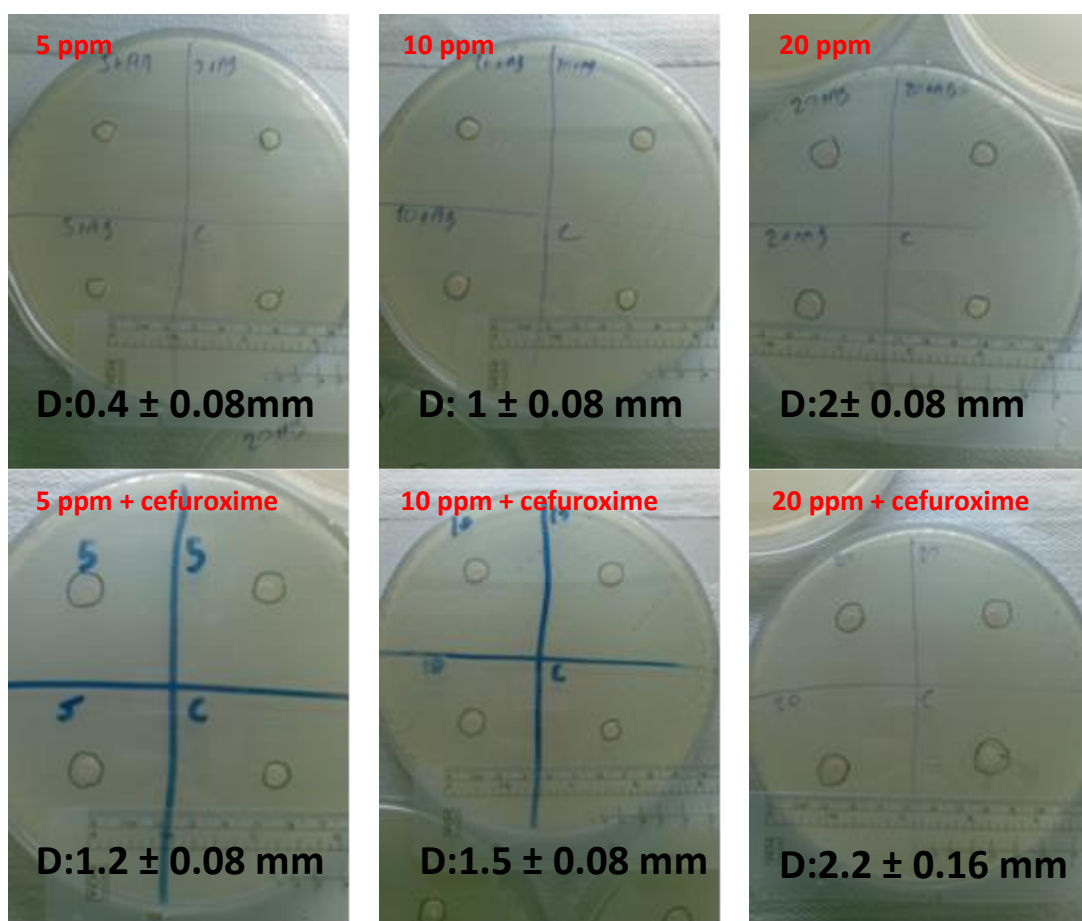


Figure 3.40. Agar diffusion tests results showing the transparent zones created around the discs loaded with different doses of AuNPs (Au8 group) alone (top row) and with different doses (5, 10, 20 ppm) of AuNPs (Au8 group) + antibiotic (cefuroxime, 4 μ g/ml) at the same time (bottom row).

3.5.3.2. Antibacterial Tests of Scaffolds

The antibacterial properties of the scaffolds were also investigated by using the other type of bacteria, *S. Epidermidis* in liquid culture. According to OD results (Figure 3.41), the adhered and supernatant bacteria were significantly lower in sample groups than the bacteria alone control group (LB). The bacteria growth was inhibited statistically in the growth medium of all sample groups (supernatant bacteria) with respect to the growth medium alone (LB supernatant bacteria). Even the groups

without AuNPs had some antibacterial effect unexpectedly considering the OD value of LB. This might have been caused by the residual antibacterial chemicals (acetic acid, and GTA) prevailing inside these scaffolds apart from the intended antibacterial effect of AuNPs. Therefore, *S. epidermidis* proliferated in the medium of silk fibroin matrix without AuNPs (SFM-E) and collagen/sericin membranes (C/S and C/S-X) better than the medium of other sample groups (CS, CS-X, CS-Au and CS-AuX). The lowest OD values of supernatant bacteria were measured for groups containing AuNPs. OD of collagen sponges containing AuNPs (CS-Au and CS-AuX) was statistically lower than CS group. Also, silk fibroin matrix with AuNPs (SFM-AuE) inhibited the bacteria growth significantly in comparison to SFM-E without AuNPs. Therefore, it was concluded that all the collagen sponges and SFM-AuE had possibly a strong inhibitory effect on the growth of bacteria in growth LB medium, on the other hand silk fibroin matrices without AuNPs (SFM-E) and collagen/sericin films did not inhibit the growth of bacteria. OD results related to bacteria adherence were too low, and so in order to understand whether the surface of different scaffold types had antibacterial property, SEM analysis was also carried out (Figure 3.42). Although the presence of bacteria was not too much on any of the scaffolds, there was a clear difference in bacteria numbers between the scaffolds with and without AuNPs. Consequently, it was supposed that AuNPs could have a role in creating an antibacterial surface coat on scaffolds.

The antimicrobial ability of citrate capped AuNPs against *S. epidermidis* in our study might be related to their small size again. It was reported that metal nanoparticles are harmful to bacteria (Chwalibog et al. 2010). It was stated that citrate capped AuNPs tend to make aggregates in solutions, especially when their concentrations was very high (Zhou et al., 2012). So, defining the antibacterial effect of citrate capped AuNPs in solutions could lead to misconceptions. In this study, antibacterial effect of bilayered scaffolds loaded with AuNPs in bacteria growth medium was investigated. So, aggregation was avoided. AuNPs inside the scaffolds probably extracted into the bacteria broth solutions and then bound closely to the surface of bacteria. During the interaction between *S. epidermidis* and AuNPs, they were trapped by the biofilm and the substance released by cells caused distortion of the cell wall (Chwalibog et al.

2010). Also, the particles interact with the building elements of the outer membrane and might cause structural changes, degradation and finally cell death. It was indicated in a study that AuNPs are more effective against gram negative organisms due to the nature of materials present in cell wall. However, the bacteria type (*S. Epidermidis*) in this study was gram-positive. Hence, the bactericidal efficacy of citrate capped AuNPs synthesized in this study was not very high.

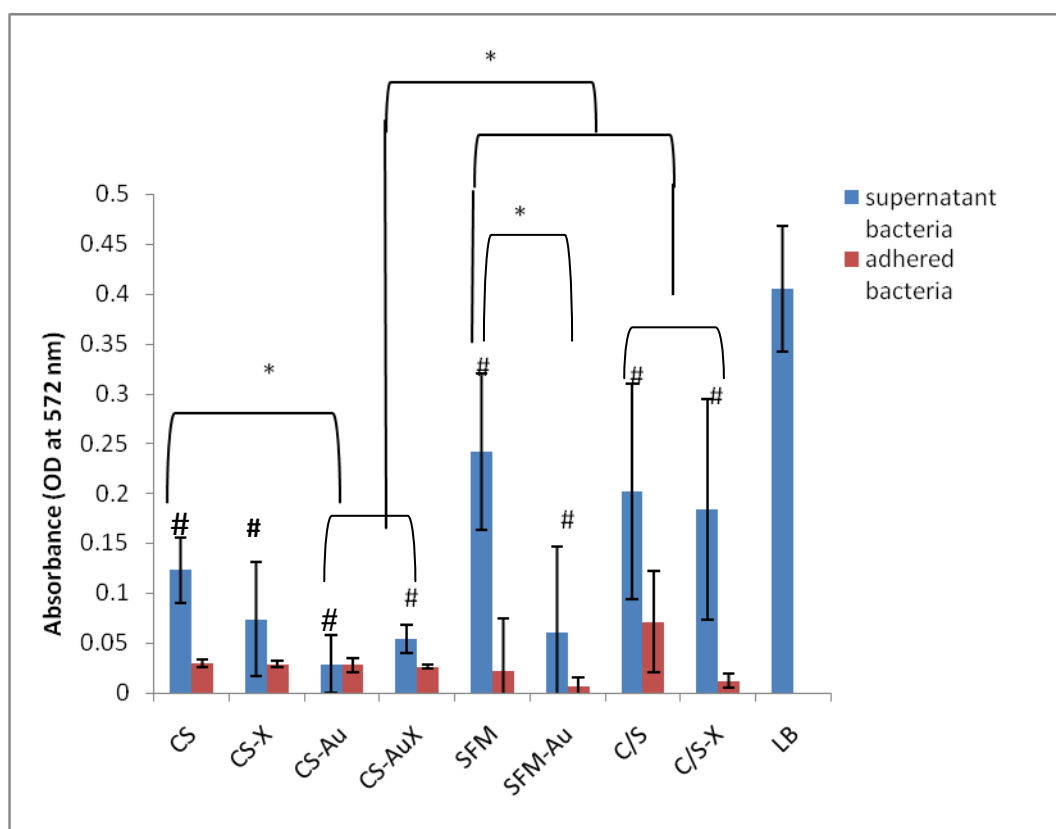


Figure 3.41. Antibacterial tests of scaffolds based on OD measurements. *: Indicating a significant difference between the groups. #: Significant difference from the control group (LB). (n=3 ±SD, p<0.05).

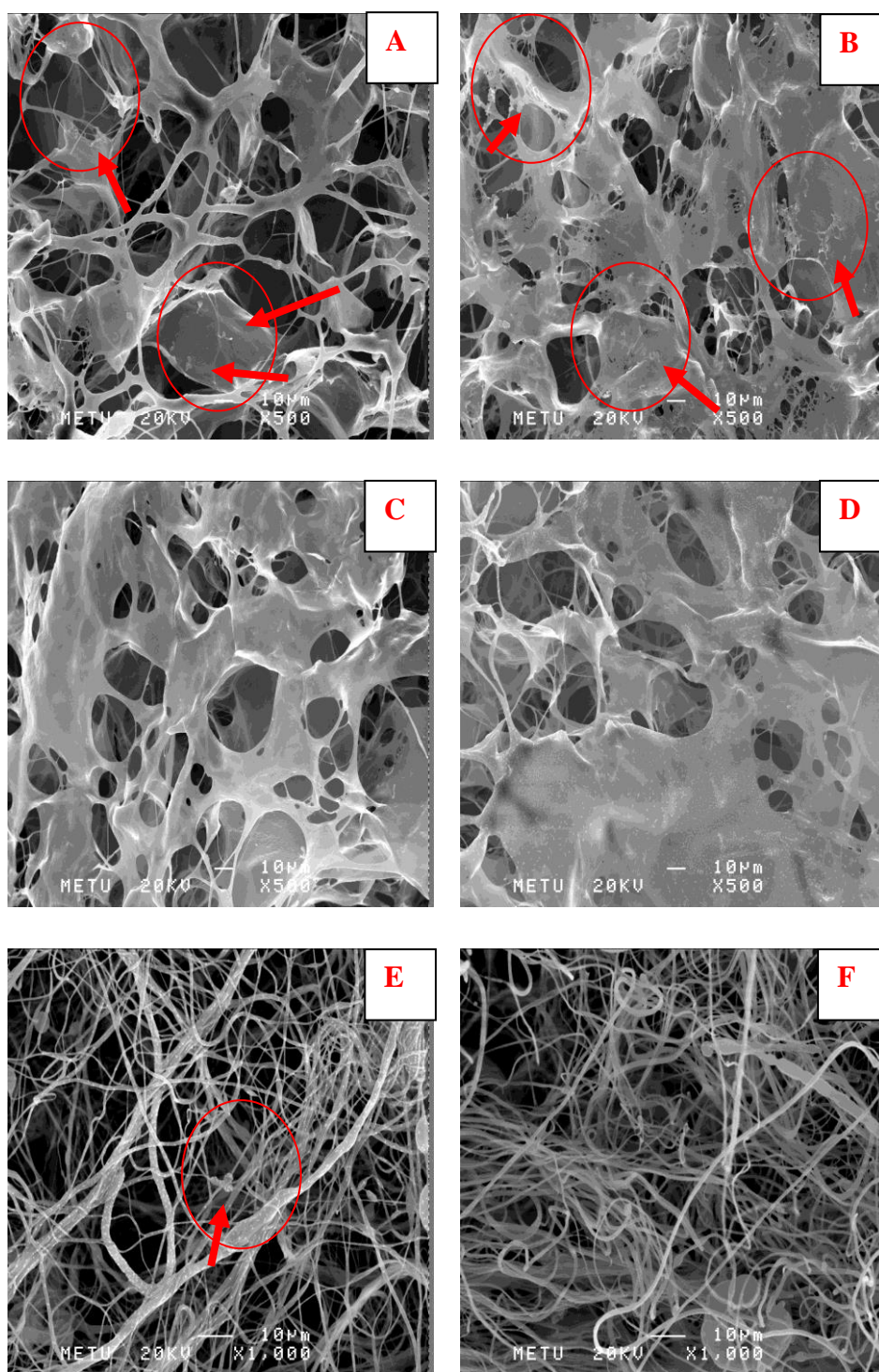


Figure 3.42. SEM micrographs showing the adhered bacteria colonies on A) CS, B) CS-X, C) CS-Au, D) CS-AuX, E) SFM-E and F) SFM-AuE. Arrows and circles in red indicate the bacteria colonies.

3.5.4. In Vivo Characterization Studies

3.5.4.1. In Vivo Rat Full-Thickness Skin Wound Healing Tests

3.5.4.1.1. The Optimization of Wound Healing Experimental Procedure

In the initial experiments of optimization study, it was observed that the wound contraction progressed more rapidly in cross-linked scaffolds (BLCS-X, BLCS-AuX) than BLSF and BLCS (Fig. 3.43). However, it was stated that a more complete wound closure has been previously observed even in control group (skin wound left without any cover) after 14 days. However, during these experiments it was also recognized that rats have opened the bandage cover on the scaffolds which caused drying of the scaffold and wounded region. Hence, it was thought that the experimental procedure should be modified.

From the optimization studies, it was thought that the wound bed had desiccated to a great extent and resulted in scar tissue formation. This situation must probably have avoided the healing of the wound. Therefore, wound contraction in any of the study groups at the end of 14th day was not so obvious. During the preliminary wound healing tests, the collagen/sericin film layer of the bilayered scaffolds were exposed to open environment. This film layer was designed to enable the water vapor transmission rate in a controlled manner (about 1300-1400 g/m²/day), which was suitable for low to medium exudating wounds. Since there was no pooling of exudates under wound in the rats, this might have caused to quick desiccation. It was decided that utilization of the collagen/sericin film layer was not suitable for this type of in vivo rat wound model due to the aforementioned reasons. Hence, collagen/sericin film layer was discarded from the in vivo tests and instead a commercial silicone membrane (permeable to oxygen, but impermeable to water vapour) was used as the outer cover in order to prevent the desiccation of the healing rat skin tissues. IobanTM surgical drape was advised as a suitable option for this purpose by Doç. Dr. Kemal Kısmet. The optimized experimental procedure was shown in Figure 3.44. There are several limitations in this study. First, rats differ

from humans in several aspects of skin healing. For example, rats have a loose skin structure that slides over muscles. In contrast to human skin, rat skin has panniculus carnosus muscle, which plays an important role in wound contraction and collagen synthesis.

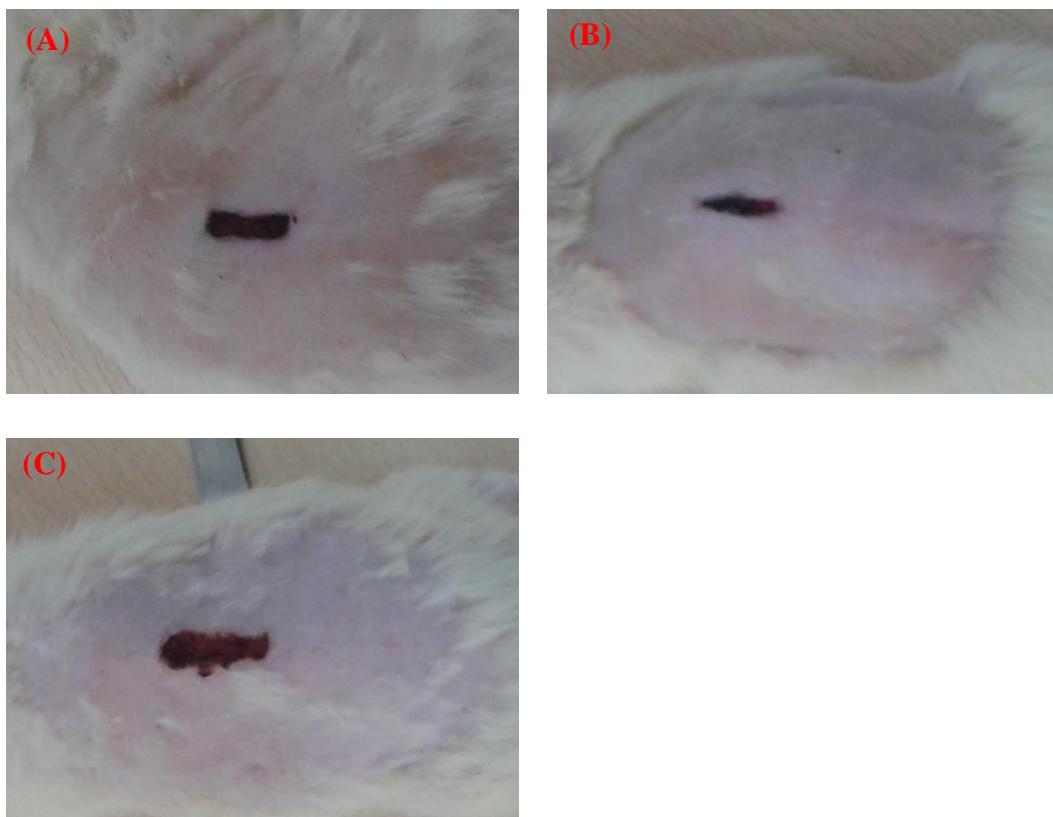


Figure 3.43. The appearance of the wounds on postoperative 14th day of preliminary experiments with the selected scaffolds: (A) BLCS, (B) BLCS-AuX, and (C) BLSF-X.

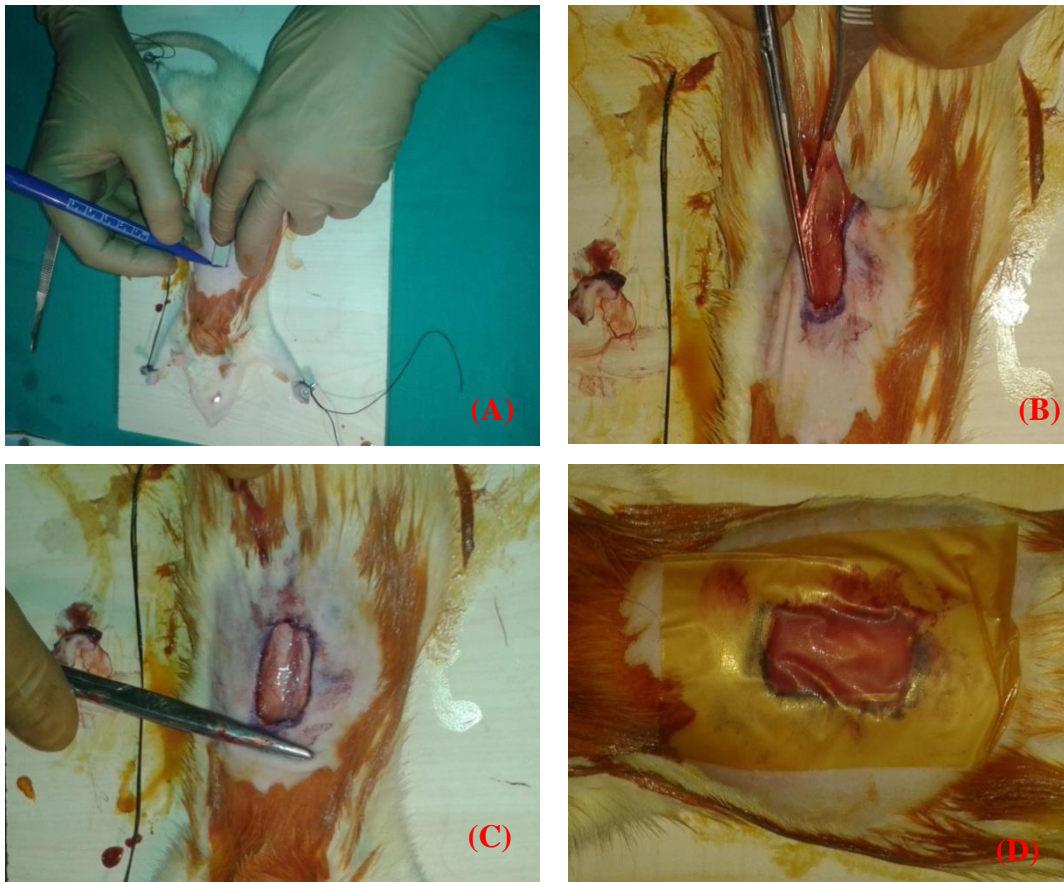


Figure 3.44. The experimental steps to create full-thickness wound model in rats: (A) drawing the wound in the size of 1x2 cm with a mould, (B) incising the wound with a skin scraper and removing the film-like thin muscle tissue under the cut-out skin (panniculus carnosus) (C) applying the test groups onto the wound area and humidifying it with PBS and (D) closing the surface of scaffolds with Ioban™ surgical drape.

3.5.4.1.2. Wound Contraction

Wound contraction areas of all the test groups on post-operative 14th day were given in Figure 3.45. Wound healing results of the wounds treated by different test groups were depicted representatively with photos taken on postoperative 14th day (Figure 3.46). By observing the wound area at defined time intervals (4, 7, 10, 14 days), the reduction in wound defect area was calculated. In the first 4 days, there was no

prominent difference of wound contraction between any of the treatment and control group (about 9-21%). Starting from 7th day, the wound contraction rate began to accelerate more clearly for any of the treated groups (29-40%) in comparison to control (about 23%). While wound contraction rates of wounds treated with skin substitutes and untreated wounds were about 44-61% and 38% at 10th day, they were 62-76% and 45% at 14th days, respectively. Although it was thought that the contraction processes were more rapid in the case of the wounds treated with skin substitutes, the differences were statistically significant ($p < 0.05$) only at 14th day (except for SF-X and MatridermTM groups). These results indicated that all the fabricated skin substitutes (except for SFM and MatridermTM) can accelerate the contraction of full-thickness wounds in normal rats.

AuNPs was used in the scaffolds to treat full-thickness skin wounds in rats to evaluate their effect. Honey was also known for its wound healing accelerating property. Hence, it was used as another component for comparison of the healing effect of different bioactive agents.

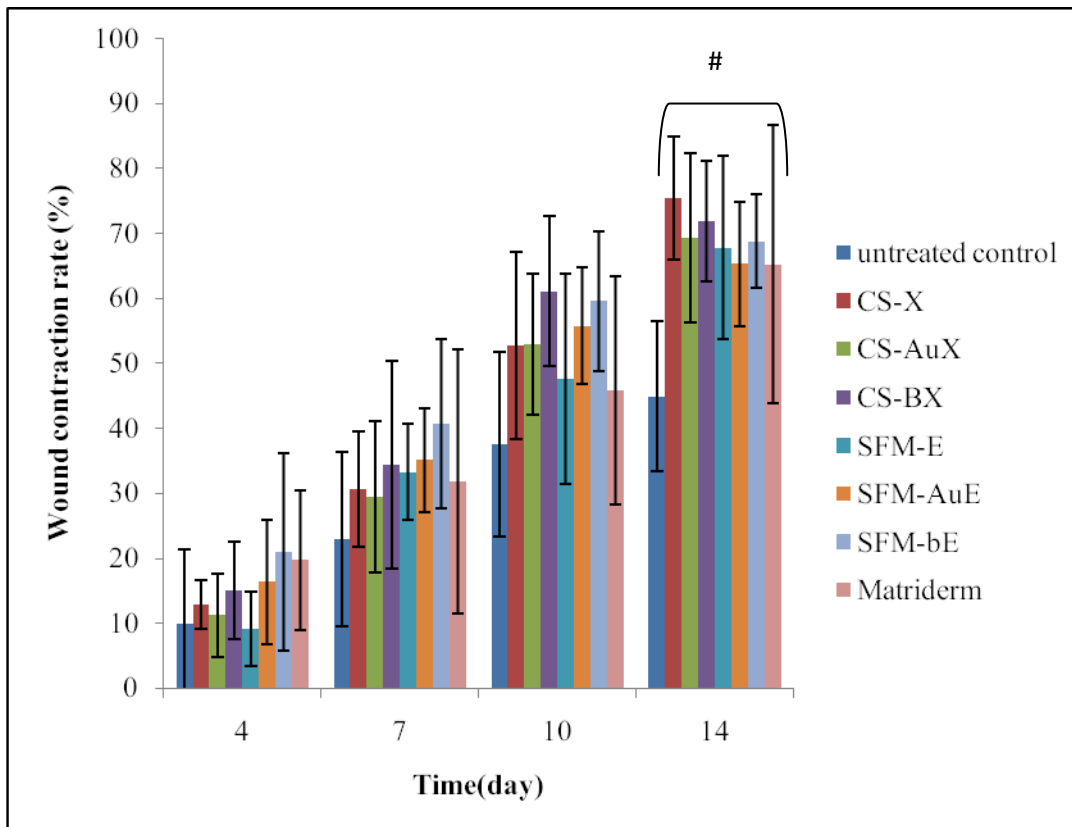


Figure 3.45. Wound contraction rates of different test groups on post-operative 4th, 7th, 10th and 14th days. #: Significant difference from the untreated control group (n=10 ±SD, p<0.05).

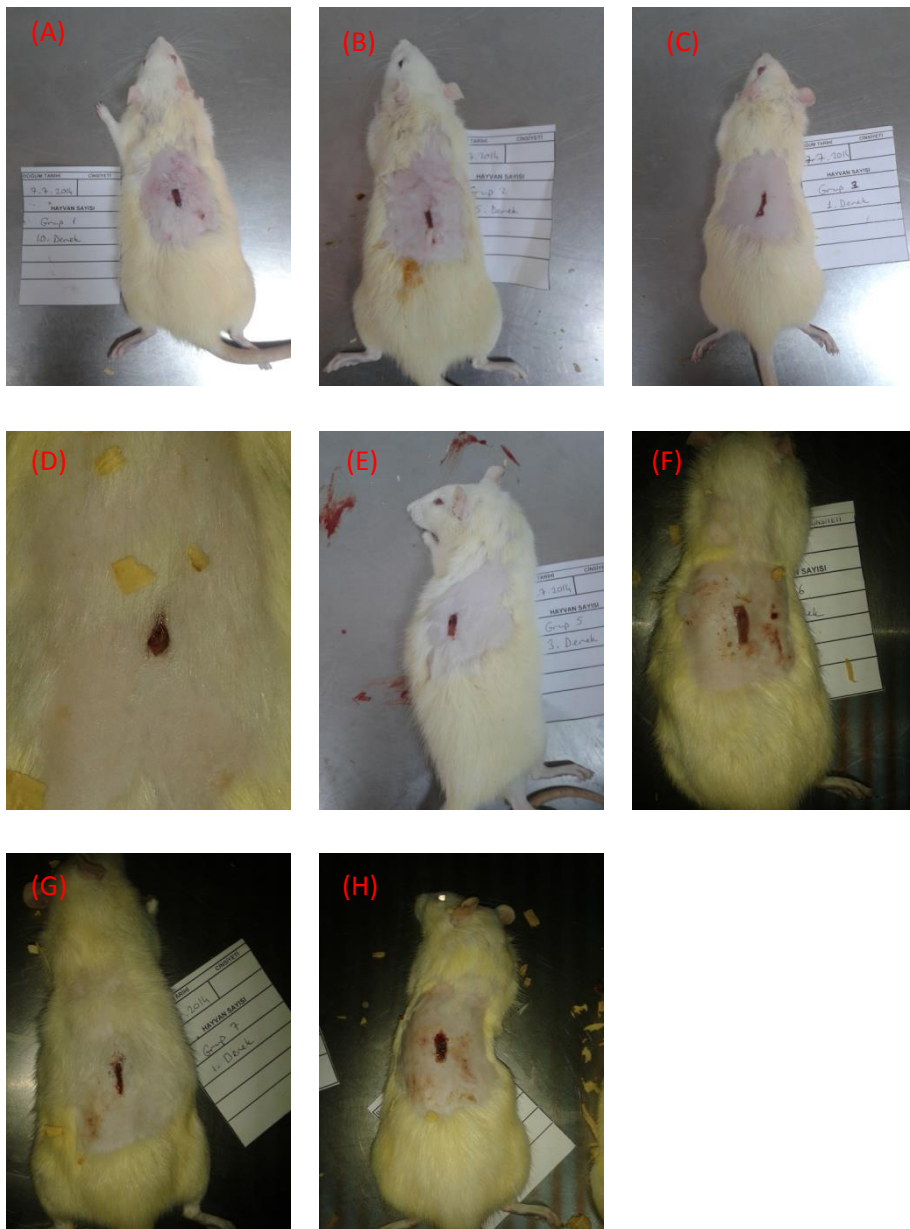


Figure 3.46. The images showing the wound contraction extent of different test groups and control on post-operative 14th day: (A) empty control, (B) CS-X, (C) CS-AuX, (D) CS-BX, (E) SFM-E, (F) SFM-AuE, (G) SFM-B, (H) MatridermTM.

3.5.4.1.3. Biomechanical Tests

Representative stress-strain curves of all groups were given in Figure 3.47 to give a rough idea about the biomechanical property of the test groups. The tensile strength in each curve was identified as the ultimate tensile stress observed. The tensile strength of an incisional wound is an assessment of the total wound strength. Also, recovery index was used to understand to what degree the wound returned to its unwounded state and to normalize the differences in the physical conditions of the animals. The elongation was measured as the extension divided by the initial gauge length of the test specimens until complete breakage. Modulus of elasticity was measured by taking the slope of the initial linear region of the stress-strain curve.

Biomechanical tests showed that collagen sponges incorporated with AuNPs or honey (CS-AuX and CS-BX) had greater resistance to rupture when compared with the other test groups (Figure 3.48 A). Although the tensile strength (UTS) of these groups was statistically similar to the other groups, they were the only groups reaching to the UTS range of normal-unwounded skin. The wounded skin in these groups could be said to recover to its original unwounded state as verified with recovery index calculation (Figure 3.48 B). No meaningful differences between the elastic modulus (E) of test groups were observed except that only E of CS-AuX was statistically higher than SFM-BE. Also, only CS-AuX had statistically similar values with the unwounded skin, on the other hand the other test groups has statistically lower E than unwounded skin (Figure 3.49A). Nearly all the groups had statistically similar elongation at break values (EAB), excluding the SFM-BE. SFM-BE group had such a loose and extensible structure that its EAB exceeded all the other groups with statistical difference than unwounded skin, untreated control, CS-X and CS-AuX (Figure 3.49B).

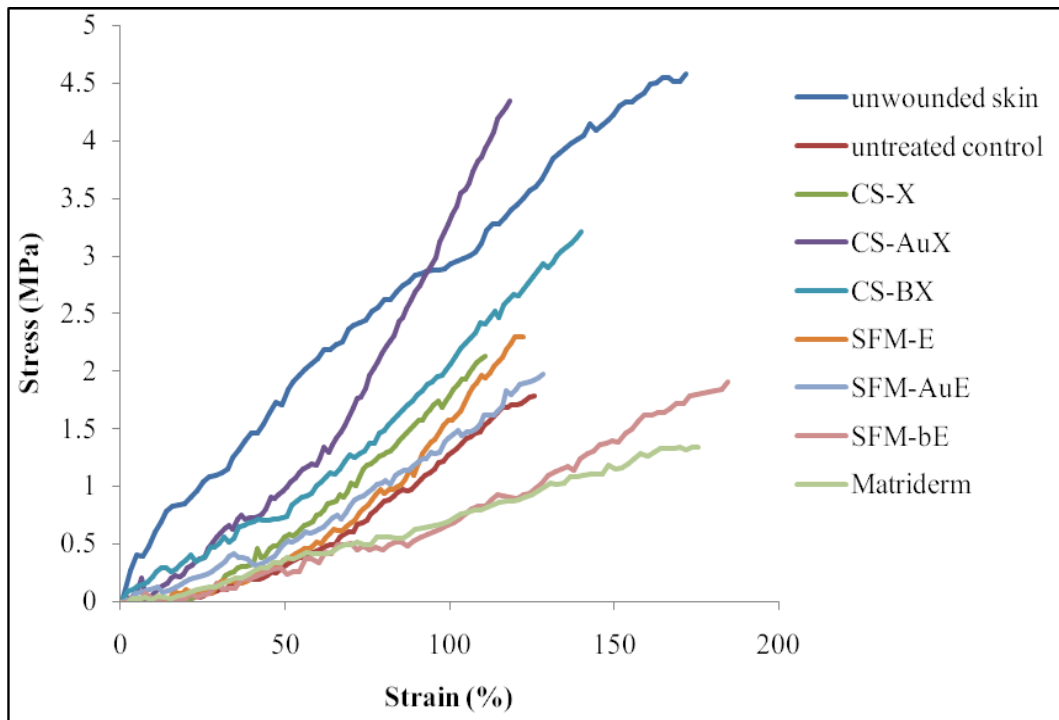


Figure 3.47. Stress-strain curves of skin biopsies taken on post-operative 14th day.

Different components are responsible for the increase of tensile strength or tensile modulus of skin wounds during the healing time. Especially the reorganization of extracellular matrix synthesized by fibroblasts (Menetrey et al., 2000) during the healing process affects the wound UTS, E and EAB. Increased tensile strength is related to the increased amount of extracellular matrix deposition in the wound bed of the skin. So, there is correlation between wound maturation (collagen maturation and cross-linking) and tensile strength (Jimenes and Rampy, 1999). The mechanical behavior properties of the skin are dominated by the dermis in normal conditions (Silver et al., 2003). Reduced mechanical properties may be related to the decrease of collagen synthesis or functional properties of collagen fibers (Quan et al., 2010; Fisher et al., 2009; Fisher et al., 2008). In our study, only a small increase in the amount of new uncross-linked collagen in the incisional gap during the 14 days period was described in the histological specimens. Therefore, it was supposed that

the difference of UTS between the test groups might be related to the process of the vascular reaction (by creation of fibrin network) of the inflammatory phase and difference in collagen network formation and organization. Also, lower tensile modulus values (softer skin samples) than normal skin observed for all the test samples (except for empty control, CS-AuX and CS-BX) could be related to the loose structure of the new collagen and fibrin fibers. As a result of this extensible, loose structure, all the test samples elongated as much as the normal skin (Figure 3.49 A). Opposing to the UTS increasing effect of fibroblasts, the density of inflammatory cells such as polymorphonuclear leukocytes and their long presence during wound healing might decelerate the dermal repair process and decrease wound UTS, because they dissolve proteins like collagen or silk fibroin with enzymes (Muehlberger et al., 2005). According to histological studies of our samples, we recorded some macrophages for the test groups (especially for MatridermTM) and the higher mechanical firmness of the wounds could be correlated to the increase of these macrophages. Thus, the collagen synthesized by fibroblasts within the proliferative phase, could be belowered in case of a severe acute inflammatory response (Muehlberger et al., 2005). Secondly, the faster course of inflammatory phase (anti-inflammatory effect of AuNP and honey) can induce the earlier initiation of collagen production and this might explain the increase of wound tensile strength as well. There are also other mechanisms of the effect of these bioactive agents on wound healing. Their antioxidant activities can improve the proliferation of cells into the injured area and so accelerate the synthesis of collagen (Suguna et al. 2002).

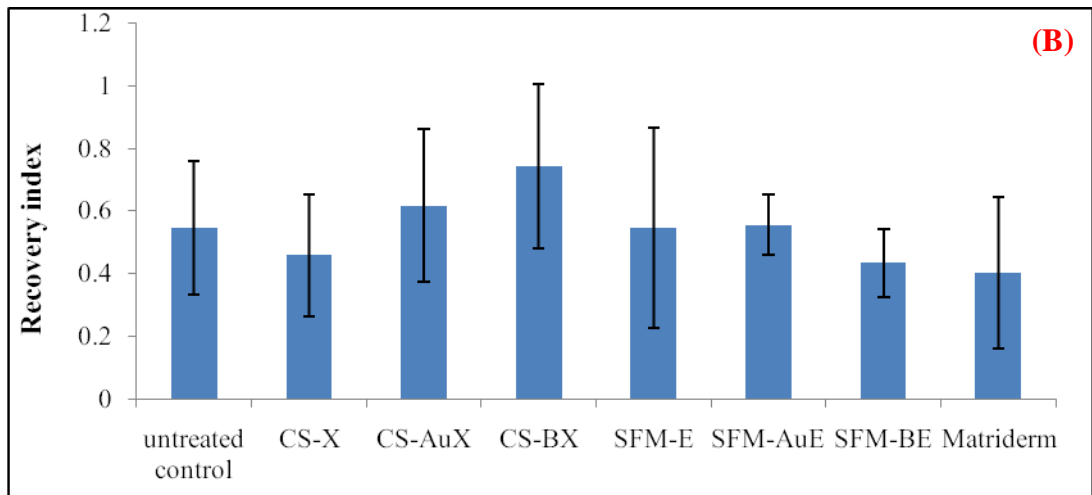
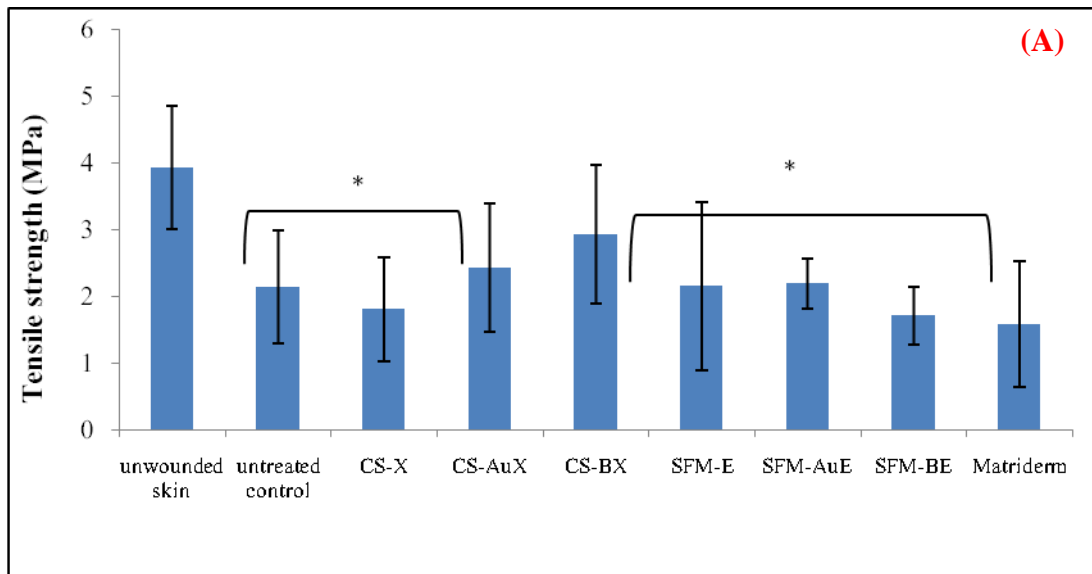


Figure 3.48. (A) Tensile strength and (B) the corresponding recovery index of skin biopsies taken on post-operative 14th day. *: Indicating a significant difference from the unwounded skin. $n \geq 6 \pm SD$

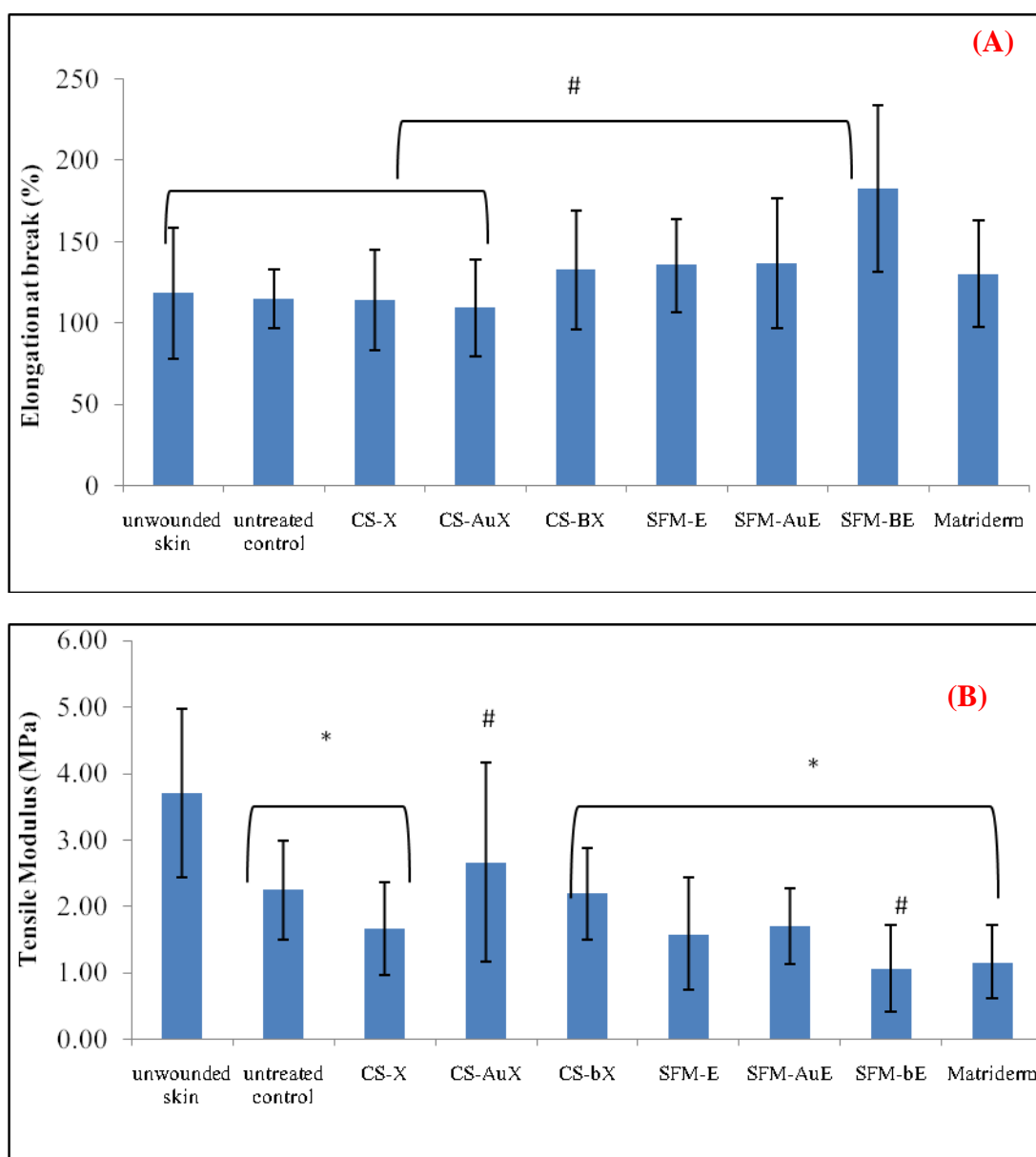


Figure 3.49. A) Elongation at break (%) and B) elastic modulus of skin biopsies taken on post-operative 14th day. *: Indicating a significant difference from the unwounded skin for $p < 0.05$. #: Indicating a significant difference between the test groups for $p < 0.05$ ($n \geq 6 \pm SD$).

3.5.4.1.4. Histopathological Analysis

Although there is a multitude of studies related to the clinical use of AuNPs, only little is known about its potential *in vivo* effects such as induction of inflammatory immune responses, possible contribution to regeneration or inhibition of skin tissue regeneration. Therefore, in the present study histopathological analysis were also performed to evaluate role of AuNPs on post wound processes. It can be stated that the data in this area of research is still largely limited. Especially, knowledge about *in vivo* effect of AuNPs is needed before its medical application in humans.

3.5.4.1.4.1. Epithelization Results

According to histopathology analysis, 14 day after the surgery, the epidermis was slightly thickened at the cut edges of test samples as a result of the mitotic activity of basal cells. The incisional wounds were slightly bridged by one layer (re-epithelization score of 1-2) of newly synthesized epithelial cells at most for the test groups (Figure 3.50). Therefore, it was still the early phase of the beginning of the keratinization of the epidermis. There was no statistical difference between any of the test groups, yet the best re-epithelization scores were measured for CS-X group and groups containing honey (CS-BX and SFM-BE). Nearly no re-epithelization (re-epithelization score of 0-1) was observed for empty control, SFM-AuE and MatridermTM groups. The migration of epithelial cells beneath the scab was seen in some of the groups (untreated control, CS-X, CS-AuX, SFM-AuE and SFM-BE) and almost complete re-epithelization was detected (CS-X and SFM-BE) (Figure 3.51). It was suggested that if study could be continued for longer periods, epidermis regeneration, that is, the epithelial thickening over the incisions would be evident and the surface keratinization would continue. Finally, the thickness of the keratin layer would be similar to the intact epidermis, and the healing of epidermis would be more complete. Yet, one of the most important outcomes of this analysis was the confirmation of the start of the re-epithelization of the tested scaffolds so that it was

concluded that there were no foreign material reaction to the scaffolds towards which epithelial cells grown.

3.5.4.1.4.2. Repair of the Wound Bed

Histological evaluation revealed that the inflammatory phase of healing was still continuing for 14 days after surgery. On the superficial part of the dermis, a necrotic tissue was observed as a result of the damage. Inflammatory phase cells seen under the tissue necrosis formed a demarcation line consisted of macrophages (neutrophils and histiocytes) and lymphocytes. Inflammatory response was surpassed in the collagen sponge groups containing AuNPs and honey to a large extent with respect to empty control and Matriderm™ (Figure 3.50). The disappearance of dermal inflammatory infiltration with fibroblast proliferation seemed to occur earlier in the collagen sponge groups (especially CS-AuX, CS-BX groups) and SFM-BE than the empty control and Matriderm™ (Figure 3.51). The primary inflammatory response occurred first and was replaced with capillary and collagen fiber formation.

The proliferative phase of healing also began 14 days after surgery. Fibroblasts were increased in number near the incisional space. Proliferation of fibroblasts and new endothelial cells with characteristic circular nuclei, which forms granulation tissue, was found at this time. The incisional space at the layer of dermis contained an extracellular matrix with a significant quantity of collagen for CS-BX and SFM-BE groups (Figures 3.50-3.51). The observation of histological sections showed vertically oriented fibroblasts (Figure 3.51). The highest score for granulation tissue was given for collagen sponge containing honey (CS-BX) followed by SFM-BE and other collagen sponge groups (CS-X and CS-AuX). Fibroblast proliferation seemed to increase in all test sample groups with respect to empty control group with the least proliferation seen in SFM-E and nearly none for Matriderm™ (Figure 3.51).

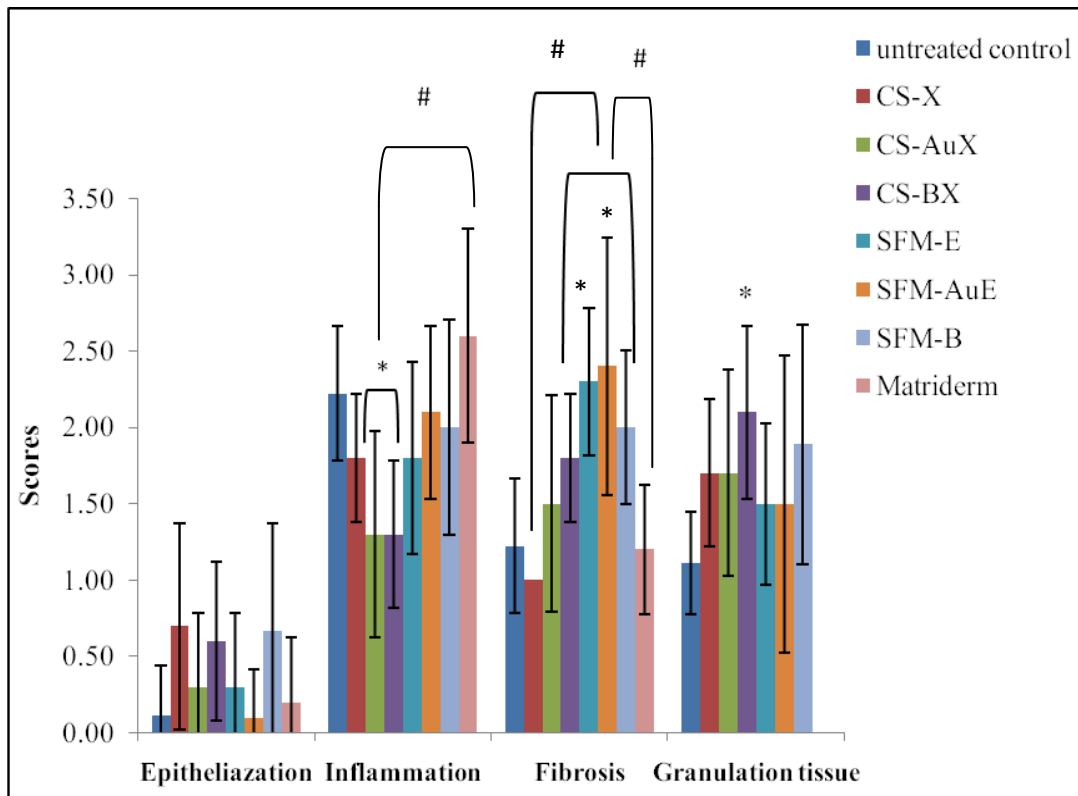


Figure 3.50. Histopathological scores of test groups (skin biopsies taken on post-operative 14th day). *: Indicating a significant difference from untreated control. #: Indicating a significant difference between test groups (n=10 ± SD, p<0.05).

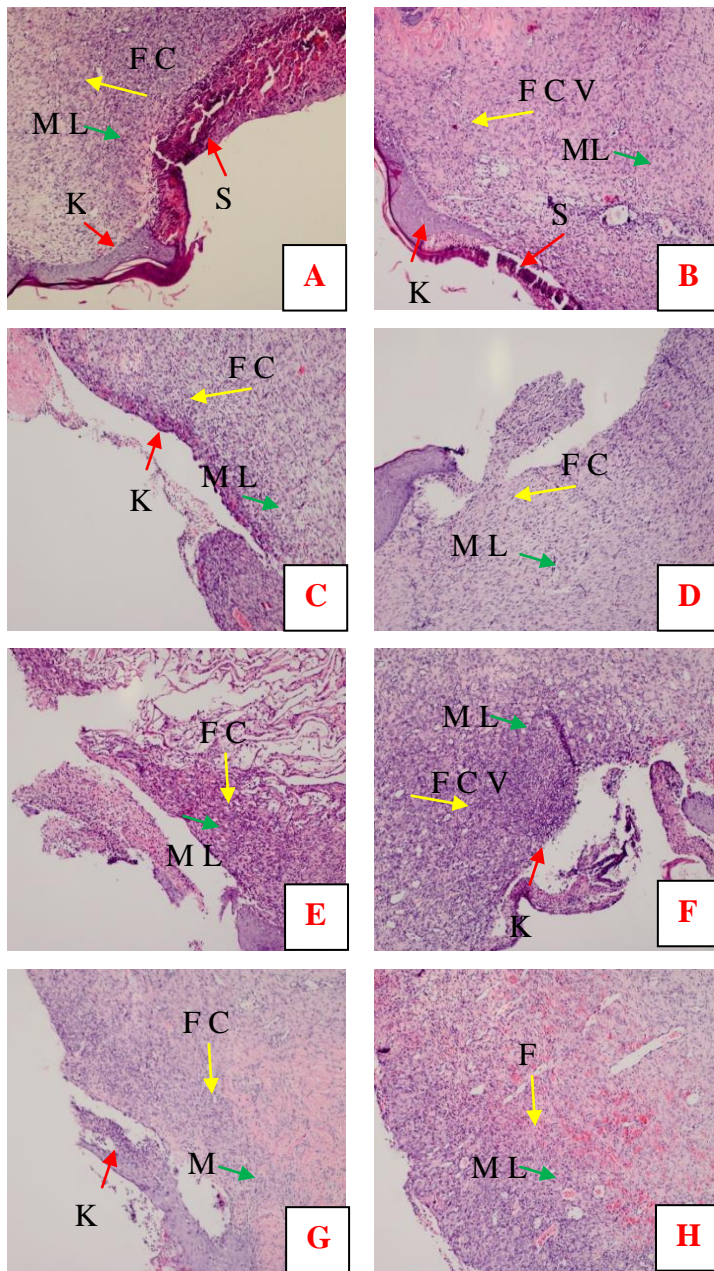


Figure 3.51. Representative images of H&E staining: (A) untreated control, (B) CS-X, (C) CS-AuX, (D) CS-BX (E) SFM-E, (F) SFM-AuE, (G) SFM-BE and (H) Matrigel™ test groups on post-operative 14th day. Red, yellow and green arrows indicate re-epithelialization (keratinocytes: K, scab: S), granulation/fibrosis (fibroblasts: F, collagen: C, vascularization: V), and inflammatory cells (macrophages: M, lymphocytes: L).

It was reported in a number of studies that silk fibroin might be a promising candidate as skin tissue scaffold (Sugihara et al., 2000; Yeo et al., 2000; Minoura et al., 1995; Santin et al., 1999). In the study of Sugihara et al. (2000) it was shown that silk fibroin film treatment on the wounds produced less inflammatory response (less neutrophil and lymphocyte infiltration) than clinically used DuoActive dressing. Compared with DuoActive dressing wound dressings, full thickness skin wounds in rats were healed seven days faster with silk films (Sugihara et al., 2000). The healing of the epidermis and dermis of rats were compared for poly (vinyl alcohol), chitosan and silk fibroin sponges alone and sponges composed of their blends. As compared with the paired and single polymer cases, the blends of PVA, chitosan and silk fibroin showed the best healing (Yeo et al., 2000).

These studies demonstrated that silk fibroin scaffolds could be an alternative skin tissue scaffold, because they might able contribute to the process of skin healing more than other polymers used with little minimal inflammatory response. In the histopathological evaluations of the scaffolds prepared in this study, we have also observed that silk fibroin groups promoted the healing process better than the untreated control with little to medium inflammatory response, but collagen based groups were better than silk fibroin groups in terms of healing of wound bed.

3.5.5. Toxicological Evaluation

Toxicological evaluations were done on one of the most successful groups (BLCS-AUX) selected according to all the characterization tests performed.

3.5.5.1. Intradermal Reactivity

In toxicological studies no undesired outcome like death, or an abnormal general condition like change in weight was observed in any of the animals during the experimental period (Table 3.6). Grade 0 and 1 erythema/edema skin reactions were

noted after injection of the extracts in physiological saline (mean score: 0.73) or control solution (mean score: 1.18) during the observation period in the test or control animals. Very slight skin reactions were observed after injection of the extracts in sesame oil as follows: Grade 2 erythema at all five sites in three test animals and grade 1 oedema at all five sites in three test animals were recorded at 24, 48, and 72 hours after injection. The total score for erythema/eschar and oedema was 9 (mean score: 3) from 24 to 72 hours after injection. Skin reactions were observed after injection of the control sesame oil as follows: grade 1 or 2 erythema at all five sites in three test animals and grade 0 or 1 edema at all five sites in three test animals at 24, 48, and 72 hours after injection. The total score for erythema/eschar and edema was 7.66 (mean: 2.55) from 24 to 72 hours after injection. The difference values were below 1.0 (-0.45 score for physiological saline extract solvent and 0.45 score for sesame oil extract solvent) showing that the test sample (BLCS-AuX) does not cause any intracutaneous (intradermal) irritation.

Up to now no data was reported on the side effects of AuNPs in the literature related to the adverse skin reactions (dermal irritation) to AuNPs. Hence, the importance of further studies of AuNPs on experimental animals for extrapolation of the results to human is essential.

3.5.5.2. Sensitization

In sensitization tests, neither an abnormal general condition nor changes in weight were observed in animals during the experimental periods. Following sensitization with topical application of gauze patch immersed in the test sample (BLCS-AuX) extract, no hypersensitive skin reaction was examined on challenged sites at 24 and 48 hours during the observation period in any of the 10 test animals. No skin reactions were noted at any of the sites in the 5 negative control animals. The lesions were graded according to the Magnusson and Kligman scale (Table 2.7). Therefore, these results indicated that BLCS-AuX did not cause hypersensitive skin reaction. According to experimental and clinical studies, when a sponge or a film made up of

xenogenic collagen was applied to the injured surface of the skin it did not cause any sensitization (Vacanti and Langer, 1998; Soo et al., 1993). However, injectable collagen was reported to cause hypersensitivity to the skin of 3% of the population according to literature data collected during pre-application tests (Delustro et al., 1990; Soo et al., 1993). The effect of AuNPs on the sensitization of skin was not investigated so far. Thus, it is necessary to conduct more animal experiments for improving the understanding of skin sensitization of AuNPs.

Table 3.6. Irritation scores (intracutaneous) in rabbits.

Test and control articles*	Animal no.	Total time (Hour) after administration			Total score	Irritation** $\Sigma(A + B)/15$	Total irritation score	Mean#	Difference of mean##
		24	48	72					
Physiological saline extract of BLCS-AuX	1	5	0	0	5	0.33	2.2	0.73	
	2	5	3	5	13	0.87			
	3	5	5	5	15	1			
-0.45									
Physiological saline (control 1)	1	10	5	5	20	1.33	3.53	1.18	
	2	5	5	8	18	1.2			
	3	5	5	5	15	1			
Sesame oil extract of BLCS-AuX	1	15	15	15	45	3	9	3	
	2	15	15	15	45	3			
	3	15	15	15	45	3			
0.45									
Sesame oil (control 2)	1	10	10	15	35	2.33	7.66	2.55	
	2	10	15	10	35	2.33			
	3	15	15	15	45	3			

Note: *Each test and control article was administered to 5 sites per animal.

**Total score (erythema and eschar formation (A) and edema formation (B) of 24, 48, and 72 hours after administration of per animal)/15 (3 grading periods (24, 48, and 72 hours after administration) \times 5 administered sites).

#Total irritation score/3 animals.

##Mean (each test article) – Mean (each control article) = Any score < 1 indicates no irritation.

3.5.5.3. Genotoxicity

It is important to determine the mutagenic characteristic of scaffold extracts used as skin substitutes containing potentially genotoxic components. The potential genotoxic elements of the scaffolds fabricated in this study are GTA and AuNPs. The potential toxic impact of AuNPs may be unpredictable. Beside particles size, surface chemistry and surface charge also play a crucial role in determining genotoxic effect. Thus, the standard bacterial reverse-mutation assay, commonly known as the Ames test (Ames, 1973) was applied in this study to assess the genotoxic effect of BLCS-AuX (Table 3.7).

For the evaluation of genotoxicity test results, if p value of the treatment group was lower than 0.05 ($p < 0.05$) when compared with the corresponding negative control, it was thought to be biologically significant; and was thought to represent the induction of a significant number of mutagenic events in the treated population. No increase in revertant frequencies were observed with the base substitution indicating tester strain TA100, TA1535 and *E. coli* WP2 for any of the tested articles, both in the presence and in the absence of S9. Similarly, no increases in revertant frequencies were observed for any of the tested articles with frameshift mutation indicating tester strain TA98 and TA1537 either in the presence or in the absence of S9 mix (Table 3.7). As a whole, this indicated that BLCS-AuX did not cause genotoxicity. Since the selected group, BLCS-Au-X contains all components-chemical treatments of other groups, it might be suggested that other related groups (BLCS, BLCS-Au and BLCS-X), might also give non-mutagenic results.

If AuNPs enter into the cells, they might interact with biological molecules, such as proteins and nucleic acids and are likely to alter the structure and function of proteins and/or cause genotoxicity. Recent works related to the genotoxicity of citrate capped AuNPs are a bit contradictory, mainly due to the differences of particles size, surface chemistry and surface charge of synthesized AuNPs in those studies. For instance; it was suggested that AuNPs capped with either sodium citrate or polyamidoamine dendrimers might exhibit in vitro genotoxicity on hepatocellular carcinoma cells and

peripheral blood mononuclear cells from healthy human volunteers even at very low concentrations (Paino et al., 2012). Also, it was demonstrated that serum coated AuNPs (20 nm) were also able to cause sustained DNA strand breaks and chromosomal breaks induced by oxidative stress in human lung fibroblasts (Li et al., 2011). It was showed in a recent work (Vecchio et al., 2012) that exposure to citrate capped AuNPs (15 nm) were able to induce genetic mutations in the germinal line of *Drosophila* (Fraga et al., 2013). The genotoxic effects of AuNPs having different sizes (2, 20 and 200 nm) were investigated by administering single intratracheal instillation into the lung of male adult Wistar rats (Schulz et al., 2012). Relevant DNA damage could not be detected in the tests and it was concluded that under the conditions of the study the different sized AuNPs tested were non-genotoxic at the given dose.

Table 3.7. Mutagenicity of test sample extracts in *S.Typhimurium* and *E. colitest* strains.

Tested article	Base-pair substitution type						Frameshift type			
	TA100		TA1535		<i>E. coli</i> WP2		TA98		TA1537	
	-S9 mix	+S9 mix	-S9 mix	+S9 mix	-S9 mix	+S9 mix	-S9 mix	+S9 mix	-S9 mix	+S9 mix
Extract of BLCS- AuX in PS	-	-	-	-	-	-	-	-	-	-
Extract of BLCS- AuX in DMSO	-	-	-	-	-	-	-	-	-	-
PS	-	-	-	-	-	-	-	-	-	-
DMSO	-	-	-	-	-	-	-	-	-	-
*Positive control	+	+	+	+	+	+	+	+	+	+

*The positive controls were given in Table 2.8

Mutagenicity was shown with “+” or “-” indicating the presence ($p < 0.05$) or absence ($p > 0.05$) of mutagenic condition, respectively. (n=3).

Genotypes are: *hisD3052, rfa uvrB, pKM101* for TA98; *hisG46, rfa, uvrB, pKM101* for TA 100; *hisG46, rfa, uvrB* for TA1535; *hisC3076, rfa, uvrB* for 1537; *trpE65, pKM101* for *E. Coli* WP2.

PS: Physiological saline (0.9% w/v NaCl).

DMSO: Dimethyl sulfoxide.

CHAPTER 4

CONCLUSION

A variety of up-to-date skin substitutes are being developed with an effort to satisfy the ideal characteristics of a successful skin substitute. In the present study, various scaffolds based on natural (collagen, silk fibroin and sericin) and synthetic polymers were evaluated for the desired properties of a successful skin substitute such as pore size and porosity, equilibrium degree of swelling, water vapour transmission rate, oxygen permeability, mechanical properties, aqueous and enzymatic degradation profiles, antibacterial assessment, in vitro biocompatibility, in vivo skin wound healing performance on rat and toxicology.

These studies indicated that all of the scaffolds fabricated in this study have optimal physico-chemical characteristics of a skin substitute and have no in vitro cytotoxicity. Especially, AuNPs incorporation into collagen sponges enhanced some of these properties, such as better mechanical properties and degradation profile, although these positive effects were not so clear and necessitates further tests for verification. In addition to these, scaffolds incorporated with AuNPs gained antimicrobial properties, which is also very important for the success of skin substitutes. Biocompatibility of all of the scaffolds was verified with cytotoxicity, cell adhesion and proliferation studies. In vivo wound healing performance of the scaffolds was compared with each other and controls (untreated control and MatridermTM). All the analysis suggested that all the groups, especially the groups containing the bioactive agents (honey or AuNPs) have equal or slightly better in vivo healing effect than MatridermTM.

For one of the most successful bilayered scaffolds (BLCS-AuX), standard tests (ISO 10993: Biological Evaluation of Medical Devices) were also preformed. The animal toxicology evaluation on BLCS-AuX was made with intradermal irritation tests (ISO

10993-10: Animal intradermal reactivity test), skin sensitization (ISO 10993-10: Closed-patch test) and genotoxicity tests (ISO 10993-3, OECD 471: Bacterial reverse mutation test). According to these tests, there were no adverse skin reactions (irritation or sensitization) or genotoxicity for BLCS-AuX.

As a conclusion, all of these skin substitutes, especially the groups containing bioactive agents (honey or AuNPs) might be valuable skin substitute materials for use in the management of skin wounds. The substantial aim of this study in long term is to develop potentially commercializable skin substitutes.

REFERENCES

Adekogbe I, Ghanem A (2005). Fabrication and characterization of DTBP-crosslinked chitosan scaffolds for skin tissue engineering. *Biomaterials* 26: 7241-7250.

Agarwal S, Mishra P, Shivange G, Kodipelli N, Moros M, Fuente JM de la, Anindya R (2014). Citrate-capped gold nanoparticles for the label-free detection of ubiquitin C-terminal hydrolase-1. *Analyst*.

Ahn JS, Choi HK, Lee KH, Nahm JH, Cho CS (2001). Novel mucoadhesive polymer prepared by template polymerization of acrylic acid in the presence of silk sericin. *J. Appl Polym Sci* 80: 274-280.

Ajibola A, Chamunorwa JP, Erlwanger KH (2012). Nutraceutical values of natural honey and its contribution to human health and wealth. *Nutr Metab (Lond)* 9: 61.

Ajibola A, Idowu GO, Amballi AA, Oyefuga OH, Iquot IS (2007). Improvement of some haematological parameters in albino rats with pure natural honey. *J Biol Sci Res* 2: 67-69.

Akturk O, Tezcaner A, Bilgili H, Deveci MS, Gecit MR, Keskin D (2011). Evaluation of sericin/collagen membranes as prospective wound dressing biomaterial. *J Biosci Bioeng* 112: 279-288.

Alberts B, Johnson A, Lewis J, Raff M, Roberts K (2002). *Molecular Biology of The Cell*; Garland Science: New York, NY, USA.

Al-Jabri A, Al Mahrooqi Z, Nzeako B, Nsanze H (2005). Inhibition effect of honey on the adherence of *Salmonella* to intestinal epithelial cells in vitro. *Int J Food Microbiol* 103(3): 347–351.

Aljadi AM, Kamaruddin MY (2004). Evaluation of the phenolic contents and antioxidant capacities of two Malaysian floral honeys. *Food Chem* 85: 513-518.

Altman GH, Diaz F, Jakuba C, Calabro T, Horan RL, Chen J, Lu H, Richmond J, Kaplan DL (2003). Silk-based biomaterials. *Biomaterials* 24: 401–416.

Ames BN (1973). Carcinogens are mutagens: their detection and classification. *Environ Health Perspect* 115–118.

Angele P, Abke J, Kujat R, Faltermeier H, Schumann D, Nerlich M, Kinner B, Englert C, Ruszczak Z, Mehrl R, Mueller R (2004). Influence of different collagen species on physico-chemical properties of crosslinked collagen matrices. *Biomaterials*. 25(14): 2831-2841.

Aoki H, Tomita N, Morita Y, Hattori K, Harada Y, Sonobe M et al (2003). Culture of chondrocytes in fibroin–hydrogel sponge. *Biomed Mater Eng* 13(4): 309–316.

Aramwit P, Sangcakul A (2007). The effects of sericin cream wound healing in rats. *Biosci Biotechnol Biochem* 71(10): 2473-2477.

Arriaga E, Navarro-Calvo AL, Díaz-Carbajal E (2011). Botanical characterisation of Mexican honeys from a subtropical region (Oaxaca) based on pollen analysis. *Grana* 50: 40-45.

Aryal S, Bahadur R, Bhattarai SR, Prabua P, Kim HY (2006). Immobilization of collagen on gold nanoparticles: preparation, characterization, and hydroxyapatite growth. *J Mater Chem* 16: 4642-4648.

Augustine R, Kalarikkal N, Thomas S (2014). Advancement of wound care from grafts to bioengineered smart skin substitutes. *Prog Biomater* 3: 103-113.

Ayutsede J, Gandhi M, Sukigara S, Micklus M, Chen HE, Ko F (2005). Regeneration of *B. mori* silk by electrospinning, Part 3: characterization of electrospun nonwoven mat. *Polymer* 46(5): 1625–34.

Badylak SF (2004). Xenogeneic extracellular matrix as a scaffold for tissue reconstruction. *Transpl Immunol* 12: 367–377.

Balasubramani G, Ramkumar R, Krishnaveni N, Pazhanimuthu A, Natarajan T, Sowmiya R, Perumal P (2014). Structural characterization, antioxidant and anticancer properties of gold nanoparticles synthesized from leaf extract (decoction) of *Antigonon leptopus* Hook. & Arn. *J Trace Elem Med Bio*.

Balasubramani M, Kumar TR, Babu M (2001). Skin substitutes: A review. *Burns* 27: 534–544.

Bechetoille N, Dezutter-Dambuyant C, Damour O, Andre V, Orly I, Perrier E (2007). Effects of solar ultraviolet radiation on engineered human skin equivalent containing both Langerhans cells and dermal dendritic cells. *Tissue Eng* 13: 2667–2679.

Beretta G, Caneva E, Facino RM (2007). Kynurenic acid in honey from arboreal plants: MS and NMR evidence. *Planta Med* 73: 1592-1595.

Beretta G, Gelmini F, Lodi V, Piazzalunga A, MaffeiFacino R (2010). Profile of nitric oxide (NO) metabolites (nitrate, nitrite and N-nitroso groups) in honeys of different botanical origin: nitrate accumulation as index of origin, quality and of therapeutic opportunities. *J Pharm Biomed Anal* 53: 343-349.

Bhardwaj N, Sow WT, Devi D, Ng KW, Mandal BB, Cho N-JJ (2014). Silk fibroin-keratin based 3D scaffolds as a dermal substitute for skin tissue engineering. *Integr Biol (Camb)* 7: 53–63.

Bhattarai N, Edmondson D, Veisoh O, Matsen FA, Zhang M (2005). Electrospun chitosan-based nanofibers and their cellular compatibility. *Biomaterials* 26: 6176–6184.

Bi L, Cao Z, Hu Y, Song Y, Yu L, Yang B, Mu J, Huang Z, Han Y (2011). Effects of different cross-linking conditions on the properties of genipin-cross-linked chitosan/collagen scaffolds for cartilage tissue engineering. *J Mater Sci Mater Med* 22: 51–62.

Biggs S, Chow MK, Zukoski CF, Grieser F (1993). The Role of Colloidal Stability in the Formation of Gold Sols. *J Colloid Interface Sci* 160:511.

Bilsel Y, Bugra D, Yamaner S, Bulut T, Cevikbas U, et al. (2002) Could honey have a place in colitis therapy? Effects of honey, prednisolone, and disulfiram on inflammation, nitric oxide, and free radical formation. *Dig Surg* 19: 306-311.

Blais M, Grenier M, Berthod F (2009). Improvement of nerve regeneration in tissue-engineered skin enriched with schwann cells. *J Invest Dermatol* 129: 2895–2900.

Blanpain C, Lowry WE, Geoghegan A, Polak L, Fuchs E (2004). Self-renewal, multipotency, and the existence of two cell populations within an epithelial stem cell niche. *Cell* 118: 635–648.

Blassa M, Candracci M, Accorsi A, Piacentini MP, Albertini MC et al (2006). Raw millefiori honey is packed full of antioxidants. *Food Chem* 97: 217-222.

Bogdanov S, Jurendic T, Sieber R, Gallmann P (2008). Honey for nutrition and health: a review. *J Am Coll Nutr* 27: 677-689.

Boyce ST (2001). Design principles for composition and performance of cultured skin substitutes. *Burns* 27, 523-533.

Boyd M, Flasz M, Johnson PA, Roberts JS, Kemp P (2007). Integration and persistence of an investigational human living skin equivalent (ICX-SKN) in human surgical wounds. *Regen Med* 2: 363–370.

Brust M, Walker M, Bethell D, Schiffrin DJ, Whyman R (1994). Synthesis of thiol-derivatised gold nanoparticles in a two-phase liquid-liquid system. *J Chem Soc, Chem Commun* 801-802.

Burygin GL (2009). On the enhanced antibacterial activity of antibiotics mixed with gold nanoparticles. *Nanoscale Res Lett* 4: 794–801.

Buttafoco L, Kolkman NG, Engbers-Buijtenhuijs P (2006). Electrospinning of collagen and elastin for tissue engineering applications. *Biomaterials* 27: 724-734.

Cao H, Chen X, Huang L, Shao Z (2009). Electrospinning of reconstituted silk fiber from aqueous silk fibroin solution. *Materials Science and Engineering C* 29: 2270–2274.

Castaneda L, Valle J, Yang N, Pluskat S, Slowinska K (2008). Collagen cross-linking with Au nanoparticles. *Biomacromolecules* 9: 3383–3388.

Chakrapani VY, Gnanamani A (2012). Electrospinning of type I collagen and PCL nanofibers using acetic acid. *Journal of Applied Polymer Science* 125: 3221–3227.

Chan TR, Stahl PJ, Li Y, Yu SM (2015). Collagen-gelatin mixtures as wound model, and substrates for VEGF-mimetic peptide binding and endothelial cell activation. *Acta Biomater.*

Chang MC, Tanaka J: FT-IR study for hydroxyapatite/collagen nanocomposite cross-linked by glutaraldehyde. *Biomaterials* 2002 23: 4811–4818.

Chen JP, Chang GY, Chen JK (2008). Electrospun collagen/chitosan nanofibrous membrane as wound dressing. *Colloids and Surfaces A: Physicochem. Eng. Aspects* 313: 183-188.

Chen L, Mehta A, Berenbaum M, Zangerl AR, Engeseth NJ (2000). Honeys from Different Floral Sources as Inhibitors of Enzymatic Browning in Fruit and Vegetable Homogenates. *J Agric Food Chem* 48(10): 4997–5000.

Chen L, Zhu C, Fan D, Liu B, Ma X, Duan Z, Zhou Y (2011). A human-like collagen/chitosan electrospun nanofibrous scaffold from aqueous solution: electrospun mechanism and biocompatibility. *J Biomed Mater Res A* 99: 395–409.

Chen YH, Dong WR, Xiao YQ, Zhao BL, Hu GD, An LB (2006) Preparation and bioactivity of human hair keratin-collagen sponge, a new type of dermal analogue. *Nan Fang Yi Ke Da Xue Xue Bao* 26: 131–138.

Chiarini A, Petrini P, Bozzini S, Pra I, Armato U (2003). Silk fibroin/poly(carbonate)–urethane as a substrate for cell growth: in vitro interactions with human cells. *Biomaterials* 24(5): 789–799.

Chithrani BD, Ghazani AA, Chan WCW (2006). Determining the size and shape dependence of gold nanoparticle uptake into mammalian cells. *Nano Letters* 6 (4): 662–668.

Chong EJ, Phan TT, Lim IJ, Zhang YZ, Bay BH, Ramakrishna S, Lim CT (2007). Evaluation of electrospun PCL/gelatin nanofibrous scaffold for wound healing and layered dermal reconstitution. *Acta Biomater* 3: 321–330.

Chow MK, Zukoski CF (1994). Gold Sol Formation Mechanisms-Role of Colloidal stability. *Journal of Colloid and Interface Science* 165: 97-109.

Chwalibog A, Sawosz E, Hotowy A, Szeliga J, Mitura S, Mitura K, Grodzik M, Orłowski P, Sokolowska A (2010). Visualization of interaction between inorganic nanoparticles and bacteria or fungi. *International Journal of Nanomedicine* 5: 1085–1094.

Connor EE, Mwamuka J, Gole A, Murphy CJ, Wyatt MD (2005). Gold nanoparticles are taken up by human cells but do not cause acute cytotoxicity. *Small* 1 (3): 325–327.

Cozad M, Bachman S, Grant S (2011). Assessment of decellularized porcine diaphragm conjugated with gold nanomaterials as a tissue scaffold for wound healing. *J Biomed Mater Res A* 99A: 426–434.

Crane E (1975). History of honey. In: Crane E, editor. *Honey: a comprehensive survey*. London: William Heinemann 439-488.

Cui Q, Yashchenok A, Zhang L, Li L, Masic A, Wienskol G, Möhwald H, Bargheer M (2014). Fabrication of bifunctional gold/gelatin hybrid nanocomposites and their application. *ACS Appl Mater Interfaces* 6: 1999–2002.

Cui Y, Zhao Y, Tian Y, Zhang W, Lü X, Jiang X (2012). The molecular mechanism of action of bactericidal gold nanoparticles on *Escherichia coli*. *Biomaterials* 33: 2327-2333.

Dal Pra I, Freddi G, Minic J, Chiarini A, Armato U (2005). Denovo engineering of reticular connective tissue in vivo by silk fibroin nonwoven materials. *Biomaterials* 26(14): 1987–99.

Daniel MC, Astruc D (2004). Gold nanoparticles Assembly, supramolecular chemistry, quantum-size-related properties, and applications toward biology, catalysis, and nanotechnology. *Chem Rev* 104: 293.

Das SK (2009). Gold nanoparticles: microbial synthesis and application in water hygiene management. *Langmuir* 25: 8192–8199.

Dash R, Acharya C, Bindu PC, Kundu SC (2008). Antioxidant potential of silk protein sericin against hydrogen peroxide-induced oxidative stress in skin fibroblasts. *BMB Reports* 236-241.

Dash R, Mandal M, Ghosh SK, Kundu SC (2008). Silk sericin protein of tropical tasar silkworm inhibits UVB-induced apoptosis in human skin keratinocytes. *Mol Cell Biochem* 311: 111-119.

Davidenko N, Gibb T, Schuster C, Best SM, Campbell JJ, Watson CJ, Cameron RE (2012). Biomimetic collagen scaffolds with anisotropic pore architecture. *Acta Biomater* 8: 667–676.

Dee KC, David A, Puleo DA, Bizios R (2002). *An Introduction to Tissue-Biomaterial Interactions*. New Jersey: Wiley-Liss, Hoboken.

Deeken CR, Fox DB, Bachman SL, Ramshaw BJ, Grant SA (2011). Characterization of bionanocomposite scaffolds comprised of amine-functionalized gold nanoparticles and silicon carbide nanowires crosslinked to an acellular porcine tendon. *J Biomed Mater Res B* 97: 334–344.

DeLustro F, Dasch J, Keefe J, Ellingsworth L (1990). Immune responses to allogenic and xenogenic implants of collagen and collagen derivatives. *Clin Orthop Relat Res* 260: 263–279.

Doillon CJ, Silver FH (1986). Collagen-based wound dressing: Effects of hyaluronic acid and fibronectin on wound healing. *Biomaterials* 7: 3–8.

Duan H, Feng B, Guo X, Wang J, Zhao L, Zhou G, Liu W, Cao Y, Zhang W (2013). Engineering of epidermis skin grafts using electrospun nanofibrous gelatin/polycaprolactone membranes. *Int J Nanomed* 8: 2077–2084.

Ehmann HM, Breitwieser D, Winter S, Gspan C, Koraimann G, Maver U, Segal M, Köstler S, Stana-Kleinschek K, Spirk S, Ribitsch V (2015). Gold nanoparticles in the engineering of antibacterial and anticoagulant surfaces. *Carbohydr Polym* 117: 34–42.

Ehrenreich M, Ruszczak Z (2006). Tissue-engineered temporary wound coverings. Important options for the clinician. *Acta Dermatoven APA* 15(1): 5-13.

Exposito JY, Cluzel C, Garrone R, Lethias C (2002). Evolution of collagens. *Anat Rec* 268: 302–316.

Exposito JY, Le Guellec D, Lu Q, Garrone R (1991). Short chain collagens in sponges are encoded by a family of closely related genes. *J Biol Chem* 266: 21923–21928.

Falanga V, Faria K (2007). Bioengineered skin constructs. *Principles of Tissue Engineering* 3(77): 1167-1185.

Fathi-Azarbayjani A, Qun L, Chan YW, Chan SY (2010). Novel vitamin and gold-loaded nanofiber facial mask for topical delivery. *Aaps Pharmscitech* 11: 1164–1170.

Felson DT, Anderson JJ, Meenan RF (1990). The comparative efficacy and toxicity of second-line drugs in rheumatoid arthritis results of two meta analyses. *Arthritis Rheum* 33: 1449–1461.

Fini M, Motta A, Torricelli P, Giavaresi G, Nicoli Aldini N, Tschon M et al. (2005). The healing of confined critical size cancellous defects in the presence of silk fibroin hydrogel. *Biomaterials* 26(17): 3527–3536.

Fischer RL, McCoy MG, Grant SA (2012). Electrospinning collagen and hyaluronic acid nanofiber meshes. *J Mater Sci-Mater M* 23: 1645–1654.

Fisher GJ, Quan T, Purohit T, Shao Y, Cho MK, He T et al. (2009). Collagen fragmentation promotes oxidative stress and elevates matrix metalloproteinase-1 in fibroblasts in aged human skin. *Am J Pathol* 174: 101-114.

Fisher GJ, Varani J, Voorhees JJ (2008) Looking older: fibroblast collapse and therapeutic implications. *Arch Dermatol* 144: 666-672.

Fleischer S, Shevach M, Feiner R, Dvir T (2014). Coiled fiber scaffolds embedded with gold nanoparticles improve the performance of engineered cardiac tissues. *Nanoscale* 6: 9410–9414.

Fraga S, Faria H, Soares M, Duarte J, Soares L, Pereira E, Costa-Pereira C, Teixeira J, Bastos M, Carmo H (2013). Influence of the surface coating on the cytotoxicity, genotoxicity and uptake of gold nanoparticles in human HepG2 cells. *J Appl Toxicol* 33: 1111–1119.

Frens G (1973). Controlled nucleation for regulation of particle-size in monodisperse gold suspensions. *Nature-Physical Science* 241: 20-22.

Fung YC (1993). *Biomechanics: Biomechanical properties of living tissues*. New York, NY: Springer Verlag.

Garcia Y, Wilkins B, Collighan RJ, Griffin M, Pandit A (2008). Towards development of a dermal rudiment for enhanced wound healing response. *Biomaterials* 29: 857– 868.

Gaspar A, Moldovan L, Constantin D, Stanciuc AM, Sarbu Boeti PM, Efrimescu IC (2011). Collagen-based scaffolds for skin tissue engineering. *J Med Life* 4: 172–177.

Geethalakshmi R and Sarada DV (2013). Characterization and antimicrobial activity of gold and silver nanoparticles synthesized using saponin isolated from *Trianthemadecandra L*. *Ind Crop Prod* 51: 107–115.

Gelse K, Pöschl E, Aigner T (2003). Collagens--structure, function, and biosynthesis. *Adv Drug Deliv Rev* 55: 1531–1546.

Gentleman E, Lay AN, Dickerson DA, Nauman EA (2003). Mechanical characterization of collagen fibers and scaffolds for tissue engineering. *Biomaterials* 24: 3805-3813.

Ghazali FC (2009). Morphological characterization study of Malaysian honey - AVPSEM, EDX randomised attempt. *Annal Microscop* 9: 93–102.

Gheldof N, Wang XH, Engeseth NJ (2002). Identification and quantification of antioxidant components of honeys from various floral sources. *J Agric Food Chem* 50: 5870-5877.

Ghosh K, Ren XD, Shu XZ, Prestwich GD, Clark RA (2006). Fibronectin functional domains coupled to hyaluronan stimulate adult human dermal fibroblast responses critical for wound healing. *Tissue Eng* 12: 601–613.

Gil-Tomas J (2007). Lethal photosensitisation of *Staphylococcus aureus* using a toluidine blue O–tiopronin–gold nanoparticle conjugate. *J Mater Chem* 17: 3739–3746.

Gong Y, Chen X, Lu Y, Yang W (2015). Self-assembled dipeptide–gold nanoparticle hybrid spheres for highly sensitive amperometric hydrogen peroxide biosensors. *Biosensors Bioelectronics* 66: 392-398.

Goodman CM, McCusker CD, Yilmaz T (2004). Toxicity of gold nanoparticles functionalized with cationic and anionic side chains. *Bioconjugate Chem* 157: 897–900.

Gopalakrishnan R, Azhagiya Singam ER, Vijaya Sundar J, Subramanian V (2015). Interaction of collagen like peptides with gold nanosurfaces: a molecular dynamics investigation. *Phys Chem Chem Phys* 17: 5172–5186.

Grace NA, Pandian K (2007). Antibacterial efficacy of aminoglycosidic antibiotics protected gold nanoparticles—A brief study. *Colloids Surf. A Physicochem Eng Asp* 297: 63–70.

Grant DN, Benson J, Cozad MJ, Whelove OE, Bachman SL, Ramshaw BJ, Grant DA, Grant SA (2011). Conjugation of gold nanoparticles to polypropylene mesh for enhanced biocompatibility. *J Mater Sci-Mater M* 22: 2803–2812.

Grant SA, Spradling CS, Grant DN, Fox DB, Jimenez L, Grant DA, Rone RJ (2014). Assessment of the biocompatibility and stability of a gold nanoparticle collagen bioscaffold. *J Biomed Mater Res A* 102: 332–339.

Gu H, Ho PL, Tong E, Wang L, Xu B (2003). Presenting vancomycin on nanoparticles to enhance antimicrobial activities. *Nano Lett* 3: 1261–1263.

Guelcher SA, Hollinger JO (2006). *An Introduction to Biomaterials. The Biomedical Engineering Series.* Boca Raton, FL: CRC Press.

Haller E, Lindner W, Lämmerhofer M (2015). Gold nanoparticle-antibody conjugates for specific extraction and subsequent analysis by liquid chromatography-tandem mass spectrometry of malondialdehyde-modified low density lipoprotein as biomarker for cardiovascular risk. *Anal Chim Acta* 857: 53–63.

Hardy JG, Lin M, Römer, Scheibel TR. (2008). Polymeric materials based on silk proteins. *Polymer* 49: 4309-4327.

Helenius G, Backdahl H, Bodin A, Nannmark U, Gatenholm P, Risberg B (2006). In vivo biocompatibility of bacterial cellulose. *J Biomed Mater Res A* 76: 431–438.

Hollander DH (1994). Interstitial cystitis and silk allergy. *Med. Hypotheses* 43(3): 155-160.

Hsu FY, Hung YS, Liou HM, Shen CH (2010). Electrospun hyaluronate–collagen nanofibrous matrix and the effects of varying the concentration of hyaluronate on the characteristics of foreskin fibroblast cells. *Acta biomaterialia* 6: 2140-2147.

Hu K, Lv Q, Cui F, Feng Q, Kong X, Wang H, et al. (2006). Biocompatible fibroin blended films with recombinant human-like collagen for hepatic tissue engineering. *J Bioactive Compatible Polym* 21(1): 23–37.

Huang L, Nagapudi K, Apkarian RP (2001). Engineered collagen–PEO nanofibers and fabrics. *J Biomater Sci Polymer Ed* 12: 979–993.

Huang WC (2007). Functional gold nanoparticles as photothermal agents for selective-killing of pathogenic bacteria. *Nanomedicine* 2: 777–787.

Huemmerich D, Slotta U, Scheibel T. (2006) Processing and modification of films made from recombinant spider silk proteins. *Appl Phys A* 82: 219–222.

Hung H-SS, Chang C-HH, Chang C-JJ, Tang C-MM, Kao W-CC, Lin S-ZZ, Hsieh H-HH, Chu M-YY, Sun W-SS, Hsu S-HH (2014). In vitro study of a novel nanogold-collagen composite to enhance the mesenchymal stem cell behavior for vascular regeneration. PLoS ONE 9: e104019.

Inoue S, Tanaka K, Arisaka F, Kimura S, Ohtomo K, Mizuno S (2000). Silk fibroin of *B. mori* is secreted, assembling a high molecular mass elementary unit consisting of H-chain, L-chain, and P25, with a 6:6:1 molar ratio. J Biol Chem 275(51): 40517–40528.

Ji XH, Song XN, Li J, Bai YB, Yang WS, Peng XG (2007). Size control of gold nanocrystals in citrate reduction: The third role of citrate. J Am Chem Soc 129:13939-13948.

Jin HJ, Chen J, Karageorgiou V, Altman GH, Kaplan DL (2004). Human bone marrow stromal cell responses on electrospun silk fibroin mats. Biomaterials 25(6): 1039–1047.

Jin HJ, Kaplan DL (2003). Mechanism of silk processing in insects and spiders. Nature 424: 1057-1061.

Jin HJ, Park J, Valluzzi R, Cebe P, Kaplan DL (2004). Biomaterial films of *B. mori* silk fibroin with poly(ethyleneoxide). Biomacromolecules 5(3):711–717.

Johnen C, Steffen I, Beichelt D, Bräutigam K (2008). Culture of subconfluent human fibroblasts and keratinocytes using biodegradable transfer membranes. Burns 34: 655–663.

Jones I, Currie L, Martin R (2002). A guide to biological skin substitutes. British Journal of Plastic Surgery 55: 185-193.

Jorge-Herrero E, Fernandez P, Turnay J, Olmo N, Calero P, Garcia R, Freile I, Castillo-Olivares JL (1999). Influence of different chemical cross-linking treatments on the properties of bovine pericardium and collagen. Biomaterials 20: 539-545.

Jung D, Minami I, Patel S, Lee J, Jiang B, Yuan Q, Li L, Kobayashi S, Chen Y, Lee K-BB, Nakatsuji N (2012). Incorporation of functionalized gold nanoparticles into nanofibers for enhanced attachment and differentiation of mammalian cells. *J Nanobiotechnology* 10: 23.

Kaplan DL (1998). Fibrous proteins—silk as a model system. *Polymer Degradation and Stability* 59: 25-32.

Kato N, Sato S, Yamanaka A, Yamada H, Fuwa N, Nomura M (1998). Silk protein, sericin, inhibits lipid peroxidation and tyrosinase activity. *Biosci Biotechnol Biochem* 62(1): 145-147.

Kearney JN (2001). Clinical evaluation of skin substitutes. *Burns* 27: 545-551.

Kellouche S. et al. (2007). Tissue engineering for full-thickness burns: a dermal substitute from bench to bedside. *Biochem Biophys Res Commun* 363: 472–478.

Khalil MI, Sulaiman SA, Gan SH (2010). High 5-hydroxymethylfurfural concentrations are found in Malaysian honey samples stored for more than one year. *Food Chem Toxicol* 48(8–9): 2388– 2392.

Ki CS, Park SY, Kim HJ, Jung H-MM, Woo KM, Lee JW, Park YH (2008). Development of 3-D nanofibrous fibroin scaffold with high porosity by electrospinning: Implications for bone regeneration. *Biotechnol Lett* 30: 405–410.

Kim H, Kim H, Matsumoto A, Chin I, Jin H, Kaplan D (2005). Processing windows for forming silk fibroin biomaterials into a 3D porous matrix. *Aust J Chem* 58: 716–720.

Kim KH, Jeong L, Park HN, Shin SY, Park WH, Lee SC et al. (2005). Biological efficacy of silk fibroin nanofiber membranes for guided bone regeneration. *J Biotechnol* 120(3): 327–339.

Kim PJ, Dybowski KS, Steinberg JS (2006). Feature: a closer look at bioengineered alternative tissues. *Podiatry Today* 19: 38–55.

Kim UJ, Park J, Kim HJ, Wada M, Kaplan DL (2005). Three dimensional aqueous-derived biomaterial scaffolds from silk fibroin. *Biomaterials* 26(15): 2775–2785.

Kim YP, Oh YH, Kim HS (2008) Protein kinase assay on peptide-conjugated gold nanoparticles. *Biosens Bioelectron* 23: 980-986.

Kimling J, Maier M, Okenve B, Kotaidis V, Ballot H, Plech A (2006). Turkevich method for gold nanoparticle synthesis revisited. *J Phys Chem B* 110: 15700-15707.

Kishore RK, Halim AS, Syazana MS, Sirajudeen KN (2011). Tualang honey has higher phenolic content and greater radical scavenging activity compared with other honey sources. *Nutr Res* 31(4): 322–325.

Ko W-KK, Heo DN, Moon H-JJ, Lee SJ, Bae MS, Lee JB, Sun I-CC, Jeon HB, Park HK, Kwon IK (2015). The effect of gold nanoparticle size on osteogenic differentiation of adipose-derived stem cells. *J Colloid Interf Sci* 438: 68–76.

Kokabi M, Sirousazar M, Hassan ZM (2007). PVA–clay nanocomposite hydrogels for wound dressing. *European Polymer Journal* 43: 773-781.

Kondo T (2007). Timing of skin wounds. *Legal Medicine* 9: 109-114.

Kumar S, Gandhi KS, Kumar R (2007). Modeling of formation of gold nanoparticles by citrate method. *Ind Eng Chem Res* 46: 3128-3136.

Kumari K, Singh P, Mehrotra G (2012). A facile one pot synthesis of collagen protected gold nanoparticles using Na–malanodialdehyde. *Materials Letters* 79: 199201.

Kundu SC, Dash BC, Dash R, Kaplan DL (2008). Natural protective glue protein, sericin bioengineered by silkworms: Potential for biomedical and biotechnological applications. *Progress in Polymer Science* 33: 998-1012.

Kuo WS (2009). Antimicrobial gold nanorods with dual-modality photodynamic inactivation and hyperthermia. *Chem Commun* 32: 4853–4855.

Kurosaki S, Otsuka H, Kunitomo M, Koyama M, Pawankar R, Matumoto K (1999). Fibroin allergy. IgE mediated hypersensitivity to silk suture materials. *J Nippon Med Sch* 66(1): 41-44.

Kwakman PH, te Velde AA, de Boer L, Speijer D, Vandenbroucke-Grauls CM et al. (2010). How honey kills bacteria. *FASEB J* 24: 2576-2582.

Labala S, Mandapalli PK, Kurumaddali A, Venuganti VV (2015). Layer-by-layer polymer coated gold nanoparticles for topical delivery of imatinib mesylate to treat melanoma. *Mol Pharm*.

Lai J-YY, Ma DH (2013). Glutaraldehyde cross-linking of amniotic membranes affects their nanofibrous structures and limbal epithelial cell culture characteristics. *Int J Nanomedicine* 8: 4157–4168.

Lanone S, Rogerieux F, Geys J, Dupont A, Maillot-Marechal E, Boczkowski J, Lacroix G, Hoet P (2009). Comparative toxicity of 24 manufactured nanoparticles in human alveolar epithelial and macrophage cell lines. *Part Fibre Toxicol* 6: 14.

Li C, Li D, Wan G, Xu J, Hou W (2011). Facile synthesis of concentrated gold nanoparticles with low size-distribution in water: temperature and pH controls. *Nanoscale Research Letters* 6: 440

Li C, Vepari C, Jin HJ, Kim HJ, Kaplan DL (2006). Electrospun silk-BMP-2 scaffolds for bone tissue engineering. *Biomaterials* 27(16): 3115–3124.

Li DX, Li CF, Wang AH, He Q, Li JB (2010). Hierarchical gold/copolymer nanostructures as hydrophobic nanotanks for drug encapsulation. *J Mater Chem* 20: 7782-7787.

Li J, Chen J, Kirsner R (2007). Pathophysiology of acute wound healing. *Clinics in Dermatology* 25: 9-18.

Li JJ, Zhou L, Hartono D, Ong CN, Bay BH, Yung LY (2008). Gold nanoparticles induce oxidative damage in lung fibroblasts in vitro. *Adv Mater* 20: 138–142.

Li M, Ogiso M, Minoura N (2003). Enzymatic degradation behavior of porous silk fibroin sheets. *Biomaterials* 24: 357–365.

Li X, Robinson SM, Gupta A, Saha K, Jiang Z, Moyano DF, Sahar A, Riley MA, Rotello VM (2014). Functional gold nanoparticles as potent antimicrobial agents against multi-drug-resistant bacteria. *ACS Nano* 8: 10682–10686.

Lin H-Y, Kuo Y-J, Chang S-H, Ni T (2013). Characterization of electrospun nanofiber matrices made of collagen blends as potential skin substitutes. *Biomed Mater* 8: 025009.

Lin YK, Liu DC (2006). Comparison of physical-chemical properties of type I collagen from different species. *Food Chem* 99: 244–251.

Lin Y-L, Jen J-C, Hsu S-H, Chiu I-M (2008). Sciatic nerve repair by microgrooved nerve conduits made of chitosan-gold nanocomposites. *Surgical Neurology* 70 S1: 9 – S1:18.

Liu SH, Zhang ZH, Han MY (2005) Nanometer-sized gold-loaded gelatin/silicananocapsules. *Adv Mater*, 17: 1862-1866.

Liu SJ, Kau YC, Chou CY, Chen JK, Wu RC (2010). Electrospun PLGA/collagen nanofibrous membrane as early-stage wound dressing. *J Membrane Sci* 355: 53–55.

Lu S, Xia D, Huang G, Jing H, Wang Y, Gu H (2010). Concentration effect of gold nanoparticles on proliferation of keratinocytes. *Colloid Surface B* 81: 406–411.

Lusby PE, Coombes A, Wilkinson JM. Honey (2002). A potent agent for wound healing? *J Wound Ostomy Continence Nurs* 29(6): 295–300.

Mahdihassan S (1985). Cinnabar-gold as the best alchemical drug of longevity, called Makaradhwaja in India. *Am. J. Chin. Med* 13: 93–108.

Mandal MD, Mandal S (2011). Honey: its medicinal property and antibacterial activity. *Asian Pac J Trop Biomed* 1: 154-160.

Manjumeena R, Elakkiya T, Duraibabu D, Feroze Ahamed A, Kalaichelvan P, Venkatesan R (2015). 'Green' biocompatible organic-inorganic hybrid electrospun nanofibers for potential biomedical applications. *J Biomater Appl* 29(7): 1039-1055.

Martin MN, Basham JI, Chando P, Eah SK (2010). Charged gold nanoparticles in non-polar solvents: 10-min synthesis and 2D self-assembly. *Langmuir* 26: 7410-7417.

McKeon-Fischer K, Freeman J (2011). Characterization of electrospun poly(L-lactide) and gold nanoparticle composite scaffolds for skeletal muscle tissue engineering. *J Tissue Eng Regen M* 5: 560–568.

Medhi B, Prakasha A, Avti K, Saikia UN, Pandhia P, Khanduja KL (2008). Effect of manuka honey and sulfasalazine in combination to promote antioxidant defense system in experimentally induced ulcerative colitis model in rats. *Indian J Experiment Biol* 46: 583-590.

Meinel AJ, Kubow KE, Klotzsch E, Garcia-Fuentes M, Smith ML, Vogel V, Merkle HP, Meinel L (2009). Optimization strategies for electrospun silk fibroin tissue engineering scaffolds. *Biomaterials* 30: 3058–3067.

Meinel L, Hofmann S, Karageorgiou V, Kirker-Head C, McCool J, Gronowicz G, Zichner L, Langer R, Vunjak-Novakovic G, Kaplan DL (2005). The inflammatory responses to silk films in vitro and in vivo. *Biomaterials* 26: 147-155.

Meinel L, Karageorgiou V, Fajardo R, Snyder B, Shinde-Patil V, Zichner L, et al. (2004). Bone tissue engineering using human mesenchymal stem cells: effects of scaffold material and medium flow. *Ann Biomed Eng* 32(1): 112–122.

Meyers MA, Chen PY, Lin AYM, Seki Y (2008). Biological materials: Structure and mechanical properties. *Progress in Materials Science* 53: 1-206.

Miladi I, Alric C, Dufort S, Mowat P, Dutour A, Mandon C, Laurent G, Bräuer-Krisch E, Herath N, Coll J-LL, Dutreix M, Lux F, Bazzi R, Billotey C, Janier M, Perriat P, Duc G Le, Roux S, Tillement O (2014). The In Vivo Radiosensitizing Effect of Gold Nanoparticles Based MRI Contrast Agents. *Small* 10: 1116-1124.

Miller SJ, Burke EM, Rader MD, Coulombe PA, Lavker RM (1998). Re-epithelialization of porcine skin by the sweat apparatus. *J Invest Dermatol* 110: 13–19.

Min BM, Lee G, Kim SH, Nam YS, Lee TS, ParkWH (2004). Electrospinning of silk fibroin nanofibers and its effect on the adhesion and spreading of normal human keratinocytes and fibroblasts in vitro. *Biomaterials* 25(7–8): 1289–1297.

Minoura N, Aiba S, Gotoh Y, Tsukada M, Imai Y (1995). Attachment and growth of cultured fibroblast cells on silk protein matrices. *J Biomed Mater Res* 29(10): 1215–1221.

Mohamed M, Sirajudeen KN, Swamy M, Yaacob NS, Sulaiman SA (2010). Studies on the antioxidant properties of Tualang honey of Malaysia. *Afr J Tradit Complement Altern Med* 7(1): 59–63.

Molan PC (1999) The role of honey in the management of wounds. *J Wound Care* 8: 415–418.

Molan PC (1999) Why honey is effective as a medicine. I. Its use in modern medicine. *Bee World* 80: 80–92.

Molan PC, Smith IM, Reid GM (1988). A comparison of the antibacterial activities of some New Zealand honeys. *J Apic Res* 27(4): 252–256.

Motta A, Fambri L, Migliaresi C (2002). Regenerated silk fibroinfilms: thermal and dynamic mechanical analysis. *MacromolChem Phys* 203(10–11): 1658–1665.

Motta A, Migliaresi C, Faccioni F, Torricelli P, Fini M, Giardino R (2004). Fibroin hydrogels for biomedical applications: preparation, characterization and in vitro cell culture studies. *J Biomater Sci Polym Ed* 15(7): 851–864.

Muehlberger T, Moresi JM, Schwarze H, Hristopoulos G, Laenger F, Wong L (2005). The effect of topical tretinoin on tissue strength and skin components in a murine incisional wound model. *J Am Acad Dermatol* 52: 583–588.

Mukherjee P, Bhattacharya R, Bone N, et al. (2007). Potential therapeutic application of gold nanoparticles in B-chronic lymphocytic leukemia (BCLL): Enhancing apoptosis. *J.Nanobiotechnology* 5: 4.

Mundo MA, Padilla-Zakour OI, Worobo RW (2004). Growth inhibition of foodborne pathogens and food spoilage organisms by select raw honeys. *Int J Food Microbiol* 97: 1-8.

Murase M (1994). Method for solubilizing and molding cocoon silk, artificial organ made of cocoon silk, and medical element made of cocoon silk. Japan Patent 06-166850A.

Muthukumar T, Prabu P, Ghosh K, Sastry TP (2014). Fish scale collagen sponge incorporated with *Macrotyloma uniflorum* plant extract as a possible wound/burn dressing material. *Colloids Surf B Biointerfaces* 113: 207–212.

Nasir NA, Halim AS, Singh KK, Dorai AA, Haneef MN (2010). Antibacterial properties of tualang honey and its effect in burn wound management: A comparative study. *BMC Complement Altern Med* 10(31):1–7.

Nguyen DT, Kim DJ, So MG, Kim KS (2010). Experimental measurements of gold nanoparticle nucleation and growth by citrate reduction of HAuCl_4 . *Adv Powder Technol* 21: 111-118.

Nirmala GA, Pandian K (2007). Antibacterial efficacy of amino glycosidic antibiotics protected gold nanoparticles—A brief study. *Colloids and Surfaces A: Physicochem Eng Aspects* 297: 63–70.

Norman RS (2008). Targeted photothermal lysis of the pathogenic bacteria, *Pseudomonas aeruginosa*, with gold nanorods. *NanoLett* 8: 302–306.

Nunes Pauli GE, Escosura-Muñiz A de la, Parolo C, Helmuth Bechtold I, Merkoçi A (2014). Lab-in-a-syringe using gold nanoparticles for rapid immunosensing of protein biomarkers. *Lab Chip* 15: 399–405.

Obaid G, Chambrier I, Cook MJ, Russell DA (2015). Cancer targeting with biomolecules: a comparative study of photodynamic therapy efficacy using antibody or lectin conjugated phthalocyanine-PEG gold nanoparticles. *Photochem Photobiol Sci*.

Oh E, Susumu K, Goswami R, Mattoussi H (2010). One-phase synthesis of water-soluble gold nanoparticles with control over size and surface functionalities. *Langmuir* 26: 7604-7613.

Paino I, Marangoni V, Oliveira R, Antunes L, Zucolotto V (2012). Cytotoxicity and genotoxicity of gold nanoparticles in human hepatocellular carcinoma and peripheral blood mononuclear cells. *Toxicol Lett* 215: 119-125.

Pan Y, Neuss S, Leifert A, Fischler M, Wen F, Simon U, Schmid G, Brandau W, Jahnke-Dechent W (2007). Size-Dependent Cytotoxicity of Gold Nanoparticles. *Small* 3: 1941–1949.

Panilaitis B, Altman GH, Chen J, Jin HJ, Karageorgiou V, Kaplan DL (2003). Macrophage responses to silk. *Biomaterials* 24: 3079-3085.

Papini R (2004). Management of burn injuries of various depths. *Br Med J* 329: 158–160.

Park JB and Lakes RS (1992). *Biomaterials*. Second ed. Plenum.

Park JB, Bronzino JD (2003). *Biomaterials: Principles and Applications*. Boca Raton, FL: CRC Press.

Park SN, Kim JK, Suh H (2004). Evaluation of antibiotic-loaded collagen-hyaluronic acid matrix as a skin substitute. *Biomaterials* 25: 3689-3698.

Park SN, Park JC, Kim HO, Song MJ, Suh H (2002). Characterization of porous collagen/hyaluronic acid scaffold modified by 1-ethyl-3-(3-dimethylaminopropyl) carbodiimide cross-linking. *Biomaterials* 23(4): 1205–1212.

Patra HK, Banerjee S, Chaudhuri U, Lahiri P, Dasgupta AK (2007). Cell selective response to gold nanoparticles. *Nanomedicine: Nanotechnology, Biology, and Medicine* 3 (2): 111–119.

Paviolo C, Chon JW, Clayton AH (2014). Inhibiting EGFR clustering and cell proliferation with gold nanoparticles. *Small*.

Peng CC, Yang MH, Chiu WT, Chiu CH, Yang CS, Chen YW, Chen KC, Peng RY (2008). Composite nano-titanium oxide-chitosan artificial skin exhibits strong wound-healing effect—an approach with anti-inflammatory and bactericidal kinetics. *Macromol Biosci* 8: 316–327.

Perni S (2009). The antimicrobial properties of light-activated polymers containing methylene blue and gold nanoparticles. *Biomaterials* 30: 89–93.

Pernodet N, Fang X, Sun Y et al (2006). Adverse effects of citrate/gold nanoparticles on human dermal fibroblasts. *Small* 2: 766–773.

Pernodet N, Fang X, Sun Y, Bakhtina A (2006). Adverse effects of citrate/gold nanoparticles on human dermal fibroblasts. *Small* 2: 766-773.

Petrini P, Parolari C, Tanzi MC (2001). Silk fibroin–polyurethanescaffolds for tissue engineering. *J Mater Sci Mater Med* 12(10–12): 849–853.

Pissuwan D, Cortie CH, Valenzuela SM, Cortie MB (2009). Functionalised gold nanoparticles for controlling pathogenic bacteria. *Trends in Biotechnology* 28: 207-213.

Powell HM, Boyce ST (2006). EDC cross-linking improves skin substitute strength and stability. *Biomaterials* 27: 5821–5827.

Prakash A, Medhi B, Avti PK, Saikia UN, Pandhi P et al. (2008). Effect of different doses of Manuka honey in experimentally induced inflammatory bowel disease in rats. *Phytother Res* 22: 1511-1519.

Quan T, Shao Y, He T, Voorhees JJ, Fisher GJ (2010). Reduced expression of connective tissue growth factor (CTGF/CCN2) mediates collagen loss in chronologically aged human skin. *J Invest Dermatol* 130: 415-424.

Quinlan E, López-Noriega A, Thompson E, Kelly HM, Cryan SA, O'Brien FJ (2015). Development of collagen-hydroxyapatite scaffolds incorporating PLGA and alginate microparticles for the controlled delivery of rhBMP-2 for bone tissue engineering. *J Control Release* 198: 71–79.

R. Rudolf, B. Friedrich, S. Stopic, I. Anzel, S. Tomic and M. Colic (2012). Cytotoxicity of gold nanoparticles prepared by ultrasonic spray pyrolysis. *J Biomater Appl* 26(5): 595-612.

Rai A, Prabhune A, Perry CC (2010). Antibiotic mediated synthesis of gold nanoparticles with potent antimicrobial activity and their application in antimicrobial coatings. *J Mater Chem* 20: 6789-6798.

Ramos-e-Silva M, Castro RMC (2002). New dressings, including tissue-engineered living skin. *Clinics in Dermatology* 20: 715-723.

Ravichandran R, Sridhar R, Venugopal JR, Sundarrajan S, Mukherjee S, Ramakrishna S (2014). Gold nanoparticle loaded hybrid nanofibers for cardiogenic differentiation of stem cells for infarcted myocardium regeneration. *Macromol Biosci* 14: 515–525.

Regiel-Futyr A, Kus-Liśkiewicz M, Sebastian V, Irusta S, Arruebo M, Stochel G, Kyzioł A (2015). Development of noncytotoxic chitosan-gold nanocomposites as efficient antibacterial materials. *ACS Appl Mater Interfaces* 7: 1087–1099.

Regnier M, Staquet MJ, Schmitt D (1997). Schmidt, R. Integration of Langerhans cells into apigmented reconstructed human epidermis. *J Invest Dermatol* 109: 510–512.

Rho KS, Jeong L, Lee G, Seo BM, Park YJ, Hong SD, Roh S, Cho JJ, Park WH, Min BM (2006). Electrospinning of collagen nanofibers: Effects on the behavior of normal human keratinocytes and early-stage wound healing, *Biomaterials* 27: 1452-1461.

Saha B (2007). In vitro structural and functional evaluation of gold nanoparticles conjugated antibiotics. *Nanoscale Res Lett* 2: 614–622.

Sanna V, Pala N, Dessì G, Manconi P, Mariani A, Dedola S, Rassu M, Crosio C, Iaccarino C, Sechi M (2014). Single-step green synthesis and characterization of gold-conjugated polyphenol nanoparticles with antioxidant and biological activities. *Int J Nanomedicine* 9: 4935–4951.

Santin M, Motta A, Freddi G, Cannas M (1999). In vitro evaluation of the inflammatory potential of the silk fibroin. *J Biomed Mater Res* 46(3): 382–389.

Schlinkert P, Casals E, Boyles M, Tischler U, Hornig E, Tran N, Zhao J, Himly M, Riediker M, Oostingh G, Puntès V, Duschl A (2015). The oxidative potential of differently charged silver and gold nanoparticles on three human lung epithelial cell types. *J Nanobiotechnology* 13: 1.

Schulz M, Ma-Hock L, Brill S, Strauss V, Treumann S, Groters S, van Ravenzwaay B, Landsiedel R (2012). Investigation on the genotoxicity of different sizes of gold nanoparticles administered to the lungs of rats. *Mutat Res* 745(1–2): 51–57.

Shakespeare PG (2005). The role of skin substitutes in the treatment of burn injuries. *Clinics in Dermatology* 23: 413–418.

Shaw IC (1999). Gold-based therapeutic agents. *Chem Rev* 99: 2589–2600.

Sheridan RL, Tompkins RG (1999). Skin Substitutes in Burns. *Burns* 25: 97–103.

Shevach M, Fleischer S, Shapira A, Dvir T (2014). Gold nanoparticle-decellularized matrix hybrids for cardiac tissue engineering. *Nano Lett* 14: 5792–5796.

Shevchenko R, James S, James S (2010). A review of tissue-engineered skin bioconstructs available for skin reconstruction. *J R Soc Interface* 7: 229–258.

Shevchenko RV, Sibbons PD, Sharpe JR, James SE (2008). Use of a novel porcine collagen paste as a dermal substitute in full-thickness wounds. *Wound Repair Regen* 16: 198–207.

Shukla R, Bansal V, Chaudhary M, Basu A (2005). Biocompatibility of gold nanoparticles and their endocytotic fate inside the cellular compartment: a microscopic overview. *Langmuir* 21: 10644–10654.

Shukla R, Bansal V, Chaudhary M, Basu A, Bhonde RR, Sastry M (2005). Biocompatibility of gold nanoparticles and their endocytotic fate inside the cellular compartment: A microscopic overview. *Langmuir* 21: 10644–10654.

Silveira PC, Venâncio M, Souza PS, Victor EG, Souza Notoya F de, Paganini CS, Streck EL, Silva L da, Pinho RA, Paula MM (2014). Iontophoresis with gold nanoparticles improves mitochondrial activity and oxidative stress markers of burn wounds. *Mater Sci Eng C Mater Biol Appl* 44: 380–385.

Silver FH (1994). *Biomaterials, Medical Devices and Tissue Engineering: An Integrated Approach*. London: Chapman and Hall.

Silver FH, Siperko LM, Seehra GP (2003). Mechanobiology of force transduction in dermal tissue. *Skin Res Technol* 9: 3–23.

Simon-Deckers A (2008). Impact of gold nanoparticles combined to X-Ray irradiation on bacteria. *Gold Bull* 41: 187–193.

Sionkowska A, Kozłowska J (2010). Characterization of collagen/hydroxyapatite composite sponges as a potential bone substitute. *Int J Biol Macromol* 47: 483–487.

Soenen SJH, Illyes E, Vercauteren D et al (2009). The role of nanoparticle concentration-dependent induction of cellular stress in the internalisation of non-toxic cationic magneto liposomes. *Biomaterials* 30: 6083–6813.

Song E, Kim SY, Chun T, Byun HJ, Lee YM (2006). Collagen scaffolds derived from a marine source and their biocompatibility. *Biomaterials* 27: 2951–2961.

Soo C, Rahbar G, Moy RL (1993). The immunology of bovine collagen implants. *J Dermatol Surg Oncol* 19: 431–434.

Sugihara A, Sugiura K, Morita H, Ninagawa T, TubouchiK, Tobe R et al (2000). Promotive effects of a silk film on epidermal recovery from full-thickness skin wounds. *Proc Soc Exp Biol Med* 225(1): 58–64.

Sugiura H, Yunoki S, Kondo E, Ikoma T, Tanaka J, Yasuda K (2009). *In vivo* biological responses and bioresorption of tilapia scale collagen as a potential biomaterial. *J Biomater Sci Polym Ed* 20: 1353–1368.

Suguna L, Singh S, Sivakumar P, Sampath P, Chandrakasan G (2002). Influence of Terminalia chebula on dermalwound healing in rats. *Phytotherapy Research*. 16: 227-231.

Supp DM, Boyce ST (2005). Engineered skin substitutes: practices and potentials. *Clinics in Dermatology* 23: 403-412.

Tamada Y (1997). Anticoagulant and its production. Japan Patent 09-227402A.

Tamada Y, Sano M, Niwa K, Imai T, Yoshino G (2004). Sulfation of silk sericin and anticoagulant activity of sulfated sericin. *J Biomater Sci Polym Ed* 15(8): 971-980.

Tan HT, Rahman RA, Gan SH, Halim AS, Hassan SA, Sulaiman SA, et al (2009). The antibacterial properties of Malaysian tualang honey against wound and enteric microorganisms in comparison to manuka honey. *BMC Complement Altern Med* 9(34): 1–8.

Tanaka K, Inoue S, Mizuno S (1999). Hydrophobic interaction of P25, containing Asn-linked oligosaccharide chains, with the H–L complex of silk fibroin produced by *B. mori*. *Insect Biochem Mol Biol* 29(3): 269–276.

Templeton AC, Hostetler MJ, Kraft CT, Murray RW (1998). Reactivity of monolayerprotected gold cluster molecules: Steric effects. *J Am Chem Soc* 120: 1906-1911.

Thomas M, Klivanov AM (2003). Conjugation to gold nanoparticles enhances polyethylenimine's transfer of plasmid DNA into mammalian cells. *Proceedings of the National Academy of Sciences* 100: 9138–9143.

Tkachenko AG, Xie H, Liu Y et al. (2004). Cellular trajectories of peptide modified gold particle complexes: Comparison of nuclear localization signals and peptide transduction domains. *Bioconjug Chem* 15: 482–490.

Tremblay PL, Hudon V, Berthod F (2005). Inosculation of Tissue-Engineered Capillaries with the Host's Vasculature in a Reconstructed Skin Transplanted on Mice. *American journal of Transplantation* 5: 1002-1010.

Trottier V, Marceau-Fortier G, Germain L, Vincent C, Fradette J (2008). IFATS collection: Using human adipose-derived stem/stromal cells for the production of new skin substitutes. *Stem Cells* 26: 2713–2723.

Tsubouchi K (1999). Occlusive dressing consisting essentially of silk fibroin and silk sericin and its production. Japan Patent 11-070160A.

Tsubouchi K, Igarashi Y, Takasu Y, Yamada H (2005). Sericin enhances attachment of cultured human skin fibroblasts. *Biosci Biotechnol Biochem* 69(2): 403-405.

Tsukada M, Hayasaka S, Inoue K, Nishikawa S, Yamamoto S (1999). Cell culture bed substrate for proliferation of animal cell and its preparation. Japan Patent 11-243948A.

Tumbar T (2006). Epithelial skin stem cells. *Methods Enzymol* 419: 73–99.

Tumbar T, Guasch G, Greco V, Blanpain C, Lowry WE, Rendl M, Fuchs E (2004). Defining the epithelial stem cell niche in skin. *Science* 303: 359–363.

Turkevich J, Stevenson PC, Hillier J (1953). The formation of colloidal gold. *The Journal of Physical Chemistry*. 57: 670-673.

Unger RE, Peters K, Wolf M, Motta A, Migliaresi C, Kirkpatrick CJ (2004). Endothelialization of a non-woven silk fibroin net for use in tissue engineering: growth and generegulation of human endothelial cells. *Biomaterials* 25(21): 5137–5146.

Unger RE, Wolf M, Peters K, Motta A, Migliaresi C, James Kirkpatrick C (2004). Growth of human cells on a nonwoven silk fibroin net: a potential for use in tissue engineering. *Biomaterials* 25(6): 1069–1075.

Vacanti JP, Langer RS (1998). Preparation of three-dimensional fibrous scaffold for attaching cells to produce vascularized tissue in vivo. US Patent 5,770,193 (MIT).

Vatankhah E, Prabhakaran MP, Jin G (2014). Development of nanofibrous cellulose acetate/gelatin skin substitutes for variety wound treatment applications. *Journal of Biomater appl* 28(6): 909-921.

Vecchio G, Galeone A, Brunetti V, Maiorano G, Rizzello L, Sabella S, Cingolani R, Pompa PP (2012). Mutagenic effects of gold nanoparticles induce aberrant phenotypes in *Drosophila melanogaster*. *Nanomedicine* 8(1): 1–7.

Venugopal JR, Zhang Y, Ramakrishna S (2006). In vitro culture of human dermal fibroblasts on electrospun polycaprolactone collagen nanofibrous membrane. *Artif Organs* 30: 440–446.

Vepari C, Kaplan DL (2007). Silk as a biomaterial. *Prog Polym Sci* 32: 991–1007.

Viator JA, Gupta S, Goldschmidt BS, Bhattacharyya K, Kannan R, Shukla R, Dale PS, Boote E, Katti K (2010). Gold Nanoparticle Mediated Detection of Prostate Cancer Cells Using Photoacoustic Flowmetry with Optical Reflectance. *J Biomed Nanotech* 6: 187–191.

Volkert AA, Subramaniam V, Haes AJ (2011). Implications of citrate concentration during the seeded growth synthesis of gold nanoparticles. *Chem Commun* 47: 478–480.

Vukovic G, Marinkovic A, Obradovic M et al (2009). Synthesis, Characterization and Cytotoxicity of Surface Amino-functionalized Water-dispersible Multiwalled Carbon Nanotubes. *Appl Surf Sci* 255: 8067–8075.

Wang J, Li QX (2011) Chemical composition, characterization, and differentiation of honey botanical and geographical origins. *Adv Food Nutr Res* 62: 89–137.

Wang J, Li YF, Huang CZ, Wu T (2008). Rapid and selective detection of cysteine based on its induced aggregates of cetyltrimethylammonium bromide capped gold nanoparticles. *Analytica chimica acta* 626: 37–43.

Wang X, Kim HJ, Xu P, Matsumoto A, Kaplan DL (2005). Biomaterial coatings by stepwise deposition of silk fibroin. *Langmuir* 21(24): 11335–11341.

Wang XH, Li DP, Wang WJ, Feng QL, Cui FZ, Xu YX, Song XH, van der Werf M, (2003). Crosslinked collagen/chitosan matrix for artificial livers. *Biomaterials* 24: 3213–3220.

Wang Y, Blasioli DJ, Kim HJ, Kim HS, Kaplan DL (2006). Cartilage tissue engineering with silk scaffolds and human articular chondrocytes. *Biomaterials* 27(25): 4434–4442.

Waters CA, Mills AJ, Johnson KA, Schiffrin DJ (2003). Purification of dodecanethiol derivatised gold nanoparticles. *Chem Commun* 540-541.

Wei G, Li C, Fu Q, Xu Y, Li H (2015). Preparation of PCL/silk fibroin/collagen electrospun fiber for urethral reconstruction. *Int Urol Nephrol* 47: 95–99.

Whelove OE, Cozad MJ, Lee B-DD, Sengupta S, Bachman SL, Ramshaw BJ, Grant SA (2011). Development and in vitro studies of a polyethylene terephthalate-gold nanoparticle scaffold for improved biocompatibility. *J Biomed Mater Res B* 99: 142–149.

When CM, Ye ST, Zhou LX, Yu Y (1990). Silk-induced asthma in children: a report of 64 cases. *Ann Allergy* 65 (5): 375-380.

White JW, Doner LW (1980) Honey composition and properties: Beekeeping in the United States. *Agric Handbook* 335: 82-91.

Yamaguchi K, Kikuchi Y, Takagi T, Kikuchi A, Oyama F, Shimura K, et al. (1989). Primary structure of the silk fibroin light chain determined by cDNA sequencing and peptide analysis. *J Mol Biol* 210(1): 127–39.

Yang C, Neshatian M, van Prooijen M (2014). Cancer nanotechnology: enhanced therapeutic response using peptide-modified gold nanoparticles. *J Nanosci Nanotechnol* 14(7): 4813-4819.

Yang SC, Wang YP, Wang QF, Zhang RL, Ding BJ (2007). UV irradiation induced formation of Au nanoparticles at room temperature: The case of pH values. *Colloid Surf A-Physicochem Eng Asp* 301:174.

Yannas IV, Burke JF, Orgill DP, Skrabut EM (1982). Wound tissue can utilize a polymeric template to synthesize a functional extension of skin. *Science* 215:174–176.

Yannas V, Burke JF (1980). Design of an artificial skin. 1. Basic design principles. *J Biomed Mater Res* 14: 65-81.

Yeo JH, Lee KG, Kim HC, Oh HYL, Kim AJ, Kim SY (2000). The effects of Pva/chitosan/fibroin (PCF)-blended spongsheets on wound healing in rats. *Biol Pharm Bull* 23(10): 1220–1223.

Zaoming W, Codina R, Fernandes-Caldas E, Lockey RF (1996). Partial characterization of the silk allergens in mulberry silk extract. *J. Investig. Allergol Clin Immunol* 6(4): 237-241.

Zawrah MF, El-Moez AS, Center D (2011). Antimicrobial activities of gold nanoparticles against major foodborne pathogens. *Life Science Journal* 8: 37–44.

Zeugolis DI, Li B, Lareu RR, Chan CK, Raghunath M (2008). Collagen solubility testing, a quality assurance step for reproducible electro-spun nano-fibre fabrication. A technical note. *J Biomater Sci Polym Ed* 19: 1307–1317.

Zhang M, Wang J, Xu W, Luan J, Li X, Zhang Y, Dong H (2015). The mechanical property of *Rana chensinensis* skin collagen/poly (L-lactide) fibrous membrane. *Materials Letters*.

Zhang YQ (2002). Applications of natural silk protein sericin in biomaterials. *Biotechnology Advances* 20: 91-100.

Zhao WA, Gao Y, Kandadai SA, Brook MA, Li YF (2006). DNA polymerization on gold nanoparticles through rolling circle amplification: Towards novel scaffolds for three-dimensional periodic nanoassemblies. *Angew Chem Int Ed* 45: 2409-2413.

Zhao X, Bichara DA, Zhou L, Kulig KM, Tseng A, Bowley CM, Vacanti JP, Pomerantseva I, Sundback CA, Randolph MA (2014). Conditions for seeding and promoting neo-auricular cartilage formation in a fibrous collagen scaffold. *J Craniomaxillofac Surg* 1-8.

Zhaorigetu S, Yanaka N, Sasaki M, Watanabe H, Kato N (2003). Inhibitory effects of silk protein, sericin on UVB-induced acute damage and tumor promotion by reducing oxidative stress in the skin of hairless mouse. *Journal of Photochemistry and Photobiology B: Biology* 71:11-17.

Zharov VP (2006). Photothermal nanotherapeutics and nanodiagnostics for selective killing of bacteria targeted with gold nanoparticles. *Biophys J* 90: 619–627.

Zhong SP, Zhang YZ, Lim CT (2010). Tissue scaffolds for skin wound healing and dermal reconstruction. *Wiley Interdiscip Rev Nanomed Nanobiotechnol* 2: 510–525.

Zhou CZ, Confalonieri F, Medina N, Zivanovic Y, Esnault C, Yang T, et al (2000). Fine organization of *B. mori* fibroin heavy chain gene. *Nucleic Acids Res* 28(12): 2413–2419.

Zhou H, Lu Q, Guo Q, Chae J, Fan X, Elisseff JH, Grant MP (2014). Vitri-fied collagen-based conjunctival equivalent for ocular surface reconstruction. *Biomaterials* 35: 7398–7406.

Zhou T, Wang N, Xue Y, Ding T, Liu X, Mo X, Sun J (2015). Development of biomimetic tilapia collagen nanofibers for skin regeneration through inducing keratinocytes differentiation and collagen synthesis of dermal fibroblasts. *ACS Appl Mater Interfaces*.

Zhou Y, Kong Y, Kundu S, Cirillo J, Liang H (2012). Antibacterial activities of gold and silver nanoparticles against *Escherichia coli* and *Bacillus Calmette-Guérin*. *J Nanobiotechnology* 10: 19.

APPENDIX A

ETHICAL APPROVAL FOR ANIMAL TESTS



T.C.
Sağlık Bakanlığı
Ankara Eğitim ve Araştırma Hastanesi
“Hayvan Deneyleeri Yerel Etik Kurulu Karar Defteri”

Toplantı No: 0018

13.05.2014

PROJENİN ADI (Varsa Kodu): Biyoaktif ajan yüklü iki katmanlı deri eşleniklerinin invivo dermal yara iyileştirme potansiyellerinin değerlendirilmesi.

SORUMLU ARAŞTIRMACI : Dr.Ömer Aktürk. Doktora Tezi
T.C.S.B.Ankara Eğitim ve Araştırma Hastanesi Genel Cerrahi Kliniği
(Dr.Ömer Aktürk, Doç.Dr.Dilek Keskin, Doç.Dr.Kemal Kısmet, Dr.Serdar Kuru, Dr.Mehmet Esat Duymuş, Dr.Ferudun Kaya, .Dr.Muzaffer Çaydere, Doç.Dr.Sema Hücümenoğlu, Prof.Dr.A.Çınar Yastı)

ARAŞTIRMAYI DESTEKLEYEN KURULUŞ(LAR): TÜBİTAK

KARAR:

295.Çalışmanın Protokol, usul, yaklaşım ve yöntem yönünden “**ETİK**” değerlendirmesinde “**UYGUN**” “**OLDUĞUNA**”/“**OLMADIĞINA**” “**OYBİRLİĞİ**” / “**OYÇOKLUĞU**” ile karar verilmiş ve araştırma için belirlenen tüm hayvan, uygulama, tetkik ve girişimlerin bedellerinin araştırma grubunca karşılanması kaydı ile çalışmanın yapılmasına ve Hastanemiz arşiv bilgi ve belgelerinin ve Hayvan Deneyleeri Laboratuvarı'nın kullanılmasına “**İZİN**” “**VERİLMİŞTİR**” / “**VERİLMEMİŞTİR**”.

Prof.Dr.Nevres AYDOĞAN
(BAŞKAN)

Doç.Dr.Yalçın ARAL

Prof.Dr.Ali Pekcan Demiröz

Doç.Dr.Nezih SUNGUR

Uz.Dr.Mustafa KOTANOĞLU

Gülcan BAŞEĞMEZ
(Sivil Üye)

Prof.Dr.Uğur KOÇER

Veteriner Hek. Cengiz YADGIN
(Raportör ve Kurul Seretere))

Doç.Dr.Kemal KISMET

Prof.Dr.Münir DEMİRCİ

Ahmet Zeki GÜLER
(Sivil Toplum Örgütü Üyesi)

CURRICULUM VITAE

1. Personal Information:

Surname, Name :	Aktürk, Ömer	
Nationality:	Turkish (TC)	
Date and Place of Birth	1 th of January 1982, Yozgat	
Marital Status:	Single	
Accommodation:	Ata Sokak 2/13 Anittepe Çankaya Ankara	
Phone:	0312 229 4756	GSM: 0544 216 7781
email	e129050@metu.edu.tr	Faks: -

2. Education:

Year of Graduation	Degree	Institution
02.2009- 01.2015	Ph. D.	METU, Engineering Sciences
10.2006- 02.2009	MS	METU, Engineering Sciences
09.2001- 06.2006	BS	METU, Mining Engineering

3. Academic and Work Experience:

Year	Enrollment	Place
05.2013- Present	Founder and manager	Remoderm Medical Biotechnology Incorporation
06.2013- 06.2014	TÜBİTAK 1512 project, coordinator	METU, Engineering Sciences Department
03.2012- 03.2013	TÜBİTAK 1002 project, project researcher	METU, Engineering Sciences Department
06.2010- 11.2011	METU BAP project, project researcher	METU, Engineering Sciences Department
12.2009- 08.2011	TÜBİTAK 1001 project, project researcher	METU, Engineering Sciences Department
06.2007- 08.2007	TÜBİTAK-British Council Scientific Frameshift project, guest researcher	London Imperial College Chemical Engineering and Chemical Technologies Department
08.2006- 08.2008	TÜBİTAK 1001 project, project researcher	METU, Engineering Sciences Department

4. Publications:

International Refereed Journals

1. Akturk O, Tezcaner A, Bilgili H, Deveci MS, Gecit MR, Keskin D. Evaluation of sericin/collagen membranes as prospective wound dressing biomaterial. J. Biosci. Bioeng. 2011; 112: 279-288.

Abstracts Published in International Refereed Conferans Proceedings

1. Akturk O, Tezcaner A, Gecit MR, Keskin D. Sericin/collagen membranes for wound healing. Proceedings of ICTE2011 II International Conference on Tissue Engineering. 2011; 279-286

International Refereed Conferans Abstracts

1. Ömer Aktürk, Dilek Keskin. Development and characterization of bilayered scaffolds incorporated with gold nanoparticles as potential skin substitutes. 26th Annual Conference of the European Society for Biomaterials, oral presentation, 2014, ESB2014, England, Liverpool.
2. Ömer Aktürk, Ayşen Tezcaner, M. Ruşen Geçit, Dilek Keskin. Sericin/collagen membranes for wound healing. II International Conference on Tissue Engineering, ICTE2011, oral presentation, 2011, Portugal, Lisbon.

National Refereed Conferans Abstracts

Ömer Aktürk, Ayşen Tezcaner, M. Ruşen Geçit, Dilek Keskin. Protein bazlı yara örtüsü hazırlanması ve biyomalzeme özelliklerinin incelenmesi. Biyomedikal Mühendisliği Ulusal Toplantısı, BİYOMUT2008, oral presentation, 2008, Ankara, ODTÜ.

5. Foreign Languages:

	Reading	Writing	Speaking
English	Advanced	Advanced	Advanced
Spanish	Advanced	Intermediate	Intermediate
German	Basic	Basic	Basic

6. HOBBIES:

Painting, ice skating, mountian skiing, bilard, voleyball, football, basketball, tenis.